

**Dissolution kinetics of biogenic silica
in marine environments**

**Lösungskinetik von biogenem Opal
in marinen Systemen**

Dirk Rickert

**Ber. Polarforsch. 351 (2000)
ISSN 0176 - 5027**

Dirk Rickert

Geomar Forschungszentrum
für marine Geowissenschaften
Wischhofstr. 1-3, Geb. 8/E
D-24148 Kiel
Deutschland

Die vorliegende Arbeit ist die inhaltlich leicht veränderte Fassung einer Dissertation, die am Graduiertenkolleg "Dynamik globaler Stoffkreisläufe im System Erde" und in der Abteilung Marine Umweltgeologie des Geomar Forschungszentrum für marine Geowissenschaften der Christian-Albrechts-Universität (CAU) zu Kiel angefertigt und im Juni 1999 der Mathematisch-Naturwissenschaftlichen Fakultät der CAU Kiel vorgelegt wurde.

	Page
CONTENTS	i
Acknowledgements	v
Abstract	vii
1. Introduction	1
2. Materials and methods	8
2.1 Sediments and sample preparation	8
2.1.1 Sediments	8
2.1.2 Sample preparation	13
2.1.2.1 Pore water extraction	13
2.1.2.1.1 Silicic acid	13
2.1.2.1.2 Aluminum	14
2.1.2.2 Sediment cleaning	15
2.2 Phytoplankton, cultured diatoms, sediment-trap and sedimentary opal	16
2.2.1 Opal samples	16
2.2.2 Acid leaching	18
2.3 Clay minerals	18
2.4 Sample characterization	19
2.4.1 Opal	19
2.4.2 Carbonate and C/N analyses	19
2.4.3 Detritus	20
2.4.4 XRD measurements	20
2.4.5 XRF measurements	23
2.4.6 Porosity	24
2.4.7 Surface area measurements (BET)	24
2.4.8 Scanning electron microscopy (SEM)	24
2.5 Dissolution experiments and calculations	25
2.5.1 Historical and theoretical background	25
2.5.2 Inflow solutions and pH measurements	28
2.5.3 Analytical techniques	29
2.5.4 Batch experiments	29
2.5.4.1 Temperature-dependent batch experiments (T-Batch)	29
2.5.4.2 Cobalt adsorption experiments	30
2.5.4.3 Alkaline dissolution experiments	31
2.5.5 Continuously stirred flow-through experiments	32
2.5.6 Temperature dependence on reaction rates	34
2.6 Modeling of pore water silicic acid	34
3. Experimental results and discussion	36
3.1 Stirred flow-through experiments	38
3.1.1 Solubility measurements	38
3.1.1.1 Introduction	38
3.1.1.2 Results	39

3.1.1.2.1	Apparent solubilities at 2°C and 25°C	39
3.1.1.2.2	Depth distribution of apparent solubilities in sediments	43
3.1.1.2.3	Effect of major cations (Mg ²⁺ , Al ³⁺)	45
3.1.1.2.4	Effect of clay minerals	54
3.1.1.3	Discussion	56
3.1.1.3.1	Laboratory and field solubilities: A comparison	56
3.1.1.3.2	Early diagenetic effects on silica solubility	58
3.1.1.3.3	Geochemical implications for early diagenetic modeling of biogenic silica dissolution	70
3.1.1.4	Conclusion	71
3.1.2	Dissolution kinetics	73
3.1.2.1	Introduction	73
3.1.2.2	Results and preliminary discussions	75
3.1.2.2.1	Apparent reaction rates at 2°C and 25°C	75
3.1.2.2.2	Depth-dependent reaction rates of sediments at 25°C	80
3.1.2.2.3	Determination of (reactive) surface area	85
3.1.2.2.4	Effects of clay minerals and coatings on biogenic silica reactivity	100
3.1.2.3	General discussion of laboratory results	105
3.1.2.3.1	Dissolution kinetics and mechanisms	105
3.1.2.3.2	Reaction rates from water column and sediments	106
3.1.2.3.3	Reactivity control on biogenic silica dissolution	108
3.1.2.3.4	Reverse weathering control on biogenic silica dissolution	114
3.1.2.3.5	Geochemical implications for early diagenetic modeling of biogenic silica dissolution	118
3.1.2.4	Conclusion	120
3.2	Pore water modeling	123
3.2.1	Introduction	123
3.2.2	Results	124
3.2.2.1	Pore water modeling	124
3.2.2.2	Benthic dissolution fluxes	128
3.2.2.3	Depth-dependent reaction rate constants	133
3.2.3	Discussion	137
3.2.3.1	Variations of benthic silicic acid fluxes	137
3.2.3.2	Initial silicic acid enrichment: Sampling artefact or rapidly dissolving biogenic silica (BSi)	138
3.2.3.3	A comparison of dissolution rate constants: Laboratory and field rates	144

3.2.3.3.1	Dissolution rates as a function of depth	144
3.2.3.3.2	What do dissolution experiments tell us about natural weathering ?	153
3.2.3.4	The benthic silica cycle in the Arabian Sea:	
	A mass balance	157
3.2.4	Conclusion	164
4.	Summary and general conclusions	166
	References	169
 APPENDIX		 183
A.1	XRF chemical bulk analysis of kaolinite, illite and montmorillonite	183
A.2.1-7	Average composition of sediments and pore waters	184
A.3.1-6	Raw data of sediment flow-through experiments	198
A.3.7	Raw data of single opal dissolution experiments	204
A.3.8	Results of aluminum flow-through experiments	205
A.3.9	Results of magnesium flow-through experiments	206
A.3.10	Results of opal/detrital clay experiments	207
A.3.11	Results of sediment flow-through experiments	208
A.3.12	Results of cobalt adsorption experiments	209
A.3.13	Results of alkaline leaching experiments with opal/clay mixtures	209
A.3.14	Results of alkaline leaching experiments with sediments	210

Acknowledgements

I would like to thank Prof. Dr. E. Suess and Priv. Doz. Dr. M. Schlüter, not only for their scientific advice but especially for their confidence in me and the liberty they gave me during my study and for the fruitful discussions and critical comments on the early stages of this thesis.

My thank goes to K. Wallmann and G. Bohrmann for discussions and for constructive comments on various aspects of this thesis.

I am very grateful for the technical assistance given by B. Domeyer, A. Bleyer, A. Lunau, R. Surberg, and A. Kolevica during the laboratory part of the thesis and during several expeditions. J. Heinze and D. Rau provided help on X-ray diffractometry and X-ray fluorescence. I would like to thank O. Schneider and C. Jung for their assistance on the scanning electron microscope and Dr. H. Lange who taught me how to work with clay minerals.

I am especially grateful to S. Wolf for his excellent assistance in carrying out the time-consuming experimental work.

I gratefully acknowledge Prof. Dr. G. Lagaly and his scientific group for allowing me access to their laboratories during BET measurements and clay mineral studies, and for the helpful discussions and comments on the results. S. Abend and K. Beneke kindly provided kaolinite and montmorillonite for my opal/clay experiments.

R. Botz and M. Schmidt have kindly provided phytoplankton samples for the laboratory studies.

I have benefited from fruitful discussions with numerous colleagues during my research on the dissolution kinetics of biogenic silica. I would especially like to mention, among others, Philippe van Cappellen, Suvasis Dixit, Olivier Ragueneau, and Justus van Beusekom.

My thanks go to the BfW Kiel-Wellingdorf and K. Bänsch who provided valuable help with the construction of several flow-through reactors which my thesis is substantially based on.

This thesis benefited greatly from corrections of E. Huetten, J. Wolf-Welling and R. Keir and last but not least from N. Schmidt who helped me with the reference list. I thank you all.

This thesis was partially supported by the Federal Ministry of Education, Science and Research (BMBF) and the German Science Foundation (DFG) within the framework of the multidisciplinary deep sea program BIGSET (BioGeochemical Transports of matter and energy in the deep-SEa).

A Ph.D scholarship of the graduate school "Dynamik globaler Kreisläufe im System Erde" funded by the German Science Foundation (DFG) is gratefully acknowledged. I wish to thank all former and present colleagues of the graduate school for the working atmosphere, for fruitful discussions within that multidisciplinary framework and for their moral support during the final stages of the thesis.

I would like to thank my parents and grandparents for their support during my studies.

Finally, I wish to thank Valérie for her patience and moral support during the nightshifts of the last months.

Abstract

The production and dissolution processes of biogenic silica (BSi) in the water column and surface sediments are important aspects for the investigation and reconstruction of present and past productivities of the ocean because biogenic silica is intimately linked to the carbon cycle. Because the controls on biogenic silica dissolution and preservation in various sedimentary environments are complex and not well defined, biogenic silica content in sediments cannot be interpreted simply as some linearly-coupled indicator of productivity. The basic processes which control the course of various geochemical cycles can only be understood with a proper kinetic framework.

In order to quantify recycling fluxes of silicic acid and to identify the processes controlling the preservation and recycling of BSi, pore water and solid phase profiles from five locations in the Arabian Sea were compared with samples derived from the Southern Ocean, the North and South Pacific, and the North Atlantic. Examining these different sedimentary regimes was expected to elucidate the key mechanisms controlling biogenic silica recycling and preservation. The benthic silica cycle in the Arabian Sea based on processing samples from 5 locations shows that the burial efficiency ranges between 7 and 17%, with the remaining percentage recycled from the sediment-water interface and from the sediment.

To understand the large variations in asymptotic silicic acid concentration-depth profiles, field measurements in combination with results gained through continuous flow-through (CFT) experiments were modeled. The experiments were carried out to directly quantify reactivity and solubility of biogenic silica under a variety of solution and solid matter conditions and under controlled saturation states. A reactivity constant gained through an alkaline leaching procedure provides a satisfactory proxy for tracking the evolution of silica reactivity decreases in the water and sediment column. Experimental solubilities measured in the deepest core sections exhibit a range of values similar to those observed in the field. These results and those gained in CFT experiments carried out with opal/clay mixtures reveal that the main environmental factor controlling the pore water build-up of silicic acid is the logarithmic ratio of detrital and biosiliceous material in sediments. The weighted average of solubilities of multiple siliceous phases yields realistic silicic acid values in sediment/pore water systems. With increasing deposition of detritus relative to biogenic silica, apparent solubility of biogenic silica within the sedimentary matrix decreases. This value represents a balance between biogenic silica dissolution releasing silicic acid and precipitation in reverse weathering reactions fixing silicic acid at the same rate.

Two possible endmember mechanisms for the formation of authigenic aluminosilicates were emphasized. A near-simultaneous dissolution-reprecipitation reaction of silicic acid and mobile aluminum escaping from relatively unstable aluminum oxides or aluminosilicates without build-up of high Al concentrations in pore waters is more likely than direct precipitation of silicic acid and aluminum from solution usually depleted in aluminum.

Old geochemists never die, they merely reach equilibrium.

Antonio Lasaga

1. Introduction

The aqueous chemistry of silica has long fascinated researchers in both the natural and applied sciences, ranging from the growth of gemstones, ancient marine sponges and so-called “marvels of complex design” [ILER, 1979], diatoms (silica-shelled phytoplankton) and radiolarians (silica-shelled zooplankton), to geothermal prospecting and power production to the catastrophic failure of high-pressure steam turbines. These and other phenomena, which can be traced to the ubiquitous presence of silica in surface waters, provide ample opportunity for the application of a chemical understanding of kinetics and thermodynamics, i.e. equilibria in the silica-water system.

The silica cycle

The marine silica cycle (Fig. 1.1) is dominated by the production and subsequent dissolution of biogenic silica (BSi) in the water column. The world ocean is strongly undersaturated in silicic acid but its cycle is in steady state, with both the eolian and

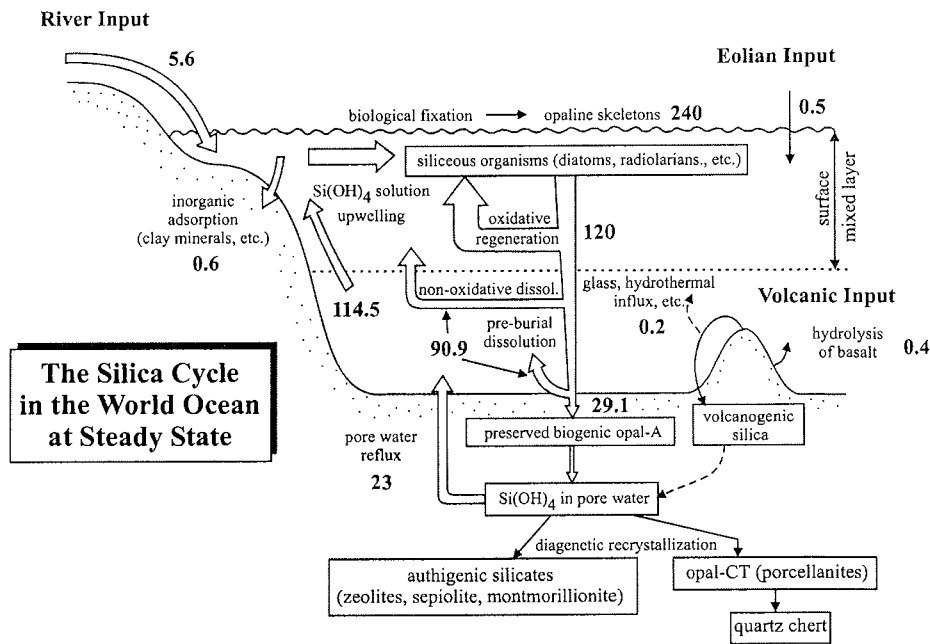


Fig. 1.1 The silica cycle in the world ocean at steady state [in: HESSE, 1988; with new data from TRÉGUER et al., 1995]. All fluxes are in teramoles of Si per year.

1. Introduction

annual input from rivers ($6.1 \text{ Tmol Si yr}^{-1}$) balanced by the burial of diatom shells in sediments. Figure 1.1 indicates the important role of the production/dissolution cycle, which exceeds the net through-put by a factor of ~ 80 [TRÉGUER et al., 1995]. The global rate of biogenic silica production in the ocean has been estimated to be between 200 and 280 Tmol Si yr^{-1} [NELSON et al., 1995; TRÉGUER, 1995]. Approximately 50% of the biogenic silica produced in the euphotic zone dissolves in the upper 100 m, leading to an estimated global export to the deep ocean of $\sim 120 \text{ Tmol Si yr}^{-1}$.

Since half of the export flux of organic carbon to the deep-sea is produced by diatoms [NELSON et al., 1995], any effort to better understand the processes determining the efficiency of the biological pump must take into account those factors which influence the relative contribution of diatoms to total primary production. Those factors, in turn, stress the importance of studying the silicon cycle in the modern oceans (Fig. 1.1) [e.g., BUESSELER, 1998; NEWTON and BOYD, 1998]. The biological pump represents the net effect of all processes which convert CO_2 into organic matter by photosynthesis in surface waters, and some fraction of the organic carbon (C_{org}) which survives heterotrophic, regenerative processes to sink into the deep-sea.

The problems

The silica cycle in the water column of the open ocean is strongly bimodal in character. In areas overlying diatomaceous sediments (in which only 10-25% of the global production of biogenic silica occurs), opal accumulation ranges within 15-25% of the silica produced in the surface layer. In other areas (in which most silica production occurs, ~ 75 -90%), however, almost no surface-produced opal is preserved. The global burial/production ratio, therefore, is only $\sim 3\%$, representing a composite of these two, very different systems [NELSON et al., 1995].

The Southern Ocean plays a major role in the global silica cycle, where more than half of the Si removal from the world ocean occurs through the accumulation of biogenic silica in Antarctic sediments [e.g., DEMASTER, 1981; LISITZIN, 1985]. The striking differences between high northern and southern Atlantic observed in the benthic silica cycle [SCHLÜTER et al., accepted] confirm the bimodal character of silica cycling mentioned above. Even if compared to the Weddell Sea (a region of fairly low BSi fluxes within the Southern Ocean), the rain rate of biogenic silica to the seafloor in the northern North Atlantic is very low and supplies only a minor contribution to the global silica cycle of the world ocean. Nevertheless, compared to the southern South Atlantic, the available particle trap data [SCHLÜTER et al., accepted] does not point to considerably lower BSi export from the surface waters of the northern North Atlantic. This stresses the importance of studying the silica cycle in the modern ocean in general and emphasizes the importance of studying the dissolution kinetics of BSi in particular.

The fate (dissolution or export) of biogenic silica produced in surface waters is strongly influenced by intrinsic factors and those which affect the dissolution (temperature, structure, degree of silicification, trace metals within the opal matrix such as Al [VAN BENNEKOM et al., 1988; VAN CAPPELLEN and QIU, 1997], organic coatings) as well as by external factors due to dissolution and/or export of BSi out of surface waters. The degree of undersaturation and the proposed non-linear dissolution kinetics of biogenic silica in highly undersaturated surface waters [VAN CAPPELLEN and QIU, 1997a,b] constitute some of these factors; other factors are the availability of silicic

acid, the formation of amorphous aggregates [e.g., SMETACEK, 1985; VON BODUNGEN et al., 1986; ALLDREDGE and GOTTSCHALK, 1989] and the type of grazers which may contribute to the enhanced export of BSi through fecal pellets [see ref. cited in NELSON et al., 1995]. Individual diatoms settling through the water column would probably not be able to reach abyssal depths, but a large portion of the diatom remains do reach the seafloor, probably as aggregates. Velocities of more than 2300 m in 10 days have been recorded by TSUNOGAI et al. [1986] in the Antarctic Ocean, suggesting that formation of aggregates is of great importance in escaping the high degree of undersaturation in the water column. Fecal pellets of the larger crustacean zooplankton can sink at rates of 100-800 m d⁻¹ [FOWLER and SMALL, 1972]. In addition, these fecal pellets are typically covered by an organic membrane [e.g., TURNER and FERRANTE, 1979], which can additionally delay silica dissolution. Recently BIDDLE and AZAM [1999] have reported enhanced silica dissolution due to the efficient removal of the organic matrix embedded in silica shells by bacterial hydrolytic attack.

With this information now available, the discrepancy between northern and southern latitudes can be explained by the growth of iron-limited diatoms which develop thicker silica shells [HUTCHINS and BRULAND, 1998; TAKEDA, 1998] than those produced in northern latitudes not being limited through iron deficiencies and by the breaking down of organic coatings through bacterial hydrolytic attacks [BIDDLE and AZAM, 1999]. SMETACEK [1999] proposes that a larger percentage of silica shells survives in HNLC (high nutrient, low chlorophyll) areas and is buried because bacterial growth may also be iron-limited and the breakdown of protective coatings may be slowed in those areas. The fraction of biogenic silica which escapes dissolution in the surface layer settles and redissolves through the water column before reaching the seafloor where most of its regeneration finally occurs [BROECKER and PENG, 1982]. Regeneration is accomplished by the dissolution of biogenic silica and other silica-bearing minerals, or by transport through the sediment-water interface, sediment burial and mixing.

Because the controls on biogenic silica dissolution and preservation in various sedimentary environments are complex and not well defined, biogenic silica contents in sediments cannot simply be interpreted as an indicator of past productivity [DEMASTER, 1981; SHEMESH et al., 1989; PICHON et al., 1992; BERGER and HERGUERA, 1992; ARCHER et al., 1993; DEMASTER et al., 1996]. It is important to first understand the processes which affect the dissolution of biogenic silica and release of silicic acid in the pore waters near the sediment-seawater interface because these processes control the amount of BSi which ultimately accumulates in sediments. These processes must be better understood before sedimentary biogenic silica can be used as a palaeoproductivity indicator, an indicator which could potentially yield valuable information about paleoenvironmental conditions, such as carbon cycling. RAGUENEAU et al. [submitted] provide a detailed review of all known physical, chemical and biological factors affecting the competition between biogenic silica recycling and preservation, beginning in surface waters and continuing to burial in deep-sea sediments. However, no consensus on the factors governing this competition exists as yet [ARCHER et al., 1993; MCMANUS et al., 1995; VAN CAPPELLEN and QIU, 1997a,b; RABOUILLE et al., 1997; RAGUENEAU et al, submitted].

1. Introduction

The answers

Pore water profiles alone cannot answer the question concerning the extent to which variable asymptotic silicic acid concentrations are induced through the biomineralization process in surface waters, or whether they are the product of an early diagenetic reaction. A number of scenarios can be imagined which would produce the constant or pseudo-constant depth-concentration profiles of silicic acid in pore waters. Given the many possible explanations [ARCHER, 1993; MCMANUS et al., 1995; MICHALOPOULOS and ALLER, 1995; VAN CAPPELLEN and QIU, 1997a,b; RABOUILLE et al., 1997; RAGUENEAU, submitted], an independent determination of the solubility and dissolution kinetics of solid biogenic silica is required to unambiguously interpret and understand silicic acid profiles measured in sediments.

In this thesis, insights into biogenic silica dissolution in both field and laboratory settings have been gained, which in turn provide answers to important questions which still puzzle biogeochemists working on the early diagenesis of biogenic silica:

- (1) How can silica be preserved in sediments in which pore water silicic acid concentrations do not reach saturation with respect to an acid-cleaned biosiliceous ooze as measured in the laboratory ($\sim 1000 \mu\text{M}$ at 4°C ; HURD, 1973)?
- (2) What controls spatial variations in asymptotic silicic acid concentrations of pore waters?
- (3) What causes apparent reactivity decreases with depth in sediments with low ($< 20\%$) biogenic silica contents ?
- (4) Is the bimodal character of the relationship between surface-layer production and benthic accumulation of silica when the northern Atlantic and Southern Ocean are compared thermodynamically or kinetically controlled by biogenic silica dissolution?

The specific objectives

Few studies so far combine field and laboratory measurements to gain an understanding of those factors which are responsible for solubility and reactivity differences in sediments either with depth or from one geographic site to another [e.g., HURD, 1973; BARKER et al., 1994; VAN CAPPELLEN and QIU, 1997a,b].

To evaluate the processes which affect pore water silica profiles and, consequently, the recycling of silicic acid fluxes across the sediment-water interface field data of silicic acid, biogenic silica and porosity have been combined and fitted to one-dimensional diagenetic equation [BERNER, 1980]. Recycling silicic acid fluxes and depth-dependent kinetic constants gained from the pore water modeling procedure as output parameters were compared with laboratory solubility plus rate data of the same sediments taken from different depth intervals.

The influence of detrital clays (kaolinite, montmorillonite, illite) and soluble cations (Al, Mg) on the dissolution kinetics of biogenic silica were studied in flow-through experiments.

Finally, results of laboratory investigations which provide important mechanistic insights into the early diagenesis of silica in deep-sea sediments have been summarized.

My sedimentary investigations, based on flow-through experiments [CHOU and WOLLAST, 1985; VAN CAPPELLEN and QIU, 1997a,b], were extended to simulate the primary solubility and reactivity signals from the overlying water column (phytoplankton, sediment trap material) and sedimentary end members (e.g., *Ethmodiscus rex* ~ 4 Myr BP). By applying such a holistic approach, that is by investigating changing sedimentary regimes in which biogenic silica is involved, primary signals from the water column or sedimentary end members, the key mechanisms controlling biogenic silica recycling and preservation were identified.

The apparent dissolution rate constants obtained by the flow-through experiments provide a satisfactory proxy for tracking the evolution of the reactivity of a biogenic silica assemblage as it sinks through the water column and is buried in the sediment column. VAN CAPPELLEN and QIU [1997a,b] working on siliceous oozes from the Southern Ocean demonstrated that the specific reactive surface area of biogenic silica decreases significantly with sediment depth. This has been shown by surface reactivity estimates using cobalt (Co) adsorption experiments [VAN CAPPELLEN and QIU, 1997b]. Since sediment facies in which opal contents are strikingly lower than in Southern Ocean sediments (< 20%) have also been processed, the use of Co adsorption experiments for tracking the evolution of the reactive surface area of silica in these sediments was less unambiguous. Thus, a reactivity rate constant in an alkaline medium, k_{NaOH} , [see also KONING et al., 1997] was used as a relative measure for a depth-dependent decrease in reactivity. Furthermore, influences of detrital clays and organic matter on this constant were examined to better predict depth distribution in sediment cores on the one hand and reactivity differences between single opal samples on the other hand.

In summary, the results, i.e. relative reactivity changes defined by flow-through experiments and k_{CFT} were fairly well represented by k_{NaOH} . Compared to flow-through experiments, both the cobalt adsorption method for opal-rich sediments [VAN CAPPELLEN and QIU, 1997 b] and the use of an alkaline apparent reactivity constant, k_{NaOH} , have the advantage of being faster and simpler to implement on a routine basis. The latter is not restricted to opal-rich sediments and provides first insights into the reactivity distribution of biogenic silica in sediments under investigation. Flow-through experiments, however, are still needed for investigations of dissolution and reprecipitation reactions of biogenic silica under natural seawater conditions and for the calibration of adsorption or measurements of reactivity in alkaline medium.

This thesis also involves and discusses modifications and extensions which can be applied to the present models of opal early diagenesis. A much more simplified fitting procedure was applied to take into account the non-linear dissolution kinetics [e.g., FLEMING, 1986; BERGER, 1994; VAN CAPPELLEN and QIU, 1997a,b; this study], solubility changes with depth, depth-dependent rate constants [VAN CAPPELLEN and QIU, 1997; this study] and subsurface gradients which may provide a seasonal imprint within pore water silicic acid profiles.

Within the framework of the multidisciplinary deep-sea program BIGSET (BIoGeochemical Transports of matter and energy in the deep-SEa), funded by the Federal Ministry of Education, Science and Research (BMBF) and the German Science Foundation (DFG), several cruises have been undertaken to quantify the flux and

1. Introduction

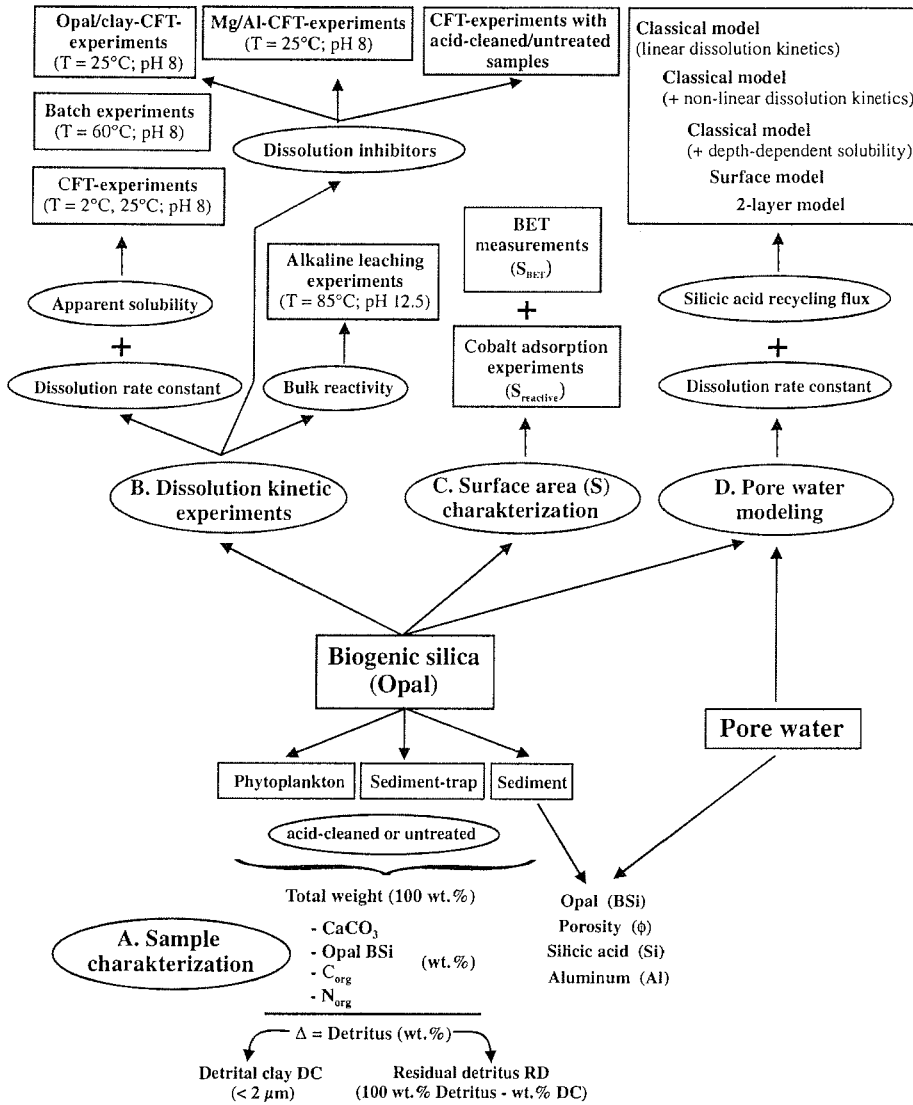


Fig. 1.2 Main scientific goals and instruments of: A. sample characterization (Chap. 2), B. dissolution kinetic experiments (Sect. 3.1), C. surface area characterization (Sect. 3.1.2), and D. pore water modeling.

turnover of material in the benthic boundary layer of 5 stations in the northern (NAST), western (WAST), central (CAST), eastern (EAST) and southern (SAST) Arabian Sea. Calculated values for recycling fluxes and steady state mass balances for these 5 sites were used to estimate the rain rate which must reach the seabed to balance burial rates and recycling effluxes. Combining those estimates with independent sediment trap data [HAAKE et al., 1993], a general box-model for the benthic silica cycle at these 5 localities with low opal accumulation was developed.

The approach

This study is divided into 4 chapters. This chapter has given an overview of the factors which stress the importance of studying the silica cycle as part of the biological pump and the dissolution kinetics of biogenic silica both in the field and in the laboratory. The previous work and the specific objectives of the present thesis have been outlined. Sample preparation and analytical methods of the opal samples from the surface water, the water column (450 m, 1000 m, 2500 m) and the sediment as well as subsequent laboratory experiments are described in chapter 2. In Chapter 3 the results of laboratory studies and modeling of pore water silicic acid are given and discussed; Section 3.1 outlines the results of flow-through experiments in terms of solubility (3.1.1) and dissolution kinetics (3.1.2). Factors which may sustainably influence the solubility of biogenic silica, such as specific cations (Mg^{2+} or Al^{3+}) or detrital minerals from which clay minerals have been investigated in more detail are part of Section 3.1.1. Factors which contribute specifically to the dissolution kinetics of biogenic silica (detrital minerals or reactive aluminum, inorganic and organic coatings as well as the specific (reactive) surface area) and methods to determine specific (reactive) surface area changes among biogenic silica samples originated various diagenetic histories are presented in Section 3.1.2. Specific (reactive) surface areas determined by means of BET-measurements or cobalt adsorption experiments are discussed in Section 3.1.2.3.3 as well as the alkaline leaching experiments which are suited to track the chemical and physical evolution of the overall biogenic silica assemblages. Section 3.2 deals with the pore water modeling of the 13 locations of studies. Finally, laboratory and field evidences on the controls on the recycling and preservation of biogenic silica in marine environments are summarized in the general conclusions of Chapter 4. Figure 1.2 summarizes the main scientific goals and instruments of A. sample characterization (Chap. 2), B. dissolution kinetic experiments (Sect. 3.1), C. surface area characterization (Sect. 3.1.2), and D. pore water modeling (Sect. 3.2).

2. Materials and methods

For the purpose of this thesis, sediment samples were selected with different opal/detritus ratios (Tab. 2.1) collected from various sedimentary regimes (Fig. 2.1). In general, cores of 6 to 40 cm length were recovered with multicorers. The geographic subregions 1-6 (Fig. 2.1) where sediments were collected are indicated in Figure 2.1 (see also Table 2.1 for further core description). This study summarizes pore water results from eight cruises. Pore water concentrations of dissolved silica (A.2.1-2.6.4, Fig. 3.4) display a large range of variation reflecting different opal contents in the cores. Geographic locations 1-6 of the sediment samples used in this study are indicated in Figure 2. Dissolution kinetics of biogenic silica in the 'untreated' sediment samples were compared with an Opal-CT/Opal-A mixture from the Maud Rise [BOHRMANN et al., 1994], Opal-A characterized by a mass occurrence of the giant diatom *Ethmodiscus rex* [ABELMANN et al., 1990], particle trap material collected from the Norwegian Sea, and untreated phytoplankton samples collected from surface water near the South Sandwich Islands. Moreover, the dissolution behavior of acid- and peroxide- cleaned samples from PS-2314-1, a cultured diatom assemblage of *Thalassiotrix antarctica*, and phytoplankton material, collected from the surface waters near the South Sandwich Islands, Norwegian Sea and Indian Ocean during several cruises, derived from laboratory cultures or a sediment trap deployed in the Weddell Sea (Tab. 2.2) was studied.

2.1 Sediments and sample preparation

Terminology and concentration units

To facilitate communication, a few of the terms and concentration units used for the subsequent description of materials, methods and results will be defined:

Dissolved silica (abbreviated: Si) is the term used for the undissociated monomeric *silicic acid* (H_4SiO_4 or $\text{Si}(\text{OH})_4$); both terms are used in this thesis. The concentration unit commonly used is $\mu\text{mol l}^{-1}$ or μM . Its anhydrous equivalent SiO_2 in its various solid phases will be referred to as silica and has a molecular weight of $\sim 60 \text{ g mol}^{-1}$. According to MORTLOCK and FROELICH [1989] *biogenic silica, opal-A* or simply *opal* (abbreviated: BSi) has an average water content of 10 wt.%. Therefore, a molecular weight of $\sim 66 \text{ g mol}^{-1}$ is assumed for further calculations. *Aluminum or dissolved alumina* (abbreviated: Al) is used to denote the aqueous Al (III) form, and *alumina* the amorphous $\text{Al}(\text{OH})_3$.

2.1.1 Sediments

Following is a short description of the sediments sampled in the subregions 1-6 (Fig. 2.1):

- (1) As an end member with almost no biogenic opal ($< 1 \text{ wt.}\%$) and an asymptotic dissolved silica concentration of $\sim 100 \mu\text{M}$, core M31/2 was selected, collected on cruise ARK-X/1 in the Norwegian Sea [SCHLÜTER and SAUTER, submitted]. Some occasional glass-like spicule sponge fragments were noticed in scanning electron micrographs (SEM) of the sediment among particles of sand and shells of foraminifera. The rare assemblages of diatom species preserved in surface sediments

2. Materials and methods

reflect the local oceanographic conditions and are quite similar to assemblages found in deep water sediment trap [KOHLY, 1998]. They do not necessarily reflect the composition of the main sedimentation event (weakly silicified species), but rather the post-bloom species composition with stronger silicified diatoms [KOHLY, 1998].

- (2) During cruise M36/6, core MC#33 was selected as being representative for the BENGAL (Benthic Biology and Geochemistry of a Northeastern Atlantic Abyssal Locality) station with an opal content between 2-3 wt.% and asymptotic pore water silicic acid concentrations of 200 μM . In contrast to Norwegian Sea sediments, the biogenic silica is diluted by large amounts of CaCO_3 in the top of the core (0-10 cm) rather than by terrigenous inflow. The stratigraphy of the core (A.2.2) follows the general Atlantic pattern of high concentrations in interglacial intervals [JANSEN et al., 1984]. Below 10 cm the carbonate content decreases markedly from ~ 70 wt.% down to 40 wt.%.
- (3) Investigations during three cruises (M33/1, SO118, SO129) in the Arabian Sea were focussed mainly on five stations in the northern (NAST), western (WAST), central (CAST), eastern (EAST), and southern (SAST) Arabian Sea. These stations are characterized by different rates of sedimentation, and different sediment regimes with extremely high carbonate contents of up to 70 wt.%. In WAST cores the highest contents of biogenic opal of ~ 5 wt.% and asymptotic pore water silicic acid concentrations of approximately 550 μM were observed. The cores deriving from other locations showed similar concentrations of extractable biogenic silica (2-3 wt.%) but pore water values ranging between 250 and 300 μM silicic acid. Throughout Indian Ocean cruises more than 10 multicorer were taken at each location so that a broad data base about pore water nutrients and sediment contents could be created. In Table 2.1 only those cores are listed which were used in laboratory experiments. In Appendices A.2.3.1 to A.2.3.5, all multicorers are listed which were used for the evaluation of pore water silicic acid or sediment contents and for the pore water modeling studies (2.6).
- (4) Surface sediments collected on cruise SO109/1 (4) are represented by pore water and sediment parameters of MC-1-3, a diatom-bearing mud, highly influenced terrigenous material from the North American continent.
- (5) Sediment material available from the Peru Basin (MC-145) collected during cruise SO106, together with porosity and nutrient data were made available for this study [HAECKEL et al., submitted]. Sediment from ~ 4000 m water depth represents a typical deep-sea clay. CaCO_3 and biogenic silica constitute a more significant contribution. This material is biogenically dominated by siliceous material in the upper part of the core (0-20 cm) (6 wt.% CaCO_3 , 20 wt.% Opal), whereas the carbonate content increases by a factor 4-5 in the lower section of the core (20-30 cm) (27 wt.% CaCO_3 , 20 wt.% Opal) [KONING et al., 1997; HAECKEL et al., submitted].

2. Materials and methods

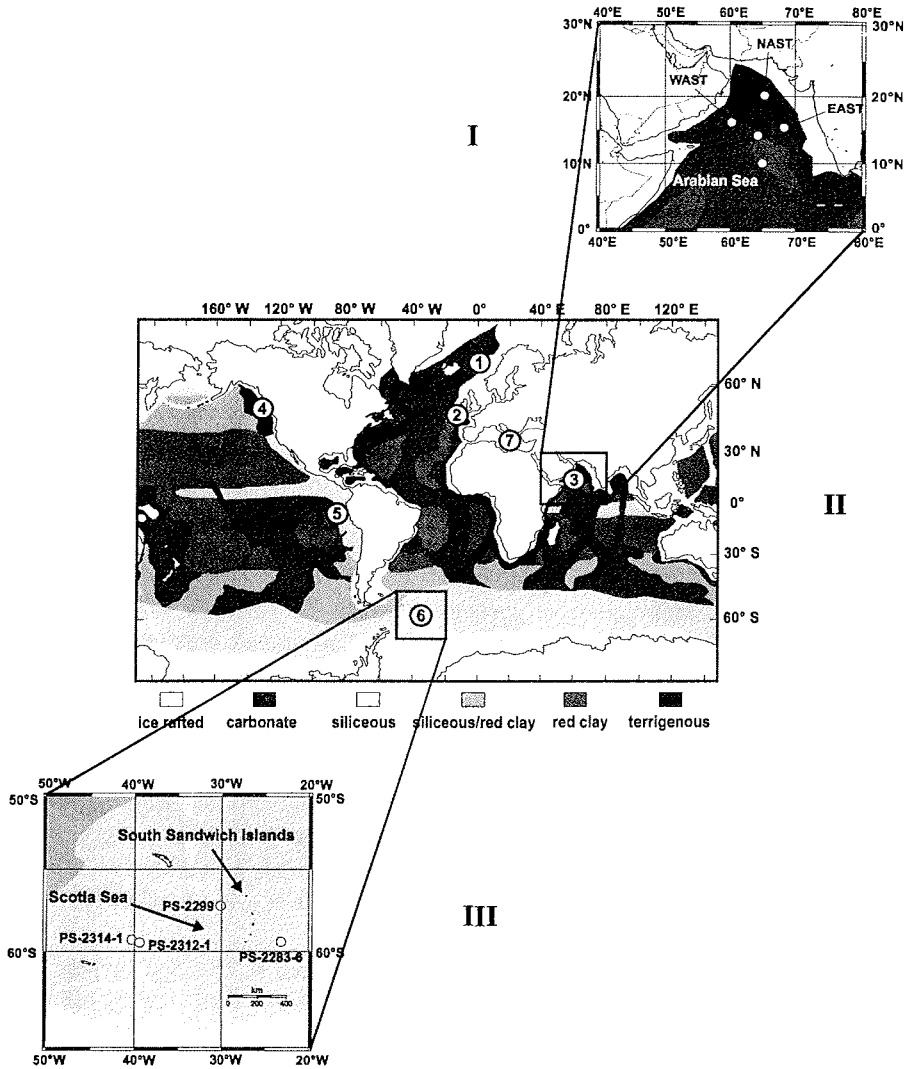


Fig. 2.1. I. Distribution of sediment facies on the sea floor of present-day oceans [reprinted from R. N. ANDERSON, 1986]. Sample locations 1-6 are listed in Tab 2.1. II. Sample locations in the western (WAST), northern (NAST), eastern (EAST), southern (SAST), and central (CAST) Arabian Sea. Note that each of these sites was sampled several times during three cruises with RV *Meteor* (M33/1) and *Sonne* (SO118, SO129). III. Site location map of 4 stations in the Scotia Sea. Sediment samples were taken during RV *Polarstern* cruise ANT-X/5 [SCHLÜTER et al., 1998]. Site 7 is represented by two sediment cores from the Discovery Basin, Eastern Mediterranean, where opal preservation is documented in hypersaline brines [WALLMANN et al., submitted].

2. Materials and methods

Tab. 2.1 Core locations and brief descriptions of cores (for locations, see Figure 2.1) taken for laboratory studies (flow-through experiments¹, batch experiments², cobalt adsorption experiments³). Alkaline extraction experiments were performed with samples from all stations. Pore water samples (2.1.2) were obtained using a squeezing technique or a centrifuging technique on sectioned cores (sample is marked with AI to indicate AI-pore water determinations) (for further description, see 2.1.2).

No.	Cruise	Station	Water depth	Sample designation	Location		Sediment facies
					Latitude	Longitude	
1	ARK-X/1	Norwegian Sea	3260	M31/2 ^{1,2}	69°59'N	03°58'E	0-5 cm calc. ooze 5-35 cm sandy mud
2	M36/6	BENGAL	4800	MC#33 ^{1,2}	48°58'N	16°28'W	foraminiferal ooze
3	M33/1	WAST	4030	MC#15 ²	16°12'N	60°18'E	foraminiferal mud
	SO118	WAST	4030	MC#53 ^{1,2}	16°13'N	60°16'E	foraminiferal mud
	SO118	NAST	3190	MC#45 ¹	20°00'N	65°35'E	foraminiferal ooze
	SO129	NAST	3190	MC#39 ^{AI}	20°13'N	65°35'E	foraminiferal ooze
	M33/1	EAST	3800	MC#28 ¹	15°35'N	68°36'E	foraminiferal ooze
	SO129	EAST	3840	MC#24 ^{AI}	15°35'N	68°34'E	foraminiferal ooze
	SO129	CAST	3950	MC#29 ^{AI}	14°25'N	64°34'E	foraminiferal ooze
	SO129	SAST	4430	MC#14 ^{AI}	10°02'N	65°00'E	foraminiferal mud
4	SO109/1	Juan de Fuca Ridge	2850	MC-1-3 ^{1,2}	45°29'N	128°02'W	diatom-bearing terrigenous mud
5	SO106	Peru-Basin	4080	MC-145 ^{1,2}	05°30'S	85°23'W	diatom-and radiolarian-bearing clay
6	ANT-X/5	Scotia Sea	4700	PS-2283-6 ^{1,2}	59°44'S	23°17'W	biosiliceous mud
	ANT-X/5	Scotia Sea	3380	PS-2299 ^{1,3}	59°51'S	23°23'W	biosiliceous ooze
	ANT-X/5	Scotia Sea	1670	PS-2312-1 ^{1,2}	59°50'S	39°42'W	biosiliceous ooze
	ANT-X/5	Scotia Sea	2330	PS-2314-1 ^{1,2,3}	59°33'S	40°31'W	biosiliceous ooze
7	D206	Discovery Basin	3580	PC9	35°20'N	21°35'E	calcareous ooze
	D206	Discovery Basin	3580	PC15	35°16'N	21°41'E	see text

- (6) A pore water data set and sediment samples from the Atlantic sector of the Southern Ocean were collected during the R.V. *Polarstern* cruise ANT-X/5 [SCHLÜTER et al., 1998]. Sediments are siliceous oozes with a negligible carbonate fraction throughout the cores but differing in the ratio of detrital material to extractable biogenic silica. Moreover, in PS-2283-6 volcanic ash particles derived from the Mount Hudson eruption in 1991 [BOHRMANN, pers. comm.; e.g., SCASSO et al., 1994] were recognized visually.
- (7) Site 7 provided biogenic opal excellently preserved under extreme brine conditions. The Discovery Basin is filled with a brine that has the highest salinities ever found in marine environments. Pore waters and water samples from the brine pool show that this brine is essentially a concentrated solution of $MgCl_2$ formed by the dissolution of bischofite ($MgCl_2 \cdot 6H_2O$) with Mg-concentrations almost ten times greater than in seawater [MEDRIFF-CONSORTIUM, 1995; WALLMANN et al., 1997; WALLMANN et al., submitted]. The Discovery Basin was investigated during cruise D206 of R.V. *Discovery* in 1993 [MEDRIFF CONSORTIUM, 1995] with two piston cores from the Basin (PC11, PC15) and one reference core (PC9) from a location outside the basin for this study [WALLMANN et al., submitted]. The preferential preservation of opal within that brine lake is documented in core PC15. Scanning electron micrographs clearly indicate radiolarians, diatoms, and - to a lesser extent - silicoflagellates particularly abundant in the sapropel S-1 layer and well preserved. No down-core differential dissolution has been recorded in core PC15. These findings are supported by measurements of biogenic opal contents [data in WALLMANN et al., submitted]. In general, a good correlation between organic carbon and biogenic opal contents for example was observed for the abundant siliceous microfossils in the organic-rich sapropel S-1 layer in PC15 and almost none was observed in PC9 in which there was observed low organic carbon contents [WALLMANN et al., submitted]. The extremely high organic matter content of the sapropel S-1 layer and the excellent preservation of siliceous microfossils may indicate that these organic coatings preserved still prevent dissolution processes. Another possible explanation for the preservation efficiency is the extraordinarily high concentration of Mg in this brine which may also act as inhibitor for opal dissolution. By means of flow-through experiments the efficiency of organic matter as well as of various concentrations of dissolved Mg in suppressing the dissolution process of biogenic silica was evaluated.

To compare natural findings by means of pore water measurements and modeling and laboratory-based dissolution measurements, pretreatment of sediment samples are avoided, as well as pore water squeezing and freeze-drying which fractures the siliceous frustules [BARKER et al., 1984], but this was assumed to be of minor consequence for the dissolution experiments at least for the solubility determination. In contrast, after acid or peroxide pretreatment which removes surface coatings (metals, organic matter) dissolution rate and the apparent solubility were significantly enhanced (see results in 3.1.2.2.4; for pretreatment consequences see e.g., HURD, 1972, 1973; LAWSON et al., 1978; WILLEY, 1980, 1997; BARKER et al., 1994).

Therefore, the remaining squeeze cakes were freeze-dried and gently disaggregated using mortar and pestle to ensure the homogeneity of the sample, but not pulverized to

2. Materials and methods

avoid major breaks in the opaline silica skeletons. The samples were not subjected to any chemical treatment apart from that carried out for cobalt adsorption experiments (3.1.2.2.3) and that necessary for dealing with fresh phytoplankton samples (3.1) to maintain the structure and properties (for example metal coatings) of the surface.

2.1.2 Sample preparation

2.1.2.1 Pore water extraction

Surface sediments taken with a multicorer were transferred to the cold room of the research vessel immediately after their recovery. They were sampled and processed within 3-4 hours at *in situ* temperatures ($T \sim 2^\circ\text{C}$). Pore water of wet sediment segments was extracted to determine nutrients (including silicic acid) by using a low pressure nitrogen squeezer and filtering the samples by $0.4 \mu\text{m}$ cellulose acetate or by a centrifuging technique, better suited for Al determination than squeezing because of lower contamination. The pore water obtained was filtered through syringe filters (for further details, see 2.1.2.2).

Samples were analyzed at different depths intervals, with a higher resolution within the first 10 centimetres. The pore water obtained was analyzed for silicic acid, nitrate plus nitrite, ammonium, and phosphate while at sea. The remaining sample volumes were stored in the cold room, or during cruises in the Arabian sea, frozen at -20°C in the dark for storage to avoid microbial degradation and assimilation activity. HCl acidification was avoided to prevent a decrease in silica concentrations which can be caused by precipitation reactions during sample storage.

2.1.2.1.1 Silicic acid

Silicic acid was analyzed using two methods; during ARK-X/1, ANT-X/5 and SO106 silicic acid was measured by autoanalyser applying the molybdenum blue method [GRASSHOFF et al., 1983]; during the other cruises similar manual colorimetric techniques were adapted [GRASSHOFF et al., 1983]. For Arabian Sea sediments (location 3, Fig. 2.1) pore water analyses from samples of all 3 cruises were taken into account and as a rule mean values of silicic acid of at least 2 profiles for each station were taken for pore water modeling studies. Uncertainties in pore water modeling and opal dissolution fluxes from pore water *ex situ* extraction are assessed separately. Pore water profiles used for the fitting procedure (3.2) are documented in Appendices A. 2.1-2.6.4.

Chemical analysis

The relative standard deviation based on 10 replicate analyses of the same pore water sample was 2.1% with $140 \mu\text{M}$ silicic acid.

Sediment heterogeneity

Pore waters from 5 to 10 multicorer tubes, taken at different multicorer casts at one site during one or all three cruises, showed concentration ranges with relative standard deviations rarely exceeding 10%. Standard deviations are often greater in the first centimetres of the core where a higher sampling resolution results in higher uncertainties. Also sampling the surface sediments in contact with bottom water leads to

higher variabilities (see also WILLEY et al., 1997). Core processing, particularly in the first section, leads to large errors because the undersaturation with respect to biogenic opal in overlying bottom water is highest. This in turn influences the flux calculations as well as reaction rate distributions (3.2.3.2).

Sediment cores with variations of silicic acid concentrations exceeding mean values were not taken into account. Disturbed cores are mainly responsible for those deviations, as well as storage time, squeezing procedures, storage temperature oscillations or simply natural patchiness.

Pore water extraction using 3 different techniques and replicate tubes of one multicorer cast

Pore water samples were obtained using a squeezer pressurizing the samples by nitrogen (1), a teflon squeezer deployed inside a glove box using helium as pressure gas (2) or by centrifuging of defined core sections (3). Relative standard deviations in most depth segments were < 3%, but increased up to 10% in some depth intervals. Our results showed that the overall patchiness of several tubes from one multicorer cast is lower compared with single tubes from multiple casts. Different squeezing techniques, however, did not result in systematic changes of profile shapes or values.

In summary, sediment heterogeneity (i.e., sediment patchiness) from several deployments of multicorers seems a major source of uncertainty. This is enhanced by the difficulty of sampling from near surface sediment. Consequently, all opal dissolution fluxes gained from pore water modeling (3.2) show uncertainties of at least 10-20% depending on the source and the physical properties of the surface sediment, which can be minimized by *in situ* whole core squeezing techniques [e.g., BENDER et al., 1987; MCMANUS et al., 1995; SAYLES ET AL., 1995]. Uncertainties become even greater (2-3 orders of magnitude) when comparing flux calculations based on gradient estimates from modeled silicic acid values at $x = 0$ [MCMANUS et al., 1995; SAYLES et al., 1995; RAGUENEAU et al., submitted] or using a simple two-point calculation between the bottom water silicic acid value and the dissolved silica content of the top 0.25 or 0.5 cm of the sediment column [e.g., HENSEN et al., 1998, RAGUENEAU et al., submitted] (3.2.2.2).

2.1.2.1.2 Aluminum

Filtered pore water samples from 4 stations (WAST, SAST, EAST, CAST) in the Arabian Sea (location (3) in Figure 2.1 and Table 2.1) were analyzed for dissolved aluminum (Al) according to HYDES and LISS [1976]. This method is based on measuring the fluorescence of the Lumogallion-Al complex at pH 5 using a 0.005% Lumogallion solution and an acetate buffer following MACKIN and ALLER [1984]. These measurements had to be corrected, however, because of a strong natural fluorescence signal due to the high DOC content in the pore water, particularly in surface sediments. To suppress both interferences from HPO_4 and from organic matter, calcium chloride solution was added [MACKIN, 1983; MACKIN and ALLER, 1984]. An Hitachi F-2000 fluorometer with an excitation wavelength of 465 nm and an emission wavelength of 555 nm was used on board.

2. Materials and methods

Cleaning procedure

The flasks and vessels used for the Al analyses were cleaned according to the procedure by VAN BEUSEKOM et al. [1997; pers. comm.]. All sampling and reaction vessels were soaked overnight with hot detergent (Extran™, Merck), rinsed thoroughly with hot tap water, ultrapure water and soaked in 1% suprapure HNO₃. This procedure had to be repeated several times on board because of the contamination of the bottles after several deployments as shown by elevated Al values.

Analyses

All analyses were carried out in a clean-air bench. The small amounts of pore water available made 5 dilution procedures necessary. Due to a change in natural fluorescence throughout the core, measurements in each sample were carried out by standard addition of three to four standards including a blank standard. The addition of CaCl₂ solution stabilized the slope of the curve which otherwise tended to decrease significantly towards the surface sediment; this was possibly caused by major interferences between added Al and DOC or HPO₄⁻ present in pore water (see natural fluorescence of the sample as indication for DOC, Fig. 3.8). The correlation coefficient r^2 (usually better than 0.99) for the slope of the standard addition curve was used as an indicator of precision. Nevertheless, measurements had to be corrected for natural fluorescence, reagent blank, and for Al content of ultrapure water, used on board. Reagent blank (3.4 ± 0.4 nM) was determined as the difference between a normal set of bottom water analyses and a set to which the double amount of reagents (CaCl₂, Lumogallion) was added. To determine the Al content of ultrapure water replicate measurements in a suite of 8 samples of deionized water yielded 2.5 ± 0.2 nM Al. Adding double the amounts of Lumogallion without CaCl₂ to another eight samples of deionized water showed an increase in Al of up to 3.5 nM. The difference of 1 nM is lumogallion blank, implying 1.5 nM Al in deionized water. The relative precision for the measurement of Al in pore water was calculated to be 3 nM or better. In the error propagation the precision of the calibration curve, the reagent blank, the measured signals, and dilution were considered.

2.1.2.2 Sediment cleaning

Cobalt adsorption experiments [VAN CAPPELLEN, 1996; VAN CAPPELLEN and QIU, 1997b] were performed to evaluate whether a reduction in density of reactive surface sites could explain the decrease in reactivity with increasing depth observed in most cores studied (3.1.2.2.3 and 3.1.2.3.2). To investigate this possibility and to quantify the influence of chemical treatment on a sediment sample (PS-2299, 20-25 cm) in terms of reactivity and/or solubility due to the removal of surface coatings such as organic matter or metal cations, a cleaning method proposed by BIEBOW [1991] was chosen. Very simple techniques were used which can be repeated several times: hydrogen peroxyde (H₂O₂) treatment to destroy organic matter, acid treatment (10% HCl) to remove carbonate, sieving (20 μ m) to remove clay minerals and settling (Atterberg method) to remove heavy minerals (> 20 μ m). It should be mentioned that by this method all diatoms < 20 μ m are removed. According to ANDERS [1997] the fraction > 20 μ m in Scotia Sea sediments provides the fraction significantly enriched in diatoms.

2.2 Phytoplankton, cultured diatoms, sediment-trap and sedimentary opal

2.2.1 Opal samples

Phytoplankton

Phytoplankton bloom samples #64 and #65 (Tab. 3.2) were collected from surface waters near the South Sandwich Islands on December 30th / 31st 1997 during RV *Polarstern* cruise ANT-XV/2. Plankton samples taken by net from surface waters of approximately 0°C consist of more or less pure natural diatom associations dominated by *Chaetoceros*, *Thalassiotrix* and *Rhizosolenia* sp. analyzed by SEM-electron microscopy. Whereas sample #64 was cleaned according to the procedure in Section 2.2.2, #65 remains untreated for further investigations.

The phytoplankton bloom sample taken at NAST (Fig. 3.1 and Tab. 3.2) with a plankton net during RV *Sonne* cruise SO129 (Feb. 1998) is dominated by diatom species, such as *Rhizosolenia* sp., a major upwelling species [NAIR et al., 1989], *Nitschia* sp., *Biddulphia* sp. as well as some radiolarians and some non-siliceous forms such as dinoflagellates (*Ceratium* and *Peridinium* are visible as well [LOCHTE, PFANNKUCHE, pers. comm.]. During Meteor cruise M21/4, the phytoplankton sampled at station 225 (Tab. 2.2) in surface waters between 0 and 50 m consisted mainly of *Chaetoceros* sp., *Rhizosolenia* sp., and *Thalassiosira* sp. [ANDERS, 1997].

Culture

The diatom species *Thalassiosira antarctica* (*T. antarctica*), originally isolated from a phytoplankton sample collected in the Weddell Sea during RV *Polarstern* ANT-IX/2-cruise, were cultured in 10 l-bottles containing clean (filtered) seawater at 0°C [for culture conditions see SCHMIDT et al., 1996 and references cited there].

Sediment trap material

Silica solubility and reactivity in samples collected in surface waters and sediment cores will be compared with biosiliceous material retrieved from sediment by means of flow-through experiments. For this purpose particle trap material (BO 1o#3) was sampled in the Weddell Sea at 450 m (kindly provided by M. SCHMIDT).

Sediment trap NB 9 in general was deployed in the Norwegian Sea at 70°00'N 04°00'E at 1000 m and 2500 m water depth. Sediments for batch- and flow-through experiments were taken at the same site. The Norwegian Sea is characterized by a relatively low diatom flux [KOHLY, 1998] that is probably the result of coprophagy (= reingestion of fecal pellets by zooplankton grazers) and coprorhexy (= mechanical destruction of fecal pellets) processes [LAMPITT et al., 1990; VON BODUNGEN et al., 1995]. *Chaetoceros*- and *Nitschia* sp. are supposed to be the most frequent at 1000 m water depth according to KOHLY [1998], but the *Thalassiosira* sp. as well as *Coscinodiscus radiatus* and *Rhizosolenia* sp. have been observed [KOHLY, 1998].

In 2500 m water depth the diatom flux seems not to change significantly with the seasons which are in good correlation with the material yielded from the upper trap. For the flow-through experiments at 2°C, sample No. 18 taken at a depth of 1000 m during a summer/winter bloom was chosen, whereas for the material collected in 2500 m water depth samples 1-6 were combined because of lacking material.

2. Materials and methods

Tab. 2.2 Samples O1-O11 from various regions applied for dissolution flow-through experiments (see also results in A.3.7).

No.	Sample	Location	T _{surface} [°C]	Notes
O1	<i>Thalassiosira antarctica</i> (<i>T. antarctica</i>) ¹		4	culture
O2	Phytoplankton bloom (NAST, SO129)	20°00'N 65°35'E	26-29	dominated by <i>Rhizosolenia</i> sp.
O3	Phytoplankton bloom (ANT-XV/2) #64 ¹	56°39'S 25°24'W	0.66	C _{org} -free, dominated by <i>Chaetoceros</i> , <i>Thalassiosira</i> and <i>Rhizosolenia</i> sp.
O4	Phytoplankton bloom (ANT-XV/2) #65 ¹	56°44'S 25°32'W	-0.34	untreated; dominated by <i>Chaetoceros</i> , <i>Thalassiosira</i> and <i>Rhizosolenia</i> sp.
O5	Phytoplankton bloom (M21/4 St. 225; 0-50 m) ¹	64°00'N 10°00'W	8.3	Norwegian Sea (06/08/92)
O6	Sediment trap (BO 1o#3; 450 m) ¹	54°20'S 03°23'W		Weddell Sea (03/07-03/30/91)
O7	Sediment-trap NB 9 (No. 18) (1000m) ²	70°00'N 04°01'E		Norwegian Sea
O8	Sediment-trap NB 9 (No. 1-6) (2500m) ²	70°00'N 04°01'E		Norwegian Sea
O9	<i>Ethmodiscus rex</i>	64°07'S 01°18'E	18-29 ²	Weddell Sea sediment, PS 1465, 425-427 cm; age ~ 4 Myr ³
O10	Opal-CT (Porcellanite horizon in PS2070-1)	65°06'S 03°37'E		Maud Rise, 471-474 cm; age ~ 4.2-4 Myr ⁴
O11	Sediment PS-2299 12.5-15 cm	59°51'S 23°23'W		Scotia Sea (see Tab. 2.1)

¹phytoplankton samples kindly provided by R. BOTZ and M. SCHMIDT.

²M. SCHLÜTER kindly made trap material available.

³ABELMANN et al. [1988].

⁴BOHRMANN et al. [1994].

Diagenetically altered biogenic silica

In addition to opal from surface waters and sediments samples from surface sediments (O11) and from deeper strata (O9, O10) were investigated. A core providing a mass occurrence of the giant diatom *Ethmodiscus rex* (*E. rex*) in Weddell Sea sediments was selected (core PS 1465, depth 425-427 cm, sample age ~ 4 Myr; for details, see ABELMANN et al. [1988]). A sample of Pliocene Opal-A/CT mixture [G. BOHRMANN, pers. comm.] taken from a 3-cm-thick porcellanite layer embedded in contact with his host sediment in 471 cm core depth (PS2070-1) in the Eastern Maud Rise was taken as well.

Phytoplankton samples described before were rinsed with distilled water, freeze-dried and cleaned according to Section 2.2.2 with the exception of sample #65 which remained untreated for the experiments.

Sediment trap material from Weddell Sea trap BO 1o#3 was acid-cleaned (2.2.2), whereas trap material from the Norwegian Sea (NB 9) as well as all other samples remained untreated.

Samples were freeze-dried and gently disaggregated with mortar and pestle to ensure the sample homogeneity of the sample and to minimize breakage.

2.2.2 Acid-leaching

To measure dissolution rates of pure siliceous material from diatomaceous sediment or phytoplankton implies a cleaning procedure which is suitable for removing organic matter, cations such as Mg^{2+} , Al^{3+} or Fe^{3+} , clays, and heavy minerals. A method used to measure oxygen isotopes must be suited to remove all oxygenated compounds which could alter the oxygen isotopic composition of diatom silica [JUILLET-LECLERC, 1984]. Thus, the method described fitted our purpose as well.

Phytoplankton blooms of biogenic silica which have not yet undergone significant dissolution processes, are enriched in biogenic silica and contamination by detrital clay is negligible. Hence, siliceous phytoplankton mixed with zooplankton such as copepods, *Tintinnids*, *Dinoflagellates* or *Foraminifera* (for example at NAST) or simple pure siliceous phytoplankton is first treated with a solution of 1% hydroxyl-amine in acetic acid [SHEMESH et al., 1995]. Then, to remove all the organic matter present, the diatom material was oxidized several times using a mixture of concentrated $HNO_3/HClO_4$ at 60°C [JUILLET-LECLERC, 1984]. After the samples were freed of organic matter, they were carefully washed with distilled water and dried at 60°C.

According to electron microscope and X-ray observations [SCHMIDT, 1997; BOHRMANN et al., 1994] as well as from Opal determination [SCHLÜTER and RICKERT, 1998] (2.4.1), the sedimentary Opal-A (*E. rex*) and Opal-A/CT mixture from the Maud Rise represent extremely pure siliceous samples. Contamination by detritus is negligible. Therefore, chemical treatment was avoided to measure chemically unaltered solubilities and reaction rates.

2.3 Clay minerals

To study the interaction of biogenic silica and clay minerals and the subsequent changes in biogenic silica solubility and dissolution rates in this mixture, clay-opal-mixtures with different opal/detritus ratios (3.1.1.2.4) were investigated. XRF-chemical analyses of the clays are given in Appendix A.1.

Clays used in our experiments were kaolinite, montmorillonite and illite. The general, albeit small impurities of kaolinite (China Clay provided by Krantz Company, Bonn), revealed by X-ray diffraction were caused by mica and feldspars. Ca-montmorillonite M50 from Milos (Greece), supplied by Südchemie AG (München) was purified according to STUL AND VAN LEEMPUT [1982], described in EWALD [1995]. Due to purification, montmorillonite is converted into the sodium form (kindly provided by S. ABEND, Institute for Inorganic Chemistry of Christian-Albrechts-University, Kiel). X-ray analyses reveal almost pure montmorillonite. Illite from the Massif Central, Le Puy (France), purified by small amounts of $CaCO_3$ and quartz was provided by K. BENEKE (Institute for Inorganic Chemistry of Christian-Albrechts-University, Kiel).

2. Materials and methods

2.4 Sample characterization

A full description of core compositions is given in A.2.1-A.2.7. Average sediment compositions, calculated from the chemical analyses (A.2.1-A.2.7), are given in Table 2.3.

2.4.1 Opal

Concentrations of biogenic silica in dry sediment or plankton/sediment-trap material were determined with a wet-chemical leaching technique according to SCHLÜTER and RICKERT [1998]. The aim of their study was to investigate the effect of pH on the release of silica and aluminum during alkaline extraction of marine sediments and to consider the effect of the clay correction procedure [DEMASTER, 1981] on the determination of BSi. The comparison suggests a narrow pH range as the most suitable for the extraction of biogenic silica, ensuring complete dissolution of BSi and minimizing the influence of non-BSi. Therefore, 0.032 M NaOH (pH 12.5) was taken as leaching agent, and a sequential leaching scheme was applied. Between 10 and 50 mg [LANDEN et al., 1996] of the sample were weighed into Falcon™ centrifuge cups and 50 ml of hot (85°C) alkaline extraction solution was added. The filled cups were immediately placed in a water bath at 85°C and agitated several times during the extraction procedure. After 0.5, 1, 2, 4, 8, and 24 hour intervals, the cups were centrifuged for 5 minutes and 1 ml of the supernatant solution was pipetted into reaction vessels for the subsequent determination of dissolved silica.

We calculated BSi (wt.%) with a modification for the evaluation of the dissolution pattern represented by 6 points. According to KONING et al. [1997] Equation 2.15 was fitted to the experimental data (2.5.4.3). The calculated BSi content (wt.%) based on the intercept of the released silica concentration and a conversion factor of 66 g mol^{-1} BSi (including a constant water content of BSi of 10% according to MORTLOCK and FROELICH [1989]). This procedure ruled out the high variance occurring when determining the intercept according to DEMASTER [1981] with a linear regression of the two or three points of the linear increase after approximately 4 hours. Due to the absence of certified Si standards, establishing absolute accuracy by this or other leaching procedures method was not possible [CONLEY, 1998]. Even for samples with a leachable BSi content of < 2%, the reproducibility of the extraction method is generally better than 10%, which allows for investigations of relative changes of BSi content in the sediments [SCHLÜTER and RICKERT, 1998]. For further description and application of wet alkaline extraction of biogenic silica to determine depth-dependent changes of apparent reactivities in sediment cores studied (Tab. 3.1) see Section 2.5.4.3.

2.4.2 Carbonate and C/N analyses

Carbonate, organic carbon and nitrogen were measured with a Carlo Erba Nitrogen Analyser 1500. The standard deviation with this method is 0.02% for nitrogen and 0.05% for carbon. Organic carbon was calculated by subtracting carbonate carbon from total carbon whereas C/N ratios were calculated from the ratio of organic carbon to total nitrogen content. The response of the Carlo Erba NA1500 is calibrated for each set of samples with four standards (Acetanilide) and three blank aluminum cups.

2.4.3 Detritus

Detrital sediments contain quartz, feldspars and clay minerals which make up the bulk of that composition [PRESS and SIEVER, 1986]. Detrital mineral contents (A.2.3.1-A.2.3.5 and Tab. 2.4) were estimated by calculation of the difference between the entire sample [wt.%] and the percentage of CaCO_3 , C_{org} , N_{org} and opal contents. In Table 2.4 that pool is further subdivided in detrital clay (DC; fraction $< 2 \mu\text{m}$) and residual detritus (RD). It must be noted that detrital contents as calculated in my thesis include authigenic aluminosilicates.

To quantify the clay-content for the cores of interest (Tab. 3.1), 10 g of 1-3 samples from different sediment sections were chosen. To remove impurities such as organic matter, carbonates, biogenic silica and ferrous oxides prior to X-ray investigation the samples were prepared according to STUL and VAN LEEMPUT [1982] as described in EWALD [1995]. The removal of biogenic silica with sodium carbonate as well as oxide removal by repeated treatment with sodium dithionite is essential to ensure an optimal dispersion during the final Atterberg treatment [MÜLLER, 1967]. The fraction $< 2 \mu\text{m}$ (wt.%) refers to the clay fraction which is quantitatively separated from the fraction $> 2 \mu\text{m}$ by means of 10-15 repeated settlings. The fractions were washed several times with distilled water and freeze-dried. The $< 2 \mu\text{m}$ detrital clay (DC) content was determined by weight, whereas the $> 2 \mu\text{m}$ residual detritus (RD) fraction was quantified by subtracting the clay content from the detrital content.

2.4.4 XRD measurements

The X-ray diffraction analysis of texture preparation according to H. LANGE (pers. comm.) was made with a cobalt anode, using 40 kV and 35 mA and applying a Philips PW 1830 generator. Scans were run between $2\text{-}45^\circ 2\theta$ using a scanning speed of $0.01^\circ 2\theta/\text{s}$.

200 mg of a freeze-dried sample was redispersed in 50 ml distilled water and agitated for 48 hours with a rotary shaker. 50 ml of a 50% $\text{MgCl}_2 \cdot 2 \text{H}_2\text{O}$ solution was added for Mg-saturation of clay minerals. Excess chloride was then removed by repeated washing with distilled water followed by centrifugation. Finally, 10 ml of a freshly dispersed 50 ml-suspension were pipetted onto a cellulose filter and filtrated to obtain an oriented clay fraction sample. Ethylene-glycol solvation was used to identify expandable (smectite) compounds. The samples were exposed to an ethylene-glycol saturated atmosphere in an exsiccator for 24 hours. Oriented samples, both untreated and ethylene-glycol solvated, were analyzed by XRD.

The results are given as qualitative estimates in Table 3.4. The average contents of major clay minerals in the $< 2 \mu\text{m}$ fraction of surficial sediments from world ocean basins (Tab. 3.5) are summarized in CHAMLEY [1989] and correspond quite well with our observations. The occurrence of chlorite and illite increases towards high latitudes.

In MC-1-3 derived from Juan de Fuca Plate (Fig. 3.1, Tab. 3.1), chlorite content is particularly high which may be due to direct erosion from the Rocky Mountains [H. LANGE, pers. comm.]. In soils of intertropical land masses characterized by a warm, humid climate [CHAMLEY, 1989] abundant kaolinite forms are present.

2. Materials and methods

Tab. 2.4. Quantitative bulk clay fraction analysis (see text). Standard deviations of mean values are given in brackets if relative deviation is less than 20%. No standard deviation means that detrital contents (DC) are not given as an overall mean value but for respective depth horizons due to significant change of detrital content with depth. Detrital clay (DC) contents from 3 cores of the Scotia Sea are given as one overall mean value. DC content in PS-2283-6 is excluded due to a significant lower clay content. Mean detrital content throughout the core is given in Table 3.3. (RD residual detritus = detrital content – DC, wt.%).

No.	Station	Depth intervals [cm]	DC (< 2 μ m) [wt.%]	Detritus [wt.%]	Mean DC (< 2 μ m) [wt.%]	RD (> 2 μ m) [wt.%]	DC/RD ratio
1	Norwegian Sea M31/2	15-20	21	94 ¹	20(1)	74	0.27
		30-35	19				
2	Bengal MC#33	4-5	17	32	17	15	1.13
		13-16	32	57	32	25	1.28
3	WAST MC#53	4-5	17	43(3)	16(1)	27(3)	0.59
		13-16	17				
		25-28	15				
3	NAST MC#45	4-5	18	44(5)	16(3)	28(6)	0.57
		13-16	16				
		25-28	13				
3	EAST MC#28	4-5	20	46(4)	17(3)	29(5)	0.59
		13-16	17				
		25-28	14				
3	CAST MC#40	4-5	10	30(5)	10(2)	20(5)	0.50
		13-16	8.5				
		25-28	12				
3	SAST MC#14-z	4-5	28	58(5)	28(2)	30(5)	0.93
		13-16	26				
		25-28	29				
4	Juan de Fuca Ridge MC-1-3	4-5	48	89(2)	48(1)	41(2)	1.2
		16-19	49				
5	Peru-Basin MC-145	4-5	44	76	44	32	1.4
		15.5-16.5	36	57	36	21	1.7
		26.5-27.5	26	59	26	33	0.79
6	Scotia Sea PS-2283-6	6-6.5	14	66	14	52	0.27
6	Scotia Sea PS-2299 PS-2312-1 PS-2314-1	12.5-15	31	49	31	18	1.7
		12.5-15	25	36	25	11	2.3
		12.5-15	23	48	23	25	0.92

¹Note: detritus [wt.%] from lower depth intervals of core M31/2 exhibit low CaCO₃ contents (XRF measurements, unpublished results). Accordingly, a detrital content of 94% was assumed as reasonable (A.2.1).

2. Materials and methods

Tab. 2.5 Qualitative mineral analysis of detrital clay fraction (Tab. 3.3) using X-ray diffraction. 0 = trace; x = present; xx = relatively abundant; xxx = dominant; -- not observed.

No.	Station	Feldsp.	Qtz.	Opal	Volc. glass	Montm.	Illite	Kaol.	Chlor.	Palyg.
1	Norw. Sea	x	x	--	--	x	xxx	xx	x	--
2	BENGAL	o	x	--	--	x	xxx	xx	x	--
3	WAST	o	x	--	--	xx	xxx	x	x	xx
3	NAST	o	x	--	--	xx	xxx	x	x	x
3	EAST	o	x	--	--	xx	xxx	x	x	o
3	CAST	o	x	--	--	xx	xxx	x	x	x
3	SAST	o	x	--	--	xx	xx	x	x	x
4	Peru-Basin	x	x	--	--	xxx	x	x	x	--
5	Juan de Fuca Ridge	x	x	--	--	xx	xx	x	xx	--
6	PS-2283-6	x	x	x	x	xx	xx	x	xx	--
6	PS-2299	x	x	x	--	xx	xx	x	xx	--
6	PS-2312-1	x	x	x	--	xx	xx	x	xx	--
6	PS-2314-1	x	x	o	--	xx	xx	x	xx	--

Tab. 2.6 Average contents of clay minerals in the < 2 μm fraction of surficial sediments from world ocean basins. Values summed to 100% [in WINDOM, 1976; reprinted in CHAMLEY, 1989]. Comparatively high abundancies of clays in a certain area are marked in bold letters.

Oceans	Corresponding sites No. (Tab. 2.1)	Chlorite	Illite	Smectite	Kaolinite
North Atlantic	1, 2	10	55	16	19
South Atlantic	6	11	47	26	16
North Pacific	4	18	40	34	8
South Pacific	5	13	26	53	8
Indian Ocean	--	10	29	46	15
Arabian Sea	3	18	45	28	9

2. Materials and methods

In the Indian Ocean, kaolinite concentrations increase slightly towards the equator resulting in the following sequence of increasing concentrations: NAST < CAST < SAST. In a West-east direction, there was abundant detrital palygorskite (indicated by reflections at 6.4 Å and a shoulder at 10 Å interfering with the illite (001) reflex) which had been removed from calcareous pedogenic crusts or evaporitic sediments and transported into the oceans [KOLLA et al, 1976]. Abundancies decrease towards station EAST. Sediments are dominated by smectite.

In North Atlantic sediments M31/2 and MC#33 kaolinite concentrations were comparably high whereas smectite contents in these cores are markedly poor.

In Peru Basin, typical deep-sea clays were observed which are dominated by smectite.

Sediments from the Scotia Sea mainly represent a mixture of illite and smectite and significant amounts of chlorite. In contrast to all other sediments, there are impurities besides quartz, mica, feldspars and other dense minerals in the < 2 μm fraction which are directly related to the supply from crystalline rocks in the oceans [WINDOM, 1976]. Small amounts of ash particles as well as residuals from Opal-A (< 2 μm), observed in PS-2283-6 are indicated by a hump between 2.7 Å and 5.7 Å. In PS-2312-1, such a hump was identified and related to small residual opal fragments since ash particles were not observed in this sample.

2.4.5 XRF measurements

The bulk chemistry of clay minerals (kaolinite, illite and Na-montmorillonite) used for flow-through experiments to investigate the influence of different opal/detritus ratios on biogenic silica dissolution kinetics (3.1.2.2.4) was determined by X-ray fluorescence (XRF) on fused beads. Oven-dried samples were pulverized in an agate mortar, dried again at 110°C to remove any atmospheric water that may have been absorbed during sample processing and stored in an exsiccator before preparing fused beads. Loss on ignition (LOI) at 1050°C was determined separately with a Rosemount CWA 5003 analyser; the gas released upon heating was analyzed with a BINOS™ infrared analyser for CO₂ and H₂O. Standards used were basalt BM for H₂O and limestone KH for CO₂.

For the preparation of fused beads, 600 ± 0.5 mg sample powder was thoroughly mixed with 3600 ± 0.5 mg of Spectroflux 100 (lithium-tetraborate Li₂B₄O₇), and a small quantity of ammonium nitrate (NH₄NO₃) was added as oxidizing agent. The mixture was melted at about 1000°C in an automated preparation line, the melt was then cast into a preheated mould and slowly cooled to avoid shattering due to thermal stress. A Philips X'Unique X-ray spectrometer was used for XRF analysis. Accuracy was tested by comparing results obtained on international standard reference substances with certified literature data [GOVINDARAJU, 1994]. The relative accuracy is ± 5% or better for all major and minor element oxides excluding Na₂O (± 20%) and ± 2% or better for SiO₂, Al₂O₃, Fe₂O₃, and CaO. For trace elements, the accuracy is better than 5% rel. For Cr, Sr, and Ba, ± 10% rel. or better for V, Zn, Rb, and Y, and ± 20% rel. or better for Sc (at concentrations > 10 ppm), Ni, Zr and Pb. All other trace elements are considered as semi-quantitative with accuracies < ± 20%. Results are shown in A.1.

2.4.6 Porosity

Porosities of the sediment samples were determined either by conductivity measurements according to JAHNKE et al. [1986] on the freeze-dried sample (samples from the Norwegian Sea and the Scotia Sea) or by using the water content of a certain sample *volume* taken after the recovery of the multicorer on board. Method 1 is unaffected by water loss during sample storage and therefore can be applied even after years, whereas samples in method 2 must be taken immediately on board, frozen, weighed before and after drying at 60°C in home laboratories. Water content in method 1 is calculated from conductivities measured after 12 h from a 10-20 mg dried sample suspended in deionized water. Conductivity measurements were carried out with a conductometer (WTW LF-191), calibrated with various dilutions of a certified seawater standard. The water content of the samples are calculated assuming a mean grain density of 2.6 g/cm³.

The reproducibility in either method is quite good (1-2%), even higher uncertainties derive from sampling heterogeneity. Nevertheless overall reproducibility of a certain set of samples are often better than 5% with higher uncertainties close to the sediment-water interface.

2.4.7 Surface area measurements (BET)

Surface area, here referred to as physical surface area (2.5.4.2), measurements according to BRUNNAUER, EMMET and TELLER (BET) [1938], were performed using a single point differential method [DIN 66 131; HAUL and DÜMBGEN, 1960, 1963] which uses nitrogen adsorption to measure surface areas. Sample preparation was identical to that of cobalt adsorption experiments (2.1.3). Comparison with a multiple-point surface area analyser (Institute for Inorganic Chemistry of Christian-Albrechts-University, Kiel) yielded no significant difference in surface area determinations. Surface area measurements showed a good reproducibility (better than 5%).

Absolute accuracy is often reported to be 10% or higher. To test the validity of our results measurements with Aerosil 200 (Degussa AG, Frankfurt, Germany) were performed. A specific surface area of 183 (\pm 4) m²/g in a triplicate measurement was determined for which a surface area of 196 m²/g was reported [DIN 66 131 in MATHIAS and WANNEMACHER [1988]. Our results are 7% lower than those which is within the limits of acceptance for BET-measurements.

2.4.8 Scanning electron microscopy (SEM)

The determination of sediment bulk composition as well as the identification of species was carried out on selected samples with a scanning electron microscope (SEM) at the GEOMAR Research Institute, Kiel with a CAM Scan CS 24 (Elektronen-Optik-Service GmbH, Dortmund).

2. Materials and methods

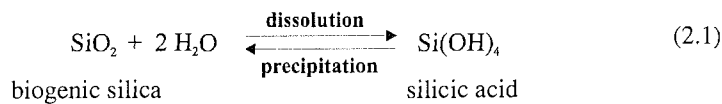
2.5 Dissolution experiments and calculations

In this chapter, general rate laws and their application in recent work on water-rock interaction in general and (biogenic) silica interaction in particular will be introduced.

2.5.1. Historical and theoretical background

The functional dependence of this rate on overall ΔG_r , the Gibbs free energy of reaction, or deviation from equilibrium, will be highlighted.

The dissolution-precipitation reaction of biogenic silica is:



A general rate law for dissolution and precipitation at constant pressure is [LASAGA et al., 1994]:

$$R_{\text{diss}} = \frac{d[\text{Si}]}{dt} = k A e^{-E_a/RT} a_{\text{H}^+}^{m_{\text{H}^+}} \prod_i a_i^{n_i} f(\Delta G_r) \quad (2.2)$$

R_{diss}	dissolution reaction rate
k	rate coefficient for dissolution reaction
A	reactive surface area of investigated substance
E_a	activation energy of dissolution reaction
R	universal gas constant ($8.314 \text{ JK}^{-1}\text{mol}^{-1}$)
T	temperature (K)
$a_{\text{H}^+}^{m_{\text{H}^+}}$	term considering the pH dependence of the dissolution reaction
$\prod_i a_i^{n_i}$	a_i incorporates other unidentified catalytic or kinetic effects (surface defect density, ion activities, e.g., Al^{3+} or Mg^{2+})
n_i	reaction order
$f(\Delta G_r)$	functional dependence accounting for variation in rate with deviation from equilibrium
ΔG_r	Gibbs free energy of reaction

The Gibbs free energy of reaction, ΔG_r ,

$$\Delta G_r = RT \ln \frac{Q}{K_{\text{eq}}} = RT \ln \frac{a_{\text{Si}}}{[\text{Si}]_{\text{eq}}} \quad (2.3)$$

and solution saturation $\Omega = [\exp(\Delta G_r/RT)]$ are equal to the ratio of the aqueous ion activity quotient or the non-equilibrium solution quotient Q , to the biogenic silica solubility (or equilibrium) constant K_{eq} , assuming ideal unit activity of the solid phase.

If the solution composition has the same stoichiometry as the solid phase (same temperature, pressure and ionic solution composition), the saturation ratio may be approximated by the above-mentioned equation in terms of molarity of dissolved silicic acid $[\text{Si}]$ and solubility value, $[\text{Si}]_{\text{eq}}$. This assumption is valid insofar as complexation, polymerization, and hydrolysis do not occur [STUMM and MORGAN, 1981; ZHANG and NANCOLLAS, 1990]. It is negligible at pH 8, but starts to occur at pH > 9 [BAES and MESMER, 1976]. For samples from the marine environment this results in

$$\Delta G_r = RT \ln \frac{[\text{Si}]}{[\text{Si}]_{\text{eq}}} \quad (2.4)$$

The rate equation 2.2 can also be simplified as long as pH, ion activities, temperature and other effects are constant. Therefore, it can be written as

$$R_{\text{diss}} = k_{\text{diss}} f(\Delta G_r) \quad (2.5)$$

where k_{diss} stand for all the other terms in Equation 2.2.

The function $f(\Delta G_r)$

The term $f(\Delta G_r)$ accounts for important variations in rate with deviation from equilibrium. The shape of function $f(\Delta G_r)$ depends on the reaction mechanism(s) operating during both dissolution and precipitation. Function $f(\Delta G_r)$ is readily obtained if the overall mechanism comprises an elementary reaction [LASAGA, 1981 a; NAGY et al., 1991]. In this case, $f(\Delta G_r)$ derived from the transition state theory (TST) is given [LASAGA, 1981 b, 1984; AARGARD and HELGESON, 1982] by:

$$f(\Delta G_r) = [1 - \exp(\Delta G_r / RT)] \quad (2.6)$$

This function satisfies two conditions: (1) $f(\Delta G_r) = 0$ at equilibrium ($\Delta G_r = 0$), and (2) $f(\Delta G_r) = 1$ at significant undersaturations. If Equation 2.6 is substituted for Equation 2.2 it follows that the dissolution rate will be independent of ΔG_r in the case of large undersaturations (large negative ΔG_r). Unfortunately, the definition of “far from equilibrium” can be used only after experiments on particular substances have been carried out. This limiting condition, termed the *dissolution plateau*, in which the dissolution rate attains a constant value vs. ΔG_r , has already been achieved in dissolution experiments with gibbsite or albite [e.g., NAGY and LASAGA, 1992; BURCH et al., 1993]. In the case of small deviations from equilibrium, $|\Delta G_r| \leq RT$, a Taylor series expansion of the exponential term in Equation 2.6 leads to a linear relation between rate and $|\Delta G_r|$. Equation 2.5 can then be simplified as follows:

$$R_{\text{diss}} = k_{\text{diss}} \frac{\Delta G_r}{RT} \quad (2.7)$$

If, furthermore, the principle of detailed balancing, or microscopic reversibility, is applicable to the overall reaction, the first derivative of f at equilibrium, $f'(0)$, is well-defined (i.e., has the same value at equilibrium if it is approached from undersaturation ($\Delta G_r \leq 0$) or super-saturation ($\Delta G_r \geq 0$)). At equilibrium, the rate of forward reaction (dissolution) is exactly equal to rate of the reverse reaction (precipitation), and both constants are related through the equilibrium constant, $[\text{Si}]_{\text{eq}}$ [RIMSTIDT and BARNES, 1980; LASAGA, 1981a]. The net rate is zero, but the forward and backward reactions proceed individually at a finite rate. As the dissolution process approaches equilibrium, the rate of backward reaction becomes finite. Thus, the net rate of reaction decreases as equilibrium is approached, ultimately becoming zero at equilibrium. The question is then: how close to equilibrium must the reaction come to before this reversible mechanism becomes significant? This is controversially discussed in the literature (DREVER, 1997). It is beyond the scope of the present thesis to provide answers to this

2. Materials and methods

question, since more data close to equilibrium are required to determine if the dependence of rate on ΔG_r is, in fact, linear [e.g., NAGY et al., 1991; NAGY and LASAGA, 1992; BURCH et al., 1993].

Substituting Equations 2.4 in 2.6 and combining the resultant expression with Equation 2.5 yields:

$$R_{\text{diss}} = k_{\text{diss}} \left(1 - \frac{[\text{Si}]}{[\text{Si}]_{\text{eq}}} \right) \quad (2.8)$$

as a first-order kinetic law. This is by far the most widely used rate expression for the dissolution of biogenic silica in which the rate depends linearly on the degree of solution undersaturation.

Many studies have reported on the dissolution rates of silica in general. Silicic acid versus time data derived from batch experiments with biogenic silica, amorphous silica or quartz were successfully fitted using Equation 2.8 [e.g., O'CONNOR and GREENBERG, 1958; VAN LIER et al., 1960; HURD, 1972a, 1973; WILLEY, 1974, 1980; LAWSON et al., 1978; KAMATANI and RILEY, 1979; HURD and BIRDWHISTELL, 1983; VAN BENNEKOM et al., 1991; BARKER et al., 1994]. This laboratory-based first-order rate law is still the standard kinetic expression in early diagenetic models of silica [KATO and KITANO, 1968; HURD, 1973; BERNER, 1974, 1980; SCHINK et al., 1975; SCHINK and GUINASSO, 1980; WONG and GROSCH, 1978; MACKIN, 1987; BOUDREAU, 1990; RABOUILLE and GAILLARD, 1990; MCMANUS et al., 1995]. The theoretical justification for the linear rate law was provided by RIMSTIDT and BARNES [1980] based on transition state theory (TST). Their assumptions have been outlined above.

Based on an experimental technique introduced by CHOU and WOLLAST [1984] which uses flow-through reactors, experimental data on reaction rates over the full range of solution saturation have become available (see also 2.5.5).

Because alteration processes in natural systems often involve solid-fluid reactions very close to chemical equilibrium, first studies concentrated on that singularly point $f(\Delta G_r = 0)$ [LASAGA et al., 1994]. Nevertheless, dramatic, non-linear behavior of dissolution and precipitation kinetics at conditions very near equilibrium were observed for kaolinite, gibbsite, albite and quartz [NAGY et al., 1991; NAGY and LASAGA, 1992; OELKERS and SCHOTT, 1992; BURCH et al., 1993; BERGER et al., 1994]. FLEMING [1985] observed such non-linear behavior for dissolution and precipitation of Ludox colloidal silica, and BERGER et al [1994] observed similar behavior for quartz dissolution rates at 300°C. Transferred to natural systems, both VAN CAPPELLEN and QIU [1997 a,b] and CARROLL et al. [1998] made the same observations under chemically complex field conditions for the dissolution of biogenic silica in Southern Ocean sediments and for the precipitation of amorphous silica in a geothermal system. RAGUENEAU et al. [1996] reported to use this technique to test several hypotheses related to biogenic opal early diagenesis. During our investigations, this non-linearity between dissolution kinetics of biogenic silica and the degree of undersaturation were observed more frequently for biogenic silica in chemically complex environments than for pure, cleaned phytoplankton samples.

These observations suggest a more generalized equation describing the dissolution rates, which account for the non-linear behavior of $f(\Delta G_r)$ [CARROLL et al., 1998]:

$$R_{\text{diss}} = k_{\text{diss}} [1 - \exp(n\Delta G_r / RT)]^m \quad (2.9)$$

where n and m are empirical constants. The shape of the Gibbs free energy function, $f(\Delta G_r)$,

$$f(\Delta G_r) = [1 - \exp(n\Delta G_r / RT)] \quad (2.10)$$

depends on the reaction mechanism(s) operating during both dissolution and precipitation. If dissolution involves one elementary reaction or a series of elementary reactions in which the dissolution rate is controlled by the slowest of the elementary reactions, then Equation 2.8 results from Equation 2.9 where m and n equal 1. If the reaction rate is controlled by more than one elementary reaction at steady state, then Equation 2.9 may be expressed by

$$R_{\text{diss}} = k_{\text{diss}} [1 - \exp(n\Delta G_r / RT)] \quad (2.11)$$

where $m = 1$. LASAGA [1981], AARGARD and HELGESON [1982] and STUMM and WIELAND [1990] offer more complete discussions of the application of TST or surface complexation theories to mineral dissolution processes.

An additional consideration is the possibility of fully non-linear rate laws. Rate laws with a functional dependence on ΔG_r of the form [BURCH et al., 1993]

$$R_{\text{diss}} = k_{\text{diss}} [1 - \exp(\Delta G_r / RT)]^m \quad (2.12)$$

have most commonly been applied to precipitation kinetics [BURTON et al., 1951]. Empirical rate laws as expressed in Equation 2.12 can also be extended to mineral dissolution processes [BLUM AND LASAGA, 1987] and have been applied to calcite dissolution kinetics [KEIR, 1980; MORSE, 1983; BERELSON, 1990]. Regardless of the mechanism, that is whether or not surface defects are involved, linear near-equilibrium conditions will never be obtained for $n \neq 1$.

Therefore Equation 2.8 changes to

$$R_{\text{diss}} = k_{\text{diss}} \left(1 - \frac{[\text{Si}]}{[\text{Si}]_{\text{eq}}} \right)^m \quad (2.13)$$

As presented in more detail later, the linear rate expression (2.8) failed to fit data gained from flow-through experiments performed at 25 °C and batch experiments performed at 60°C with sediment samples of different opal/detritus ratios (see 3.1.2.2.1 and 3.2.2.2.2). In contrast, Equation 2.13 leads to reliable results. Nevertheless, the linear rate equation 2.8 can successfully be applied to fit data obtained by flow-through experiments with different phytoplankton samples. These aspects are discussed in (3.1.1) and (3.1.2) in more detail.

2.5.2. Inflow solutions and pH measurement

In all batch- and flow-through experiments of this study bicarbonate-buffered, artificial seawater is used which ensures almost natural conditions. The composition of the artificial seawater (Salinity 35.0) is based on DICKSON [1993] for preparing artificial seawater buffers. Reagent grade salts were added to Milli-Q™-purified water. To avoid any kind of artifacts triggered by the use of organic acid as buffer substances, the pH of the inflow solutions was buffered by adding 2 mmol/l sodium bicarbonate and by aeration with filtered air containing atmospheric CO₂. Before, throughout, and after

2. Materials and methods

each experiment the pH of the inflow solution was monitored and kept at $\text{pH } 8 \pm 0.2$. Once the pH has been established after 1-2 days of aeration and a pH has been adjusted by the addition of small amounts of concentrated HCl or NaOH solution, the pH stays constant over several weeks. Dissolved silica was added using standardized stock solutions of NaSiO_3 in 5 N NaOH.

According to DICKSON [1993], pH electrodes were calibrated using BIS (2-amino-1,3-propanediol) and 2-aminopyridine in artificial seawater as buffers in the neutral pH range (pH 7 to 9). Resulting pH values are defined on the 'total' hydrogen ion concentration scale. Measurements of pH were carried out with a precision pH meter Model PHM 85 (Radiometer Copenhagen). The pH electrode was allowed to equilibrate for at least 15 min. in experimental solution before samples or standards were analyzed.

2.5.3. Analytical techniques

All aqueous elements were determined by inductively coupled plasma-atomic emission spectroscopy (ICP-AES). A Jobin Yvon ICP spectrometer was used to control the stability of seawater composition (Na, K, Mg, Ca) and to analyze changes in Si concentrations during the course of the experiments. Deviations in the composition of artificial seawater can be ignored. In addition, changes in Co and Mg if present during batch adsorption measurements (3.1.2.2.3) or Mg flow-through experiments (3.1.1.2.3), were measured using ICP-AES.

The reproducibility of this technique is better than 2%, in most cases better than 1% using Y as internal standard. The concentrations of the investigated solutions are at least one order of magnitude greater than the detection limits of the analytical techniques. Standards were measured in background electrolyte solutions identical to the diluted composition for artificial seawater to directly correct them for matrix effects. Differences in the analyzed silica concentrations using either ICP-AES or the molybdate method (2.1.2.1) were not observed. This suggests that the total dissolved silica is present as monomeric silicic acid [CARROLL et al, 1998]. For this reason ICP-AES was used for silica analyses to ensure a good reproducibility and accuracy to detect even small differences between the inflow and outflow solutions throughout the flow-through experiments.

2.5.4 Batch experiments

2.5.4.1 Temperature-dependent batch experiments (T-Batch)

As stated in 2.5.1, early experiments were conducted in batch reactors. A batch reactor is a vessel containing a fixed volume of solution, commonly buffered at a particular pH, and a certain mass of solid [DREVER, 1997]. Results from batch experiments performed are not the object of this thesis. Nevertheless, batch experiments performed at 60°C (see below) were used to complement results from flow-through experiments in cases where there was not enough material. Following is a description of the batch experiments.

500 mg or 100 mg (in case of pure biogenic silica or siliceous oozes from the Scotia Sea) of dried and further untreated sediment was placed in a 50 ml polypropylene centrifuge tube; artificial seawater (2.5.2) was added. The mixtures were agitated continuously using a rotary shaker to ensure homogeneous dispersion.

Samples were checked periodically for Si concentration to follow the rate of dissolution, the sample bottle was resealed after a pipetted sample of 2 ml was removed and replaced by 2 ml of silica-free, artificial seawater, a compromise between the necessity of sampling and guaranteeing a closed system throughout the experiment. Batch experiments were performed at three different temperatures (2°C in the cold room, 19°C in a temperature regulated laboratory, and 60°C in a drying oven). The observed temperature variations ($\pm 1^\circ\text{C}$) during each of the experimental runs produce negligible uncertainties.

In the high-temperature (60 °C) runs, the closeness to equilibrium was judged by the point at which dissolved silica showed no change in two successive time intervals, in the case of sediment from station WAST also by duplicate runs at the same temperature. Due to a lack of time, no equilibrium values for batch experiments performed at 19 °C and 2°C were achieved after 4 months. This is not surprising since WILLEY and SPIVACK [1997] reported an experimental time period of ~7 years in batch experiments carried out with untreated sediments.

Dissolution rates were calculated by differentiation of time-dependent [Si] increase with respect to time t .

2.5.4.2 Cobalt adsorption experiments

Cobalt adsorption experiments according to VAN CAPPELLEN and QIU [1997b], were performed to evaluate changes in *reactive surface area* with increasing depth as exposed by siliceous skeletons in sediments. The specific surface area which is commonly determined by an inert gas adsorption measurement (= *physical surface area*, Sect. 2.4.7) must first be distinguished from the *reactive surface area*, the number of reactive silanol ($\equiv\text{Si-OH}$, $\equiv\text{Si-O}^-$) groups exposed per unit surface area or surface site density. The reactive site area is by far the most difficult to quantify in the natural environment because of the presence of non-biosiliceous sediment constituents. In this case the interpretation of the BET surface area is not as straightforward as is it for pure siliceous ooze. Any clay minerals or oxides present will distort the results by contributing a large surface area. Co adsorption experiments are useful to reflect the relative changes of surface site densities of silanol groups with increasing depth when applied to detritus-poor sediments [VAN CAPPELLEN, 1996; VAN CAPPELLEN and QIU, 1997b], where interferences due to adsorption of Co^{2+} onto non-biosiliceous surface sites are small. Samples PS-2314-1 and PS-2299 were taken as representatives of the Scotia Sea sediment type which is characterized by high biogenic silica and low detrital contents. Sediment preparation has been described in Section 2.1.3. The effect of preparation on surface area changes was also documented by measuring BET surface areas for both the treated and untreated sediments (3.1.2.2.3). These experiments were performed according to VAN CAPPELLEN and QIU [1997b]; 0.5 g of each sample was placed in a 50-ml centrifuge tube, and buffered with 20 mg CaCO_3 which was added to the sample. 50 ml of dissolved cobalt solution (30 ppm) in deionized water was also added. Blank tests showed a negligible uptake of Co^{2+} by the CaCO_3 . The experimental conditions produce a stable final pH between 7 and 7.2. The centrifuge tubes were kept on a rotary shaker for 3 weeks at 20°C. During that time, small solution aliquots (100 μl) were taken with the highest sampling frequencies at the beginning of an experiment. Dissolved cobalt was measured with ICP-AES as outlined above (2.5.3).

2. Materials and methods

2.5.4.3 Alkaline dissolution experiments

In this thesis focus has been placed on changes in dissolution kinetics triggered by the heterogeneity of reactive sites or by the aging of reactive surface areas; these can be measured either by means of flow-through experiments over a full range of undersaturation or by batch studies. These methods are extremely laborious; therefore, to document relative changes in reactivity among biogenic opal of various origin, the alkaline extraction technique used to determine biogenic silica contents in sediments (2.4.1) was applied. The assumption is that alkaline dissolution mimics natural processes but accelerates the naturally much slower dissolution process [SHEMESH et al., 1989]. Essentially, alkaline extraction is based on the assumption that there are two silica fractions, each exhibiting distinct dissolution kinetics: quickly dissolving amorphous silica and slowly dissolving silica-bearing phases (for example clays, feldspars and quartz). The dissolution rate of biogenic silica in an alkaline medium can be approached by a first order kinetic model:

$$\frac{d[\text{BSi } \%]}{dt} = -k_{\text{NaOH}} [\text{BSi } \%]_t \quad (2.14)$$

$[\text{BSi } \%]_t$	amount of BSi [wt.%] in the sample at t
$[\text{BSi } \%]_0$	amount of BSi [wt.%] in the sample at t = 0
k_{NaOH}	apparent alkaline rate constant for the decay of the mixture [h^{-1}]

This approach is an idealized opal dissolution rate which decreases exponentially with time. The first-order rate constant (k_{NaOH}) or the reactivity of biogenic silica is assumed to be constant. However, the assumption that biogenic silica has a constant reactivity is not consistent with field and laboratory studies. Nevertheless, it was possible to apply first order kinetics to model biogenic silica dissolution in 0.032 M NaOH taking into account the slow dissolution of clay minerals for example as a constant simultaneous and independent process [DEMASTER, 1981; KONING et al., 1997]. This leads to

$$[\text{BSi}_{\text{diss}} \%]_t = [\text{BSi } \%]_0 [1 - \exp^{-k_{\text{NaOH}} t}] + b_{\text{NaOH}} t \quad (2.15)$$

Here, $[\text{BSi}_{\text{diss}} \%]_t$ is the fraction of silica SiO_2 [wt.%] already dissolved and recalculated from the concentration of silicic acid [$\mu\text{mol l}^{-1}$] present in the solution at time t. The solid-solution ratio, a volume correction due to the sequential sampling procedure, and a constant water content of BSi of 10 wt.% [MORTLOCK and FROELICH, 1989] were taken into account. The slope of the linear part of the curve, b_{NaOH} [h^{-1}], can be attributed to the leaching of detrital components. To calculate $[\text{BSi } \%]$, Equation 2.14 was fitted to the experimental data using the Origin™ software. Both constants (k_{NaOH} and b_{NaOH}) can be treated as apparent rate constants which summarize the effects for the biosiliceous phase and the detrital phase on the silicic acid concentration in solution.

To interpret the effects of present detrital clay minerals in the sediment sample during alkaline extraction and subsequent changes in alkaline dissolution constant, the time evolution of aluminum concentration in solution was monitored. Dissolved aluminum was measured by fluorescence spectroscopy using the Lumogallion method

(HYDES and LISS, 1979). In further experiments the effect of organic and inorganic coatings on the alkaline dissolution constant was investigated. Results gave valuable insights into major processes which may occur when different detrital clay minerals are present in the sediment matrix and when the main source of silicic acid is biogenic silica (3.1.1.2.4).

2.5.5 Continuously stirred flow-through experiments

Fifteen stirred flow-through reactors which can be driven simultaneously using a multiple magnetic stirring system temperature-controlled in a temperature regulated water bath (Fig. 3.2) were constructed. These reactors are particularly well-suited for investigations of dissolution kinetics as a function of the degree of disequilibrium (2.5.1) [e.g., CHOU and WOLLAST, 1984; NAGY et al., 1990, 1991; NAGY and LASAGA, 1992; BURCH et al., 1993]. Constant temperature (2°C or 25 °C) and pH (7.8-8) conditions in artificial seawater (2.5.2) were used. The major advantages of such open systems compared to closed batch experiments are [e.g., CHOU and WOLLAST, 1985] the following:

1. A constant degree of undersaturation can be maintained throughout the experiment.
2. pH and temperature can easily be investigated by changing the inflow solution, in contrast to a closed batch experiment where at least two variable changes take place simultaneously, namely the degree of undersaturation and the effect of different solution composition. In flow-through experiments it is necessary to ensure that the substance of interest is not altered chemically, thus jeopardizing the compatibility of experiments, during the course of an experiment series.
3. Steady state conditions can be achieved.
4. Solubility and dissolution/precipitation kinetics can be measured during the same course of an experiment.
5. Possible contributions to measured reaction rates of reaction products and secondary phases newly formed (which cannot be ruled out in a batch experiment) can be avoided. To which extent this is fulfilled for heterogeneous sediments will be discussed in Section 3.1.2.3.3.

Experimental methodology

Each reactor cell (volume 50 cm³) was built of transparent acrylic glass to ensure visual control during the stirring process. The fluid in the reactor was stirred with a Teflon-coated magnetic stirring bar. Both cell ends are closed by 0.45 µm nylon filters, supported by plastic grids and Teflon screw-on caps in which a small headspace and flow channels ensure the in- and outflow of the solution. A large stock (10 l) of inlet solution was prepared for each degree of undersaturation. From this, 500-1000 ml aliquots were used to supply the reactors during an experiment. In each experiment, 500 mg sediment usually was added to the reactor without

any pretreatment (2.1.1) and filled with inflow solutions (2.5.2) at a rapid flow rate. The reactors were closed and placed in the water bath. Once all 15 reactors were filled, the flow-rate was reduced to the constant value desired; then stirring was begun. A variable peristaltic pump was used to circulate the test solution through the reactor.

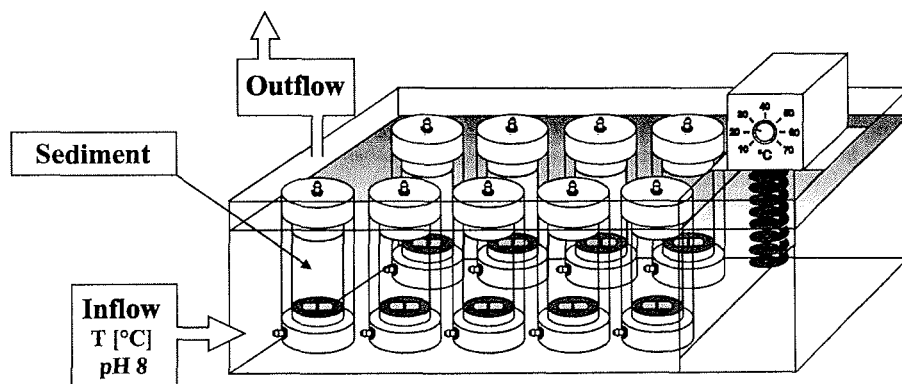


Fig. 2.2 Schematic illustration of stirred continuous flow-through (CFT) reactor technique. Inflow solution was added to the reactor with a peristaltic pump. Tygon tubing was used for interconnecting all parts of the system.

Tygon tubing was used to interconnect all parts of the system. The experiments were performed either at 25 °C or at 2°C in a cold room at ambient atmospheric pressure.

The dissolution rates were measured as a function of the degree of undersaturation by varying the silicic acid concentration or the flow rate of the inflow solution. In contrast to the experiments generally performed (passing through a succession of steady states with the same sediment sample), these experiments were run in parallel, taking 7-8 sediment samples of the same depth interval and using inflow solutions of different degrees of undersaturation with respect to the solubility of the sample. This mode was applied for two reasons:

- (1) Surface properties which may change during a course of undersaturation states are nearly the same for each run.
- (2) Different solid/solution ratios are avoided and the relative loss of BSi due to dissolution is less than 5-10% using sediment samples with various biogenic silica contents.

Flow-rates were changed with respect to biogenic silica content of the sample studied to ensure measurable differences between the inflow and outflow concentrations of silicic acid (for calculations, see below). For opal-rich sediments, flow rates typically fell into the range of 2-7 ml/h depending on the degree of undersaturation. Flow-rates exceeding these velocities were avoided because higher velocities led to extensive clotting and adhesion of sediment samples and phytoplanktonic material to the flow-through apparatus, which in turn led to a time-dependent decrease in silicic acid outflow values and, hence, in dissolution rates because the exposed surface area was decreased. These obviously artificial values were ignored in our calculations.

First, dissolution rates and solubilities of different sediment types were determined to evaluate whether different apparent asymptotic silicic acid values in the field truly reflect equilibrium between pore water and siliceous phases in sediments. Sediment flow-through solubilities and reaction rates from different sediment horizons were measured. Generally the topmost sample, a sample at 3-4 cm and another sample at the end of the core was taken.

Experiments with clay/opal mixtures were performed to study the dissolution behavior of biogenic silica in the presence of various detrital clays and to verify that asymptotic silicic acid values in pore waters are controlled by various opal/detritus ratios [VAN CAPPELLEN and QIU, 1997 a,b].

In particular, the relative effects of Mg and Al as protective agents have been studied using artificial seawater solutions with constant silicic acid and an increasing concentration of both Al and Mg. For calculations of dissolution rates and saturation states as well as for a detailed description of all experiments performed, see (2.1).

2.5.6 Temperature dependence on reaction rates

Since flow-through experiments were performed at two different temperatures (2°C, 25°C) due to reactivity differences among pure opal samples and sedimentary samples, measured reaction rates must be recalculated for a comparison.

Temperature dependence on dissolution or precipitation rates is significant and typically expressed using the Arrhenius law:

$$k = A e^{-E_{app}/RT} \quad (2.16)$$

where A is the pre-exponential factor and E_{app} is the apparent activation energy of the reaction. Here, temperature dependencies of apparent rate constant were not determined explicitly; but this has been studied extensively in the past. LASAGA [1984] points out that recent work in mineral solution reaction still leads to an average of approximately $E_{app} = 15 \text{ kcal/mol}$ (62.8 kJ/mol).

RIMSTIDT and BARNES [1980] determined the dissolution rates for four silica polymorphs with values ranging from 60 to 76 kJ/mol. In flow-through experiments activation energies in the range of 48-72 kJ/mol were obtained [VAN CAPPELLEN and QIU, 1997b]. Recently, CARROLL et al. [1998] have determined an activation energy value of $61 \pm 1 \text{ kJ/mol}$ for amorphous silica precipitation studies deploying flow-through experiments. As an average value obtained in flow-through experiments [Van Cappellen and Qiu, 1997 b] an activation energy of $\sim 60 \text{ kJ/mol}$ was applied to recalculate reaction rates determined in flow-through experiments at 25°C for *in situ* temperatures of $\sim 2^\circ\text{C}$. From Equation 2.16 we obtain

$$\ln k_2 = \ln k_1 + \frac{E_a}{R} \left[\frac{1}{T_1} - \frac{1}{T_2} \right] \quad (2.17)$$

with $R = 8.314 \text{ kJ/mol}$ and $T [^\circ\text{K}]$.

2.6 Modeling of pore water silicic acid

Pore water silicic acid concentrations increased in the upper centimeters of sediments. This trend can be attributed to the dissolution of opaline skeletal debris [e.g., HURD, 1973; BERNER, 1974, 1980; FANNING and PILSON, 1974; SCHINK et al., 1974, 1975; ALLER and BENNINGER, 1981].

But the survival of these microfossils, which do often appear to be well-preserved in the sedimentary record, represents something of an enigma [SCHINK et al., 1975], since pore waters are seldom saturated with respect to solubilities obtained for acid-cleaned opaline silica [$\sim 1000 \mu\text{M}$; HURD, 1973]. A desire to understand the factors which affect interstitial profiles and control the preservation of opal has motivated a number of

2. Materials and methods

modeling studies [e.g., ANTIKOUCHINE, 1967; HURD, 1973; WOLLAST, 1974; FANNING and PILSON, 1974; BERNER, 1974, 1980; SCHINK et al., 1975; SCHINK and GUINASSO, 1980; BOUDREAU, 1990 a,b; MCMANUS et al., 1995; RABOUILLE et al., 1997].

The approach chosen here is to utilize a one-dimensional, diagenetic reaction-transport model (3.2.2.1) and exponential fit functions to describe pore water silicic acid, porosity and biogenic silica distribution in deep-sea sediments, and to apply this model to extract rate constant values from biogenic silica dissolution as well as fluxes of silicic acid through the sediment-water interface at each station. The depth-dependent variations in porosities and opal contents in the sediments have been taken into account to determine depth-dependent apparent rate constants $k_B(x)$ from the reaction rate $R(x)$ (Eq. 3.22) for silicic acid release due to opal dissolution. This approach does explicitly account for the dynamics of the solid opal component, which would lead to two non-linear algebraic equations, one each for the solute and the dissolving solid. The most complete description available for the silica-opal system has been formulated by SCHINK and GUINASSO [1980]. This model is sufficiently complex to warrant its evaluation by advanced numerical methods, which is beyond the scope of this thesis. Mathematical descriptions and results deriving from the model approach used in this thesis are compared with experimental results in Section 3.2.

3. Experimental results and discussion

Experimental strategy to determine the nature of opal dissolution

The silicic acid concentrations of pore waters in sediments are generally related to the rain rate, burial rate and reactivity of biogenic silica. Accordingly, pore water concentrations vary widely, i.e. in the sediment cores under investigation from 100 μM to almost 800 μM depth in the upper 40 cm (Fig. 3.4). However, the solubility determined for acid-cleaned biogenic or synthetic amorphous silica [1000 μM at 4°C HURD, 1973] in natural environments is rarely attained during early diagenesis which suggests that the apparent solubility is specific for various opal compositions, affected by some other chemical processes (for example incorporation of trace metals [LEWIN, 1961; ILER, 1973; VAN BENNEKOM et al., 1979; VAN BEUSEKOM, 1991]), or that dissolution kinetics are slowed down.

The generally accepted linear rate law (Eq. 3.8) derived from batch experiments has led to extensive modeling studies (see references in Section 2.5.1). Accordingly, the pore water profiles were fitted, and values of apparent silica solubilities and rate constants were derived from the fit. Many diagenetic models are able to simulate profiles of silicic acid in the sediments, but in order to interpret very distinctive variations in asymptotic silicic acid concentrations, independent measurements of silica solubility and reactivity were required. Based on an experimental technique using flow-through reactors [CHOU and WOLLAST, 1984], experimental data on reaction rates over a wide range of undersaturation has become available, and results derived from different mineral dissolution studies give strong evidence for non-linear dissolution behavior with increasing departure from equilibrium [e.g., NAGY et al., 1991; NAGY and LASAGA, 1992; BURCH et al., 1993]. Studies using colloidal silica [FLEMING, 1985], quartz [BERGER et al., 1994] and biosiliceous oozes from the Southern Ocean [VAN CAPPELLEN and QIU, 1997a,b] also confirm non-linearity in solubility behavior for the silica system. In addition, a depth-dependent decrease of surface reactivity has been determined [VAN CAPPELLEN and QIU, 1997a,b].

In Southern Ocean sediments the relative magnitudes of asymptotic concentrations and experimental solubilities are inconsistent [VAN CAPPELLEN and QIU, 1997a,b]. This stresses the need for further investigations to reexamine Southern Ocean sediments and to extend those results to sediments of differing depositional settings. By investigating different sedimentary regimes, the key mechanisms, which control biogenic silica recycling and preservation are expected to be better constrained.

Fifteen continuous flow-through (CFT) reactors were designed and used (Fig. 2.2) for dissolution kinetic studies and solubility measurements employing sediments and almost pure opal samples of various origins (phytoplankton, sediment trap material, surface sedimentary opal, diagenetically altered opal-A/CT) (3.1.1 and 3.1.2). In order to learn whether reduced surface reactivities are the product of biomineralization processes in the water column or represent early diagenetic reactions in sediments, the sedimentary results were compared with those obtained from the analysis of phytoplankton samples collected in surface waters or sediment traps. Pure biogenic silica samples are advantageous because of no interferences by accompanying minerals. The reasons for the striking difference between high northern and southern latitudes

3. Experimental results and discussion

observed for the benthic silica cycle in the Atlantic Ocean [SCHLÜTER et al., accepted] will be considered based on dissolution kinetics of the samples from the water column.

Experimental solubilities measured on the deepest sections of the cores exhibit a relative order of values similar to those observed in the field (3.1.1.3). Moreover, a general decrease in both the solubilities and reaction rates was observed throughout the cores (3.1.1.2.2 and 3.1.2.2.2). Based on these initial observations, dissolution kinetic experiments and solubility measurements with different opal/detrital clay mixtures (3.1.1.2.3) were carried out to address the question of whether detrital clay minerals play an active role in regulating solubility values of biogenic silica in compositionally different sediments. By maintaining inflow Si concentrations at almost constant values in the flow-through experiments the influence of Mg^{2+} and Al^{3+} cations were studied which may be active in controlling the kinetics of dissolution [e.g., LEWIN, 1961; KASTNER et al., 1977; KENT and KASTNER, 1985; VAN BENNEKOM et al., 1989, 1991; VAN CAPPELLEN and QIU, 1997a,b; DIXIT and VAN CAPPELLEN, 1998] (3.1.2.2.3). The relative change of (reactive) surface area throughout an investigated core was evaluated using both BET-measurements and the cobalt (Co) adsorption experiments proposed by VAN CAPPELLEN and QIU [1997b]. Furthermore, an alkaline leaching procedure was performed. Resulting apparent rate constants k_{NaOH} (3.1.2.2.4) were suitable for determining relative reactivity changes with depths, even in opal-poor sediments.

The results from batch experiments performed at 60°C [RICKERT, unpublished results] are used to improve or to add information for the subsequent discussion of results derived from flow-through experiments. Temperatures as high as 60°C were necessary to determine solubility values in this kind of experiments because in batch experiments performed at 2°C or 19°C equilibrium was not attained presumably because of secondary precipitation reactions [RICKERT, unpublished results]. These results documented general difficulties associated with experiments performed in closed systems, such as batch reactors, in which heterogeneous reactions occur. Therefore, the measurement of dissolution rate constants in batch experiments in the presence of other sedimentary components are difficult to interpret [RICKERT, unpublished results]; however, a more detailed description of these experiments will not be included here.

Finally, exponential fit functions to describe the measured property distributions such as depth-dependent silicic acid and biogenic opal concentrations, as well as porosity profiles were applied as input parameters for a diagenetic reaction-transport model [BERNER, 1980]. This model yields fluxes of silicic acid from the sediment to the overlying water column and depth-dependent reaction rates. Assuming either linear or non-linear dissolution kinetics, rate constants $k_B(x)$ for the dissolution kinetics of biogenic silica within the sediment matrix were determined. These vary with depth following our laboratory results (3.3).

3.1 Stirred flow-through experiments

3.1.1 Solubility measurements

3.1.1.1 Introduction

How can the solubility of biogenic silica be defined ?

To find out what the solubility or saturation concentration of biogenic silica really is, or if it in fact has a unique value [WILLEY et al., 1997], the term "solubility" must be accurately defined: *the solubility* of biogenic opal can be defined as the solubility of either synthetic silica in seawater at 2°C (~900 μM , WILLEY, 1980) or acid-cleaned silica valves in seawater at 4°C (~1000 μM , HURD, 1973).

Although amorphous biogenic silica is the most soluble silica-containing phase in sediments, only a very few of the interstitial waters studied reached a concentration of ~1000 μM and hence were saturated relative to this solid phase used in laboratory experiments. For example, biogenic silica from the Zaire (Congo) deep-sea fan has a very low solubility of just 350 μM [VAN BENNEKOM et al., 1989], which has been attributed to the incorporation of aluminum into the silica structure. Therefore, it must be assumed that the solubility of biogenic silica is controlled by multiple variables and does not have one predetermined value, thus, a new question arises:

What controls solubility ?

In order to address this question, flow-through experiments on well-mixed suspensions from various deep-sea sediments in different depth intervals were carried out (Tab. 2.1 and Fig. 2.1). Following the results of solubility measurements of biogenic silica are presented.

To find out whether asymptotic silicic acid values measured in pore waters are surface- controlled [e.g., ARCHER et al., 1993], these silica solubilities and reactivities were compared with measurements of opal samples collected in surface waters or sediment traps and diatom deposits of Pliocene or Miocene age (Tab. 2.2). For experimental reasons flow-through experiments with sediments were performed at 25°C and for single opal samples at 2°C. Reaction rate constants were converted to *in situ* temperature (~2°C) using an activation energy of 60 kJ/mol (2.5.6).

The formation of secondary aluminosilicates in marine sediments was postulated over 30 years ago as a potentially important control on the chemistry of the oceans [e.g., MACKENZIE and GARRELS, 1966; MACKIN and ALLER, 1986; MICHALOPOULOS and ALLER, 1995]. Until now, however, this reverse weathering process has been largely discounted because of insufficient direct evidence. In a second set of measurements, the control which clay minerals exert on the dissolution rate of biogenic opal was investigated. Therefore, samples composed of a mixture of opal-rich sediment from the Southern Ocean (PS-2312-1 12.5-15 cm, Tab. 2.1) and on various amounts of nearly pure kaolinite, montmorillonite, and illite (Sect. 2.3 and A.1) were investigated.

The important role of Al in early diagenesis of silica has been investigated previously in extensive studies [e.g., OKAMOTO et al., 1957; LEWIN, 1961; ILER, 1973; WILLEY, 1975; MACKIN, 1987; VAN BENNEKOM et al., 1989; VAN BEUSEKOM et al., 1995; SCHLÜTER, 1990; VAN CAPPELLEN and QIU, 1997a; DIXIT and VAN CAPPELLEN, 1998]. The influence of Al on silica solubility has previously been studied exclusively in batch

3. Experimental results and discussion

reactors or/and based on pore water measurements. In batch experiments, however, silicic acid release changes periodically and the possible coprecipitation with soluble Al occurs may cause an apparent decrease in silicic acid release from synthetic or biogenic silica with time (2.5.4).

Flow-through reactors are particularly well suited to investigate the influence of different amounts of soluble Al on the dissolution behavior of biogenic opal: The undersaturation state of silicic acid can be maintained constant over a fairly narrow range and a steady state difference between silicic acid concentration in the inflow and outflow solution at various Si/Al ratios is a relative indicator for the solubility caused by adsorption of Al at the surface of biogenic silica or by coprecipitation of soluble Al and Si.

Aluminum concentrations in seawater range between 0.5 and 5 nM [ORIANI and BRULAND, 1986; MEASURES and EDMOND, 1990] and in pore water between < 10 nM [East China Sea: MACKIN and ALLER, 1984] and 400 nM [Weddell Sea: SCHLÜTER, 1990]. Because it is not clear whether the range of dissolved silica in sea- or pore water is large enough to impose significant differences on the solubility or dissolution rate of biogenic silica, experiments were undertaken to determine if coprecipitation of dissolved silica with aluminum is likely to occur; we used siliceous ooze from the Scotia Sea (PS-2312-1; 10-12.5 cm).

Different ratios of dissolved Si/Al in artificial seawater were used as inflow solutions and the siliceous ooze as dissolving material. Results are discussed under consideration of recent experiments performed by DIXIT and VAN CAPPELLEN [1998] (3.1.1.3.2). These authors performed the same kind of experiments by means of flow-through reactors and presented results for aluminosilicate precipitation and adsorption isotherms of Al(III) on biogenic silica.

With the same kind of sediments and experiments, we also looked into the role of Mg in preventing pore waters from becoming saturated with respect to pure biogenic silica [HURD, 1973]. Such an influence was supposed by WALLMANN et al. [submitted] in sediments derived from the Discovery Basin (PC15; Tab. 2.1).

In cold room experiments ($T = 2^{\circ}\text{C}$) the dissolution behavior of a freshly collected phytoplankton sample from the Bransfield Strait (ANT-XV/2, #65; Tab. 2.2) which were untreated to retain its organic coating was compared with an acid-cleaned sample (#64) from the same trapping.

3.1.1.1 Results

3.1.1.2.1 Apparent solubilities at 2°C and 25°C

Solubility measurements: Principles

Flow-through experiments were performed as outlined in Section 2.5.5 (Fig. 2.2). Typically, 6-8 silicic acid solutions with concentrations between $30\ \mu\text{M}$ and $1800\ \mu\text{M}$ were chosen as input parameter; the solutions were pumped through the reactors with flow rates which ensured a measurable difference between the inflow (Si_{in}) and outflow (Si_{out}) due to dissolution or precipitation. The former case results in $\text{Si}_{\text{out}} > \text{Si}_{\text{in}}$, whereas the latter is indicated by $\text{Si}_{\text{out}} < \text{Si}_{\text{in}}$. Flow rates used for silica-rich sediments from the Scotia Sea (Fig. 2.1) as well as those from single opal samples (Tab. 2.2) were typically in the range of 2-7 ml/h. Flow rates exceeding these values were avoided because they

3. Experimental results and discussion

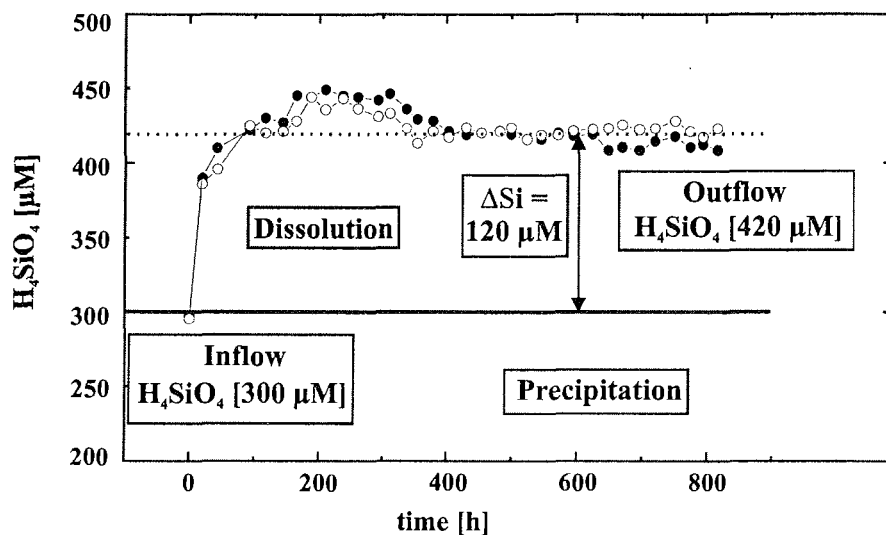


Fig. 3.1 Silicic acid concentrations as a function of time obtained in the outflow of the continuously-stirred flow-through (CFT)-reactor; the experiments performed in duplicate (open and black circles) were started with a silicic acid concentration of $300 \mu\text{M}$. Rates were calculated from the difference between the outflow and inflow solution concentrations (Eq. 3.6, Sect. 3.1.2.2.1) after the outflow solution had reached steady state. Positive rates ($\text{Si}_{\text{out}} > \text{Si}_{\text{in}}$) indicate net dissolution, negative rates ($\text{Si}_{\text{out}} < \text{Si}_{\text{in}}$) would correspond to net precipitation. Solubility is the rate equals zero ($\text{Si}_{\text{out}} = \text{Si}_{\text{in}}$) (Fig. 3.2). It should be mentioned that each data point in Fig. 3.2 originated from a measurement outlined here.

would lead to extensive clotting and adhesion of samples to the reactor wall or filter grids. Due to that limitation, undersaturation could not be maintained above 50% for the highly reactive, acid-cleaned phytoplankton sample derived from NAST site (Arabian Sea; Fig. 2.1). This is discussed in Section 3.1.2.2.1 in further detail. For silica-poor sediments (BENGAL, Norwegian Sea or Arabian Sea sediments, Fig. 2.1) in contrast, flow rates have to be maintained between 0.3-1.5 ml/h to obtain a measurable difference between inflow and outflow solution.

The biogenic silica dissolution rate was determined when the experiments had reached steady state. This was indicated by outflow solution concentrations that ceased changing with time (Fig. 3.1). In general, one set of experiments lasted 12-18 days depending on flow rate and time for reaching a steady state value. Inflow and outflow ("steady state") samples were analyzed for dissolved silicic acid as outlined before (2.5.3). Generally the number of analyses at the beginning of an experimental run was less and increased at the end of the run when steady state values appeared (Appendices A.3.1-A.3.6).

Undersaturation with respect to sedimentary biogenic silica is present when the outflow is higher than the inflow solution concentration and supersaturation when the outflow concentration is lower. As indicated in Figure 3.2 the apparent solubility ($\text{Si}_{\text{out}} = \text{Si}_{\text{in}}$) can be determined by interpolating negative and positive rates nearest to equilibrium (normally 3-4 data points are used). Values gained from experiments at $T = 2^\circ\text{C}$ were derived from extrapolating positive rates (net dissolution) to the x-axis because reliable results obtained in the oversaturation state were lacking. Apart from these apparent solubilities, the dissolution or precipitation kinetics were determined

during the course of the same experiment; results and reaction rate determinations are outlined in Section 3.1.2.2 and Tab. A.3.11.

Sediment solubilities

In terms of apparent silica solubilities measured in the deepest sections of the sediment cores at 25°C and pH 8, the cores can be divided into four distinct groups (Fig. 3.2):

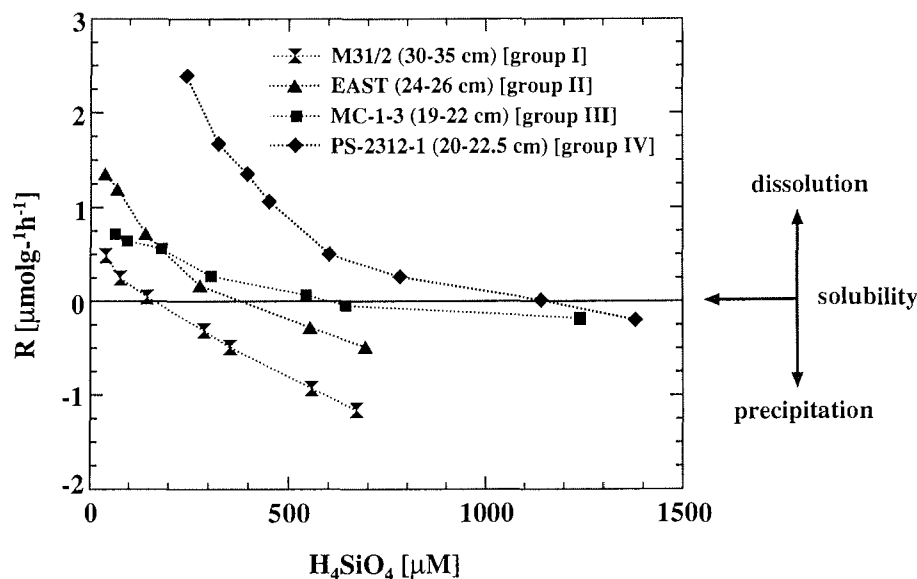


Fig. 3.2 Steady state dissolution rates per unit mass biogenic silica as a function of silicic acid concentrations in the outflow solutions (for calculations see Section 3.1.2.2.1). Positive rates indicate net dissolution, negative rates correspond to net precipitation (Fig. 3.1). The results are grouped into 4 types (discussed in the text); each is represented by one core throughout the following description.

- I. Sediments from the Norwegian Sea (M31/2) with the lowest BSi contents of all exhibit a solubility value of $\sim 170 \mu\text{M}$.
- II. Sediments from the BENGAL area (MC#33) and from most sites of the Arabian Sea (NAST MC#45, SAST MC#14, and EAST MC#28) fall into a fairly narrow range of solubilities ($300\text{-}400 \mu\text{M}$).
- III. Sediments from the Arabian Sea (WAST MC#53), the Juan de Fuca Plate (MC-1-3), and the Peru Basin (MC-145) comprise the third group with solubilities on the order of $600\text{-}800 \mu\text{M}$, with the highest values from sediments of the Peru Basin. This group is also characterized by a striking flat pattern of reaction rates versus depth (Fig. 3.2).
- IV. Siliceous oozes from the Scotia Sea (PS-2283-6, PS-2299 and PS-2312-1) have typical solubilities of $900\text{-}1100 \mu\text{M}$. These sediments, however, display systematically lower values than those reported by VAN CAPPELLEN and QIU [1997 a, b] in siliceous oozes from Southern Ocean (Indian Sector).

3. Experimental results and discussion

Opal samples from the water column and the sediments

Apparent silica solubilities ($T = 25^\circ\text{C}$ and $\text{pH } 8$) measured in 2-3 different depth intervals deploying flow-through experiments are given in Figure 3.4 (a complete list is given in Table A.3.11). For comparison, the pore water profiles of each core are also shown.

The dissolution behavior of opal samples, either acid-cleaned or almost untreated as well as fairly fresh (phytoplankton or sediment traps) or diagenetically altered (Opal-A and Opal-CT from various sedimentary regimes), was determined at 2°C and $\text{pH } 8$.

These experiments were conducted in a similar fashion as the previously described flow-through experiments by letting the samples pass through a succession of steady states using the same sample [e.g., VAN CAPPELLEN and QIU, 1997a]. In order to enhance the exchange of successive inflow solutions the reactor was rinsed with a new solution at a high flow rate before the flow rate was again reduced to the desired constant value during the course of the experiment. The data set (A.3.7.1) was plotted as rate R [$\mu\text{mol g}^{-1} \text{h}^{-1}$] versus silicic acid concentration in the outflow solution. In Table 3.2 apparent solubilities and average sample compositions are given. Rate constants are presented in Section 3.1.1.2.1.

A great variance of the apparent solubilities did not occur. Uncertainties were assumed to be less than 10%. Interestingly, an untreated diagenetically altered sample (~ 4 Myr, Tab. 2.2) from a porcellanite horizon (Maud Rise) shows the same apparent solubility as an acid-cleaned, freshly taken phytoplankton bloom sample (e.g., Pn-M21/4, Fig. 3.3 and Tab. 3.2). Lowest solubilities ($\sim 1000 \mu\text{M}$), however, were reached by untreated or acid-cleaned sediment trap material (1000m and 2500m) and by plankton sample O2 (Fig. 3.3, Tab. 3.2) from surface waters of the Arabian Sea (NAST) dominated by *Nitschia* sp.

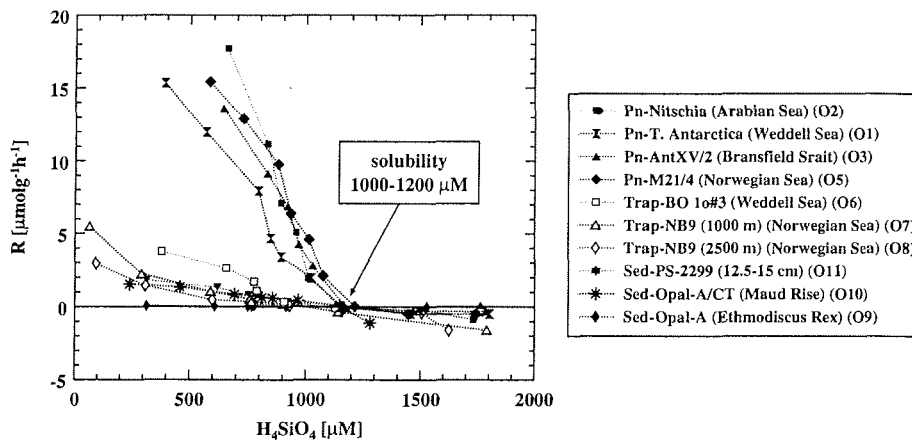


Fig. 3.3 Steady state dissolution rates of opal samples O1-O3 and O5-O11 (Tab. 2.2) as a function of silicic acid concentrations in the outflow solutions ($T = 2^\circ\text{C}$, $\text{pH } 8$). Solubility values of all samples (Tab. 3.2) fall into a fairly narrow range ($1000\text{-}1200 \mu\text{M}$). Reaction rates, however, vary by 1-2 orders of magnitude depending on whether the samples represent phytoplankton (Pn), trap material (trap, open symbols) or sediment (Sed) (3.1.2). A complete list of data is given in Tab. A.3.7 and A.3.8.2. Solid/solution ratios and reaction rates are listed in Tab. A.7. Results in terms of rates versus silicic acid concentration measured in the outflow are documented in Fig. 3.3.

3. Experimental results and discussion

Tab. 3.2 Major components and apparent solubilities of an acid-cleaned siliceous ooze (PS-2299 10-12.5 cm), untreated sedimentary opal samples (O9, O10), untreated (O7, O8) and acid-cleaned (O6) sediment-trap material, and untreated (O4) or acid-cleaned phytoplankton samples (O1, O2, O4, O5) obtained by means of flow-through reactors. Note that C_{org} and N_{org} were not detectable after acid-cleaning (2.2.2).

ID.	Sample	Apparent solubility [$\pm 10\%$] ¹	Opal [wt.%] ²	CaCO ₃ [wt.%]	C _{org} [wt.%]	N _{org} [wt.%]	Detritus [wt.%]
O1	Pn- <i>T. antarctica</i>	1150	95	--	--	--	5
O2	Pn- <i>Nitschia</i> sp.	1060	88	--	--	--	12
O3	Pn-ANT-XV/2 #64	1150	100	--	--	--	0
O4	Pn-ANT-XV/2 #65	970	37	--	8.3	1.4	53.3
O5	Pn-M21/4	1200	88	--	--	--	12
O6	Trap-BO 1o#3	1040	95	--	--	--	5
O7	Trap-NB9 (1000m)	1000	8	64.3	6.2	0.72	21
O8	Trap-NB9 (2500m)	1000	11	32.3	6.5	1	48.2
O9	Sed-Opal-A/CT	1200	100	--	--	--	0
O10	Sed- <i>Ethmo. rex</i>	1200	100	--	--	--	0
O11	Sed-PS-2299 (10-12.5 cm) acid-cleaned	1190	83	--	--	--	17

¹Due to the sampling procedure an uncertainty of ~10% is expected.

²Analytical error is less than 5%. Nevertheless, opal content may be over- or underestimated by $\pm 10\%$ when assuming a water content of biogenic opal according to MORTLOCK and FROELICH [1989].

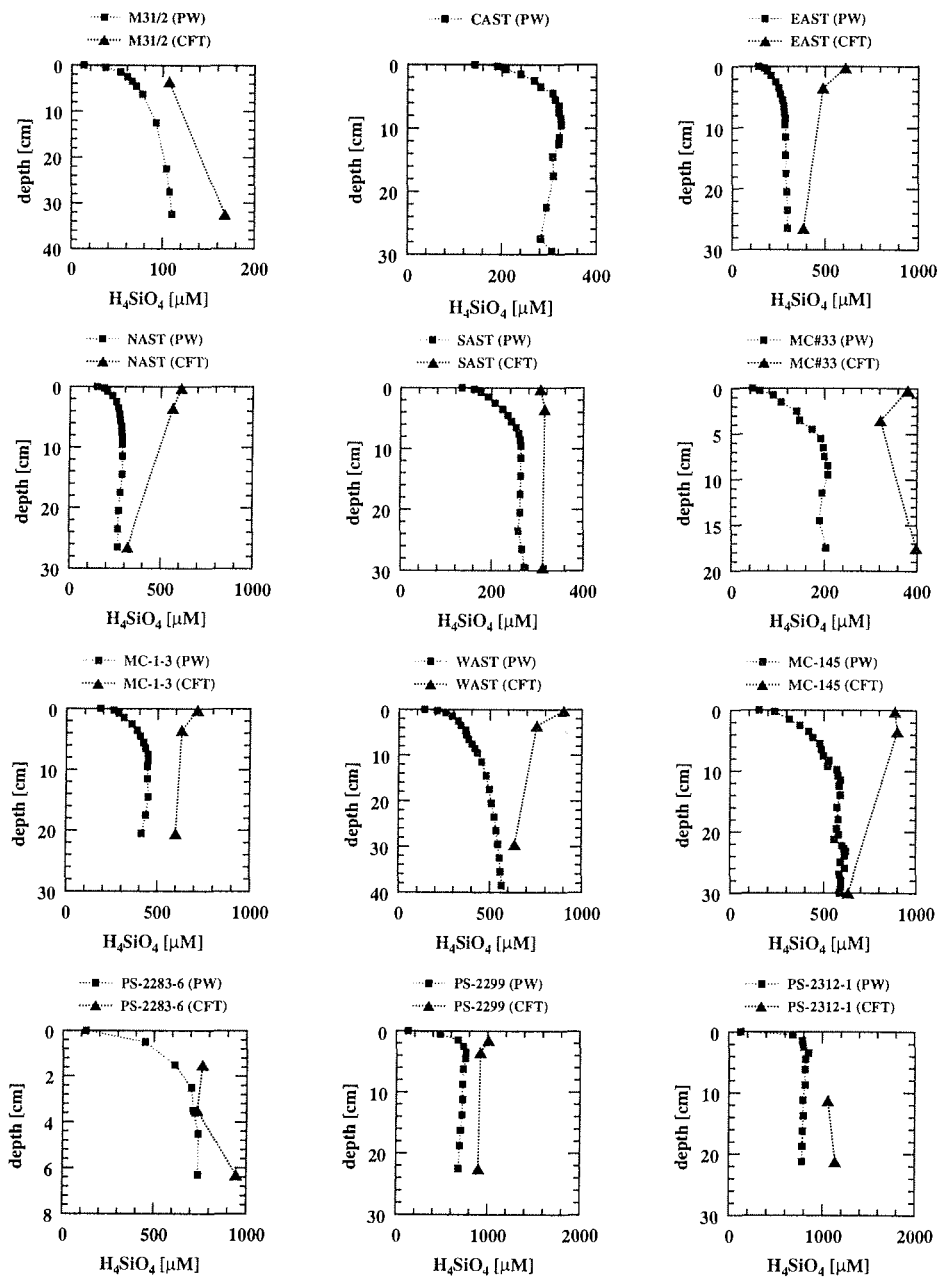
The factors, which may result in the significant decrease in reactivity (Tab. 3.3) when comparing phytoplankton (Pn) samples with sediment trap (Trap) or sediment (Sed) samples are discussed in detail in Section 3.1.2.3.

3.1.1.2.2 Depth distribution of apparent solubilities in sediments

The concentration versus depth profiles of silicic acid in pore waters from the 13 stations investigated in this study vary between 100 μM (group I: Norwegian Sea), 200-300 μM in the calcareous oozes (group II: BENGAL, NAST, CAST, EAST, SAST), 400-600 μM in sediments from Juan de Fuca Ridge, Peru Basin and WAST (group III), and 700-800 μM in Scotia Sea sediments (IV) at ambient bottom water temperature (~ 2°C). In Figure 3.2 the results from solubility measurements by flow-through experiments from the deepest sediment segments at 25°C and pH 8 are outlined.

3. Experimental results and discussion

Fig. 3.4 Apparent silica solubility profiles in the cores, measured at 25°C and ambient pressure by continuous flow-through reactors (CFT), and pore water silicic acid profiles from 12 selected stations. Note: CFT experiments were not carried out with CAST and PS-2314-1 (not shown) sediments.



3. Experimental results and discussion

Experimental solubilities, albeit providing higher values for temperature differences, exhibit a relative order of values similar to those observed in the field. In fact, laboratory results were considered which represent the part of the pore water profile where asymptotic silicic acid values were obtained. Silicic acid values measured in pore waters from the upper part of the core do not represent solubility values since they are affected by major transport processes mentioned in Section 2.6. With the exception of M31/2 and PS-2312-1 apparent solubilities of biogenic silica in sediment samples taken from three depths intervals were determined. For M31/2 and PS-2312-1 only two depth segments were investigated.

Three different trends are defined by the CFT solubilities. The solubilities tend to decrease with depth as outlined in Figure 3.4 (EAST, NAST, MC-1-3, WAST, MC-145, PS-2299), remain almost constant throughout the core (SAST, PS-2312-1), or tend to increase with depth (M31/2, PS-2283-6). Very similar patterns were observed in batch experiments performed at 60°C [RICKERT, unpublished results]. In the following those factors are highlighted which are supposed to cause a downward decrease in apparent solubilities observed in most of the cores.

3.1.1.2.3 Effect of major cations Al(III) and Mg(II)

The role of aluminum in the preservation of BSi

The role of aluminum is by far the most frequently discussed topic in dissolution kinetics of biogenic silica. The basic work was done by LEWIN [1961]. She has observed that diatom tests which had been rinsed with a solution containing aluminum at a pH below 6 showed lower silica solubilities than tests which had not been treated. Experimental work by ILER [1973] has shown that the solubility of amorphous silica decreased with increasing concentrations of aluminum due to the formation of an aluminosilicate surface on the colloidal silica particles. Another explanation for the strong effect of small amounts of Al on silica dissolution has been given by ILER [1973]: The incorporated Al produces additional negative charges on silica surfaces, repelling OH⁻ which otherwise would catalyse the dissolution. Experiments with natural phytoplankton samples from different oceanic regions have indicated that the dissolution of diatom frustules is lowered by high aluminum contents [VAN BENNEKOM, 1980, 1981; VAN BENNEKOM et al., 1988; VAN BEUSEKOM et al., 1991]. Laboratory experiments of VAN BEUSEKOM [1991] with the diatom *Thalassiosira eccentrica*, cultured in seawater with different Al/Si ratios, revealed that both the dissolution rate and the equilibrium concentration between frustules and dissolved silica decreased with increasing aluminum content in the frustules. The incorporation of Al may occur in surface waters. Such a primary signal exported to the deep-sea may cause pore waters to remain undersaturated with respect to a pure siliceous ooze.

Nevertheless it remains the question as to whether apparent asymptotic pore water silicic acid values are solely caused by the aluminum-content of the frustules since the frustules evolve from phytoplankton of different regions and from different species [VAN BENNEKOM, 1981; VAN BENNEKOM et al., 1988, 1991].

3. Experimental results and discussion

Does Al in pore waters play a key role in biogenic silica diagenesis ?

In seawater (pH ~ 8), the predominant form of dissolved alumina is $\text{Al}(\text{OH})_4^-$, although some aluminum may be bound to complexes with organic matter [SACKETT and ARRHENIUS, 1962]. Aluminum which passes through the 0.45 μm Millipore membrane filter is considered as dissolved. WILLEY [1975a] has thoroughly investigated the removal of aluminum from seawater in the presence of silicic acid, amorphous silica or various sediments. According to her, 0.5 ppm or 18.5 μM Al were stable in Sargasso seawater of 2°C (which originally contained less than 20 μM Si and 0.37 μM Al). WEY and SIFFERT [1961] found that about 74 μM Al were stable in NaCl solution at pH 8 at room temperature. The presence of sufficient dissolved silica, however, causes coprecipitation of silica with aluminum; the product of the reaction is an aluminosilicate. WILLEY (1975a) concluded that the concentrations of dissolved silica in seawater and interstitial waters which are usually much higher than the concentration of aluminum ($\text{Al} < 500 \text{ nmol l}^{-1}$) is not the controlling factor for dissolved silica in those waters.

Since a quantitative relationship between dissolution rate, the concentration of aluminum in solutions and processes occurring at the SiO_2 interface are not presently known [DOVE, 1995], flow-through experiments were conducted which are suited to examine both the effect of aluminum on the solubility as well as on the dissolution kinetics of biogenic silica.

Willey [1975a] previously found that dissolved alumina can also coprecipitate with dissolved silica from seawater enriched with both compounds. Here, concentrations of Al and Si remained stable in the artificial seawater inflow solution throughout the experiment up to concentrations of 37 μM Al at 25°C and pH 8. This was confirmed by measuring the inflow solutions before and after each run. The Al concentration in the last run (C/C'#3), however, tended to decrease during the course of the experiment. A coprecipitation with silicic acid was visible and measurable by a continuous decrease of silicic acid and aluminum in the inflow solution throughout the experimental run. The solutions enriched in both compounds showed a decrease in both components of ~ 20 μM (- 10%), thus suggesting a ratio of ~ 1:1 in the precipitate. The latter mentioned outflow values in Figures 3.5 and 3.6 and Table A.3.8, are thus be viewed with caution because of the metastability of the inflow solution and the consequently large uncertainties associated with the rate calculation.

The inflow solutions containing 0.090, 0.190, 0.650, 1.9, 2.5, and 37 μM Al as well as the solution with 290 μM at the beginning and ~270 μM at the end of the run were prepared by diluting stock aluminum standard solution in artificial seawater containing dissolved silica of 300 μM . In order to test the loss of aluminum that has not resulted from interaction with the sediment but with the flow-through apparatus, solutions of low aluminum concentrations ($\text{Al} = 0.037$ and $0.090 \mu\text{M}$) were run through an empty reactor for more than one week, which resulted in a negligible loss of aluminum. Therefore, adsorption by the flow-through system (e.g., walls, filters) is excluded.

Thus, eight subsamples of 0.5 g of siliceous ooze (PS-2312-1; 10-12.5 cm) not subjected to any prior chemical treatment were flushed with inflow solutions of a nearly constant silicic acid concentration ($300 \pm 10 \mu\text{M}$) and spiked with increasing concentrations of aluminum in 3 succeeding experimental runs. The inflowing solutions were pumped at a rate of 2.6 (± 0.1) ml/h. Each solution was run in duplicate (indicated

3. Experimental results and discussion

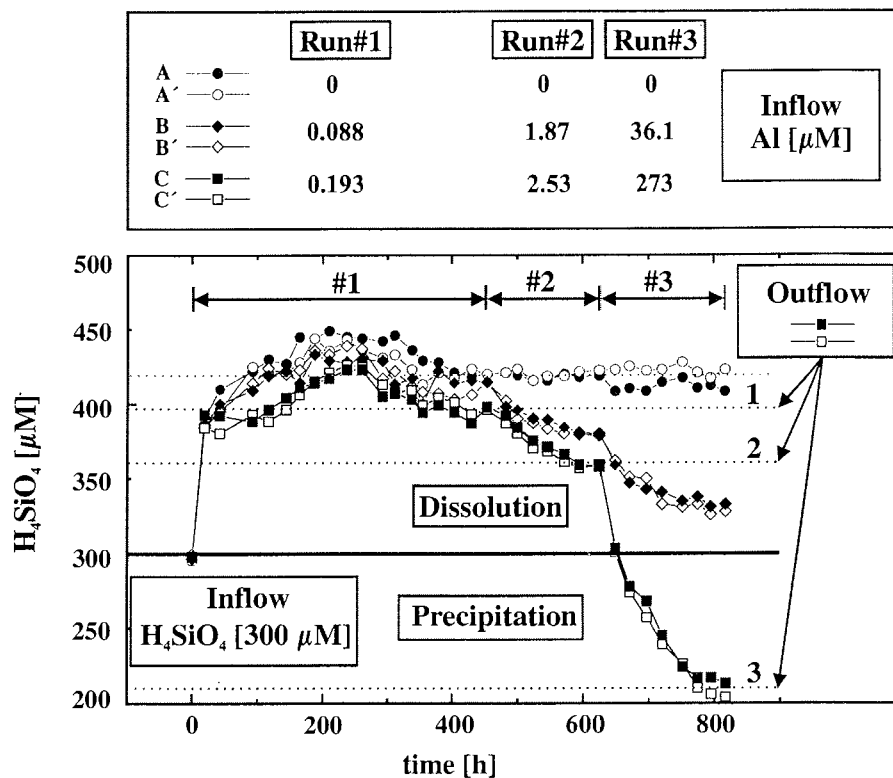


Fig. 3.5 Siliceous ooze sample PS-2312-1 (10-12.5 cm) was rinsed with increasing concentrations of aluminum (III) in artificial sea water spiked with 300 μM silicic acid. Open and filled symbols indicate duplicate runs. Run A and A' represent a single silicic acid solution without further addition of aluminum. Al concentrations reflect inflow solutions which exhibit stable concentrations during the course of a run except those taken for the last run (see text). Arrows 1-3 indicate stable outflow concentrations of silicic acid for duplicate run C and C' (open and filled squares) with various inflow concentrations of Al(III) (1: 0.193 nM; 2: 2.53 nM; 3: 273 nM). Run D/D' (Al : 650 nM) is not shown but indicated in Fig. 3.6 and A.3.8.

by the open or filled symbols in Figure 3.5), resulting in a total of 8 solutions for the first run (A/A', B/B', C/C', D/D' with filled/open symbols) and 6 solutions for the succeeding runs. The flow-reactors D and D' (results are not indicated in Figure 3.5; see Figure 3.6 and A.3.8) were only used during the first experiment. The blank solutions (A/A') not spiked with aluminum were run in two reactors reflecting more or less stable conditions throughout the runs (indicated by circles in Figure 3.5).

The silicic acid concentrations in the outflow solutions 1, 2, 3 for experiments C/C' (squares) and the stable outflow concentrations of silicic acid in the blank run (circles) reveal the influence of soluble aluminum relative to the blank runs.

3. Experimental results and discussion

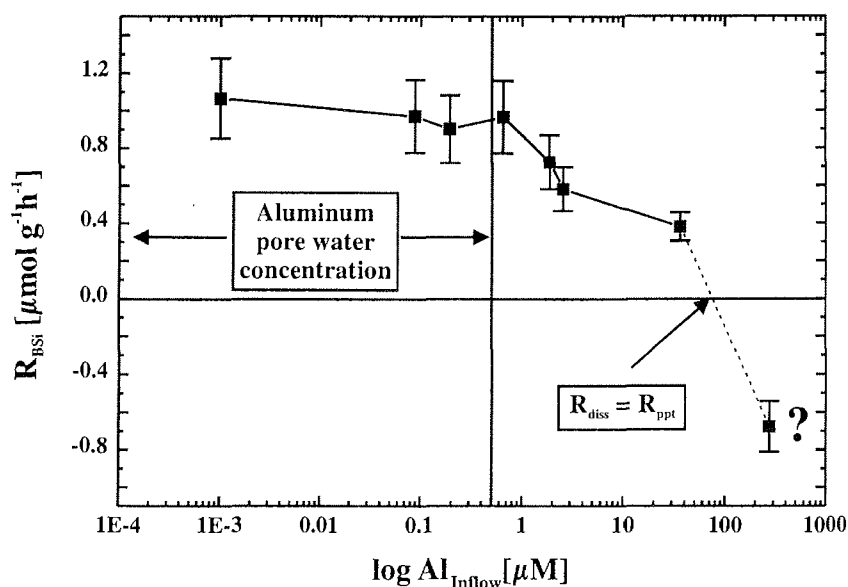


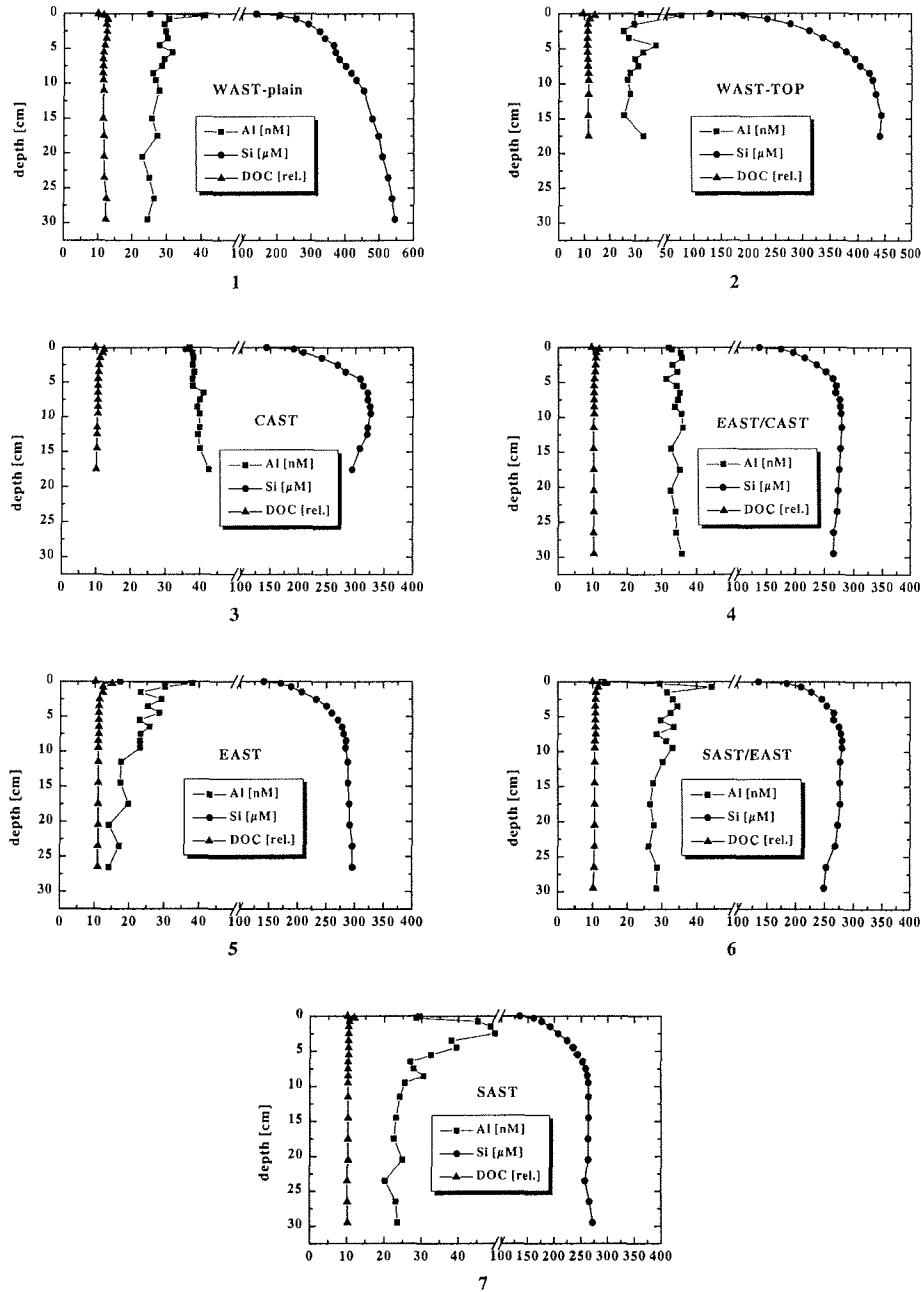
Fig. 3.6 Net rates of silicic acid release calculated using Equation 3.6 (3.1.2.2.1) Permitting uncertainties, flow-through experiments with Al concentrations of $< 0.65 \mu M$ cause no coprecipitation of silicic acid with soluble aluminum (experiments D and D' are also indicated, see text and Tab. A.3.8) and rates of silicic acid release remain constant. The presence of sufficient Al ($\gg 0.65 \mu M$), however, causes coprecipitation of silica with aluminum revealed by a sharp decrease in $[Si_{out}]$ (Fig. 3.5) or R_{BSi} . Silicic acid concentrations in the outflow changes as a consequence of the coprecipitation between 200-400 μM . The last point (question mark) is coupled with large uncertainties due to coprecipitation of silicic acid and aluminum in the inflow solution (see text). Nevertheless, a clear tendency is obvious.

Aluminum concentrations in the outflow solutions were also monitored continuously in filtered samples. The Lumogallion fluorometric method as described for seawater analyses (2.1.2.2) [HYDES and LISS, 1976] was used for the determination of aluminum concentrations in the outflow and inflow solutions up to 3.7 μM . Due to a negligible contamination, Al analyses were performed without standard addition and addition of $CaCl_2$ (2.1.2.2). Aluminum standards were prepared in artificial seawater used as inflow solution in the blank run without prior addition of silicic acid. The relative precision of duplicate measurements was 10% or better for aluminum; Al ($\geq 37 \mu M$) and Si analyses were performed by ICP-AES (2.5.3).

As long as inflow concentrations of Al do not exceed values $\geq 0.65 \mu M$ (Fig. 3.6, Tab. A.3.8), a measurable decrease, was not observed. Al concentrations $\geq 2-3 \mu M$ (Fig. 3.5, run #2 and #3; Fig. 3.6, Tab. A.3.8), however, result in a significant decrease of outflowing silicic acid concentrations. This may be caused by coprecipitation or a decrease of reactivity due to Al adsorption. The effect of the coprecipitation or adsorption reaction was determined by comparing silicic acid values in an Al-free solution with those of Al-spiked solutions (Fig. 3.5). Figure 3.6. reveals the corresponding decrease in calculated reaction rates. The calculation of reaction rates is described in Section 3.1.1.2.

3. Experimental results and discussion

Fig. 3.7 Pore water silicic acid and aluminum profiles at 7 stations in the Arabian Sea (locations and data in A.2.7). Whereas silicic acid values increase with depth, Al data show a decrease below the surface maximum towards mean values of ~ 30 nM. Natural fluorescence pore water samples measured during the aluminum analysis was used as an indication of dissolved organic carbon (DOC) [CADDÉE and LAANE, 1983]. A coincidence of surface maxima in Al with surface maxima of DOC is noticeable.



3. Experimental results and discussion

Results from run C/C' were included in both Figures 3.5 and 3.6 because apart from high uncertainties due to coprecipitation of silicic acid with aluminum which already begun in the inflow solution, the tendency of a decreasing reactivity is noticeable at least for a qualitative description of this run.

Final aluminum concentrations measured in the outflow solutions of all experiments scatter around the value measured for the background solution, but never exceed mean values of 10 nM, the detection limit for that kind of Al analysis. In Section 3.1.1.3.2 the processes responsible for the almost complete removal of aluminum in the experiments are discussed. Coprecipitation or adsorption seems to be most effective in the presence of a solid phase as indicated by the almost complete removal of Al in the reactor, whereas coprecipitation in the inflow solution at 25°C requires sufficiently high Al:Si ratios [see also WILLEY, 1975a].

Al in pore waters

Al concentrations measured in pore waters are the result of heterogeneous reactions, including the release by aluminous solid phases, such as clay minerals or gibbsite, coprecipitation with dissolved silica, and removal by solid surfaces. VAN CAPPELLEN and QIU [1997a] proposed from their studies on the dissolution kinetics of biogenic silica that the range of asymptotic pore water silica concentrations may to a large extent reflect variations in the relative supplies of biogenic silica and soluble aluminum to the sea floor.

For further discussions new pore water aluminum profiles are presented. These were measured on SO129 cruise at WAST, CAST, EAST and SAST as well as on intermediate stations WAST-TOP, EAST/CAST, SAST/EAST (the latter destinations are not indicated in Fig. 2.1). Site locations, silicic acid and aluminum profiles are given in A.2.3.1-A.2.3.5 and A.2.7. The concentration of aluminum in pore waters usually differs from that of silicic acid by a factor of ~ 1,000. Obviously pore water measurements alone cannot provide the answer to the question as to whether variable pore water aluminum levels are responsible for the variability observed in asymptotic pore water silicic acid values or apparent solubilities (see Figs. 3.7 and 3.8 and subsequent discussions).

Apparent solubility values of biogenic silica gained from asymptotic pore water concentrations are highly variable from one location in the ocean to another as shown in pore water profiles of the Arabian Sea (Figs. 3.4 and 3.6). Pore water silica concentrations increase from bottom water values of ~140 μM to asymptotic values of ~550 μM (WAST-plain), 450 μM (WAST-TOP) or 300 μM (NAST, CAST, EAST, SAST and intermediate stations).

The aluminum distributions are characterized by sharp maxima just beneath the sediment-water interface with concentrations ranging between 40 to 80 nM coinciding with maxima in natural fluorescence (~ DOC), nitrate, phosphate and ammonia [RICKERT, unpublished data; Fig. 3.9). The significant maxima within the first centimetre may be related with communities of microbial decomposer organisms; their excretions probably cause the high ammonia values. Organic matter remineralization results in increasing nitrate concentrations.

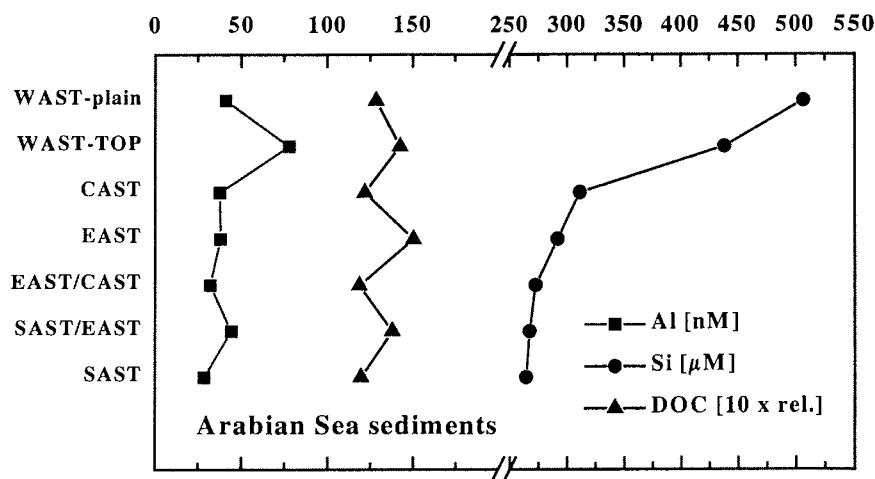


Fig. 3.8 Distribution of asymptotic silicic acid concentrations below 10 cm, maxima of dissolved alumina near the sediment-water interface and natural fluorescence [\propto DOC, see CADÉE and LAANE, 1983], observed in the first centimetres of Arabian Sea sediments (Fig. 3.7). A slight tendency of covariation between natural fluorescence and Al is poorly indicated by some maxima and minima. A correlation between aluminum and asymptotic silicic acid values, however is lacking. Therefore, it is spurious that soluble aluminum controls silicic acid values in pore waters. This is also supported by the CFT-experiments which emphasize the role of aluminum on the dissolution kinetics of biogenic silica and were described above (3.1.1.2.4). For locations see Fig. 2.1, data are given in A.2.3.1-A.2.3.5 and A.2.7.

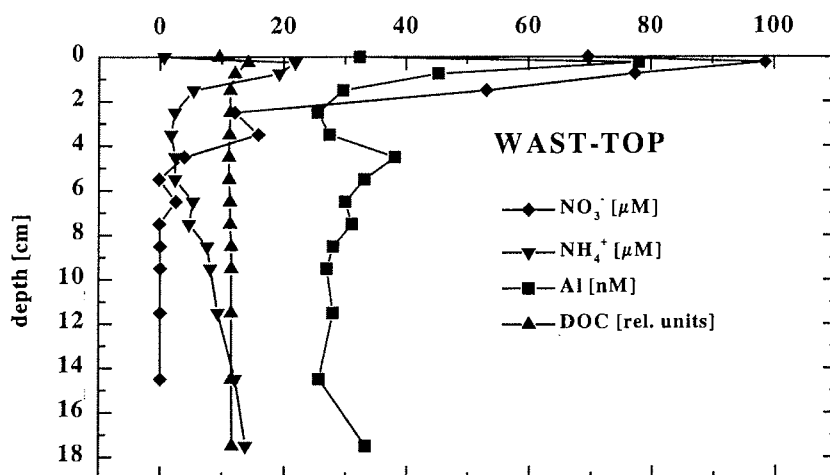


Fig. 3.9 Dissolved nitrite, nitrate, phosphate, ammonia, aluminium and natural fluorescence from WAST-TOP station [RICKERT, unpublished data]. Nutrient maxima observed in the first centimetre correlate well with the observed maxima in Al and DOC concentrations suggesting one underlying process (see also Fig. 3.8).

3. Experimental results and discussion

This process is also favored by rather high enzymatic activity in the first centimetre, indicating that the greatest part of the organic matter is degraded at the sediment surface. The silicic acid concentrations which were shown in Figure 3.7.2 increase continuously with depth. The profiles of dissolved Al (MC#35, WAST-TOP) show a sharp decrease below the sediment-water interface towards mean values of ~35 nM (Fig. 3.9). Similar trends were observed for almost all sites whereas at CAST and EAST/CAST (Fig. 3.7) the topmost Al-maximum is less significant. At CAST a slight increase with depth is observed.

Variable asymptotic pore water silicic acid concentrations observed in the cores of the Arabian Sea cannot be explained solely by a diagenetic interaction between biogenic silica and soluble aluminum. In the following section (3.1.1.2.4) experimental evidence is provided for the hypothesis that reverse weathering reactions [SILÉEN, 1961; MACKENZIE and GARRELS, 1966; MACKIN and ALLER, 1986] may occur in recent marine sediments soon after deposition and may be responsible for the variability around asymptotic pore water silicic acid concentrations.

The role of Mg in preservation of BSi

Before the important role of detrital minerals is discussed, results of some experiments performed to find out whether opal preservation observed in core PC15 (Discovery Basin, Mediterranean Ridge, Tab. 2.1) may be induced by some extraordinarily high concentrations of soluble Mg in interstitial waters [MEDRIFF-CONSORTIUM, 1995; WALLMANN et al., 1997; WALLMANN et al., submitted].

To simulate the influence of Mg on the dissolution kinetics of biogenic silica in general the same kind of experiments were carried out as those outlined for the influence of soluble Al using again siliceous ooze sample PS-2312-1 (10-12.5 cm) in 9 parallel runs (E/E', F/F', G/G', H/H', I). Two were run in duplicate respectively (excepting the last one), but instead of aluminum successively increasing concentrations of Mg-spiked artificial seawater were used as inflow solutions. Prior to various Mg inflows, the sediments were allowed to equilibrate for approximately 1 week with artificial seawater commonly used for the flow-through experiments (3.1.2.2.1) containing 300 μM silicic acid and 57 mM magnesium (A.3.9). After sampling No. 8 (188 h) inflow solutions (except those in blank run E and E') were replaced by artificial seawater spiked with increasing concentrations of Mg. Inflow solutions were prepared as outlined in Section 2.5.2. The composition given in DICKSON [1993] was modified with respect to magnesium by further addition of reagent grade $\text{MgCl}_2 \cdot 6 \text{H}_2\text{O}$. This resulted in soluble magnesium concentrations of 0.057 M, 0.23 M, 0.92 M, 1.82 M and 3.5 M and 300 μM silicic acid. Due to coprecipitation at extremely high concentrations of magnesium with silicic acid during preparation of the inflow solutions, Si concentrations could not be maintained at 300 μM . Figure 3.9 indicates such a decrease in silicic acid concentration during storage in the inflow solution from ~ 300 μM to ~ 140 μM when Mg concentrations between 0.057 M and 3.5 M were used. Once, silicic acid concentration had reached that lower value, it remained constant throughout the experiment. Figure 3.9 reveal that net dissolution rates decrease with increasing concentration of Mg in artificial seawater. A Mg concentration of 3.5 M in the inflow solution results in a net precipitation indicated by a negative rate of 0.18 $\mu\text{mol g}^{-1} \text{h}^{-1}$

3. Experimental results and discussion

(Fig. 3.9, A. 3.9). Magnesium concentrations in the outflow were stable after 2-3 days of solution exchange in the reactor.

If Mg concentrations did not influence the dissolution kinetics of biogenic silica an increase in silicic acid release would be expected. This was expected even under high ionic strength conditions (see discussion in Section 3.1.1.3.2) since undersaturation increased from 0.7 to 0.9 assuming a constant solubility value of $1060 \mu\text{M}$ observed for PS-2312-1 (12.5-15 cm) (A.3.6.3, Fig. 3.10). Just the opposite was the case, net silicic acid release, given as dissolution rates, decreased (Fig. 3.9).

The concentration of 5.5 M magnesium observed in pore waters of PC15 [e.g., WALLMANN et al., 1997] can be realized if 1 kg of $\text{MgCl}_2 \cdot 6 \text{H}_2\text{O}$ is dissolved in 1 litre water. Such a solution is extremely metastable. The complete dissolution of added salt required temperatures of $\sim 60^\circ\text{C}$. Slow cooling tends to stabilize the solution, but only minor agitation again induced spontaneous precipitation. Therefore, flow-through experiments were conducted at 'stable' concentrations of 3.5 M magnesium in artificial seawater. Nevertheless, a clear trend of reduced silicic acid release from siliceous ooze sample PS-2312-1 is obvious from decreasing reaction rates (Fig. 3.9, A.3.9) towards high concentrations of magnesium.

Whereas the role of magnesium is obvious but supposed to be limited to extreme environments with more concentrated solutions of MgCl_2 , the role of Al for opal

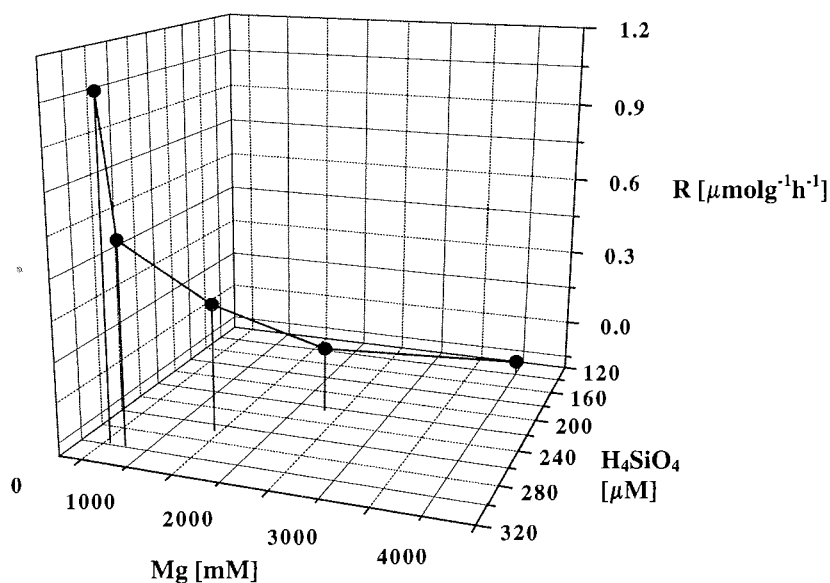


Fig. 3.9 Rates of silicic acid release as a function of magnesium concentration in the outflow. Silicic acid concentration in the inflow solution varied due to a coprecipitation during preparation between 300 (Mg 57-230 mM) and 140 μM (Mg 3500 mM). The influence of extraordinary high concentrations of magnesium on the dissolution kinetics of biogenic silica is striking despite the enhancement of undersaturation in the inflow solution and suggests to cause opal preservation in Discovery brine core PC15 [e.g., WALLMANN et al., submitted].

3. Experimental results and discussion

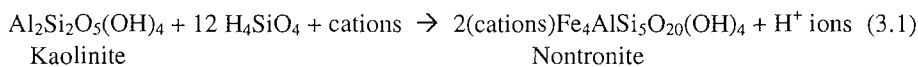
preservation in pore waters is at least an open question since a significant effect requires unnaturally high aluminum concentrations (3.1.1.2.3 and 3.1.1.3.2).

Following the effect of detritus on solubility of biogenic silica which ought to be differentiated from the effect of pore water aluminum.

3.1.1.2.4 Effect of clay minerals

Quartz, feldspars and clay minerals make up the bulk composition of detrital minerals [PRESS and SIEVER, 1986]. Detritus as used in my thesis (2.4.3) include all non-biosiliceous mineral phases [see also VAN CAPPELLEN and QIU, 1997a,b].

The deposition of clay-type aluminosilicates or detrital clay in general may independently regulate the build-up of pore water silicic acid concentrations either by sorption processes [e.g., GEHLEN et al., 1993] or by inducing 'reverse weathering' reactions [e.g., MACKENZIE and GARRELS, 1966; STOFFYN-EGLI, 1982; MACKIN and ALLER, 1986; MICHALOPOULOS and ALLER, 1995] such as a possible nontronite production through reaction of kaolinite, dissolved silica and other cations if silicic acid concentrations exceed 250 μM [LERMAN, 1979]:



This formation of authigenic clay during early sedimentary diagenesis can be accounted to "reverse weathering" or "reconstitution" (SIEVER, 1968) processes which returns to the ocean-atmosphere system the H^+ lost during weathering and removes excess metal cations and silicic acid, thereby preventing the ocean becoming alkaline [MACKENZIE and GARRELS, 1966].

In further considerations the clay minerals are treated as the detrital fraction, however being aware that the clay fraction (DC) does not reflect the detrital fraction as a whole in marine sediments. In Arabian Sea sediments for instance, DC is only 50% of residual detritus (RD) (Tab. 2.4), resulting in opal/detrital clay ratios of ~ 0.16 .

In order to investigate the effect of detrital clay minerals, kaolinite, montmorillonite and illite on the dissolution behavior of biogenic silica, 3.75 g of each clay mineral were mixed with 0.25 g of biosiliceous ooze sample PS-2312-1 (12.5-15 cm, 64 wt.% opal) which yield a final opal/detrital clay ratio of 0.042. Flow-through experiments with opal/clay mixtures were performed in parallel at $T = 25^\circ\text{C}$ and pH 8 with 5-6 silica-spiked inflow solutions in the range of 35 μM to 712 μM (Fig. 3.5). Flow velocities were varied from 0.2 to 1.5 ml/h. Steady state was reached after ~ 400 h. Time-dependent changes in the outflow solutions are shown in Table A.3.10.

In the presence of detrital clay minerals the apparent solubility of biogenic opal sampled at site PS 2312-1 (12.5-15 cm) decreases significantly (Fig. 3.5), suggesting that the removal of silicic acid induced by detrital minerals is one of the mechanisms by which the interstitial pore waters maintain their composition. Kaolinite, montmorillonite and illite in general reveal the same behavior in suppressing the solubility of biogenic silica, whereas the crossover points determined by interpolation of data points near equilibrium are different. Kaolinite, followed by montmorillonite and illite are most effective in preventing biogenic silica from reaching *in situ* solubility value of sediment PS 2312-1 (10-12.5 cm).

3. Experimental results and discussion

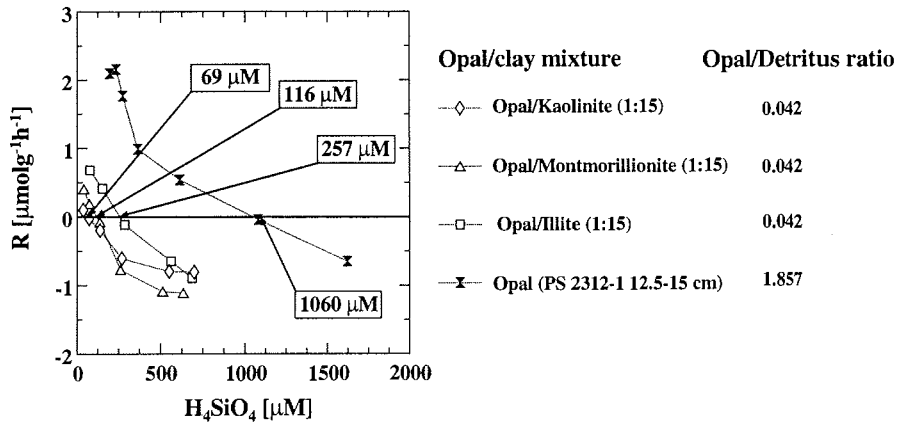


Fig. 3.10 Flow-through experiments with mixtures of opal (PS-2312-1 12.5-15 cm) and clay (kaolinite, montmorillonite, illite). Mixtures with opal/clay(detritus) ratios of 0.043 were applied. Rates of silicic acid release vs. the silicic acid concentration in the outflow. A clear reduction of apparent solubility is obvious in comparison with solubility values of pure sedimentary biogenic opal (PS-2312-1 12.5-15 cm) in the host sediment, i.e. 63-257 μM compared to 1060 μM .

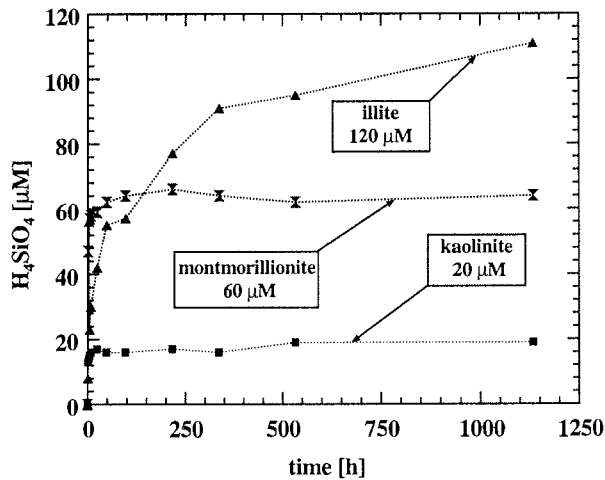


Fig. 3.11 Changes in silicic acid concentration in artificial sea water-clay slurry containing (pH 8, $T=20^\circ\text{C}$) kaolinite, montmorillonite and illite. Final concentrations reached after ~ 1100 h are shown. The relative order of values exhibits those obtained in flow-through experiments where 15:1-mixtures of clay minerals and siliceous ooze (PS-2312-1) were examined (Fig. 3.4).

3. Experimental results and discussion

Experiments performed by SIEVER and WOODFORD [1973] with pure clay minerals and silica-spiked solutions in 7-days batch experiments suggest a reaction order (illite < kaolinite < montmorillonite) slightly different from my results (kaolinite < montmorillonite < illite). Following their results, illite would be most effective in silica uptake, whereas in my results (Fig. 3.10) silica uptake by illite is at least effective.

To confirm the results we also conducted batch experiments. 1 g of pure clay minerals was treated with 50 ml of buffered artificial seawater (2.5.2) and continuously shaken at 20°C to investigate whether the sum of silicic acid released after ~1100 h exhibit the relative order of values observed in flow-through experiments. The results are given in Figure 3.11 and suggest that our sequence kaolinite < montmorillonite < illite is reproducible.

3.1.1.3 Discussion

3.1.1.3.1 Laboratory and field solubilities: A comparison

One of the aim of the laboratory experiments was to interpret the large variations in asymptotic pore water silicic acid concentrations which can be reproduced but not explained by applying pore water modeling techniques alone (3.2). Flow-through experiments were particularly useful to unambiguously answer the question of a thermodynamic and/or kinetic control of biogenic silica dissolution in marine sediments. Moreover, considering sediment samples from different depth intervals it was possible to examine the depth-dependency of apparent solubilities and dissolution kinetics.

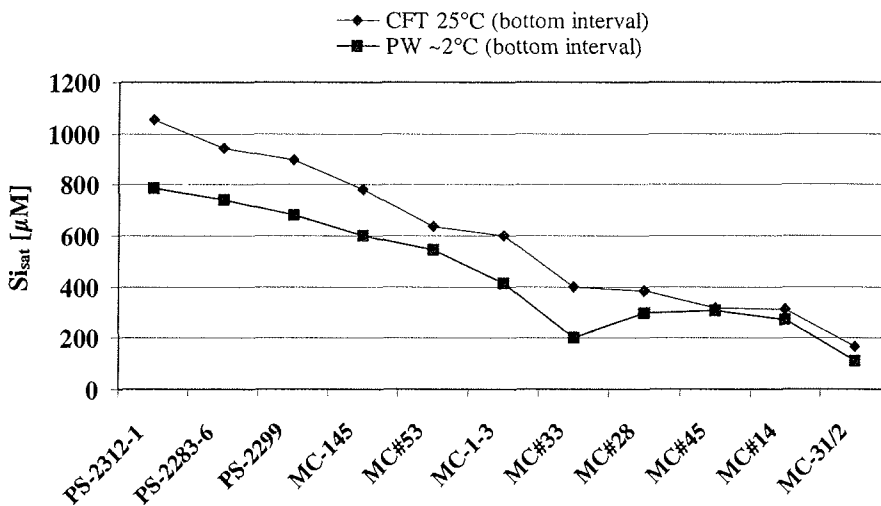


Fig. 3.12 Comparison between pore water asymptotic silicic acid concentrations (squares) measured at *in situ* temperatures (~2°C) and experimental solubilities (diamonds) in flow-through experiments measured in the deeper core sections at 25°C. The relative magnitude of the asymptotic concentrations and experimental solubilities show a strikingly good correlation.

3. Experimental results and discussion

A system with asymptotic behavior of a depth-dependent solubility is different from that with a kinetic inhibition. In the first case, asymptotic silicic acid concentration and apparent solubilities measured in flow-through experiments are expected to be similar to or lower than the predefined value ($< 1000 \mu\text{M}$ at 4°C in seawater; HURD, 1973). In the second case, the kinetically inhibited system, the asymptotic concentration and apparent solubility is still the solubility of amorphous silica ($\sim 1000 \mu\text{M}$). Such solubilities are only seldom measurable, e.g. as those reported by HESSE [1988 and pers. comm.] in deep-sea drilling cores or in flow-through experiments carried out with pure opal samples (3.1.1.2.1). Since concentrations were determined with chemically untreated sediment samples at 25°C at ambient pressure in artificial seawater and bicarbonate buffered at pH 8 these cannot be compared directly with asymptotic silicic acid values ($T \sim 2^\circ\text{C}$, water depth ranges from 1670 to 4800 m). However, we would at least expect that solubilities measured at the deepest section of the cores exhibit a range and a relative distribution of values similar to those observed in the fields.

The variation among asymptotic pore water silicic acid concentrations ($T \sim 2^\circ\text{C}$, pH ~ 8) is on the order of $700 \mu\text{M}$ for all 13 cores. Solubilities measured in laboratory flow-through experiments ($T = 25^\circ\text{C}$, pH 8) at the deepest section of 11 cores range from ~ 200 to $\sim 1100 \mu\text{M}$. Most striking, however, is the observation that the relative distribution of apparent solubilities measured in flow-through experiments and obtained from pore water silicic acid values is indeed quite similar (Fig. 3.12).

Therefore, the data obtained by pore water sampling or flow-through experiments lend support to the concept that apparent biogenic silica solubilities in an assemblage with other detrital minerals represent a weighted average of the solubilities of the various siliceous components. Thus, asymptotic silicic acid values truly reflect apparent solubilities of biogenic silica within a complex sedimentary matrix.

Data obtained in VAN CAPPELLEN and QIU [1997 a] in contrast do not support the concept that pore water silica generally build-up to the point at which the equilibrium solubility of the dissolving biogenic silica is reached since apparent solubilities in their study reveal a concentration range three times lower than the asymptotic pore water silicic acid concentrations in their approach. The relative magnitudes of asymptotic concentrations and experimental solubilities do not match either. I suppose from the different results that the electrolyte applied (0.7 N NaCl: VAN CAPPELLEN and QIU [1997a,b]; artificial seawater: this study) is one of the major reasons for the general difference. Since an intercomparison of both methods and reactor-types has not yet been undertaken, slightly differences of the independent performed flow-through experiments are listed in Table 3.1.

These differences are not mentioned to give preference to one method over the other but to draw attention to the problems which are to be encountered with any method used in laboratories. Even if the same method is used in several laboratories [e.g., CONLEY, 1998] patterns in the measurements remain which are related to specific methodologies or treatments. An intercomparison should establish the accepted range of variability in measurements and to focus on the individual treatment of specific problems to bring about a closer collaboration between laboratory and modeling scientists.

3. Experimental results and discussion

Tab. 3.1 Experimental set up of independently performed flow-through experiments on the dissolution kinetics of biogenic opal in Southern Ocean sediments [VAN CAPPELLEN and QIU, 1997 a,b] and sediments from various sedimentary regimes (this study, Fig. 2.1 and Tab. 2.1)

Properties	VAN CAPPELLEN and QIU [1997 a,b]	This study
Flow-through reactor	Suspended magnetic stir bar	Simple magnetic stir bar on the bottom of the reactor
Inflow solution	0,7 M NaCl buffered with TRIS	Artificial seawater (S = 35) according to DICKSON [1993], bicarbonate buffered (2 mM)
Sediments	Southern Ocean sediments with 16-76% opal	Sediments from various regions (Fig. 2.1, Tab. 2.1) with 1-63% opal
Experimental performance	Same sediment for a succession of inflow solutions with various silicic acid concentrations	Parallel runs of typically 7-8 single reactors filled with the same sediments but different silicic acid concentrations respectively

Thus, the question still remains what the solubility of biogenic silica really is-if it in fact can be expressed with a uniquely defined value. Further studies with flow-through experiments seem to be needed whose results can be compared between different laboratories to unambiguously answer the question which is the ‘best’ solubility, an asymptotic silicic acid value obtained in pore waters [SCHINK and GUINASSO, 1980] or a solubility value obtained by flow-through experiments [VAN CAPPELLEN and QIU, 1997a; RABOUILLE et al., 1997].

For further discussions and the subsequent modeling (3.1.1.3.3 and 3.2) the conflict was circumvented because flow-through solubilities from the sediments of my study confirm the *ad hoc* assumption of SCHINK and GUINASSO [1980] setting Si_{sat} equal to the observed asymptotic concentration (Fig. 3.12).

3.1.1.3.2 Early diagenetic effects on silica solubility

Besides the question which solubility is treated as the more or less “best value” the more important question is, which factors are controlling asymptotic pore water silicic acid values in general. The questions still debated [NELSON et al., 1995; RAGUENEAU et al., 1997, 1998; SCHLÜTER et al., accepted] are which mechanism leads to a more efficient opal preservation in regions of silica accumulation (Chap. 1), where global silica production makes up only ~10-25% of the total silica produced by diatoms [TRÉGUER, 1995], and whether the opal content of the sediment is a proxy for production in surface waters or controlled by regional different preservation efficiencies.

Based on laboratory results of this thesis, two possible mechanisms are discussed that may operate in the sediment to prevent biogenic silica from reaching solubility values expected for an acid-cleaned biogenic silica (1000 μ M at T = 4°C; Hurd, 1973) and lead to the formation of authigenic phases: (a) The presence of soluble Al [VAN CAPPELLEN and QIU, 1997a,b] or (b) the occurrence of reverse weathering reactions taking up silica by detrital clay minerals without substantial build-up of dissolved Al-intermediates

which does not preclude its involvement but suggest a near-simultaneous dissolution-precipitation process.

Early diagenetic imprint from the water column

The marine silica cycle is dominated by the production and subsequent dissolution of biogenic silica in the water column. In this context it is mentioned that there is no *a priori* reason to assume that the opal types entering the sediment have all the same solubility since WILLEY et al. (1980) reported that short-time aging processes without changing the bulk chemistry leads to a decrease in solubility of chemically-pure X-ray amorphous silica of approximately 20%. This process, however, is assumed to be of minor importance for the water column where rather high degrees of undersaturation prevent reprecipitation of less soluble amorphous silica in contrast to results from closed batch systems where saturation was maintained over a considerable period of time (WILLEY et al., 1980). But in the sediment column, aging processes may be an important process to alter biogenic silica assemblages (see below).

On the other hand, opal formation and subsequent dissolution resistance may also be affected by the trace element chemistry of the surface waters: Aluminum was mentioned to be important [LEWIN, 1963; VAN BENNEKOM et al., 1991] and confirmed by laboratory results [VAN BEUSEKOM, 1995]. A decrease in reactivity and solubility with increasing Al/Si ratios within the structure of silica skeletons was indicated. Hence, such structural change due to metal incorporation, in this thesis referred to as *primary alteration* of biogenic silica, is differentiated from *secondary alteration* such as organic or inorganic surface coatings, which either exists until being decomposed or forms by interaction between the hydroxyl groups present at the surface and several metals, for example Al, Be, Fe, Ga, Gd, and Y [LEWIN, 1961; Iler, 1973] or Mg [ILER, 1973; KASTNER, 1977]. Such phases may be active in lowering the silica reactivity since dissolution through such a phase is kinetically inhibited and the thermodynamic behavior for a secondary precipitate cannot *a priori* be treated the same as pure biogenic silica.

BSi was cleaned with hot oxidizing acids (2.1.3) to remove organics as well as secondary precipitates caused by possibly adsorbed or bound cations. Therefore, measurements of solubility which differ significantly from the value proposed for acid-cleaned biogenic silica ($\sim 1000 \mu\text{M}$ at 4°C ; HURD, 1973) provide strong evidence for the incorporation of trace amounts of Al or other possible trace metals and their importance for the dissolution kinetics of biogenic opal.

Solubility values of $1000\text{-}1200 \mu\text{M}$ measured for these acid-cleaned phases (phytoplankton (Pn) and particle trap material (Trap)) as well as sedimentary opal samples (Sed) of recent or ancient origin gave no clear evidence for an early diagenetic imprint and subsequent solubility decrease due to the incorporation of trace metals (Fig. 3.15). Nevertheless, lower values were measured in those opal samples containing a significant load of detrital material as well as organic matter.

Acid-cleaned sediment PS-2299 (10-12.5 cm) has almost the same solubility value obtained for a fresh phytoplankton sample from surface waters. However, the untreated material from PS-2299 (Fig. 3.4) as well as PS-2312-1 from the same region (Fig. 3.14) exhibit a marked decrease in solubility.

3. Experimental results and discussion

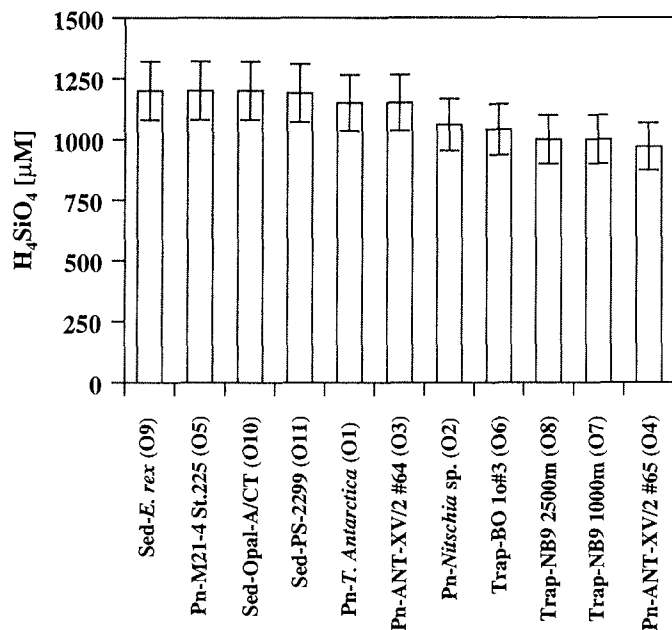


Fig. 3.13 Apparent solubility values for phytoplankton samples (Pn), particle-trap material (Trap), and sedimentary opal (Sed) determined by flow-through experiments at 2°C and pH 8; a slight decrease from 1200 μM to ~1000 μM dissolved silicic acid is apparent in samples (see text). Solubility values were obtained as described in Section 3.1 (see also Fig. 3.3).

Untreated opal samples from sediments, for example a sample consisting of a pure, well-known giant diatom *Ethmodiscus rex* [ABELMANN et al., 1988; BOHRMANN et al., 1994] exhibit no early diagenetic solubility reduction either. Solution resistance of *Ethmodiscus rex*, which has been mentioned previously by SHEMESH et al. [1989], thus may have kinetic reasons (3.1.2.3.1). Results are not surprising since Al concentrations in surface waters of the North Atlantic [6-8 nM; OLAFSSON, 1983] and the Weddell Sea (< 3 nM, MORAN et al., 1992) was significantly lower than in those surface waters where VAN BENNEKOM et al. [1991] observed such a dramatic reduction in solubility. Surface waters of the Arabian Sea were reported to be enriched in dissolved alumina [VAN BEUSEKOM, 1995]. Thus, a slight solubility decrease observed for phytoplankton sample O2 (Tab. 2.2) may be caused by that slightly enhanced aluminum content of surface waters. Whether this solubility decrease is caused by incorporated Al or the slight detrital load (Tab. 3.2) or is simply hidden in the uncertainties of the measurement remains speculation.

In summary, the bimodal character between northern and southern Atlantic Ocean is not supported by large solubility differences among the silica remains during their descent through the water column.

Early diagenetic imprint of the sediment column

Pore water profiles of dissolved silica are usually interpreted as a result of silica early diagenesis. Net dissolution of deposited diatom frustules causes an increase in pore water silica with depth towards apparent solubility. Pore water profiles alone cannot answer the question of solubility changes with depth since profiles in the top section are particularly controlled by other processes such as diffusion or advection through compaction or biologically mediated processes (bioirrigation, bioturbation). These solubility decreases imply further diagenetic interaction between silicic acid and silica-bearing minerals, i.e. reverse weathering reactions [LERMAN, 1979] or interaction of soluble constituents with opal surfaces after burial. Aluminosilicates which are formed during early diagenesis in sediments (*Tertiary alteration*) act as protective layers of biogenic silica. This results in a decrease of apparent solubilities (Fig. 3.4).

With the exception of cores PS-2283-6 and M31/2, solubilities tend to decrease throughout the cores toward values which are generally in good agreement with asymptotic silicic acid values determined in the pore waters (Figs. 3.4 and 3.12). In Figure 3.14, three locations were chosen to illustrate the bimodal distribution (Chap. 1) comparing the northern and southern latitudes [NELSON et al., 1995; SCHLÜTER et al., accepted]. Since phytoplankton samples from different regions do not provide major differences in apparent solubilities (Fig. 3.13, Tab. 3.2) these values were considered as a primary signal from surface waters for both regions. Apparent solubilities of phytoplankton assemblages recalculated for $T = 25^\circ\text{C}$ ($\text{pH } 8$, $p = 1 \text{ atm}$) using the empirical relationship of KAMATANI et al. [1988] ($\sim 1740 \mu\text{M}$) were compared with solubility changes of underlying sediments of the Norwegian Sea (M31/2), the northern Arabian Sea (NAST) and the Scotia Sea (PS-2299).

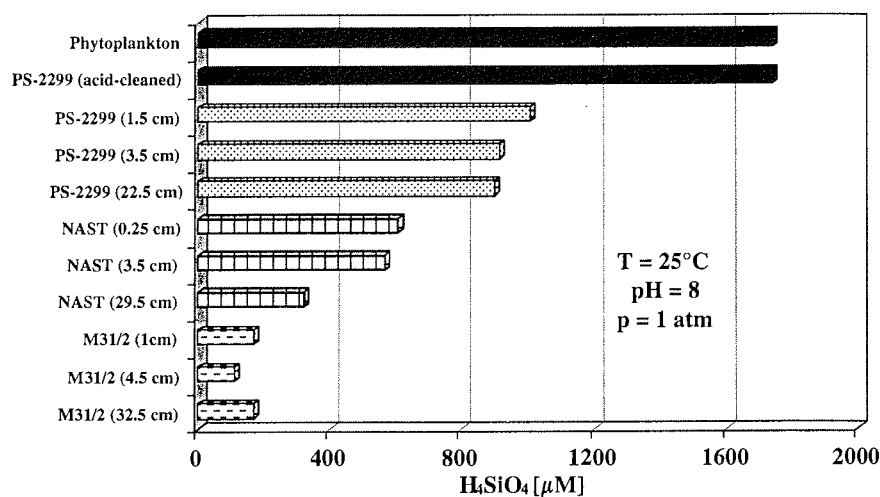


Fig. 3.14 Comparison of solubilities at $T = 25^\circ\text{C}$ of either acid-cleaned phytoplankton or acid-cleaned sediment sample PS-2299 (10-12.5 cm) (Tab. 3.2), and untreated sediment samples from the Scotia Sea (PS-2299), the Arabian Sea (NAST, MC#45) and the Norwegian Sea (M31/2); either 3 different depth horizons show a dramatic decrease of solubilities in the near-surface horizon. Solubility value from the first depth horizon in M31/2 was estimated from batch experiment performed at 60°C (see text).

3. Experimental results and discussion

The existing data suggest that a steep general decrease from surface solubilities towards apparent solubilities at greater depth exists in the first cm below the seafloor. In particle traps at a depth of 1000 m and 2500 m in the Norwegian Sea (NB 8, not shown here), the material also tends to show slightly decreasing solubilities with depth (Tab. 3.2). Solubility values of Southern Ocean sediments decrease only slightly with depth. They remain at fairly high levels throughout the core, whereas solubility values in M31/2 are more than 5 times smaller. The solubility value for the first depth interval (1 cm) of M31/2 was estimated from batch experiments performed in artificial seawater at 60°C [Rickert, unpublished data]. These measurements show almost the same apparent solubility values for both surface and bottom intervals. Thus, surface solubility value estimated for flow-through experimental conditions ($T = 25^{\circ}\text{C}$, $\text{pH } 8$, $p = 1 \text{ atm}$) should almost be equal to bottom value determined, i.e. $\sim 170 \mu\text{M}$. Comparing high northern and southern Atlantic sediment cores biogenic silica contents vary by a factor of ~ 50 . Thus, a logarithmic relationship between opal content and solubility value is expected and is defined by the empiric Equations 3.2 and 3.3 illustrated in Figure 3.18 (see further below).

The role of aluminum

VAN CAPPELLEN and QIU [1997a,b] assume that the first decrease in solubility at the sediment-water interface is related to the increased levels of dissolved aluminum experienced by the diatom debris immediately after reaching the seafloor. The increase in Al levels at the sediment-water interface is proposed to result in an uptake of Al^{3+} by the siliceous surfaces immediately after deposition [VAN BEUSEKOM and VAN BENNEKOM, 1997].

Flow-through experiments were carried out with increasing aluminum concentrations to investigate whether increasing aluminum levels in an open system result in a noticeable decrease in apparent silicic acid concentrations. Assuming that a decrease of reaction rate indicates a tendency of solubility decrease due to the formation of authigenic phases at the surface of biogenic silica, the data gained by aluminum flow-through experiments (3.1.1.2.3) suggest that aluminum levels have to exceed values of 650 nM in inflow solutions to show striking effects on the dissolution behavior of biogenic silica. VAN BENNEKOM et al. [1991] have shown that both the dissolution rate and the equilibrium solubility of diatom silica decrease with incorporated Al; the effect of incorporated aluminum is evident when Al is added in concentrations of $\sim 100 \text{ nM}$. Much higher concentrations were used in LEWIN's [1961] study.

In contrast to recent experiments of DIXIT and VAN CAPPELLEN [1998] significant higher solid/solution ratios were taken in my experiments. This ensures measurable differences of outflow and inflow solution to quantify the retardation effect of various Al on the dissolution behavior of biosiliceous tests. WILLEY et al. [1975] observed that Al removal was most complete in the presence of sediments, and most rapid in the case of amorphous silica, suggesting that the solid phase acts both as a source of dissolved silica which subsequently removes dissolved alumina by coprecipitation, and as a surface which removes aluminum from solution by adsorption (Fig. 3.15).

Since DIXIT and VAN CAPPELLEN [1998] have focused on the adsorption/coprecipitation behavior of dissolved aluminum in the presence of biogenic silica, i.e. on the formation of authigenic aluminosilicates, they used significantly

3. Experimental results and discussion

smaller amounts of biogenic silica to obtain measurable aluminum concentrations in the outflow. Because of the low solid/solution ratio, however, differences of silicic acid in the inflow and outflow solution were not measurable [DIXIT, pers. comm.].

Pore water data from interstitial waters of Arabian Sea sediments also do not support a correlation between low aluminum concentration and high interstitial asymptotic silicic acid values. Pore water silicic acid values among the cores vary between 300 and 600 μM , whereas apparent aluminium levels are about the same. More strikingly, however is a slight positive correlation between subsurface maxima of aluminum, dissolved organic matter [rel. units] and other nutrients (Fig. 3.9) observed in Arabian Sea sediments. For Arabian Sea sediments such a correlation is most obvious for the sites WAST-TOP, EAST and SAST/EAST (Figs. 3.7 and 3.8). This suggests one underlying process, possibly related to adsorption-desorption reactions of aluminum-DOC complexes and the destruction of such complexes in deeper sections by mineralization processes. These would release aluminium which subsequently adsorbs onto mineral surfaces or coprecipitates with silicic acid.

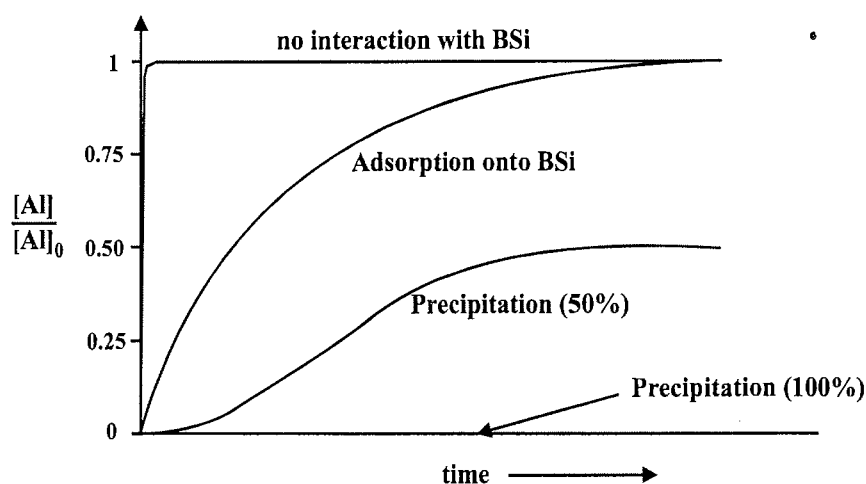


Fig. 3.15 Major processes involved in the interaction of aluminum in contact with sediment and siliceous phases [from: DIXIT and VAN CAPPELLEN, 1998; see also: WILLEY et al., 1975]. The ratio of soluble aluminum measured in the outflow $[Al]$ to aluminum in the inflow $[Al]_0$ in open flow-through systems is plotted versus time. The ratio $[Al]/[Al]_0$ decreases after a sufficient time-span to such an extent that coprecipitation occurs. No interaction with a solid phase would result in negligible decrease as for the adsorption case. In case of adsorption the concentrations of the outflow solution increases slightly towards inflow concentration until surface sites are fully occupied. 100% coprecipitation (possibly coupled with adsorption reactions) was observed in our experiments, since aluminum concentrations were not measurable in the outflow (see text) or the time span of the experiment was too short for reaching 100% adsorption.

3. Experimental results and discussion

Combining the information gained in both experimental approaches [DIXIT and VAN CAPPELLEN, 1998; RICKERT, this thesis] it may be assumed that the level of aluminum found in seawater and interstitial waters of most deep-sea sediments ($[Al] \ll 600 \text{ nM}$) is too low to be the controlling factor for dissolved silica or that the time is indeed too short to demonstrate such a retarding effect in laboratory experiments.

In summary, pore water silicic acid concentrations in the Arabian Sea as well as flow-through experiments gave evidence that soluble Al is not the controlling factor on biogenic silica solubility as long as Al is not incorporated into the silica structure, a process (*primary alteration*) which occurs in surface waters [VAN BENNEKOM et al., 1989; VAN BEUSEKOM, 1991].

On the other hand laboratory experiments by MACKIN [1989] or MICHALOPOULOS and ALLER [1995] and natural occurrence of authigenic phases on silica particles [e.g., HURD, 1973] gave evidence to the fact that the formation of precipitates in the presence of a silicic acid source (glass beads) and clay mineral suspensions is possible. This suggests that a similar reaction may also occur in the presence of biosiliceous material.

Given my laboratory and field results and the latter [MACKIN, 1989; MICHALOPOULOS and ALLER] observations, another mechanism explain low pore water aluminum concentrations, that is the formation of aluminosilicates which are able to contribute to lower apparent solubility values of biogenic silica. These form during early diagenesis of biogenic silica in sediments and do not require a measurable source of soluble aluminum but involve Al by near-simultaneous dissolution-precipitation reactions (Sect. 3.1.2.3.4, Fig. 3.37; see also MICHALOPOULOS and ALLER, 1995).

The role of magnesium

The role of magnesium was focused in experiments which were conducted with the aim to study and simulate conditions of opal preservation in hypersaline brine lakes of Discovery Basin in the western part of the Mediterranean Ridge [e.g., MEDRIFF-CONSORTIUM, 1995; WALLMANN et al., 1997; WALLMANN et al., submitted]. We observed the important role of Mg^{2+} (max. $\sim 5.5 \text{ mol/l}$) in core PC15 as one possible reason for the abundance of well-preserved siliceous microfossils (max. opal contents of $\sim 32 \text{ wt.}\%$). Based on our experimental results (Fig. 3.9), two explanations for opal preservation under extreme Mg-saline conditions are possible:

- (1) Mg^{2+} has extremely high hydration numbers, therefore a great capacity to reduce the amount of free water available to silica solubility [MARSHALL and WARAKOMSKI, 1980]. Since we used artificial seawater in all the experiments instead of 0.7 M NaCl [VAN CAPPELLEN and QIU, 1997 a,b; Tab. 3.1], this may also explain the general lower apparent solubilities and reactivities observed in Southern Ocean sediments of my study compared with corresponding results of VAN CAPPELLEN and QIU [1997a,b].
- (2) The presence of silica and extraordinary high concentrations of Mg^{2+} may influence the formation of authigenic clays [FRITZ et al., 1987; BADAUT and RISACHER, 1983] reducing the apparent silica solubility. In experiments with saline waters, amorphous silica combined with magnesium-rich solutions was reported to form a Mg-hydroxysilicate resembling sepiolite [KENT and KASTNER, 1985]. The mineral sepiolite may form readily on the surface of opal [CHRIST et al., 1973] if conditions in the sediment are favourable to Mg^{2+} adsorption. This decrease in the overall

3. Experimental results and discussion

dissolution rate is embedded in the term $_{11}a_i$, expressed in Equation 2.2 (Sect. 2.5.1); a_i incorporates the unidentified catalytic or kinetical inhibitory effects of Mg^{2+} .

The dissolution of biogenic silica and a subsequent reprecipitation of released silicic acid in diagenetic silicates is extremely site specific, even at the microscale, and is ultimately strongly dependent on silica solution chemistry. Therefore, the influence of magnesium with resulting opal preservation may be significant in the hypersaline brines of Discovery basins, but it should not be taken as a feature for opal preservation under normal marine conditions.

The role of detrital clay minerals

We assumed the detrital content as important phase in regulating solubility values throughout the core which in general showed a slight decrease in solubility (Fig. 3.4). With the increasing deposition of detrital minerals, relative to the input of biogenic silica, the departure of apparent solubility based on asymptotic silicic acid values from a solubility value of a pure biosiliceous ooze is proposed to increase [MACKIN, 1987]. Because biogenic silica is no longer the only component controlling the build-up of silicic acid in pore waters, the system will no longer equilibrate with chemically pure amorphous silica. Rather detrital minerals should be involved in the process of dissolution of amorphous and not well-defined silicates and subsequent reprecipitation of secondary precipitates.

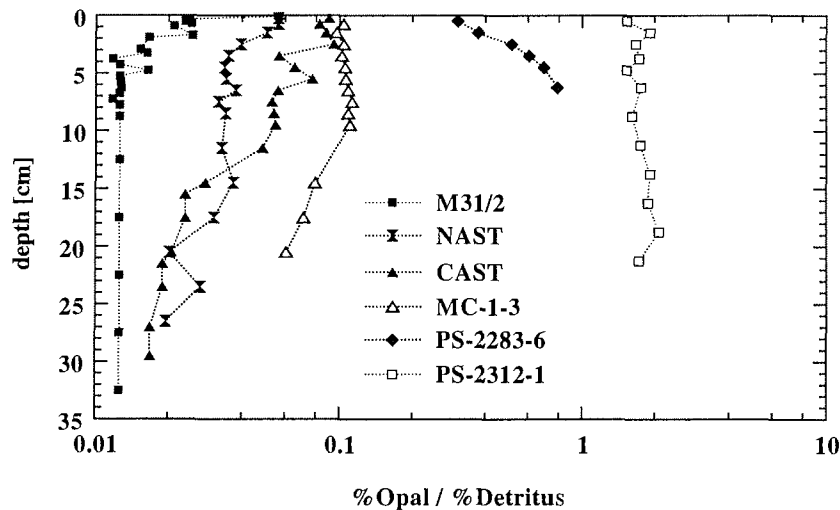


Fig. 3.16 Typical pattern of ratios of biogenic opal and detrital contents as a function of depth (data in A.2.1-A.2.6.4). For reasons of clarity 6 typical patterns were chosen. A comparison of most profiles with the results of solubility measurements follow the general trends observed in Fig. 3.4. For M31/1 we assumed a constant trend with depth (below 8 cm depth) (see footnote, Tab.2.4)

3. Experimental results and discussion

Flow-through experiments with distinct opal/detrital clay ratios (Fig. 3.10) were performed to show the significant lowering of apparent solubilities measured in sample PS-2312-1 (12.5-15 cm) where a significant load of additional detrital clay is present. The results were most significant for kaolinite/opal mixtures (15:1), lowering the apparent solubility by a factor of 15, followed by montmorillonite/opal mixtures (15:1) with a lowered solubility by a factor of 10 and less significant for illite/opal mixtures (15:1) with a decrease by a factor of 4 compared with siliceous ooze sample PS-2312-1 (Fig. 3.10).

Experimental evidence, in conjunction with pore water profiles and sediment opal/detritus ratios (Fig. 3.16) support the hypothesis that reverse weathering reactions [SILÉEN, 1961; MACKENZIE and GARRELS, 1966; MACKIN and ALLER, 1989; MICHAPOLOPOULOS and ALLER, 1995] may occur in recent marine sediments soon after deposition and may explain the variability around different asymptotic pore water silicic acid concentrations (Fig. 3.10). In the following section we will discuss the general pattern for the opal/detritus ratio observed (Fig. 3.16) and focus on the main environmental reasons which appear to cause marked differences between the cores.

In Figure 3.16 a significant decrease is shown for M31/2 in the upper section. With almost constant opal contents (~1 wt.%), but a dramatic decrease in additional CaCO₃ from almost 80% at the top to ~6% at 5 cm depth, the opal/detritus ratio changes by a factor of ~5. A subsequent decrease in solubility is expected.

Batch experiments performed at 60°C [Fig. 3.17; RICKERT, unpublished results] were carried out to reveal the relative order of solubility changes as expected from the opal/detritus ratio with a decrease and subsequent increase towards the bottom of the core where opal contents show an increase. The temperature of 60°C was essential to reach a solubility value in reasonable experimental times. Batch experiments at 2°C and 19°C failed to reach equilibrium probably due to the kinetic control of Si and Al release by secondary precipitates.

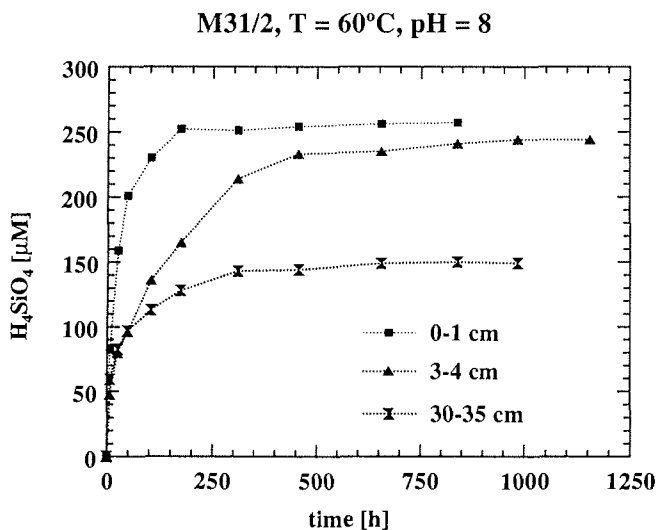


Fig. 3.17 Change in silicic acid concentration of untreated sediments from core M31/2 in artificial sea water (pH 8) at 60°C reveal differences in reactivity as well as differences in apparent solubilities (see text).

3. Experimental results and discussion

A more general pattern is represented by sediments derived from NAST location (Arabian Sea, Fig. 2.1) with a steady decrease of the opal/detritus ratio with depth. Apparent solubilities as shown in Figure 3.4 follow that decrease. Opal/detritus ratios from Southern Ocean sediments PS-2312-1 (Fig. 3.16), PS-2299 and PS-2314-1 do not change markedly with depth. Thus, apparent solubilities obtained in flow-through experiments do not exhibit a clear trend with depth either (Fig. 3.4). This is in general agreement with results from VAN CAPPELLEN and QIU [1997 a,b]. Clearly different, however, is the observation of a significant increase of solubility in PS-2283-6 (Fig. 3.4), accompanied by an increase in opal/detritus ratios (Fig. 3.16). The lower apparent solubilities measured in the first centimetres are supposed to be related to volcanic ash debris from the Mount Hudson eruption in 1991 [BOHRMANN, pers. comm.; e.g., SCASSO et al., 1994]. Dissolution of these ash particles may produce high levels of aluminum [VAN CAPPELLEN and QIU, 1997a,b] or may have distinctly lower solubility values in comparison to biogenic opal and thus cause overall lower apparent solubilities.

Experiments by MACKENZIE and GARRELS [1965] and MACKENZIE et al. [1967] revealed that clay minerals can release silicic acid to *seawater* depleted of the element and take it up from solution in enriched *seawater*. The uptake also involves dissolved cations and leads to the formation of new, poorly-defined aluminosilicate phases. SIEVER and WOODFORD [1973] considered silicate reconstitution a doubtful mechanism for a partial control of silica and cation composition of seawater but assumed it to be a reasonable mechanism in *interstitial waters*.

Although the release-uptake of silica between clays and solution is quite complex, there is evidence that in some cases silica behaves as if it were adsorbed, equilibrating rather rapidly after changes in composition or in temperature [e.g., GIFFORD and FRUGOLI, 1964; MCKEAGUE and CLINE, 1963; FANNING and PILSON, 1971; SIEVER and WOODFORD, 1973], whereas in other cases silica is released or incorporated slowly [MACKENZIE and GARRELS, 1965; MACKENZIE et al., 1967; WOLLAST, 1967; SIEVER and WOODFORD, 1973]. SIEVER and WOODFORD [1973] studied the interaction of clays in various natural waters. They found that the rate of silica release or uptake was time-dependent, being more rapid at first. Clays placed in silica-rich water would remove soluble silica from the aqueous phase whereas clays placed in silica-poor water would release silica. These reactions appear to involve an adsorption-desorption process followed by diffusion-controlled, bulk phase reactions. WOLLAST [1967], LUCE et al. [1972] and others have observed such processes as well. We already mentioned a nontronite formation in 20 cm sediment depth was described. Silicic acid concentration of $\geq 250 \mu\text{M}$ are sufficient for that possible sink of dissolved silica in seawater (Eq. 3.1) [LERMAN, 1979 and Sect. 3.1.1.2.4]. HURD [1973] has reported about iron, magnesium and calcium aluminosilicates which may represent the minerals forming on the surface of opal. All diagenetically formed aluminosilicates as well as detrital minerals in general are active reducing the solution rate as well as the apparent solubility of biogenic silica since aluminosilicate minerals have their own specific thermodynamically defined solubility value. The apparent solubility value, thus a weighted average of the solubilities of different siliceous phases, is the result of this implying that dissolution and reprecipitation rates at equilibrium are nearly the same.

3. Experimental results and discussion

The solubility of acid-cleaned sample PS-2299 (10-12.5 cm) closely agrees with that of fresh diatoms collected in surface waters (Figs. 3.13 and 3.14), whereas untreated samples from the same sediment exhibit significantly lower values (Figs. 3.4 and 3.14). This is consistent with the hypothesis that early diagenetic processes at the silica surface exert to a significant degree control on the build-up of silicic acid in sediments. Since an acid-cleaning procedure [see also HURD, 1973] results in the removal of diagenetically altered surface layers and authigenic surface precipitates from the particles, it is not surprising that solubilities of untreated samples are lower. Nevertheless, untreated biogenic silica samples observed in deeper sections of cores PS 1465 (Weddell Sea) and PS-2070-1 (Maud Rise) with an age of ~ 4 Myr at the sediment-water interface reveal almost the same solubility as acid-cleaned sedimentary opal from surface sediments. The reason for this observation is the fact that these samples are fairly pure opal samples (see analyses in Tab. 3.2). Considering their reactivity in terms of dissolution rate constants, k_{CFT} , however, significant lower values than those for acid-cleaned sediment samples were observed (Tab. 3.4, Sect. 3.1.1.2.1). This phenomenon will be discussed in Section 3.1.2.3.3.

Combining apparent solubilities from pore waters ($T \sim 2^\circ\text{C}$) with the logarithmic ratio of the detrital and biosiliceous contents of the sediments (A.2.1-2.6.4), results in an inverse relationship (Fig. 3.18) which can be divided in two sections with different slopes following these empirical relationships:

$$[1.8 \geq x \geq 0.32] \quad \text{Si}_{\text{sat}} = -363 x + 804 \quad (3.2)$$

$$[0.32 \geq x \geq -0.91] \quad \text{Si}_{\text{sat}} = -126 x + 727 \quad (3.3)$$

Hereby x is the logarithmic ratio of detrital and biosiliceous contents of the sediments. $x = 0.32$ corresponds to an asymptotic silicic acid value of $\sim 700 \mu\text{M}$. Silicic acid concentrations $< 700 \mu\text{M}$ are best described by Equation 3.2, whereas lower ratios are best explained by Equation 3.3. Since this equation is only fed by the limited data set reported in this study and by results of VAN CAPPELLEN and QIU [1997 a,b], it should be treated as a first approximation to describe silicic acid values as a function of sedimentary composition in deep-sea sediments with respect to siliceous phases at a given temperature and ambient pressure. The depth-dependent solubility distributions among the cores which are not visible *a priori* in pore water silicic acid concentrations due to transport processes, but measurable in flow-through experiments, are best explained by the differences in opal/detritus ratios. Clearly, dissolved interstitial silicic acid concentrations may react with the major cations (for example Mg^{2+}) as well as with the minor cations of seawater such as Al^{3+} . But since experiments as well as the pore water data on aluminum in Arabian Sea sediments do not support a significant role of aluminum, we think that reverse weathering reactions [e.g., SILLÉN, 1961; MACKENZIE and GARRELS, 1966; LERMAN, 1979; STOFFYN-EGLI, 1982; MACKIN, 1989; MICHALOPOULOS and ALLER, 1995] are the most favored process controlling the build-up of silicic acid in pore waters. Thus the dissolution of biogenic silica resulting in increasing silicic acid concentrations is balanced by the precipitation of silicic acid in the presence of detrital materials with distinctly lower solubilities than an acid-cleaned siliceous ooze. This is in general agreement with the conclusions of VAN CAPPELLEN

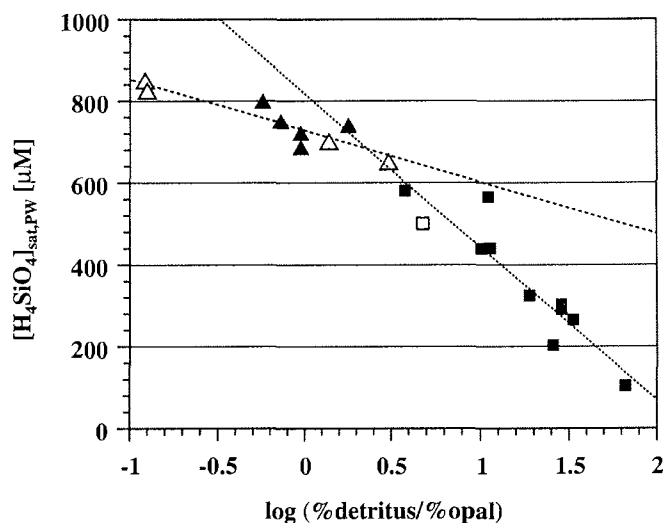


Fig. 3.18 Relationships (I. squares, II. triangles) between sediment composition and pore water silicic acid (filled symbols). The assumed asymptotic silicic acid concentrations measured at depth are plotted against the logarithmic ratio of the average detrital and biogenic opal contents of the cores (Tab. A.2.1-A.2.6.4). Results of VAN CAPPELLEN and QIU [1997 a,b] for the Southern Ocean are included (open symbols).

and QIU [1997]; the magnitudes of asymptotic silicic acid values and experimental solubilities of biogenic opal in the deepest section of the cores, however, exhibit the same relative order of values. Thus, in my opinion, the role of aluminum in pore waters is less important than proposed by VAN CAPPELLEN and QIU [1997]. Indeed opal/detritus ratios control the silicic acid levels measured in pore waters, which in turn control dissolved alumina levels.

The source of Al which is needed in some reactions forming aluminosilicates during early diagenesis of biogenic silica [MICHALOPOULOS and ALLER, 1995] may be unstable amorphous Al oxides or highly weathered aluminosilicates. Since there is no significant evidence for usually high concentrations of dissolved aluminum throughout the pore water which may be high enough ($Al > 600$ nM, inferred from Al flow-through experiments, Fig. 3.6) to significantly influence silicic acid values in the experiments, I favor a close coupling of dissolution and reprecipitation reactions without build-up of dissolved Al intermediates. This mechanism does not preclude its involvement in a near simultaneous dissolution-precipitation process [e.g., MICHALOPOULOS and ALLER, 1995] but aluminum in pore waters where concentrations do not support a large involvement in precipitation reactions to that extent that the solubility of biogenic silica is significantly lowered. The two proposed mechanisms to form authigenic minerals during early diagenesis and to control the build-up of pore water silicic acid are (Fig. 3.37, Sect. 3.1.2.3.4):

- (A) Simultaneous dissolution and precipitation (MICHALOPOULOS and ALLER, 1995; RICKERT, this thesis)
- (B) Coprecipitation of silicic acid and aluminum (VAN CAPPELLEN and QIU, 1997a,b)

3. Experimental results and discussion

Actually, the concept of reverse weathering has not gained wide acceptance because of the lack of direct evidence for precipitation of significant amounts of diagenetically formed minerals. Indeed, the identification of such newly formed solid phases by XRD is extremely difficult due to its often amorphous structure. Nevertheless, LERMAN [1979] reported the occurrence of nontronite. There, the very fine size fraction ($< 0.2 \mu\text{m}$) of the sediment and low concentrations of authigenic phases in the bulk sediment point to the general difficulties that are encountered in identification of the mineral sinks for dissolved chemical species in sediment-pore water regimes. Additionally, a rapid clay mineral formation in Amazon Delta sediments [MICHALOPOULOS and ALLER, 1995] and laboratory experiments with glass beads as a source of silicic acid [MACKIN, 1989] reveal that reverse weathering may indeed constitute a major sink for silicic acid in marine environments.

3.1.1.3.3 Geochemical implications for early diagenetic modeling of biogenic silica dissolution

For the description of early diagenesis of biogenic silica in the sediment column, models with a single rate expression representing the net production of dissolved pore water silicic acid from dissolving silica [e.g., SCHINK et al., 1975; BOUDREAU, 1990; RABOUILLE and GAILLARD, 1990] are used to interpret local profiles of silicic acid and biogenic opal. In modeling pore water silicic acid or even in laboratory studies, all predictions are largely a function of the total saturation deficit ($1 - \text{Si}/\text{Si}_{\text{sat}}$) (Eq. 2.8). Hereby it is important to know whether a theoretical value of Si_{sat} , for example based on the solubility of amorphous opal, or an apparent value measured in flow-through experiments is best to be taken. Another possibility is *ad hoc* setting Si_{sat} equal to the observed asymptotic pore water silicic acid values [SCHINK and GUINASSO, 1980]. Possible modifications to present models are now discussed taking into account the present laboratory results of solubility control in deep-sea sediments (3.1.1.3.2):

The asymptotic concentration

The fact that the theoretical solubility of amorphous silica is rarely attained at shallow depths during early diagenesis is attributable to the additional content of non-biosiliceous phases which leads to a balance of dissolution/precipitation reactions and finally to lower apparent silica solubilities than that of pure biosiliceous ooze.

In addition to this effect, the kinetics of dissolution become inhibited (3.1.2), but this is not directly attributable to a general decrease of solubility with depth, since solubility values in flow-through experiments carried out with artificial seawater are in general agreement with pore water silicic acid concentrations, although reaction rate constants vary by orders of magnitudes (3.1.2.2, Fig. 3.23).

The depth-dependent reduction of solubility by surface inhibition processes are taken into account by replacing $[\text{Si}]_{\text{sat}}$ (Eq. 2.8) with an appropriate depth-dependent function (3.2.3.3.1). This should preferably be calculated by an appropriate mechanistic model based on results from flow-through experiments for each sampling interval or could be calculated from the proposed expressions (Eqs. 3.2 and 3.3) and measurements of depth-dependent detrital/opal contents as well. Accordingly the preservation of biogenic silica represents no longer „something of an enigma“ [SCHINK et al., 1975], but can

unambiguously be attributed to the overall thermodynamic control of apparent solubility by the detritus/opal ratio (Eq. 3.2 and 3.3).

Other early diagenetic reactions

Whereas experiments and field data of this study were focused on early diagenetic processes, other mineralogical and chemical changes in the silicic acid-silica system remain unconsidered, for example transformations of opal-A to opal-CT or crystalline quartz which occur well below the top metre of sediments with increasing depth [CALVERT, 1971; KASTNER et al., 1977; WILLIAMS et al., 1985; WILLIAMS and CRERAR, 1985; HESSE, 1988].

My experiments provide strong evidence for formation of aluminosilicates or at least for the possibility of other silica-bearing minerals (for example clays), adjusting the asymptotic silicic acid value below the solubility of biogenic silica (Fig. 3.10).

Therefore, the conservation equation for dissolved silica (Eq. 3.17) should include at least two rate expressions, one representing the production of pore water silicic acid, the other accounting for its precipitation through non-biosiliceous phases (for example clay minerals) [BOUDREAU, 1990; VAN CAPPELLEN and QIU, 1997 a]. Thus, the diagenetic equation (Eq. 3.12) in Section 3.2.2.1 becomes:

$$\frac{d}{dx} \left(\varphi(x) D_s \frac{dSi}{dx} \right) + \varphi(x) R(x)_{pw} - \varphi \sum_{j=1}^m R_{clay} = 0 \quad (3.4)$$

The aim of my thesis was to identify the processes which are responsible for the change in reactivity and solubility of biogenic silica in different sediment types. The implications of these processes, i.e the incorporation of the experimental findings in numerical models should be encouraged in existing numerical model approaches (for further recommendations see BOUDREAU [1990] and references cited there).

Input of multiple opal types differing in the solubility and reactivity constant values

Solubility differences among different opal types can also be taken into account [BOUDREAU, 1990], although we have not obtained a distinct solubility difference between the various types of opal samples. Therefore, it is assumed that lower solubilities are best explained by early diagenetic interaction of biosiliceous ooze as a bulk phase and other non-siliceous phases. Different solubilities of the multiple opal types *must* be taken into account if evidence of significant incorporation of aluminum into the structure of siliceous microfossils and the subsequent decrease in solubility is given as reported for the Zaire deep-sea fan by VAN BENNEKOM et al. [1989].

3.1.1.4 Conclusion

The main findings from the experimental and field data are:

- (1) Asymptotic pore water concentrations of dissolved silica in changing sedimentary regimes vary from ~100 μM to almost 800 μM .
- (2) Apparent solubilities of biogenic silica determined by means of continuous flow-through experiments in untreated sediment samples (of the deepest section of 11

3. Experimental results and discussion

cores) exhibit a relative order of values similar to those asymptotic values observed in the field.

- (3) Asymptotic silicic acid values truly reflect an equilibrium between pore water and a multi-component siliceous solid phase system; these values should be treated as apparent solubilities of biogenic silica.
- (4) In general, apparent solubilities tend to decrease with sediment depth suggesting the inclusion of a depth-dependent saturation value in the early diagenetic models of biogenic silica dissolution.
- (5) With increasing deposition of detritus, relative to biosiliceous material, the departure of apparent solubility from solubility of an acid-cleaned siliceous ooze ($\sim 1000 \mu\text{M}$, 4°C) increases systematically.
- (6) Flow-through experiments performed with clay/opal mixtures reveal a drop of solubility when detrital clays are present.
- (7) The main environmental factor which controls the build-up of dissolved silica in sediment pore water is the ratio of detrital and biogenic silica content in the sediment. The apparent solubility value is a weighted average of solubilities of the siliceous phases present in the sediment.
- (8) Experimental evidence and pore water aluminum data suggest that dissolved alumina levels are unlikely to control dissolved silica concentrations. However, the role of Al in silica early diagenesis will be further debated.
- (9) Since no evidence for high Al concentrations in the pore waters of deep-sea sediments is given which would lead to measurable interaction between dissolved Al and Si, a close coupling of dissolution and precipitation reactions (reverse weathering reactions) without build-up of dissolved Al intermediates is favored; this mechanism does also not preclude the involvement of Al in near simultaneous dissolution-precipitation processes.
- (10) Extremely high concentrations of magnesium ($\sim 5.5 \text{ M}$) control the preservation of opal in hypersaline brines.
- (11) Minor solubility differences ($1000\text{-}1200 \mu\text{M}$) between single opal samples which were determined by means of flow-through experiments ($T = 2^\circ\text{C}$, $\text{pH } 8$) do not support the idea that solubility differences among different opal samples explain the bimodal character of northern and southern Atlantic.
- (12) From a chemical point of view, a kinetic control (for example degree of silicification, surface area, organic and inorganic coatings) is favored as an explanation for different preservation efficiencies. This control is closely coupled to a biological control, i.e. the bulk of biogenic silica escapes dissolution in the water column where the efficiency of bacterial removal of the organic matrix from diatom shells is inhibited under iron deficiency (BIDDLE and AZAM, 1999).
- (13) Solution resistance of *Ethmodiscus rex*, a giant diatom ($\sim 4 \text{ Myr BP}$) is kinetically-controlled largely because of an extremely small specific surface area ($\sim 2 \text{ m}^2/\text{g}$); the thermodynamically-controlled solubility value is comparable to that of acid-cleaned phytoplankton samples.

3.1.2 Dissolution kinetics

3.1.2.1 Introduction

Recent investigations on the dissolution kinetics of amorphous silica have provided a valuable insight into many of the factors affecting dissolution rates. A general rate law (Eq. 2.2) for dissolution and precipitation which combines all these factors is given in LASAGA et al. [1994]. The most widely used expression to fit silicic acid versus time data measured in batch experiments on mostly pure biosiliceous materials was already mentioned. The measurements followed a first-order kinetic law in which the rate depends linearly on the degree of undersaturation (Eq. 2.8) [e.g., O'CONNAR and GREENBERG, 1958; HURD, 1972; WOLLAST, 1974; LAWSON et al., 1978; KAMATANI et al., 1988]. Laboratory-based experiments by means of flow-through reactors [e.g., CHOU and WOLLAST, 1984], provided striking evidence for non-linear dissolution and precipitation kinetics (see Section 2.5 and references cited there). For the silica-system it was FLEMING [1985] who first observed an exponential increase of the dissolution rate with increasing undersaturation. BERGER et al. [1994] observed such a non-linear behavior for quartz and recently VAN CAPPELLEN and QIU [1997a,b] published the first results of flow-through experiments performed on biosiliceous oozes from the Southern Ocean. These data also disagree with the linear rate law generally used to describe the dissolution kinetics of biogenic silica.

To estimate the effect of non-linear dissolution kinetics on opal dissolution in the water column where the undersaturation is low the first flow-through experiments were conducted on almost pure opal samples (phytoplankton as well as diagenetic altered opal-A/CT, Sect. 2.2, Tab. 2.2). In the sediment regime, the effect of non-linear dissolution kinetics would be most dramatic in some few topmost millimetres where departure from apparent solubility is greatest [VAN CAPPELLEN, 1996; VAN CAPPELLEN and QIU, 1997a,b].

Mineral substitution reactions in which primary minerals dissolve and secondary minerals precipitate are typical under natural conditions. Thus, it is important to understand these processes not only isolated from each other but also with their interactions. Previous studies carried out by means of flow-through experiments have usually been performed on well-defined mineral assemblages [e.g., DOVE and CRERAR, 1990; NAGY and LASAGA, 1991; NAGY and LASAGA, 1992; BURCH et al., 1993]. Other batch or flow-through experiments performed on biogenic silica provide results from a distinct environmental setting [e.g., HURD, 1973; VAN CAPPELLEN and QIU, 1997a,b; RAGUENEAU et al, submitted].

Dissolution experiments described in this thesis were carried out to examine the decrease in reactivity of biosiliceous remains produced in the euphotic zone as they evolve, during their transfer to the sea floor and after deposition in various sedimentary environments. A comparison of the dissolution kinetics in opal-dominated samples (phytoplankton samples and biosiliceous oozes) with the behavior of sediments with minor biogenic silica content provides major insights on the controlling factors of solubilities and reaction rates. Flow-through reactors are suited for studying dissolution kinetics while maintaining constant pH, temperature, electrolyte composition and undersaturation with respect to biogenic silica or to possible secondary phases. Furthermore, it is possible to directly monitor reactivity decreases of biosiliceous

3. Experimental results and discussion

remains within the sedimentary column without yielding the answer to which extent those variations are due to reduced specific reactive surface areas or the preferential dissolution of a more reactive fraction.

In free-drift, batch reactor experiments, however, one cannot distinguish between rate changes due to changing undersaturation of the solution and alteration of the solid silica due to secondary reactions [e.g., DREVER, 1997; VAN CAPPELLEN and QIU, 1997a,b].

The flow-through and batch experiments (2.5.4.1) provide important evidence that possible interfering secondary reactions may only be successfully suppressed in sediments enriched with biogenic silica (siliceous oozes or pure opal samples), i.e. almost homogeneous samples. In sediments dominated by other than biosiliceous phases, significant evidences for heterogeneous reactions were gained, particularly when using artificial seawater.

Another key parameter of the dissolution rate of biogenic silica is the amount of reactive surface area exposed by the skeletal particles [e.g., HURD, 1973, 1983; KAMATANI and RILEY; DOVE and ELSTON, 1992; VAN CAPPELLEN, 1996]. The reactive surface area, however, is probably the most difficult one to quantify in natural environments [e.g., DOVE and RIMSTIDT, 1994; CASEY and WESTRICH, 1993; VAN CAPPELLEN, 1996]. Surface areas are conventionally determined by gas adsorption methods based on the BET theory [BRUNAUER, EMMETT and TELLER, 1938] (2.4.7). It has commonly been assumed that surface areas determined on dried samples provide a good proxy for fitting surface areas available for dissolution or precipitation reactions. A systematic study of HURD et al. [1981] using the nitrogen gas adsorption method has made it clear that BET surface areas of biosiliceous samples in deep-sea drilling cores indeed decrease, but on time scales which by far exceed those (1000-10000 years) relevant for surface sediments of interest. Thus, if the specific surface area of these particles does not change with depth, the total surface area and consequently the dissolution rate R should be proportional to the concentration of biogenic silica in the sediment. Most models of silica early diagenesis (Eq. 2.27, Sect. 2.6) are based on this assumption, yet it will be proven that this assumption is only partly fulfilled.

VAN CAPPELLEN and QIU [1997a,b] observed a decrease in reaction rate constants with sediment depth while the BET surface areas maintained constant. This observation indicated that a decrease in reactivity is not matched by a corresponding change of BET surface areas. Surface reactivity is more likely represented by *reactive* surface area, i.e. surface densities of silanol ($\equiv\text{Si-O}$) groups exposed by the skeletal particles [e.g., WIRTH and GIESKES, 1979; FLEMING, 1986; BRADY and WALTHER, 1990; DOVE and ELSTON, 1992; DOVE and RIMSTIDT, 1994]. Furthermore, in the standard kinetic expression used to account for silicic acid production in early diagenetic models of biogenic silica it is usually assumed that the net rate of pore water silicic acid production is directly proportional to the bulk concentration of biogenic silica at a given depth [e.g., SCHINK et al., 1975; RABOUILLE and GAILLARD, 1990]. The relative changes of the net rate of silica dissolution observed in Southern Ocean sediment cores [VAN CAPPELLEN, 1996], however, are much larger than those of the biogenic silica concentration. Accordingly, it seems unlikely that this linear relationship mentioned before can account for relative changes in reactive surface area. The reactive surface area is, however, as difficult to quantify in natural environments as BET areas of

3. Experimental results and discussion

biogenic silica in mixed sediment samples. Sediments represent a mixture of primary and secondary minerals besides biogenic opal. Thus, it is extremely difficult to apportion the total physical (BET) area between these different phases to yield an opal surface area. Any present clay minerals or oxides can distort the results by adding an unknown but often large amount of surface area (Tab. 3.5).

Cobalt adsorption experiments applied to determine relative changes in reactive surface area in Southern Ocean sediments [VAN CAPPELLEN, 1996; VAN CAPPELLEN and QIU, 1997a,b] have the advantage of being faster and simpler than flow-through experiments; unfortunately, this method has to be restricted to rather pure siliceous oozes.

In this thesis, the evolution of reaction rate of biogenic opal in heterogeneous sediments is documented by flow-through experiments over the full range of undersaturation with respect to biogenic silica. Additionally an alkaline leaching technique is proposed for the determination of surface reactivity changes throughout the core, without being restricted to almost pure siliceous oozes or samples. Depth distributions of rate constants k_{NaOH} determined using that technique were compared with results derived from the cobalt adsorption method [VAN CAPPELLEN, 1996; VAN CAPPELLEN and QIU, 1997] as far as this seemed justified for the samples of interest. Only two sediment cores from the Southern Ocean were chosen due to the restricting factors mentioned above. Moreover, the results of BET measurements taken from untreated and treated acid-cleaned sediment samples or opal samples are presented.

An important question that has still to be addressed deals with the bimodal character of biogenic silica, that is the puzzling relation of “high productivity (75-90% of the world production) and low preservation” of opal in the northern Atlantic [NELSON et al., 1995; SCHLÜTER et al., submitted] and “low productivity (10-25% of the world production) and high preservation” of opal in the southern Atlantic.

The laboratory results of sediment, phytoplankton or particle trap material, i.e. reaction rate constants representing water column processes and variations of dissolution behavior in connection with sediment/pore water processes, and important constraints created by these kinetic signals are discussed.

3.1.2.2 Results and preliminary discussions

3.1.2.2.1 Apparent reaction rates at 2°C and 25°C

Rate determination: Principles

In flow-through experiments, rates were determined after steady state was reached, i.e. when silicic acid concentration of the outflow was observed constant in several consecutive samples (Fig. 3.1). Accordingly, number of analyses of the outflow solutions were enhanced at the end of the run. Because the sediment suspension is well-mixed the influences of mass-transport, for example by diffusion due to gradients within the system gathered, are negligible. Solution composition in the reactor can be taken as identical to that of the collected outflow solution [e.g., BURCH et al., 1993]. The analysis of rate data collected from a mixed-flow reactor is possible from a simple mass balance at steady state, expressed in the following formula:

3. Experimental results and discussion

$$\frac{dn_{\text{Si}}}{dt} = 0 = v \cdot \Delta[\text{Si}] - S_{\text{BSi}} \cdot m_{\text{BSi}} \cdot R' \quad (3.5)$$

n_{Si}	number of moles of Si in reactor solution [μmol]
v	volume flow rate [l h^{-1}]
$\Delta[\text{Si}]$	difference between outflow and inflow solution of Si in experiment [$\mu\text{mol l}^{-1}$] $\Delta[\text{Si}] = [\text{Si}]_{\text{out}} - [\text{Si}]_{\text{in}}$ (Fig. 3.1)
S_{BSi}	BET specific surface area [$\text{m}^2 \text{g}^{-1}$]
m_{BSi}	mass of extractable biogenic silica within the sediment [g]
R'	dissolution rate determined by continuous flow-through (CFT) reactor [$\mu\text{mol m}^{-2} \text{h}^{-1}$]

In this formulation, dissolution rates (R_{diss}) are positive and precipitation rates (R_{ppt}) are negative. With $R = R' S_{\text{BSi}}$ steady state rates are calculated rearranging the right-hand side in Equation 3.5:

$$R = \frac{v \cdot \Delta[\text{Si}]}{m_{\text{BSi}}} \quad (3.6)$$

Since the determination of BET surface areas for an assemblage of various species with different degrees of silicification and within a heterogeneous sediment matrix effected by clay minerals, is somewhat arbitrary (3.1.2.1), an expression for rates of silicic acid release to solution per unit mass biogenic silica was assumed to be more reliable [VAN CAPPELLEN and QIU, 1997a,b].

The error in rate calculation using Equation 3.6 is dominated by the uncertainties of $\Delta[\text{Si}]$ ($\leq 5\%$). These result from the standard deviation of averaged concentrations during steady state and from the mass loss Δm ($\leq 5\%$) caused by the dissolution of biogenic silica during the course of the experiment. The amount of solid silica during an experiment can be treated as approximately constant. The uncertainty of flow rate is not greater than 0-1%. Accordingly, the error in rate from Equation 3.6 does not exceed the magnitude of $\pm 10\%$, but would increase significantly if surface areas with absolute accuracies of $\pm 10\%$ are included. A better reproducibility ($\sim 5\%$) is achieved from the single point BET measurements (2.4.7) used in this study.

Rate dependence on solution saturation state

The dependence of measured steady state dissolution rates R_{CFT} using continuous flow-through (CFT) reactors on solution saturation state is shown in Figure 3.19. The functional dependence $f(\Delta G_r)$ accounting for the variation of the rate with the deviation from equilibrium according to the general rate law for dissolution and precipitation [e.g., LASAGA et al., 1994] (Eq. 2.2) can be expressed by $(1 - [\text{Si}]/[\text{Si}]_{\text{eq}})$, the relative degree of undersaturation (2.5.1). The linear rate law, which is almost universally used by geochemists to describe the dissolution and precipitation kinetics of biogenic and amorphous silica (Eq. 2.8 or 2.13 with $m = 1$) [e.g., O'CONNOR and GREENBERG, 1958; HURD, 1973; WILLEY, 1974; KAMATANI and RILEY, 1979; VAN BENNEKOM et al., 1991; BARKER et al., 1994], was applied to the data from flow-through experiments on single opal samples at 2°C (Fig. 3.19). Kinetic data collected from flow-through experiments with sediments at 25°C and batch experiments deployed at 60°C [RICKERT, unpublished

3. Experimental results and discussion

results] over the full range of undersaturation could not be dealt with in that way. The data fitted to Equation 2.13 provide that $m = 1$ is not as universal as considered before [see also VAN CAPPELLEN and QIU, 1997 a,b) and suggest a more complex dissolution mechanism.

On the basis of Equation 2.13 (Sect. 2.5.1) reaction rate constants k_{diss} [yr^{-1}] from flow-through experiments were obtained:

$$R_{\text{diss}} = k_{\text{diss}} \left(1 - \frac{[\text{Si}]}{[\text{Si}]_{\text{eq}}} \right)^m \quad (2.13)$$

These values are compared with k_{B} [yr^{-1}] [e.g., SCHINK et al., 1975] derived from pore water fitting procedure in Section 3.2.3.3.2.

Apparent reaction rates of opal samples at 2°C

To track the evolution of reactivity decreases among biogenic silica assemblages due to preferential elimination of more reactive particles or due to surface aging processes [VAN CAPPELLEN, 1996], dissolution-flow through experiments were carried out with BSi samples collected in the water column at various depths, surface sediment samples from different depth horizons and deeply buried diagenetically altered biogenic silica (3.1.1.2.1).

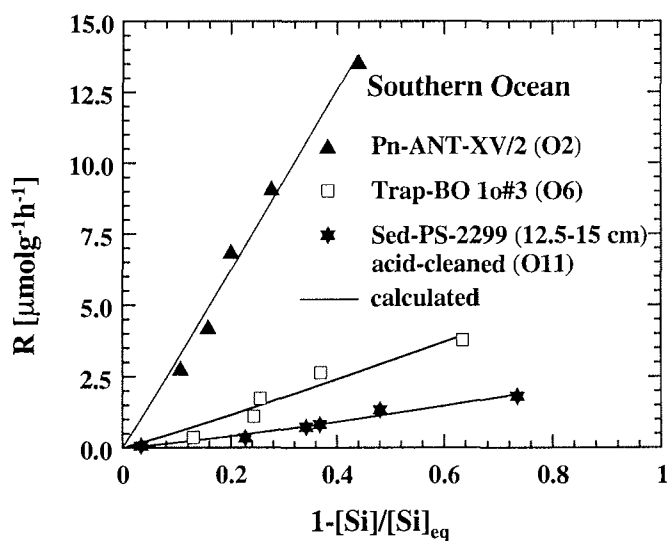


Fig. 3.19 Dependence of silica dissolution rate at 2°C and pH 8 of Southern Ocean acid-cleaned phytoplankton (Pn), siliceous particle trap (trap) and sediment (Sed) samples on the degree of undersaturation of the reactor solution. The rate data and symbols are the same as those in Fig. 3.3. The degree of undersaturation is calculated using solubility values inherited from extrapolation of dissolution rates to the x-axis of Fig. 3.3 (see text). Data for these three samples fitted to Equation 3.13 (straight line) come to $m \sim 1$. It must be noted that we did not consider the full range of undersaturation. Thus, the obvious linearity is restricted to the given undersaturation states.

3. Experimental results and discussion

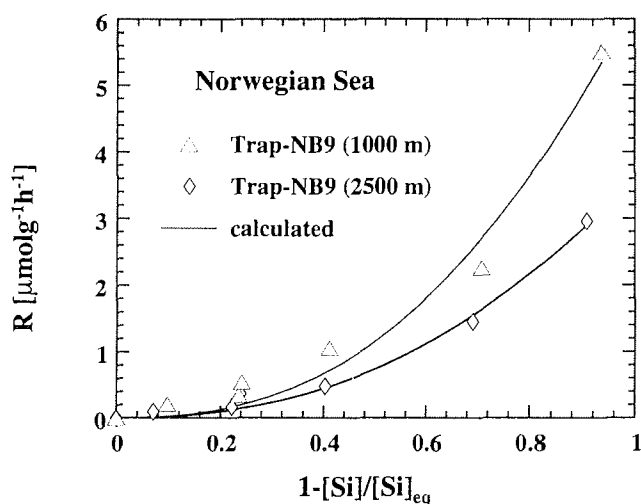


Fig. 3.20 Silica dissolution rates at 2°C and pH 8 measured on untreated sediment trap material from Norwegian Sea. Here, data were fitted to a fully non-linear rate law (Eq. 2.13) with $m \neq 1$. The transition from a linear towards a non-linear behavior is most obvious when exceeding undersaturation states > 0.5 . Note, that reactivity decreases with depth. Again, rate data and symbols used are the same as those in Fig. 3.3.

Apparent solubilities of the opal samples vary within a fairly narrow range (1000-1200 μM at $T = 2^\circ\text{C}$ and $\text{pH} = 8$; Tab. 3.2). The silicic acid production can be ascribed entirely to biogenic silica dissolution because these samples contain almost pure biosiliceous remains with the exception of untreated samples (Pn-ANT-XV/2, Trap-NB9 (1000m), Trap-NB9 (2500m)). These untreated samples provide the lowest solubility values among single opal samples ($\sim 1000 \mu\text{M}$). But Figure 3.3 (3.1.1.2.1), implying that although a significant variation in solubility occurs, i.e. thermodynamic behavior changes, the dissolution kinetics exhibit striking differences. In terms of reaction rates versus degree of undersaturation, biosiliceous remains in the water column settling down to the sediment water interface were investigated. A clear reduction in opal reactivity was observed for acid-cleaned Southern Ocean samples compared to phytoplankton material from the same region (Fig. 3.19). Samples were taken in surface waters, at 450 m depth and from the sediment.

A clearly linear dependence of the dissolution rate at 2°C and pH 8 on the degree of undersaturation could be observed below 0.75 ($> 300 \mu\text{M}$), i.e. 75% of saturation, for acid-cleaned sediment sample PS-2299 (10-12.5 cm), below 0.64 ($> 400 \mu\text{M}$) for particle trap material BO 10#3 and below 0.5 ($> 600 \mu\text{M}$) in case of phytoplankton from surface waters of the Bransfield Strait. This is in general agreement with the results of VAN CAPPELLEN and QIU [1997 b]. They reported a transition to faster dissolution kinetics (c.f., see Figure 3.20) at degrees of undersaturation which were greater than 0.8 (80% of saturation), i.e. they needed silicic acid concentrations below 200 μM to observe the transition towards non-linear dissolution kinetics.

3. Experimental results and discussion

Tab. 3.4 Summary of calculated dissolution rate constants (k_{CFT}) and constants m_{CFT} from flow-through experiments measured on single opal samples from the water column and the sediment, either untreated or acid-cleaned ($T = 2^\circ\text{C}$, pH 8, artificial seawater). $[\text{Si}]_{\text{sa}}$, the apparent solubility, was determined as described in Section 3.1.1.2.1. k_{CFT} and m_{CFT} are fitted parameters of measured steady state dissolution rates versus a relative degree of undersaturation (Eq. 3.13). Including the specific surface area S results in surface-independent reaction rate constants k' . Uncertainties from fitting procedures are given in brackets.

ID.	Sample	Apparent solubility [$\pm 10\%$] ¹	k_{CFT} [yr^{-1}]	k'_{CFT} [$\mu\text{molm}^{-2}\text{day}^{-1}$]	m_{CFT}	S [m^2/g]	Notes
O1	Pn- <i>T. antarctica</i>	1150	15(1)	65(5)	1.1(1)	9.6	acid-cleaned
O2	Pn- <i>Nitschia</i> sp.	1060	26(2)	48(4)	0.97(7)	22	acid-cleaned
O3	Pn-ANT-XV/2 #64	1150	19(2)	33(4)	1.0(1)	23	acid-cleaned
O4	Pn-ANT-XV/2 #65	970	0.91(3)	4.1(2)	1.1(1)	9.4	untreated, C_{org} -rich
O5	Pn-M21/4	1200	18(2)	45(5)	1.0(1)	17	acid-cleaned
O6	Trap-BO-1o#3	1040	3.5(6)	16(3)	1.1(2)	9.0	acid-cleaned
O7	Trap-NB9 (1000m)	1000	3.6(2)	---	2.4(3)	---	untreated, C_{org} -rich
O8	Trap-NB9 (2500m)	1000	2.1(1)	---	2.3(2)	---	untreated, C_{org} -rich
O9	Sed-Opal-A/CT	1200	1.26(5)	0.78(3)	1.02(4)	67	untreated
O10	Sed- <i>Ethmo. rex</i>	1200	0.052(6)	1.0 (1)	1.1(2)	2.1	untreated
O11	Sed-PS-2299 (10-12.5 cm)	1190	1.6(1)	1.22(9)	1.2(1)	53	acid-cleaned

Since other factors (e.g., organic matter and origin) are involved, a direct comparison of untreated samples (Tab. 3.4) with those retrieved from the Southern Ocean and with acid-cleaned phytoplankton from surface waters of the Norwegian Sea does not seem to be straightforward. For these particular samples, however, a transition from slower linear to faster linear dissolution kinetics was obtained; an additional approximation is the application of a fully non-linear rate law [KEIR, 1980; MORSE, 1983] as given in Equation 2.13 with $m \neq 1$. Kinetic constants k_{CFT} [yr^{-1}] or k'_{CFT} [$10^{-6}\text{mol m}^{-2} \text{s}^{-1}$], including the rate parameters specific surface areas (2.4.7), the apparent exponents m , and apparent solubilities (Tab. 3.2) are summarized in Table 3.4.

3. Experimental results and discussion

3.1.2.2.2 Depth-dependent reaction rates of sediments at 25°C

For water column samples a clear reduction of reactivity was observed and quantified with reaction rate constants calculated from Equation 2.13 (Tab. 3.4). Clearly, just two samples showed significant deviations from the linear dependence of reaction rates on relative departure from equilibrium under conditions outlined in the previous section.

In Figure 3.2 the consequences of increasing detritus/opal ratios were demonstrated, namely decrease in solubility values. Again, samples of the four groups outlined in Section 3.1.1.2.1 (Fig. 3.2) were used to show principle shapes obtained by means of flow-through experiments. Different dependencies on silicic acid saturation state according to reaction order m were calculated by fitting data to Equation 2.13. The dissolution rates obtained for particular samples from deepest sediment horizons are near-linear at relative degrees of undersaturation less than 0.5. With increasing distance from that point, however, there is a more or less pronounced transition in the functional dependence of the dissolution rate on the relative departure from equilibrium, more obvious in sample PS-2312-1 (20-22.5 cm), a siliceous ooze. Accordingly, it must be emphasized that kinetic transition is dependent on the saturation state of the solution (see also VAN CAPPELLEN and QIU, 1997 b). The non-linear path is more obvious in sediment sections near the sediment-water interface and tend to more pronounced linear behavior at the deepest section of the core (e.g., MC-1-3, Fig. 3.22). Non-linear behavior seems to be most pronounced in samples of high biogenic silica content (for example PS-2312-1), considering the samples from the deepest section of the cores (Fig. 3.21).

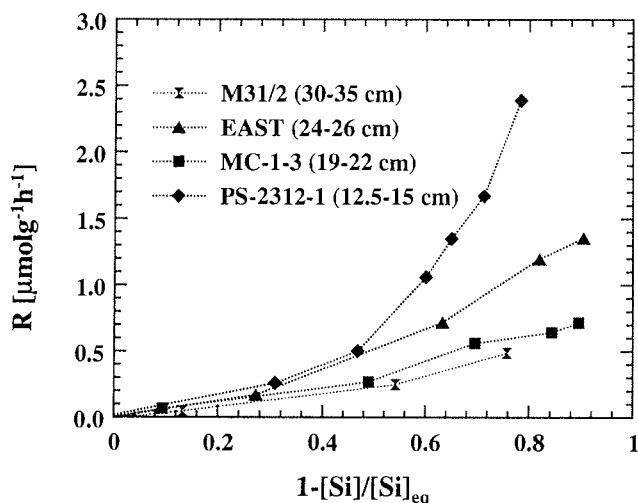


Fig. 3.21 Experimental dissolution rates per unit mass biogenic silica at 25°C and pH 8 (artificial seawater) as a function of the relative degree of undersaturation of the reactor solution with respect to apparent solubility of BSi in respective sediments. The rate data plotted are the same as those in Fig. 3.2 which represent 4 different groups of sediments considering solubility values. The degree of undersaturation is calculated using apparent silica solubility $[Si]_{eq}$ values determined by interpolation of positive and negative rates nearest to the equilibrium (see text in Section 3.1.1.2.1 & Fig. 3.2). Here, results from sediments of the deepest sections of the cores were selected. They reveal a non-linear dependence on the degree of undersaturation, mostly pronounced in sediments of high biogenic silica content, whereas those from silica-poor sediments show the least deviation from the linear rate law with, where $m \sim 1$.

3. Experimental results and discussion

Temperature also tends to shift the kinetic transition to lower degrees of undersaturation [VAN CAPPELLEN and QIU, 1997b] (c.f., results from batch and flow-through studies at 25°C and 60°C, respectively, Fig. 3.22).

In general, a decrease of apparent solubilities with depth was obtained. The results of the flow-through experiments (Fig. 3.22) reveal that such a decrease is accompanied by a decrease in reactivity. Dissolution rates as a function of the degree of undersaturation and depth suggest a subdivision of the cores into three groups according to their dissolution behavior.

Sediment samples of group A (Fig. 3.22) show marked changes between all three depth horizons. Due to a lack of sediment material from the topmost section of the core only results from two horizons (> 4 cm) were available in the Norwegian Sea (M31/2). Nevertheless, the results from batch experiments performed at 60°C [RICKERT, unpublished results, Fig. 3.22 A*] or alkaline reaction rate constants (k_{NaOH}) (Fig. 3.31, Sect. 3.1.2.2.4) reveal a sharp reactivity decrease with sediment depth starting from the topmost horizon (< 4 cm) of M31/2.

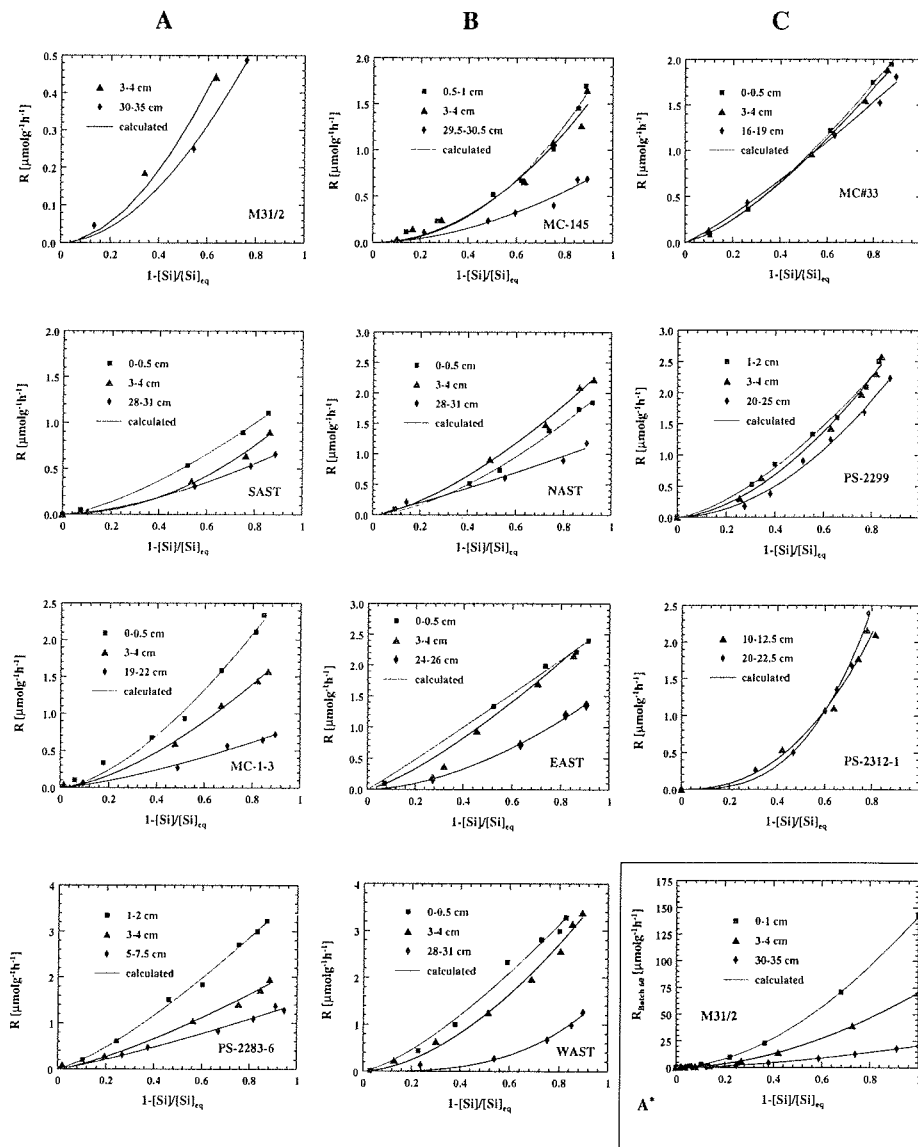
Samples of group (B) revealed similar behavior with respect to reactivity in the top sections. A steep drop, however, is obvious from the top to the bottom sample. Sediments from group C only slightly changes with depth.

Applying Equation 2.13 to fit the data derived from experiments yields reaction rate constants k_{CFT} which are compared in Figure 3.23. In most of the cores studied, the dissolution rate constant k_{CFT} decreases with depth. An exception is core PS-2312-1 (20-22.5 cm), where an increase with depth was observed in flow-through experiments. This 'outlying' constant, however, is most probably driven by uncertainties, since batch experiments (60°C) [RICKERT, unpublished results] and apparent alkaline reactivity constants (60°C) [RICKERT, unpublished results] and apparent alkaline reactivity constants reveal a decrease in reactivity with depth (3.1.2.2.3). Rate constants in the top sections of the cores vary by a factor of ~ 4-5, i.e. 0.5-2.5 yr⁻¹ among the cores. In the samples from the bottom of the cores this range tended to decrease within ~ 0.5-1.5 yr⁻¹. WAST sediments on the right and SAST sediment on the left hand of Figure 3.23 roughly border the range of dissolution constants observed in flow-through experiments. According to Figure 3.23, two phenomena are obvious:

- (1) Reaction rate constants vary by a factor of 3-5 among the cores independent of depth (A.3.11).
- (2) The general rate drop by a factor 1-3 with depth implies:
 - (a) that the surface reactivity of the silica particles during early diagenesis decreases progressively through reduction of surface silanol groups and the formation of bridging Si-O-Si-bonds at the solid-solution interface [e.g., VAN CAPPELLEN and QIU, 1997 b], and/or
 - (b) that the extent of surface coatings due to adsorption [e.g., VAN CAPPELLEN and QIU, 1997a,b] and reverse weathering reactions increases [e.g., MICHALOPOULOS and ALLER, 1995], and/or
 - (c) that biomineralization in surface waters of the oceans produces a mixture of biogenic silica particles with *a priori* variable surface reactivities and/or degrees of silicification (e.g., iron-limited diatoms make thicker shells according to HUTCHINS and BRULAND [1998] or TAKEDA [1998]), and/or

3. Experimental results and discussion

Fig. 3.22. Depth distributions of biogenic silica dissolution rates as a function of the degree of undersaturation for 11 core locations (Fig. 2.1; Tab. 2.1). All samples reveal more or less pronounced deviations from a non-linear dissolution kinetics according to Equation 2.8 (see text). Silica dissolution rates generally decrease with depth in a sediment core (A, 3.11). A. Samples with marked decreases between different horizons. B. Samples with small reactivity change in the upper section but significant decrease towards bottom sediment. C. Sediments with small reactivity changes throughout the core. For comparison, samples from M31/2 (A*) in the lower right derived from batch experiments carried out at 60 °C and pH 8 in artificial seawater [RICKERT, unpublished results]. Different scales were used for the reaction rates.



3. Experimental results and discussion

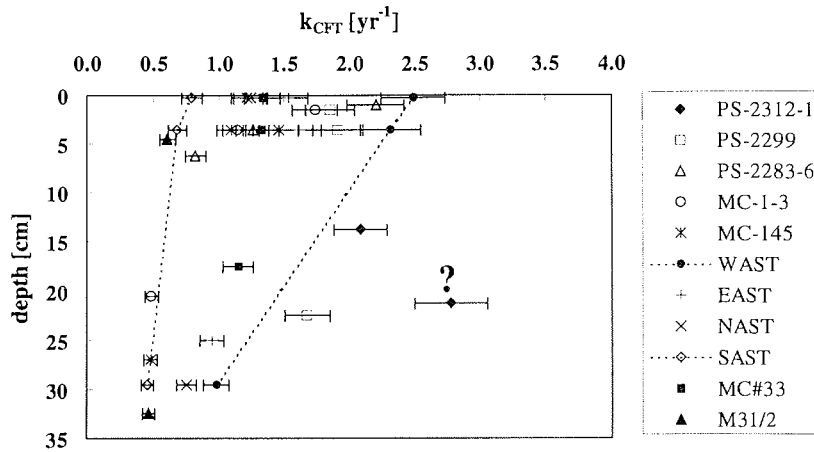


Fig. 3.23 Depth distribution of reaction rate constants k_{CFT} [yr^{-1}] at 25°C and pH 8 determined for 11 sediment cores (see Tab. 2.1 and Fig. 2.1 for location) by means of flow-through experiments. Rate constants were calculated fitting rate data versus degree of undersaturation to Equation 2.13 (see text). The error bars represent the estimated analytical uncertainties of the rate determinations. Rate constant PS-2312-1 (20–22.5 cm) is most probably faulty (see text). A complete list of rate constants k_{CFT} , reaction orders m and solubilities with depth is given in A.3.11.

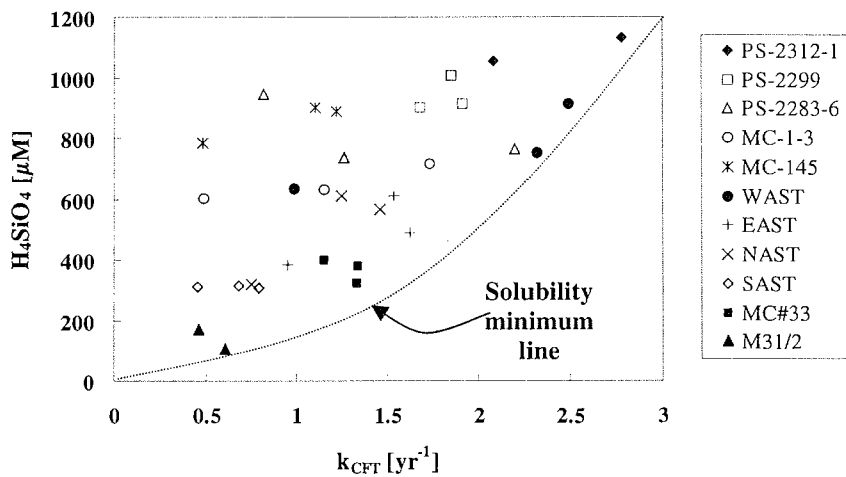


Fig. 3.24 Solubilities $[\text{Si}]_{\text{sat}}$ as a function of kinetic constants k_{CFT} at 25°C and pH 8. The figure demonstrates a fairly weak correlation between laboratory derived apparent solubilities and kinetic constants. Below dashed line, here refer to as solubility minimum line, no data were observed suggesting a common underlying process which put constraints towards the interplay of thermodynamic and kinetic behavior (see text).

3. Experimental results and discussion

- (d) that the type of opal changes during dissolution in the water column and early diagenesis processes in the sediments is due to preferential dissolution of more reactive opal types resulting in remaining, less reactive opal for reasons that still have to be considered [e.g., MIKKELSEN, 1979; VAN CAPPELLEN, 1996], and/or
- (e) that the solid phase SiO_2 that is contributing the dissolved silica [WILLEY and SPIVACK, 1997] is completely dissolved.

Considering Figure 3.24 where the obtained solubility values (A. 3.11) are plotted against reaction rate constants from the same depth horizons, it could be inferred from the dashed line that some reaction rate constants can only produce solubilities which exceed the values plotted with this line since there is no data point below it. Even more striking is the reverse: Low dissolution rate constants do not consequently cause low solubility values. A k_{CFR} value of 0.5 yr^{-1} corresponds to apparent solubility values of $\sim 200 \mu\text{M}$ (M31/2), $\sim 300 \mu\text{M}$ (SAST), $\sim 600 \mu\text{M}$ (MC-1-3) or $\sim 800 \mu\text{M}$ (MC-145). These values were obtained from bottom samples of the respective cores. There does not seem to be any systematic difference in rate constant values between cores of high opal (PS-2299, PS-2312-1, PS-2283-6) and sediments with lower biogenic silica contents. For example rate constants from WAST sediments with an opal content of 5 wt.% lie in the same range (including uncertainties) as sediments retrieved from the Southern Ocean with opal contents of $> 50 \text{ wt.}\%$. To construct a correlation between apparent solubility values and kinetic constants using the data points in Figure 3.24 would lead to arbitrary conclusions keeping in mind that some of the cores under investigation show an extreme decline in kinetic constants with increasing depth (for example compare MC-1-3 or MC-145 in Figures 3.23 and 3.24) although solubility values do not markedly change. If solubility values also change significantly, the correlation may work, but kinetic constants should not *a priori* be mixed with thermodynamic ones.

The factors responsible for a decline in silica solubilities were already mentioned, for example increasing deposition of detritus, relative to biosiliceous materials [VAN CAPPELLEN and QIU, 1997a,b], variable incorporation of trace metals for example Al [LEWIN, 1961; ILER, 1979; VAN BENNEKOM et al., 1991; VAN BEUSEKOM et al., 1991] or variable concentrations of Al in pore waters [VAN CAPPELLEN, 1997a,b] (3.1.1.2). The main environmental factor controlling the build-up of dissolved silica in pore waters is the logarithmic ratio of detrital and biosiliceous material (3.1.1.3.1). The way they interact is either constrained by pore water aluminum concentrations [VAN CAPPELLEN and QIU, 1997 a,b] or through reverse weathering reactions [e.g., MACKENZIE and GARRELS, 1965; MACKIN, 1987; MICHALOPOULOS and ALLER, 1995] (3.1.2.3.4).

Below, two different methods to determine relative changes of reactivity of biogenic silica in individual heterogeneous sediment matrices and various depths and in single opal samples are introduced. These methods have the advantage of being much faster compared to flow-through experiments. Whether they are applicable to the relative changes of surface reactivity is discussed.

3.1.2.2.3 Determination of (reactive) surface area (S_{reactive})

The rate constants k_{CFr} for biogenic silica are constant for a given temperature, pH and electrolyte composition. Moreover, they were treated as independent from the degree of undersaturation, as can be seen in Equation 2.13 which is used to fit rates versus undersaturation data from the flow-through experiments. This is illustrated in Figure 3.24 where apparent reaction rates are plotted versus apparent solubilities.

Flow-through experiments have demonstrated that the reactivity of biogenic silica decreases more or less significantly with depth in single opal samples retrieved from different depth of either the water or the sediment column.

Specific surface areas obtained from BET surface area measurements do not exhibit the systematic reactivity decrease of surficial sediments of the Southern Ocean (VAN CAPPELLEN, 1996). VAN CAPPELLEN and QIU [1997a,b] reported that a progressive reduction of the surface density of reactive sites during burial may continue even at depths where apparent saturation occurs and there is no net release of silicic acid. This led to the assumption that the preferential dissolution of a more reactive fraction of siliceous remains, is less important in the sediment column [VAN CAPPELLEN, 1996].

The factors which contribute to the depth-dependent variations and among the samples in general still must be deciphered. Accordingly, BET measurements on opal-rich cores from Scotia Sea were carried out with sediment samples from different depth segments to determine *physical surface areas* (2.4.7); cobalt adsorption experiments on two of these cores were carried out to estimate *reactive surface areas* (2.5.4.2). Since the latter measurements are restricted to almost pure biosiliceous samples, a fitting procedure recently reported by KONING et al. [1997] was applied to the alkaline leaching experiments to all sediments and opal samples under investigation. These results were compared with those from surface area measurements, cobalt adsorption and flow-through experiments. The application of alkaline leaching constants for the estimation of reactive surface areas in sediment samples and the factors which may influence the reliable interpretation of these constants were evaluated and discussed in the following and Section 3.1.2.2.4.

BET surface areas

In Figure 3.25 depth distributions of BET surface areas for the Scotia Sea sediments PS-2299 and PS-2314-1 are compared. In general, untreated sediment samples provide distinctly lower surface areas compared to acid-cleaned samples suggesting that significant inorganic or organic surface matrices interrelated with biogenic silica are active in reducing *physical surface areas* which may in turn lead to reduced *reactive surface areas* by a factor of 2-3. Another possible explanation for the enhanced surface area may be a better disaggregation of the particles after acid-cleaning procedure (2.2.2) or simple a shift towards enlarged values due to enhanced biogenic silica contents of the sample due to a removal of acid-soluble phases and subsequent enrichment of biogenic silica during the cleaning procedure.

Whether such a dramatic decrease is likely to be caused by organic coatings surface areas of the phytoplanktonic samples ANT-XV/2 #64 and #65 (Tab. 3.4) were compared. Surface areas of treated and untreated phytoplankton differ by a factor of 4-5 depending on the amount of organic coatings and/or detritus still present (Tab. 3.5). The same increase could be

3. Experimental results and discussion

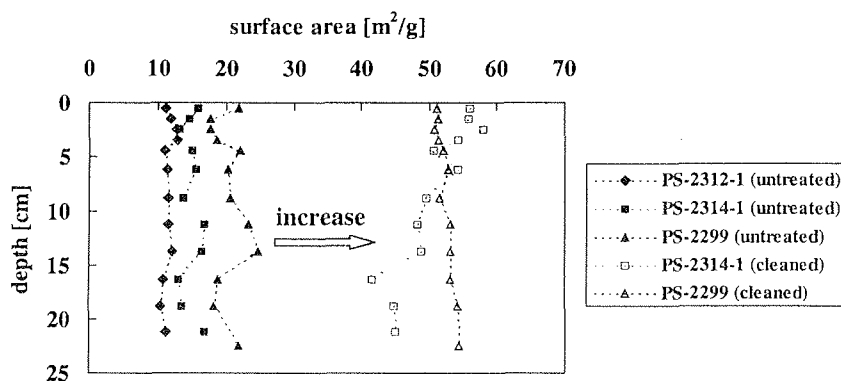


Fig. 3.25 Depth-distribution of N_2 single point BET specific surface areas measured either in untreated (filled symbols) or peroxide- and acid-cleaned (open symbols) (2.1.1.2) bulk sediment samples from the Scotia Sea (Tab. 2.1). The cleaning procedure caused a dramatic increase in the observed surface areas. The increase is a factor of 1-2 higher than expected from an increase in opal content from ~ 50% to 70%. Untreated surface areas remain essentially unchanged with depth (see also PS-2299, cleaned), whereas acid-cleaned sediment sample PS-2314-1 shows a marked decrease with depth. Data are given in A.2.6.2-A.2.6.4.

Tab. 3.5 The specific surface areas S_{BET} determined with single-point N_2 BET measurements of sediments at 4-5 cm depth either untreated or acid and peroxide treated (2.2.2). For sediments of the Scotia Sea, whole-core average values are given. Standard deviations throughout the core are given in brackets.

Sample	Sediment type	S_{BET} [m^2/g], untreated	S_{BET} [m^2/g], treated
M31/2	calcareous, sandy	8.7	
MC#33	calcareous	12	
WAST	calcareous	16	54
NAST	calcareous	14	
EAST	calcareous	18	
CAST	calcareous	17	
SAST	calcareous	20	
MC-1-3	siliceous, detrital	37	
MC-145	siliceous, detrital	35	
PS-2299	siliceous	21(2)	53(2)
PS-2312-1	siliceous	12(1)	
PS-2314-1	siliceous	15(1)	51(5)
Diatom ooze ¹	siliceous	18-32	
Foraminiferal ooze ¹	calcareous	1-10	
Fine sand ¹	detrital	1-5	
Foraminiferal grey clay ¹	calcareous, detrital	10-30	
Red clay, deep ocean ¹	detrital	25-90	

¹For comparison, specific surface areas of oceanic sediments are listed [in LERMAN, 1979].

3. Experimental results and discussion

found in the multi-component sediment sample MC#53 (WAST) with a specific surface area of 16 m²/g before and 54 m²/g after pretreatment. This increase after acid-pretreatment, however, may also be caused by a shift of the carbonate dominated sediments towards mainly siliceous-detrital dominated ones for which higher surface areas are reported in LERMAN [1979] (Tab. 3.6). Surface or internal matrices (for example incorporated Al according to VAN BEUSEKOM [1991] or VAN BENNEKOM et al. [1991]) can also play an important role in lowering reaction rates of biogenic silica in sediments and in the water column. Since the solubility determinations (Tab. 3.2) have not provided significant differences among acid-cleaned samples incorporated Al should play a subordinate role in lowering the reactivity among the samples in this study.

Variations in the alkaline reaction rate constant k_{NaOH} due to inorganic or organic surface matrices or coatings will be discussed in Section 3.1.2.2.4. Table 3.4 summarizes BET surface areas of almost pure biosiliceous samples. Samples from 4-5 cm sediment depth of each core were taken to determine site-specific variations of these heterogeneous oceanic sediments with various opal contents. Surface areas from less biosiliceous sediments, however, do not represent surface area of biogenic silica in those sediments, but an estimated average of all sedimentary components.

Co adsorption experiments

In many mineral dissolution rate studies the reactive surface area (S_{reactive}) is assumed to be the same as or at least proportional to the bulk surface area measured with BET technique. VAN CAPPELLEN [1996] propose a cobalt (Co) adsorption technique [DUGGER et al., 1964; JAMES and HEALY, 1972] to evaluate surface reactivity changes with depth which were not correlated with surface area (BET) changes.

In fact, the uptake of Co^{2+} ions varies with the distribution of silica reactivity throughout the core, and the technique seems to be suitable for estimation of the specific aqueous reactive surface area or the ($\equiv\text{Si-O}^-$) sites covering the surface of amorphous biogenic silica. Parts of the surface which are 'reactive' will participate in the dissolution process, while the rest of the surface will not participate. Furthermore, depth-dependent variations in cobalt adsorption capacities of biogenic silica were compared with the results of flow-through and alkaline leaching experiments.

In Figure 3.26, the principle pattern suggests that Co^{2+} cations can be used as a probe for reactive surface sites of biogenic silica. The silicic acid concentration tends to overshoot with respect to biogenic silica solubility during the first hours accompanied by a sharp drop in pH. After 50-100 h, silicic acid concentrations tend to stabilize at values of ~1600-1700 μM ; solutions become saturated. Cobalt concentrations in the solution tend to decrease sharply during the first 24 hours due to formation of exchangeable complexes between Co^{2+} and surface [$\equiv\text{Si-O}^-$]-groups [HATHAWAY and LEWIS, 1969], followed by a constant decrease reflecting the irreversible incorporation of metal cations into solid-state structures [CHISHOLM-BRAUSE et al., 1990] (Figure 3.26 reveal adsorption pattern: $\text{Co}_{\text{ads}} = \text{Co}_0 - \text{Co}_{\text{sol}}$; Co_{ads} = Co adsorbed, Co_0 = Co in solution at $t = 0$; Co_{sol} = Co in solution at time t). Even after 500 h, the irreversible incorporation of Co^{2+} is still going on. Though minor variations occur, the Co uptake decreases slightly with depth.

3. Experimental results and discussion

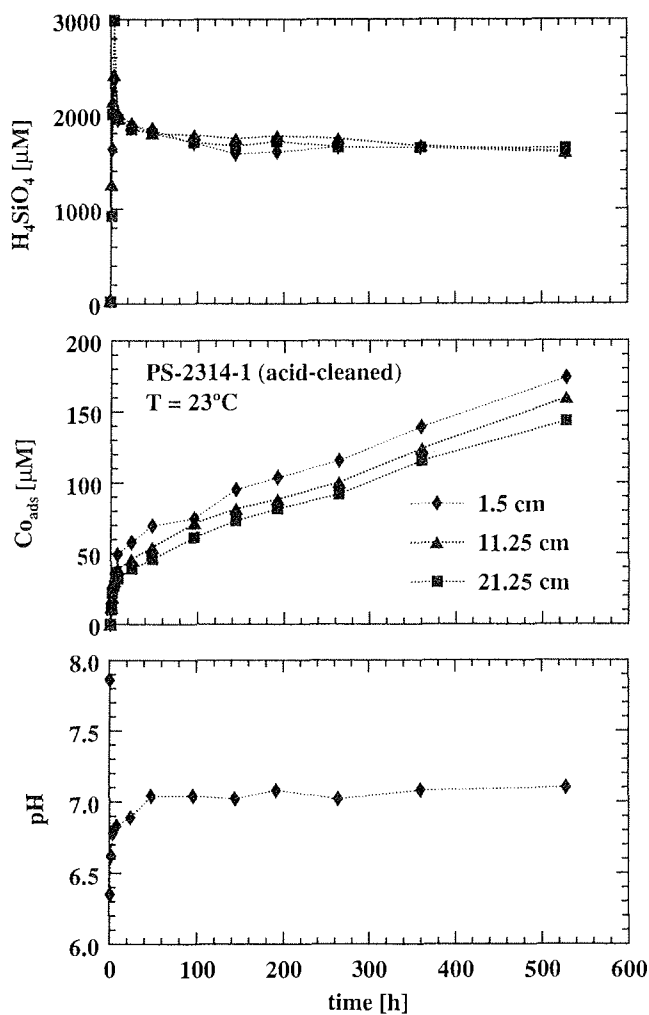


Fig. 3.26 Cobalt adsorption experiments at 23°C. Adsorption experiments were deployed by direct addition of cobalt solution to 0.5 g sediment sample (PS-2299 & PS-2314-1 + 20 mg $CaCO_3$) [VAN CAPPELLEN and QIU, 1997b]. Silicic acid [μM] (above), adsorbed Co^{2+} [μM] (middle), and pH (bottom) as a function of time. The pH dependence was nearly the same throughout the depth intervals, but never exceeded pH 7.1.

Evaluation of Co_{ads} versus time plot

Adsorption curves (Fig. 3.26, middle) show an early rapid adsorption due to the reversible exchange of cations on the surface, followed by a slower linear increase representing the irreversible incorporation of Co^{2+} into the silica structure (see above). The rapid Co^{2+} uptake at the first step of the experiments was assumed as a relative measure of surface site density and determined by extrapolating the linear portion of the adsorption curve back to zero time. This analytical problem was solved with a fitting procedure of the adsorption curves using the following empirical expression:

$$Co_{ads} = \frac{a_1 t}{a_2 + t} + a_3 t \quad (3.6)$$

where Co_{ads} is the adsorbed cobalt concentration [μmol]. The parameters a_1 [$\mu\text{mol l}^{-1}$], a_2 [s], and a_3 [$\mu\text{mol l}^{-1}\text{s}^{-1}$] are sediment-specific constants and outflow parameters from the fitting procedure for a given temperature and solution properties (for example pH, ionic strength).

To calculate the constants, Equation 3.6 was fitted to the experimental data with the commercial software Origin™. The goodness-of-fit indicator, χ^2 , of the data obtained to the theoretical curves was compared with the r^2 statistic. The results were all well described by the theoretical curves with r^2 values typically > 0.9 . χ^2 is defined as:

$$\chi^2 = \frac{\sum_{i=1}^n (f(x_i) - y_i)^2}{n - N} \quad (3.7)$$

where $f(x_i)$ is the value calculated at x_i , y_i is the measured value, n is the number of data points, and N is the number of parameters.

Extrapolating the flat linear part of the curve back to time zero is mathematically solved by assuming $t \gg a_2$; then Equation 3.6 can be reduced to

$$Co = a_1 + a_3 t \quad (3.8)$$

This linear expression simply describes the incorporation of cobalt into the silica structure with time t , starting with the already adsorbed Co concentration (= reversibly adsorbed) a_1 and h the kinetic constant a_3 .

In summary, a_1 is used as a value of the surface capacity of biogenic silica for exchangeable Co^{2+} , which is nearly independent of the initial amount of soluble Co^{2+}

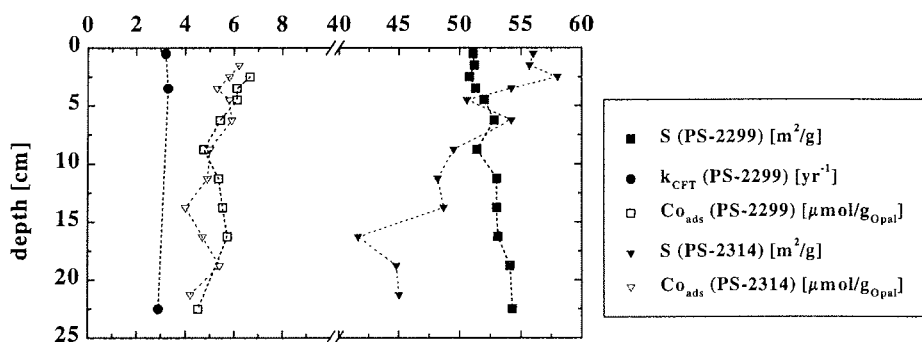


Fig. 3.27 Results of cobalt adsorption experiments of acid-cleaned sediments PS-2299 and PS-2314-1 (open lined squares and triangles) reveal specific surface areas (S) (filled black squares and triangles), surface capacities of respective core [$\mu\text{mol } Co_{ads}/g_{Opal}$] and k_{CFT} , the apparent dissolution constant of PS-2299 (filled black circles), with depth (A.3.12). With the exception of the specific surface areas of PS-2314-1 which tend to decrease with depth, sediment properties are quite similar for opal rich-sediments.

3. Experimental results and discussion

added as long as the dissolved Co^{2+} concentration after 100 h of reaction does not drop below $100 \mu\text{M}$ [VAN CAPPELLEN and QIU, 1997 b]. The results of the acid- and peroxide-cleaned cores PS-2299 and PS-2314-1 reveal only slight decreases of surface reactivity [$\mu\text{mol Co}_{\text{ads}}/\text{g}_{\text{Opal}}$]. The results of flow-through experiments for PS-2299 revealed no marked decrease with depth either (Fig. 3.27). The cobalt adsorption method, however, is limited to opal-rich sediment; it cannot be applied to the other cores under investigation where interferences due to adsorption of Co^{2+} onto non-biosiliceous surfaces would distort the results (2.5.4.2).

Apparent reactivity rate (k_{NaOH}) in alkaline solution (pH 12.5)

Surface reactivity estimates of biogenic silica using the Co adsorption method [VAN CAPPELLEN and QIU, 1997b] in cores in which opal contents are strikingly lower than in Southern Ocean sediments ($< 20\%$) lead to ambiguous results for reasons described above. Accordingly, the use of a reactivity rate constant in alkaline medium [see also KONING et al., 1997] has been optimized as a relative gauge for depth-dependent decrease in (surface) reactivity. Furthermore, the influence of detrital clays as well as organic matter on this constant has been highlighted to better interpret the depth distributions of this constant in sediment cores and the reactivity differences between single opal samples. Apparent reaction rates can, thus, be rapidly determined in alkaline solution and provide insights into the bulk reactivity of biogenic silica in sediments where BET measurements or the cobalt adsorption method seem not to be suitable.

The dissolution of biogenic silica from natural sediments in high pH and high-temperature (85°C) leaching solutions may be assumed to mimic natural processes at greatly enhanced speeds [e.g., SHEMESH et al., 1989; KONING et al., 1997]. This assumption sounds arbitrary at first, but the validity of this basic assumption as well as the usefulness of alkaline leaching constants for reactivity estimates has been proved.

All single opal samples, sediment trap samples and sediment samples, as well as opal samples (PS-2312-1 12.5-15 cm) mixed with different clay contents, had to be analyzed for biogenic silica content in 12.5 M NaOH applying the leaching technique [SCHLÜTER and RICKERT, 1998; 2.4.1 and 2.5.4.3]. Samples were taken at 6 time intervals, most frequently at the beginning and less frequently at the end of the leaching procedure (2.4.1 and 2.5.4.3) to evaluate k_{NaOH} , the rate constant for the decay of biogenic silica at pH 12.5 and $T = 85^\circ\text{C}$ or, abbreviated, the alkaline rate constant. This should be treated as a parameter representing the overall reactivity of biosiliceous fragments in the sample at a certain depth.

Since samples were not pretreated (except for freeze-drying) results involve individual organic, inorganic coatings, and matrices as well as the influence of non-biosiliceous components. Thus, this alkaline reactivity constant should be treated as an apparent rate constant. Including the slow dissolution of clay minerals as a constant, simultaneous and independent process according to DEMASTER [1981], leaching curves were fitted using Equation 2.15. The biogenic silica content, and the constants k_{NaOH} and b_{NaOH} which account for the sample distribution of opal and detrital reactivity were obtained as results. The use of an automated, wet chemical leaching method according to MÜLLER and SCHNEIDER [1993] (not used in this study) can further enhance the reproducibility of the leaching procedure and the accuracy of the subsequent fitting procedure (KONING et al. [1997] used between 600 and 1200 data points which

minimizes the error in each constant). Reproducibility for each constant and [BSi%] is generally better than 10%.

Clay minerals and Al release

In Figure 3.28 modeled depth-dependent leaching curves of 6 time intervals are shown. The initial slopes reflect reactivity, characterized by k_{NaOH} , the alkaline rate constant of the biogenic silica assemblage in the sediment matrix. k_{NaOH} values tend to decrease with depth accompanied by a general drop in opal contents. Obviously, a significant shift in sediment composition is accompanied by k_{NaOH} variations. This is only partly true for opal-rich sediment (see below). To prove the validity range of alkaline extraction experiments it is necessary to review the results of a leaching procedure for opal/clay mixtures, which were used in part in flow-through experiments for elucidating the influence of detrital clays on silica solubilities (3.1.1.2.4). Figure 3.29 shows the results of such a study for the detrital clays kaolinite, montmorillonite and illite as well as for CaCO_3 mixed with different amounts of the siliceous ooze sample PS-2312-1 (12.5-15 cm).

This study demonstrates the measurable effects of clay minerals in sediment samples on the apparent dissolution kinetics of biogenic opal in an alkaline medium. This is most striking when detrital contents exceed those of biogenic opal by more than an order of magnitude. Again, a logarithmic dependence becomes visible, as outlined above in a discussion of the solubility of biogenic opal in the presence of detrital minerals (3.1.1.3.2). A dramatic drop in reactivity expressed by k_{NaOH} is obvious in the presence of kaolinite. Again, it is kaolinite which reveals the greatest effects on the dissolution kinetics of biogenic silica (see also the dramatic decline in apparent solubility of PS-2312-1 in the presence of significant amounts of kaolinite (Figs. 3.10 and 3.29).

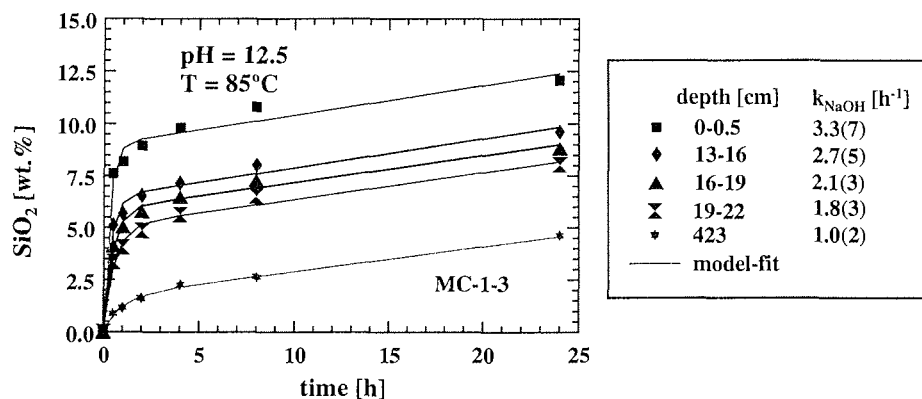


Fig. 3.28 Modeled leaching curves for core MC-1-3 at 4 depth intervals. Comparing depth intervals, considerable decrease in opal content, i.e. a shifting to lower opal/detrital ratios (A.2.4) is accompanied by a considerable differences in the initial silica release. This decrease continues when a sample taken from KAL-1-4 (423 cm) from the same site is considered. The initial slope of the curves characterized by k_{NaOH} (Eq. 2.15, Sect. 2.5.4.2) reflects the reactivity of the biogenic assemblage in the sediment matrix.

3. Experimental results and discussion

It is assumed that one underlying process influences both the net release of silicic acid measurable in the outflow solution of flow-through experiments, yielding apparent rate constants k_{CFT} and apparent solubility values $[\text{Si}]_{\text{sat}}$, and the release of silicic acid in alkaline leaching experiments.

The release of aluminum during alkaline extractions has been quantified. This release may be the reason for the striking differences among the clay minerals since in all cases the release of aluminum from kaolinite is 2-3 times higher than for the other clay minerals. A closer look at the XRF analyses of the clay minerals used in the present study (A.1) reveals the differences in $\text{Al}_2\text{O}_3/\text{SiO}_2$ ratios which increase in the following order:

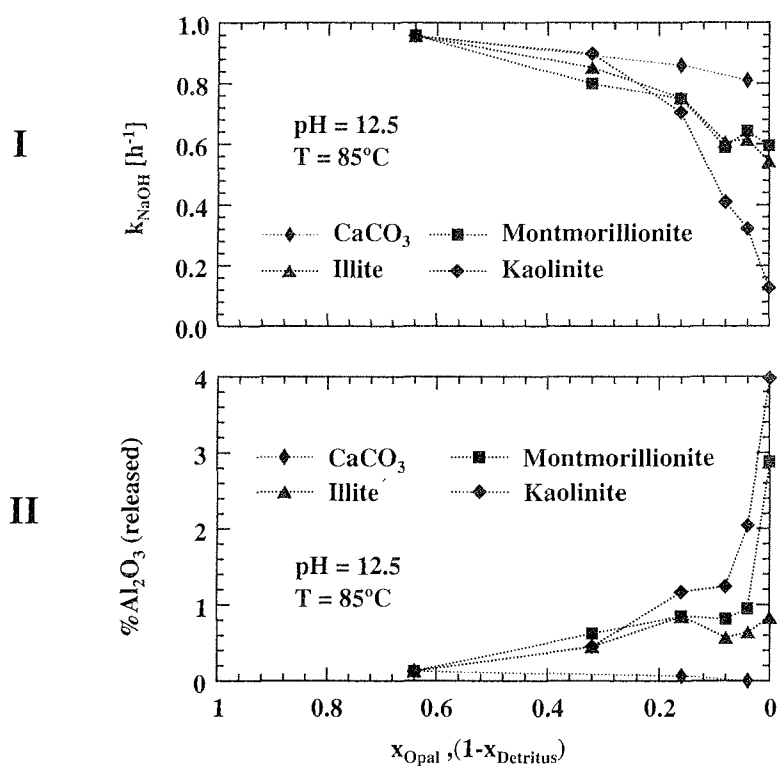


Fig. 3.29 I. Dissolution kinetics of biogenic silica (PS-2312-1, 12.5-15 cm, $x_{\text{Opal}} = 0.64$) in alkaline solution (pH 12.5) at 85°C as a function of weight ratio of opal (x_{Opal}) in the mixture; natural detrital content of siliceous ooze is ~ 36%. The addition of detrital clay minerals to siliceous ooze sample PS-2312-1 accounts for a drop in k_{NaOH} ; a dramatic decrease was observed for kaolinite. II. The reason for this is thought to be an enhanced release of aluminum from kaolinite which may lead to subsequent precipitation under consumption of silicic acid and causes a drop in k_{NaOH} . Aluminum release increases markedly for kaolinite, to a lesser extent for montmorillonite and illite when $x_{\text{Opal}} < 0.1$. The addition of CaCO_3 also seems to cause a decrease of reactivity but this is by far less extensive than for detrital minerals. This decrease, however, is attributable to residual detrital contents in sediment PS-2312-1 (see text). k_{NaOH} , as well as Al values released during opal dissolution are given in A.3.13.

Illite < montmorillonite < kaolinite. Such an alkaline solution behavior is also to be expected from the compositional point of view. In Figure 3.29, the decrease in the alkaline reactivity constant k_{NaOH} (I) is shown, which correlates well with the increase in aluminum in solution (II).

The lowering of reaction rate constants in the presence of CaCO_3 is at first surprising but may be explained by a precipitation of a calcium-containing aluminosilicate. The aluminum needed for this reaction was present since natural siliceous ooze (PS-2312-1) was applied for the mixtures which already contains 36 wt.% detritus, that is some 25 wt.% of detrital clay and 11 wt.% residual detritus (Tab. 2.4). Small but measurable amounts of aluminum in alkaline solution of the pure sediment sample PS-2312-1 as well as for 1:3 or 1:15 mixtures with CaCO_3 were determined during extraction; a tendency towards lower Al release with increasing CaCO_3 was evident (Figure 3.29).

Al determination

Al release was also monitored throughout opal determinations since aluminum provides valuable insights into the sediment structure where opal is embedded and information on whether or not easily soluble aluminosilicates are present (see description above). According to the basic assumption of alkaline extraction (fast dissolution kinetics of BSi and slow dissolution kinetics of non-BSi), a striking increase of dissolved silica is expected at the beginning and a slow and gradual increase at the end due to a slow, gradual dissolution of clay minerals.

In contrast to this assumption, the temporary increase in the concentration of dissolved aluminum (given as wt.% Al_2O_3 released with respect to total sediment) reveals a pattern quite similar to the release of silicic acid [SCHLÜTER and RICKERT, 1998; BRACK, 1997; BRACK and RICKERT, in prep.]. This in turn leads to slight overestimations of silicic acid release when a linear correction procedure is assumed to determine biogenic silica contents in natural sediments [DE MASTER, 1981].

The initial release of Al (given as wt.% Al_2O_3 released), i.e., during opal dissolution, was calculated according to DEMASTER [1981] using the intercept of the linear part of the extraction curve. Concentrations after 4, 8 and 24h were considered for the linear regression procedure. A depth-dependent release of Al, expressed as wt.% Al_2O_3 during opal dissolution, is documented in A.3.15. Average values from 12 cores are given in Figure 3.30.

The aluminum release rate for Pacific cores MC-1-3 (Juan de Fuca Ridge) and MC-145 are 3-4 times higher than that for the rest of the cores during alkaline leaching of biogenic silica after 2-4 hours of extraction. That means, some 12-16 wt.% of SiO_2 released during that time must be attributed to clay mineral dissolution, assuming an average value of ~ 4 for the $\text{SiO}_2/\text{Al}_2\text{O}_3$ ratio calculated from the slopes of SiO_2 and Al_2O_3 release between 4 to 24 hours. In turn, this must lead to large overestimations in silica content and, consequently, in all rate constants calculated on the basis of silica contents. This, however, does not affect the conclusion of this thesis. To address the problem of BSi determination in sediments which has already been discussed for over 30 years [e.g., CHESTER and ELDERFIELD, 1968; EISMA and VAN DER GAASST, 1971; HURD, 1972; LEINEN, 1977; EGGIMANN et al., 1980; DEMASTER, 1981; LEINEN, 1985;

3. Experimental results and discussion

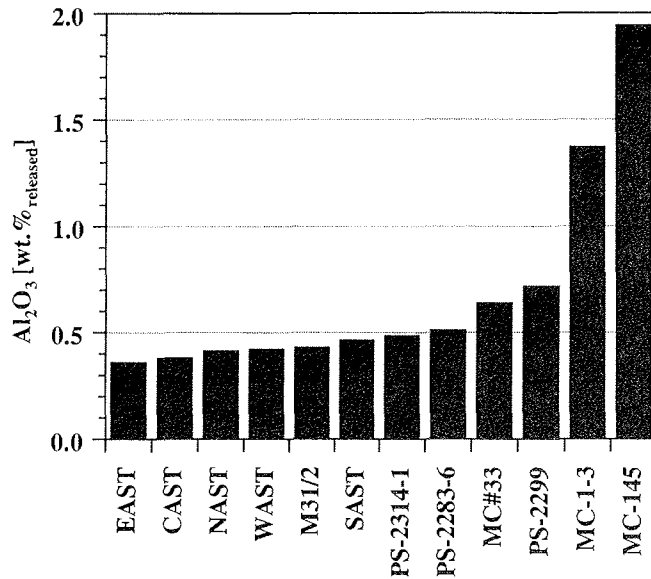


Fig. 3.30 Initial Al release (given in wt.% Al₂O₃) during alkaline leaching (pH 8, T = 85°C) of sediments. In most cores the release of aluminum is ~ 0.5 wt.%, whereas a significant release was observed for Pacific cores MC-1-3 (Juan de Fuca Plate) and MC-145 (Peru Basin). A qualitative estimate of dominant clay minerals is given in Tab. 2.5.

MORTLOCK and FROELICH, 1989; DEMASTER, 1991; MÜLLER and SCHNEIDER, 1993; BRACK, 1997; CONLEY et al., 1998; SCHLÜTER and RICKERT, 1998; BRACK and RICKERT, in prep.] in detail within the framework of this thesis would lead too far.

Nevertheless, this problem should be kept in mind for the discussion of rate constants in flow-through experiments, alkaline leaching procedures and pore water modeling on the basis of several 50-100% overestimated silica contents for the Pacific cores.

Important, however, for this thesis is the fact that the presence of obviously easily dissolving aluminosilicate phases in the two cores mentioned above are of high significance for the topic investigated here. The consequences for the dissolution kinetics of biogenic silica in those sediments are discussed in detail in Section 3.2.3.3.1 since pore water profiles are thought to be markedly affected by easily dissolving clay minerals.

Similar insights have been obtained for the constant b_{NaOH} , which was calculated from the procedure of fitting silicic acid versus a defined time pattern (see above) and reflecting the silicic acid release from non-biosiliceous phases. The resulting values determined were homogeneous for most cores within the range $0 < b < 0.1$ at pH 8 and T = 85°C (A.3.15). Significantly higher values, however, for the cores MC-1-3, MC-145, and PS-2283-6 vary between 0.1 and 0.35 h⁻¹.

k_{NaOH}: A reactivity but (non-)sensitive parameter ?

Depth distribution of k_{NaOH} are first compared with results of single depth horizons examined in flow-through experiments (Fig. 3.31) to estimate reactivity differences throughout the core. Sediment samples were chosen in the same order used in Figure 3.22 (A-C, A*). For M31/2 two depth horizons are represented by means of flow-through experiments; batch experiments at 60°C (A*) add more information to the subsurface depth horizon with the depth distribution of k_{Batch60} .

A first assessment reveals that k_{NaOH} from alkaline extraction (85°C, pH 12.5) is highly variable (for example MC#33, MC-145, SAST). Striking anomalies observed in k_{NaOH} versus depth pattern (Fig. 3.31), for example at SAST site between 4 and 8 cm sediment depth, may reflect short-term variations in opal/CaCO₃ or opal/detrital influxes or compositions. A general drop in k_{NaOH} values observed in some cores, e.g. EAST (< 10 cm) or MC-145 (< 20 cm), may be due to a general climate change, i.e. the transition from the last glacial to the Holocene in MC-145 [HAECKEL, pers. comm.].

Even more important within the framework of this thesis is the fact that k_{NaOH} values seem also to be excellent proxies for the depth-dependent changes in reactivity of biogenic opal embedded in a complex matrix of various non-biosiliceous minerals; results from flow-through (triangles) or batch experiments performed at 60°C [RICKERT, unpublished results] reveal almost the same depth-dependent behavior. A closer look, however, shows more or less remarkable deviations for both MC#33 and PS-2283-6 from a common trend of opal-rich (BSi > 20 wt.%) and opal-poor (BSi < 20 wt.%) sediments.

Opal-rich sediments (PS-2283-6, PS-2299, PS-2312-1, PS-2314-1 (not shown)) reveal k_{NaOH} versus depth pattern without distinct deviations from an almost constant, only slightly decreasing trend. PS-2283-6, however, reveals a striking decline in k_{CFT} pattern. VAN CAPPELLEN and QIU [1997a,b] have also reported a decreasing trend for k_{CFT} versus depth pattern in siliceous oozes. In the following section (a) these phenomena - almost no change in k_{NaOH} and striking variations in k_{CFT} pattern of opal-rich sediments - will be discussed in further detail. MC#33, in contrast, reveals only slight deviations in k_{CFT} (Fig. 3.22), but dramatic decreases with depth in k_{NaOH} versus depth pattern.

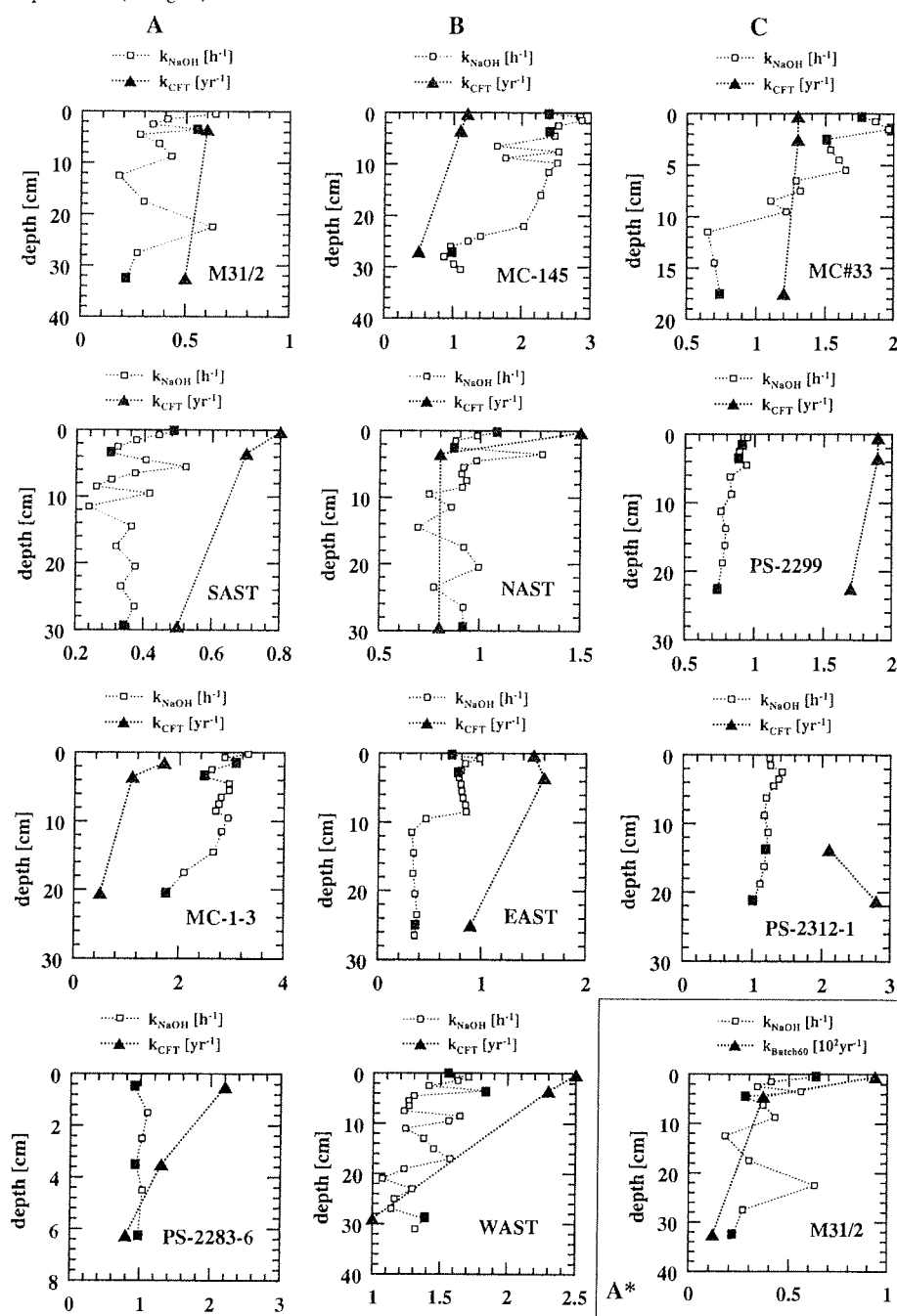
For a more detailed interpretation of rate constants calculated from results of flow-through or alkaline leaching experiments, results of the dissolution kinetics of biogenic silica in the presence of other silica-bearing phases are discussed in the following.

(a) Enhanced opal preservation due to ash particles from Mount Hudson eruption in 1991 ?

Sediment characteristics have been outlined in Section 2.1.1, where ash particles visible in the topmost sections of PS-2283-6 were mentioned. Following, experimental evidences are given to reveal that the differences in both constants are mainly caused by the ash of the Mount Hudson eruption in 1991 [e.g., SCASSO et al., 1994].

3. Experimental results and discussion

Fig. 3.31 Comparison of alkaline extraction constant k_{NaOH} [h^{-1}] and results of flow-through experiments in terms of k_{CFT} [yr^{-1}] (for groups A-C, see Section 3.1.2.2.2 and Fig. 3.22). Framed patterns A* (lower right) are results from batch experiments performed at 60°C and pH 8 in artificial seawater [RICKERT, unpublished results]. Filled squares in k_{NaOH} pattern indicate depth intervals chosen for flow-through experiments (triangles).



3. Experimental results and discussion

The instability of volcanic glasses and ash in deep-sea sediments is well documented [e.g., BONNATI and NAYUDU, 1965; MORGENSTEIN, 1967; KELLER, 1970]. A number of silicate and ferromanganese minerals result from this alteration process. It has also been reported [RIEDEL and ABERDEEN, 1957] that radiolarians and diatoms are better preserved when mixed with volcanogenic sediments. The mechanism of this preservation is yet unclear. Possible explanations are mentioned below. Flow-through experiments performed with volcanic glass particles [STRONCIK-TREUE, pers. comm.] at pH 8 and at 25°C in artificial seawater showed that ash particles have distinctly lower reaction rates and solubilities than biogenic opal. From a thermodynamic point of view ash particles in siliceous oozes should more readily act as silicic acid acceptor since the solubility of these ash particles is lower [STRONCIK-TREUE, pers. comm.]. Kinetically spoken, these ash particles may act as an inhibitor for biogenic silica dissolution. Their framework should easily be able to release aluminum, assuming that glass dissolution is treated as a congruent dissolution process. In turn, Al may simultaneously reprecipitate with silicic acid and other cations provided by ambient seawater to form aluminosilicate phases of low solubility as long as predominant biogenic silica is active, producing silicic acid for such reprecipitations.

In summary, ash particles at pH 8 and 25°C should lower the solubility values of biogenic silica; thus, they are considered as detritus, which, in turn, regulates the build-up of silicic acid. This is in agreement with solubility results presented here. Solubilities increase because detrital ash/opal ratios decrease with depth (3.1.1.3.2). A decrease in reactivity observed in k_{CFT} values during flow-through experiments may then be explained by the additional aluminum source. Close to the water-sediment interface, biogenic silica surfaces have not yet undergone extensive aging and, thus, exhibit rather high reactivities [VAN CAPPELLEN and QIU, 1997a,b]. With increasing depth, however, rapidly increasing levels of silicic acid thermodynamically force ash particles to release aluminum for reprecipitation reactions occurring on biogenic silica or glass particles. This leads to extensive aging of both biogenic opal and ash particles. The mechanism which causes a decline in reactivity with time (depth) and a better preservation of biogenic opal in volcanogenic sediments as mentioned above [RIEDEL and ABERDEEN, 1957] will be discussed again considering reverse weathering reactions (3.1.2.3.4). The latter explanation sounds plausible enough, but the question remains as to why this decline is not indicated by the alkaline leaching constant k_{NaOH} , which remains fairly constant with depth.

One explanation is that the alkaline leaching method is less sensitive compared to the continuous flow-through (CFT) technique. The dissolution rate constants obtained in CFT experiments at 25°C (2°C) seem to be the result of a kinetically controlled dissolution reaction. From a kinetic point of view, most reactive sites or species are responsible for dissolution kinetics measured in flow-through experiments; accordingly, these experiments and k_{CFT} values focus on the most reactive sites or species within the sample and sensitively react if reactive site densities [VAN CAPPELLEN and QIU, 1997b] or the reactivity of the most soluble biosiliceous particles decrease with depth for reasons summarized in Section 3.1.2.1.1. Alkaline leaching experiments and k_{NaOH} values are thermodynamically controlled for the high temperature (85°C) and high pH (12.5) conditions used. k_{NaOH} values thus represent the opal assemblage as bulk opal.

3. Experimental results and discussion

To demonstrate the effectiveness of the methods proposed, let us again take a closer look at Figure 3.29. Obviously, a marked decrease in reactivity indicated by k_{NaOH} requires non-biosiliceous contents which exceed those of biosiliceous contents by at least a factor of 2-5. It is not surprising, then, that nearly constant values were observed instead of patterns similar to those found in sediments with low BSi content. The biosiliceous assemblages predominant in Southern Ocean sediments seem to dissolve as bulk opal and reactivity differences are barely detectable. Flow-through experiments performed at pH 8, $T = 25^\circ\text{C}$ and seawater conditions, however, are more sensitive to most reactive sites or particles demonstrated for PS-2283-6 in Figure 3.31. This reactivity decrease is probably induced by the ash particles (see above).

For PS-2299 and PS-2314-1 only slight reactivity decreases were measured by cobalt adsorption experiments (Fig. 3.27). Flow-through experiments confirmed these observations and do not reveal significant reactivity decreases for PS-2299 with depth (Fig. 3.21).

In Figure 3.29 one explanation for a slight reactivity decrease when biosiliceous remains dominate the sample has been given. A small change in x_{Opal} or in the opal/detritus ratio reveals only slightly different k_{NaOH} values. For $x_{\text{Opal}} < 0.1$, however, small changes towards lower opal contents significantly enhance the ratio of aluminum/silicic acid release which may be the reason for a striking decrease in k_{NaOH} (Fig. 3.31, for example M31/2, MC-145, MC#33).

(b) 'Impurities' in the sediment record of MC#33

Figure 3.31 reveals almost opposite behavior in the silica-poor sediment record of MC#33. Reactivity constants under extreme conditions (pH 12.5, $T = 85^\circ\text{C}$) show a marked decrease with depth, whereas only slight differences in k_{CFT} are observed in flow-through reactors. Given explanation (a) above, behavior in an alkaline medium is not surprising since detrital minerals are dominant here. Biogenic silica contents decrease from 1.7% to 0.7% with depth. This in turn leads to a more than 100% change of $\text{Al}_2\text{O}_3/\text{SiO}_2$ ratios released during the first 2-4 hours by sediments for different depth horizons ($x_{\text{Opal}} \rightarrow 0$ in Figure 3.29). This is thought to lead to increasing precipitation rates of aluminosilicate phases in the closed vessel, particularly since detrital minerals are present which can act as a precursor for precipitation from the solution. Flow-through reactors, on the other hand, represent an open system. Critical oversaturations of silicic acid to possible lower soluble aluminosilicate phases should not develop since silicic acid concentrations remain below oversaturation states throughout the experimental run. An assessment of flow-through experiments will be presented later (3.1.1.3.1). Since remaining particles in BSi-poor sediments examined in flow-through experiments do not raise inflow silicic acid concentrations by more than a few micromoles, the difference between inflow and outflow solution does not change significantly if 1 or 2 percent of biogenic silica is present in the solid. Therefore, the dissolution rates and k_{CFT} values calculated by that difference (Eq. 3.6) do not vary significantly with depth. In fact, this was observed for MC#33. Nevertheless, in other cores with low BSi content (M31/2, NAST, SAST, WAST) significant changes with depth in both parameters have been observed. A possible explanation for this observation are more reactive particles remaining in the topmost sections of the cores which are possibly already dissolved in MC#33 (see (c)).

(c) The 'intermediates'

As outlined before an extreme reactivity decrease of biosiliceous remains in some sediment cores with various, but low (< 10%) opal contents (M31/2 (A*), NAST, SAST and WAST) was observed in the topmost and/or between the top and the bottom of the core. This was indicated by both parameters (k_{CFT} and k_{NaOH}). Such behavior may be explained by highly reactive siliceous remains present in the topmost section of the core; therefore, the reactivity decrease is most striking in the topmost section of the cores due to preferential dissolution of most soluble particles [e.g., WILLEY and SPIVACK, 1997] or significant aging processes [e.g., VAN CAPPELLEN and QIU, 1997a,b]. In these cores, both methods show a sensitive behavior since both thermodynamic, i.e. apparent solubility (3.1.1.2.2, Fig. 3.4), and kinetic properties (reactive sites, species composition) of the samples change markedly with depth. The pore water fitting procedure also revealed evidence for a significant reactivity decrease between the topmost and following sediment sections (3.2.2.3, Fig. 3.9). From pore water fitting such striking differences within the topmost sections were not obtained for MC#33 (b), which fits remarkably well the observation of flow-through experiments (Fig. 3.31).

(d) Pacific sediments (MC-1-3 and MC-145) and apparent rate constants

Special observations based on alkaline extractions of Pacific sediments have been outlined above. Highly soluble aluminosilicate phases are thought to be present since 12-16% of the present clay minerals were already dissolved during the first four hours of alkaline leaching at 85°C and pH 12.5. This was indicated by the highest aluminum release in all sediments of investigation. A closer look at k_{NaOH} reveals that the alkaline extraction constant is also influenced by highly soluble aluminosilicates. In most cores k_{NaOH} values of $\sim 0.5\text{-}1\text{ h}^{-1}$ (Fig. 3.31 and A.3.15) were observed. Those of MC-1-3 and MC-145 ($\sim 1\text{-}3\text{ h}^{-1}$) suggest that silicic acid released by those clay minerals may be partly involved in k_{NaOH} . Distinctly higher values for b_{NaOH} (see above) and the dissolution constant of clay minerals (Eq. 2.15; Sect. 2.5.4.3) also indicate the presence of easily soluble aluminosilicate phases in sediments of the Peru Basin. Another explanation for high k_{NaOH} and b_{NaOH} values may be the presence of extremely easily soluble biogenic opal tests, but because of the simultaneous presence of high aluminum concentrations after extraction the first explanation is favored. In addition, dissolution rate constants in flow-through experiments have not proved that easily dissolved biogenic silica shells are present. The dissolution rate constants lie within the range of constants determined in all cores (Fig. 3.23). It cannot be precluded, however that simultaneous precipitation reactions occur in the reactor which probably causes the overall flat pattern (Fig. 3.2 and 3.21). A dynamic balance between dissolving biogenic silica and reprecipitation reactions induced by the highly soluble aluminosilicates may also cause such low decreasing constants calculated for the depth-dependent kinetic constants (3.2.3.3.1, Fig. 3.48).

In Section 2.5.5 the advantages of flow-through reactors as open systems in contrast to batch reactors (2.5.4) were addressed. One of the major advantages of the open system is the fact that the formation of secondary precipitates can be ruled out. In fact, flow-through experiments performed with volcanic glass particles have provided that reprecipitation reactions occur unless a solubility value for these glass particles was

3. Experimental results and discussion

attained [STRONCIK-TREUE, pers. comm.]. Accordingly, the list of advantages (2.5.5) needs to be corrected at least for investigations of heterogeneous sediments examined in artificial seawater. Given the possibility that reprecipitation reactions occur in such heterogeneous phases, it is important to underscore the fact that dissolution rate constants observed in flow-through reactors must also be treated as *apparent rate constants*. A modified silicic acid release from biogenic silica would be detectable in outflow solutions if simultaneous precipitation reactions in the reactor occurred. These reactions may be induced through the easily soluble aluminosilicates which at least act as an Al source needed to precipitate silicic acid from inflow solution and/or released by biogenic silica tests (3.1.2.3.3). In other words, flow-through experiments in which

1. biogenic silica is present,
2. easily soluble non-biosiliceous phases are present,
3. artificial seawater as inflow solution with major ions needed for precipitation reactions is provided

are likely to produce rate constants which represent an overall process, i.e. dissolution and precipitation under natural conditions, but do not produce single dissolution rate constants for biogenic silica dissolution over the full range of undersaturation (see further discussion in 3.1.2.3.3).

3.1.2.2.4 Effects of clay minerals and coatings on biogenic silica reactivity

Flow-through experiments with various opal/detritus ratios

In the previous chapter the results of alkaline extractions of biogenic opal from sediments and synthetic clay/opal mixtures in terms of the constant k_{NaOH} have been outlined. The results were used to present the *a priori* argument that results from alkaline extraction experiments mirror processes that occur in natural environments under seawater conditions. The following experiments will now demonstrate that the explanations above are indeed useful to reasonably describe opal dissolution in seawater conditions (pH = 8 and T = 25°C).

A comparison of k_{CFT} and k_{NaOH} values (Fig. 3.31) is treated on a scale of reactivity trends. For this purpose, the results of flow-through experiments with opal/clay mixtures have been used. This was done to prove that apparent solubilities of biogenic silica actually decrease in the presence of detrital materials towards values which can be observed in natural pore water/sediment regimes of varying composition (3.1.1.2.3 and 3.1.1.3.2), but which are far below saturation with respect to pure biogenic silica. The experiments were performed using different undersaturation states of silicic acid and results were fitted using Equation 2.13.

Because only a sparse data set was available, particularly in the undersaturated region, a first order rate law was chosen to describe apparent reaction rates versus undersaturation values (Fig. 3.32). In this special case of opal/detritus ratio = 0.042 Figure 3.10 (3.1.1.2.4) and Figure 3.32 imply that a first order rate law is a good approximation as long as undersaturations < 0.7 are considered. Rate constants display the same relative order determined by alkaline extraction. A closer look at Figure 3.10 (3.1.1.2.4) reveals that reaction rates of both PS-2312-1 and the illite mixture tend to

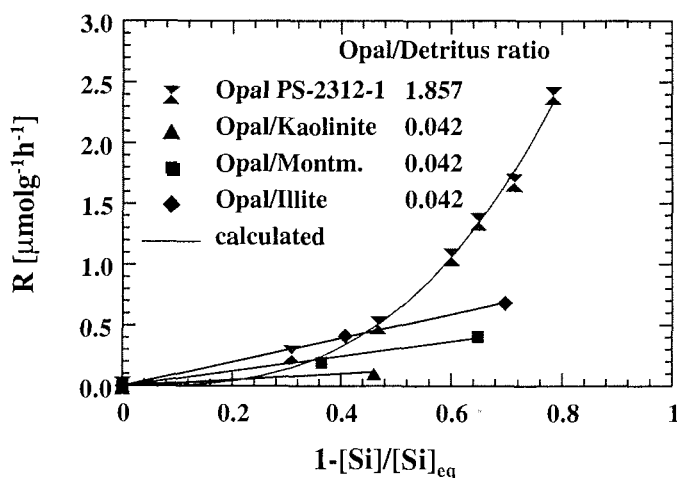


Fig. 3.32 Apparent dissolution rates of sedimentary biogenic silica (PS-2312-1 12.5-15 cm) measured by CFT technique at pH = 8 and T = 25°C in artificial seawater with clay minerals (kaolinite, montmorillonite or illite) as a function of the degree of undersaturation. An opal/detrital clay ratio of 0.042 was used. Straight lines represent results fitted to Equation 2.13. Obviously, the presence of clay minerals tends to depress the dissolution rate constant k_{CFT} as well as the reaction order m compared to the pure sediment sample. The shift in solubility (not shown) has already been mentioned in Section 3.1.1.2.4 (Fig. 3.10).

coincide when approximately halfsaturation is reached, whereas rates for montmorillonite and kaolinite remain lower. Halfsaturation corresponds to $\sim 500 \mu\text{M}$ for the pure sediment sample PS-2312-1, but only $\sim 130 \mu\text{M}$ for opal/illite, $\sim 60 \mu\text{M}$ for opal/montmorillonite and $\sim 35 \mu\text{M}$ for an opal/kaolinite mixture. Apparent dissolution rate constants k_{CFT} measured in artificial seawater at T = 25°C and pH 8 decrease from $3.6(4) \text{ yr}^{-1}$ for untreated sediment samples (opal/detritus ratio ~ 1.9) to $1.0(1)$, $0.61(6)$, or $0.25(3) \text{ yr}^{-1}$, mixed with illite, montmorillonite and kaolinite, and opal/detritus ratios of 0.04. Again, a drop in reactivity is most striking for kaolinite/opal mixtures.

In summary, the results, both k_{NaOH} and k_{CFT} distributions in sediment cores are yet to be investigated and compared, yet it is important to note that both these constants tell stories which lie inbetween those told of above for cores MC#33 and PS-2283-6. Only when both constants and the release of aluminum during extraction are monitored will the factors which may be active in regulating dissolution kinetics in closed batch reactors under extreme conditions which lead to alkaline dissolution constants, in open flow-through systems under ambient conditions which result in k_{CFT} values, and in natural sediment/pore water systems be identified.

Effect of organic and inorganic coatings

As has been previously mentioned, changes in surface areas occur due to acid pretreatment of sediment samples and must be considered. In some results - particularly those in which acid and peroxide cleaning procedures were undertaken prior to experiments - an additional effect on reactivity rate constants due to organic and inorganic coatings, here referred to as "surface coatings" must be emphasized.

3. Experimental results and discussion

Flow-through experiments in artificial seawater at $T = 2^\circ\text{C}$ and $\text{pH } 8$ and alkaline leaching procedures ($T = 85^\circ\text{C}$, $\text{pH } 12.5$) with the pretreated phytoplankton sample ANT-XV/2 #65 and the untreated organic-rich phytoplankton sample ANT-XV/2 #64 (Tab. 3.2) for major components) show drastic differences. Surface coatings cause a reactivity decrease by a factor of ~ 2 in alkaline leaching experiments given k_{NaOH} , but results in a decrease factor of ~ 20 in flow-through experiments expressed by k_{CFT} (Fig. 3.33). Obviously, again a lower sensitivity of the overall leaching attack under extreme conditions in contrast to a 'soft' attack under buffered seawater conditions at 2°C was observed. This unusual dissolution behavior was also found in untreated or acid- and peroxide- pretreated sediment samples from the Scotia Sea (PS-2299) (Fig 3.33).

It should be mentioned first that the experiment with the acid-cleaned sediment sample was conducted at 2°C , whereas experiments with the untreated sediments (20-25 cm) were performed at 25°C but recalculated for 2°C using a constant activation energy of 60 kJ/mol (2.5.6.1). In Figure 3.33 results are given for acid-cleaned and untreated phytoplankton and sediment samples. Table 3.6 summarizes the measured chemical and physical properties of both acid-cleaned and untreated samples. It becomes obvious that acid pretreatment in both samples enhances surface areas by at least a factor of two, suggesting that $k_{\text{NaOH}} [\text{h}^{-1}]$ differences between treated and untreated samples are the result of a reduced surface area due to organic and/or inorganic surface coatings of highly porous material.

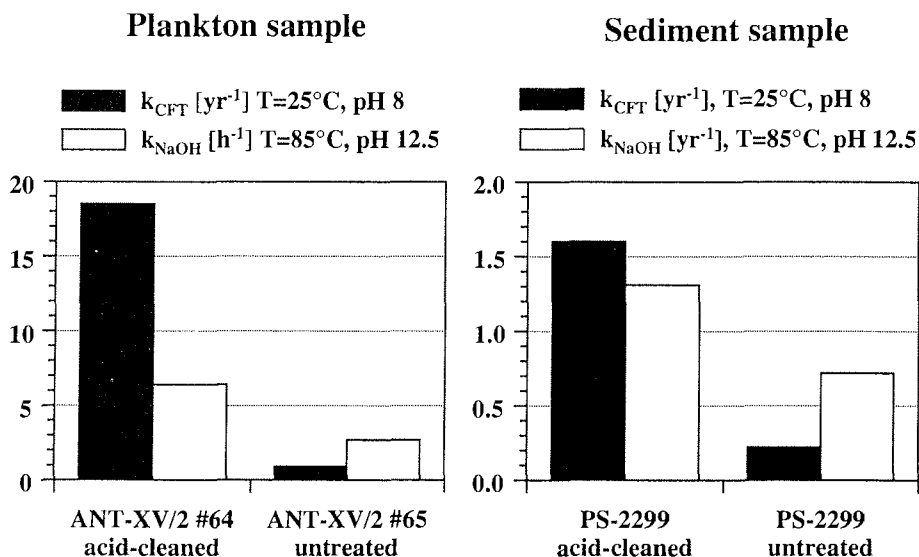


Fig. 3.33 Effect of surface coatings on the reactivity of phytoplankton sample ANT-XV/2 and sediment sample PS-2299. Alkaline rate constants k_{NaOH} and dissolution rate constants k_{CFT} of flow-through experiments reveal the same tendencies but different sensitivities. Whereas k_{NaOH} decreases only by a factor of ~ 2 , the dissolution rate constant in seawater at $\text{pH } 8$ and $T = 25^\circ\text{C}$ drops by a factor of 20 in the case of phytoplankton and by a factor of ~ 8 in the case of sediment sample due to surface coatings (note different scales). Again, the effect of less sensitivity of k_{NaOH} is obvious. This is an order of magnitude

3. Experimental results and discussion

Tab. 3.6 Chemical and physical properties of a sediment sample from PS-2299 and phytoplankton sample ANT-XV/2 either acid-cleaned or untreated. Sediment contents are average values.

Properties	Phytoplankton ANT-XV/2		Siliceous ooze PS-2299	
	Acid-cleaned (#64)	Untreated (#65)	Acid-cleaned	Untreated
Opal [wt.%]	100	37	83	49
Detritus [wt.%]	0	53	17	50
C _{org} [wt.%]	0	8	0	1
O/D	--	0.70	4.9	0.98
Solubility	1150	970	1190	680 ¹
k _{NaOH} [h ⁻¹] pH 12.5, T 85°C	6.4	2.7	1.3	0.72
k _{CFT} [yr ⁻¹] pH 8, T 2°C	19	1.0	1.6	0.22 ²
m _{CFT}	1	2.7	1.2	1.9 ³
S [m ² /g]	23	9.4	53	21

¹pore water concentration.

²recalculated from flow-through experiments performed at 25°C using E_a = 60 kJ/mol (2.5.6.1).

³calculated from flow-through experiments performed at 25°C.

For k_{NaOH} values including surface areas values of 1.9 and 1.3 μmol m⁻² s⁻¹ for untreated and acid-cleaned siliceous oozes from PS-2299, and 16 or 15 μmol m⁻² s⁻¹ for untreated and acid-cleaned phytoplankton samples were determined. KAMATANI et al. [1988] have reported a slightly lower surface increase of 1.4-1.8 times when a leaching procedure with either HNO₃ and H₂O₂ or 2N HCl at 100°C was applied for two hours. But the increase in the surface area alone cannot explain such striking differences in k_{CFT} values. For untreated and acid-cleaned siliceous ooze samples k_{CFT} values of 0.3 or 1.2 μmol m⁻² day⁻¹, for plankton samples either untreated or acid-cleaned values of 4.1 and 32 μmol m⁻² day⁻¹ were determined. It must be assumed that surface reactivities in terms of surface silanol groups increase substantially. This suggests that the low dissolution rates of untreated samples are primarily the result of inhibitors adsorbed at the surface, such as Mg [HURD, 1973] or Al [ILER, 1979; VAN CAPPELLEN and QIU, 1997 a,b], or of reprecipitates, i.e. aluminosilicate phases [HURD, 1973; MICHALOPOULOS and ALLER, 1995]. This may also suggest that a preferential dissolution of the more reactive silica fractions now escaped from surface coating occurs; the two effects last mentioned are likely to be attributed to the approximately tenfold difference in the reaction rate constant k_{CFT} between untreated and treated phytoplankton samples and comparatively slight differences in k_{NaOH}.

It is important to emphasize, that this effect is more obvious in constants obtained in flow-through experiments in which the dissolution reactions of lowest activation energy are favored; the kinetically controlled reaction is shifted towards a preferential attack of most reactive sites. Accordingly, surface coatings act as extreme inhibitors for such a

3. Experimental results and discussion

surface-controlled reaction. At higher temperatures and pH levels the process is more probably thermodynamically controlled; non-selective overall attack occurs, resulting in complete dissolution within a few hours. Slight reactivity differences are difficult to distinguish in flow-through experiments carried out with silica-rich cores (for example PS-2299, Fig. 3.31). In these cores no striking reactivity decrease with depth has been observed. An exception for silica-rich cores under investigation is PS-2283-6 likely due to the occurrence of the ash layers (see above).

The difference remaining in surface changes of sediments is clearly smaller by a factor of ~ 4 compared to the phytoplankton sample since the abundance of easily soluble fractions in sediments is smaller. These fractions have already been dissolved in the water column or during early diagenetic processes. Nevertheless, flow-through experiments performed at 2°C still shift reactions towards lowest activation energies of the remaining fractions. Thus, kinetic constants for the dissolution of the remaining, most soluble fractions have most probably been observed. Again, k_{NaOH} reveals only minor differences when acid-cleaned or untreated siliceous ooze samples in surface changes are compared.

Another aspect which is prominent when comparing results in Table 3.6 is that for silica-rich samples significant deviations from a linear rate law were observed in those cases in which coatings were present. This suggests that deviations from linearity ($m \neq 1$ in Eq. 2.13) may also be a function of surface coatings. For acid-cleaned phytoplankton samples no transition from linear towards a more complex dissolution behavior was observed (Fig. 3.19), but since the dissolution behavior of phytoplankton was not studied at degrees of undersaturations which exceed values of 0.7 (3.1.1.2.1), no conclusions can be drawn on this topic at the moment.

A kinetic transition occurs in untreated sediment and sediment-trap samples when a critical degree of undersaturation is reached (Figs. 3.20, 3.22 and 3.32). Whether this is caused by preferential dissolution along defects [VAN CAPPELLEN and QIU, 1997b] or by transition from a surface-coating controlled dissolution mechanism towards a thermodynamic controlled mechanism caused by higher undersaturations in solution remains unclear. In fact, FLEMING [1986] observed such non-linear behavior, even for a clean synthetic silica, suggesting that such behavior may also be found in ongoing flow-through experiments with phytoplankton.

Summarizing the results of organic and inorganic coatings, it is not possible to rule out a considerable reduction in surface reactivity due to surface-adsorbed inhibitors, since reaction rates increase by some orders of magnitude when samples are pre-cleaned. Accompanying increases in surface areas, albeit not fully correlating with increasing opal contents in the sample, may explain the increase of k_{NaOH} values which does not vary noticeably with or without surface coatings compared to the fairly large differences in k_{CFT} values.

Accordingly, the use of k_{NaOH} records in those cases where opal contents are small ($< 10\%$) and k_{CFT} values are less sensitive (for example MC#33) is suggested to provide an idea of reactivity distribution throughout the core. The use of flow-through constants is more appropriate in silica-rich samples in which a reaction at low temperatures follows the reaction path of lowest possible activation energy. A reactivity decrease which is caused by surface aging in siliceous oozes [VAN CAPPELLEN and QIU, 1997a,b] may also be assigned by cobalt-adsorption experiments (see above), but it will barely be

detectable in the overall bulk constant k_{NaOH} . Even the smallest reactivity differences occurring depth-dependent or from one site to another can be registered by one of the latter methods. Slightest differences in silica-poor sediments are most effectively assigned by k_{NaOH} , slight differences in silica-rich sediments are well assigned by k_{CFT} , the use of cobalt-adsorption experiments, albeit restricted to silica-rich sediments can assign absolute amounts of reactive surface sites if they have been calibrated with flow-through experiments [VAN CAPPELLEN, 1996].

The use of both constants, Co-adsorption methods and, additionally, initial Al releases during alkaline leaching result in unambiguous qualitative and/or quantitative estimates of biogenic silica reactivity even within a complex sedimentary matrix.

3.1.2.3 General discussion of laboratory results

3.1.2.3.1 Dissolution kinetics and mechanisms

A *non-linear dependence* of biogenic silica dissolution on the degree of undersaturation was expected, since recent results in different silica-water systems [FLEMING, 1986; BERGER et al., 1994; VAN CAPPELLEN and QIU, 1997a,b] have provided evidence that the generally accepted linear rate law is in fact non-linear, at least when considering high degrees of undersaturation. Since most previous laboratory data were derived from batch reactor measurements, it is not surprising that the data obtained have been fitted satisfactorily into linear rate expressions. In batch reactors the experimental system moves relatively quickly out of the fast kinetic regime which was observed in flow-through experiments when the relative degrees of undersaturation and reaction rates are highest (for example > 0.5 for PS-2312-1 at 25°C and pH = 8, Fig. 3.32).

As previously discussed (3.1.2.2.1), a transition in the functional dependence of dissolution kinetics on the relative degree of undersaturation was not observed in preliminary cold room experiments. These experiments were preliminary insofar as experimental conditions do not permit the maintenance of undersaturation states usually observed in natural environments. This is due to high release rates of silicic acid, in particular for acid-cleaned phytoplankton and particle trap material, and limitations of flow-rate due to adhesion and clotting effects when flow velocities exceed 7 ml/h. VAN CAPPELLEN and QIU [1997b] report undersaturation states > 0.8 at $T = 2^\circ\text{C}$ needed for a transition towards faster kinetics. Nevertheless, untreated phytoplankton (ANT-XV/2 #65) and particle trap material from the Norwegian Sea, as well as untreated sediment samples of various origins, exhibit a highly non-linear dependence on undersaturation. This is best expressed by a fully non-linear rate law (Eq. 2.13) previously applied to precipitation kinetics [e.g., BURTON et al., 1951] or to calcite dissolution kinetics [KEIR, 1980; MORSE, 1983].

The reaction order m obtained for most untreated sediments falls into a fairly narrow range ($1 < m < 2$; see A.3.11). Reaction orders obtained in bottom samples of silica-rich cores PS-2312-1 and WAST ($m = 2.4-3.1$) are somewhat higher for reasons which must be assessed further. In general, results do not follow the theoretical justification for the linear rate law based on the transition state theory (TST) [RIMSTIDT and BARNES, 1980]. However, the application of TST to overall reactions requires that two critical assumptions be made concerning the nature of the overall reaction:

3. Experimental results and discussion

1. A single rate-limiting reaction step must exist involving the irreversible break-down of the activated complex to form dissolved or precipitated products.
2. The rate-limiting step must be identified as an elementary reaction with activation energies significantly higher than those of all other steps, for example the hydrolysis of bridging Si-O-Si oxygens by adsorption of H₂O before the removal of Si(OH)₄ after a subsequent water attack [e.g., LASAGA and GIBBS, 1990].

Overall reactions between minerals and fluids, particularly in the presence of additional surface coatings and other mineral phases such as biogenic silica in heterogeneous sediments and organically coated phytoplankton samples, however, seem to be more complex than adsorption and hydrolysis reactions.

The number of publications which report non-linear dissolution kinetics of various minerals has increased rapidly [e.g., KEIR, 1980; NAGY et al., 1991; DEVIDAL et al., 1992; NAGY and LASAGA, 1992; BURCH et al., 1993; BERGER et al., 1994; VAN CAPPELLEN and QIU, 1997 a,b, CARROLL et al., 1998] since the introduction of flow-through reactor techniques. These provide the possibility of controlled experiments for temperature, pH, electrolyte composition and the degree of undersaturation to approach the critical level of undersaturation, at which a transition towards faster dissolution occurs. Such a transition towards faster dissolution kinetics reveals that dissolution typically proceeds by selective attack at specific sites of a mineral or an amorphous phase. VAN CAPPELLEN and QIU [1997a,b] propose micropores, suture surfaces between silica spherules and compositional defects such as embedded silanol groups, water and organic molecules.

It is important, however, to mention again that calculated reaction orders in organic-rich phytoplankton and particle trap material exceed those commonly found throughout the cores. For phytoplankton sample ANT-XV/2 #65 m = 2.7(3), for trap sample NB9 (1000 m and 2500 m) m = 2.3(2) and 2.4(3) were obtained. This suggests that without pretreatment phytoplankton samples provide sites of highest surface energy which systematically decrease during settling and after burial in sediments in early diagenetic time scales of deep-sea settings (1,000-10,000 years). This reactivity decrease may be caused by reprecipitation reactions, elimination of surface silanol groups and formation of O-Si-O bridges [VAN CAPPELLEN and QIU, 1997 a,b], or a shift in species composition towards less soluble species due to a preferential dissolution of most soluble particles.

A general decrease in solubilities (3.1.1.3.1 and Fig. 3.4), albeit mostly driven by the logarithmic ratio of detritus/opal contents (Fig. 3.18, Sect. 3.1.1.3.2) can also be attributed to a loss of excess free surface energy [VAN CAPPELLEN and QIU, 1997b]. The progressive elimination of reactive surface sites is sometimes accompanied by a successive, albeit small decrease of reaction order m (PS-2283-6, MC-1-3, MC-145, NAST, MC#33).

3.1.2.3.2. Reaction rates of water column and sediments

Figure 3.34 reveals that dissolution rate constants determined by flow-through experiments and recalculated for 2°C ($E_a = 60$ kJ/mol) (2.5.6) decrease by 1-4 orders of magnitude from fresh acid-cleaned phytoplankton towards buried sedimentary biogenic silica. It may be useful to mention that temperature differences between 25°C (~ surface

3. Experimental results and discussion

water of the Arabian Sea) and the seafloor ($\sim 2^\circ\text{C}$) can account for a decrease of the rate constant by a factor of ~ 8 .

The dissolution of single opal samples has been widely reported [KAMATANI, 1969; HURD et al., 1972, 1973; LAWSON et al., 1978; KAMTANI and RILEY, 1979; KAMATANI, 1982; VAN BENNEKOM et al., 1988, 1991] and measured in labs on fresh dead phytoplankton and sedimentary opal skeletons; acid-cleaning was reported to enhance reaction rates by 1-2 orders of magnitude [e.g., LAWSON et al., 1978; KAMATANI, 1982]. Reported reaction rates there are very similar to the results presented here: they are highly variable from one species to another and yield first order rate constants in the range of 27 yr^{-1} for $T = 2^\circ\text{C}$ and pH 8. The highest reactivity can be found in an acid-cleaned phytoplankton sample from NAST (Arabian Sea). It is dominated by weakly silicified *Rhizosolenia* sp., a major upwelling species [NAIR et al., 1989; HAAKE et al., 1993] with $k_{\text{CFT}} \sim 30 \text{ yr}^{-1}$. This value is highly consistent with results from sediment traps by BRZEZINSKI and NELSON [1995]. They reported rates of biogenic dissolution occurring in the upper 300 m of the water column prior to export of $\sim 0.06 \text{ day}^{-1}$ ($= 21.36 \text{ yr}^{-1}$).

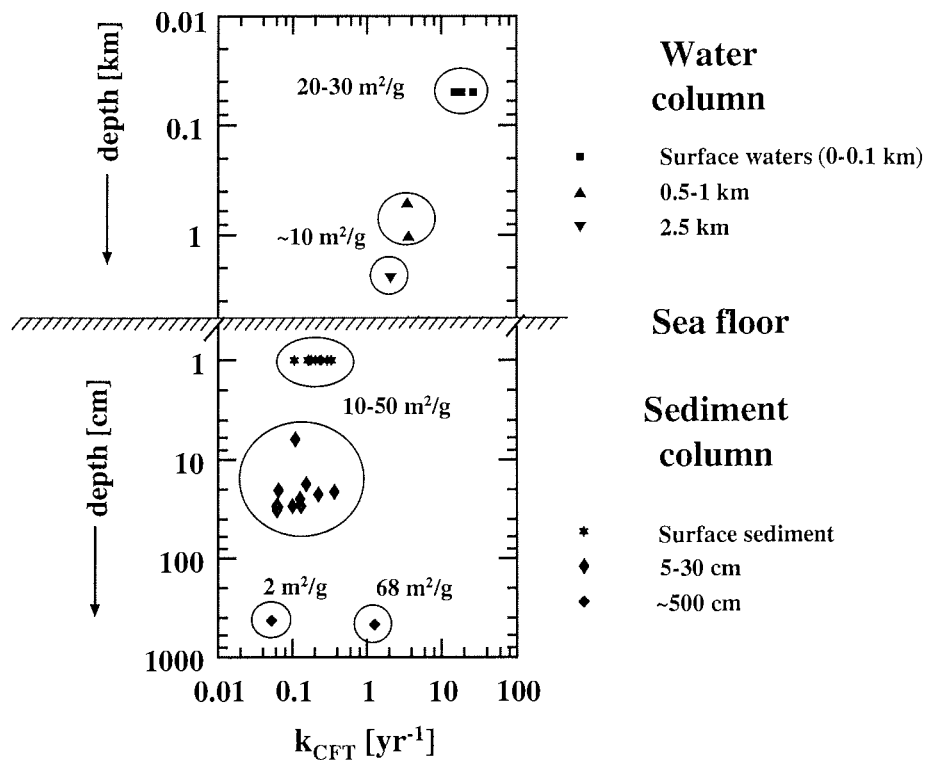


Fig. 3.34 Rate constants determined by flow-through experiments in samples from the water column (acid-cleaned or untreated) and sediment from various depths (untreated) reveal a decrease with depth (\sim age) due to reasons which are discussed below. An extraordinary high rate constant measured for Opal-A/CT sample from Maud Rise or a low rate constant for an *Ethmodiscus rex* sample from the Weddell Sea sediment can be mainly attributed to the large ($68 \text{ m}^2/\text{g}$) - or low ($2 \text{ m}^2/\text{g}$) - surface areas of the samples.

3. Experimental results and discussion

The lowest reactivity ever reported in the literature for a single species reveals the giant diatom *Ethmodiscus rex* with $k_{\text{CFT}} \sim 0.05 \text{ yr}^{-1}$. Including the low surface area, however, supplies higher net dissolution rates than opal-A/CT (Maud Rise) (Tab. 3.4). For untreated trap material from the Norwegian Sea and acid-cleaned trap material from the Weddell Sea values of $2\text{-}4 \text{ yr}^{-1}$ were obtained, showing slight differences with depth. Apparent dissolution rate constants between 0.05 and 0.36 yr^{-1} were observed for the sediments under investigation. It is also remarkable that there is a difference in dissolution rate constants by almost a factor of ~ 7 between the cores and when comparing reaction rates from the top and the bottom of the core.

In the following section laboratory results in terms of reactivity are summarized and discussed.

3.1.2.3.3 Reactivity control on biogenic silica dissolution

A fundamental variable that is central in any rate law, whether on the atomic or the field scale, is the reactive surface area [LASAGA, 1995]. Obviously mineral surface areas are needed to normalize reaction rates that are measured in the laboratory or in the field. The fundamental rate constant k' [DOVE, 1995], for instance, is written in terms of $\text{mol m}^{-2} \text{ s}^{-1}$. The reaction rates measured in flow-through experiments must be considered as bulk reaction rates when combining the rate constants k [yr^{-1}] - reflecting the reactivity of the most soluble species or reactive sites (see below) - with BET surface areas, since BET powder measurements combine areas of less reactive sites with more reactive sites. VAN CAPPELLEN [1996] has reported that BET surface areas in siliceous oozes remain essentially unchanged, whereas reaction rates vary by a factor of 3 with depth.

This observation supports the assumption that N_2 BET surface areas do not constitute a satisfactory proxy for the reactive surface area of biogenic silica in sediments. For cores PS-2299 and PS-2314-1 BET surface areas were determined on untreated and treated samples and revealed considerable increases in surface area after pretreatment (Fig. 3.25), albeit relative depth-distribution in both cases remains fairly constant in PS-2299 or decreases only slightly in PS-2314-1 (Fig. 3.27). Since neither k_{CFT} nor cobalt adsorption capacities change dramatically with depth, the statement above [VAN CAPPELLEN, 1996] cannot be proved. Even more striking is the observation that k_{CFT} values of two distinct samples from core PS-2299, one untreated and one acid-cleaned, normalized to enhanced surface areas provided remaining reactivity differences by a factor of ~ 4 . This observation was also made for untreated and acid-cleaned phytoplankton samples ANT-XV/2 #64 and #65, but remaining differences by a factor of ~ 8 revealed that changes in k_{CFT} values cannot be approximated by applying a predefined technique of considering surface area changes only (Figs. 3.33, 3.35 and 3.36).

Inorganic and organic coatings can obviously also be active in decreasing or blocking reactive sites of biogenic silica during settling and burial. This leads to a reactivity decrease of at least one order of magnitude, compared to results of phytoplankton or sediment trap material, which is in agreement to previous findings [e.g., LAWSON et al., 1978; KAMATANI, 1982]. VAN CAPPELLEN and QIU [1997a,b] have observed only slight differences in reactivity when comparing untreated and H_2O_2 -washed sediments but large differences in cobalt adsorption experiments, and concluded that a reduction of surface reactivity is not caused by the formation of protective organic

coatings but, rather, by a decrease in reactivity sites. Acid-cleaning of the samples was avoided by the latter [VAN CAPPELLEN and QIU, 1997a,b] for reasons of reactivity and solubility changes [HURD, 1973] discussed in Section 3.1.2.2.3.

Both acid-cleaning and H_2O_2 -pretreatment at $100^\circ C$ were used to remove both inorganic and organic coatings. These seem to be persistent if no activation energy (heating) is applied; both, however may lead to variations in cobalt adsorption capacities through blocking of silanol groups or adsorption. It cannot be precluded that such pretreatment has drastically altered reactivity behavior towards a surface of fewer silanol groups and increasing O-Si-O-bridges [VAN CAPPELLEN and QIU, 1997b]. This may explain the uniform cobalt capacities found after pretreatment, but would not explain why k_{CFT} for untreated samples does not change with depth. It appears that deep-sea siliceous oozes behave very differently from one site to another and that the factors which affect dissolution kinetics are not predictable simply by pore water modeling studies alone without corresponding laboratory evidences.

A comparison of k_{CFT} and k_{NaOH}

In principle, the decrease in net dissolution rates measured in most cores when dealing with a distinct sediment core or comparing cores from different sites (Fig. 3.22) is a result of surface reactivity decreases [VAN CAPPELLEN and QIU, 1997a,b], the preferential dissolution of more soluble phases [e.g., MIKKELSEN, 1979] and/or the progressive increase of inorganic surface coatings [e.g., HURD, 1973]. The determination of reactive surface areas of biogenic silica in non-biosilicious oozes is clearly more difficult than for siliceous oozes since ion adsorption methods [VAN CAPPELLEN, 1996] as well as surface area determinations (BET) in heterogeneous sediment samples must deal with multi-component surface areas where partitioning between biogenic silica and non-biosiliceous minerals can be executed only arbitrarily.

As a further extension of adsorption experiments alkaline reaction rate constant k_{NaOH} as a bulk reactivity parameter for the investigated sediments has been established. This procedure has the advantage of being even faster than adsorption measurements. Moreover, it combines the determination of biogenic silica with reactivity determinations during the same experimental course and is not restricted to biogenic silica-rich sediments. Recently, KONING et al. [1997] also reported the use of this bulk parameter to estimate reactivity differences in cores. In their study, the problem of finding an explanation for changes in k_{NaOH} values representing the reactivity of the respective mixture as a whole remained.

A large data base, including laboratory experiments, which evaluates major controls on constant k_{NaOH} , namely influences of increasing inorganic and surface coatings, is presented here. This constant is useful both for predicting reactivity differences of different species in almost pure siliceous samples (Fig. 3.35) and for tracking principle downcore reactivity shapes of biosiliceous remains in a heterogeneous sediment matrix observed in flow-through experiments (Fig. 3.31). When comparing different parameters to determine 'parts' of the reactive sites of single opal samples it becomes obvious that k_{NaOH} and k_{CFT} correlate well in all samples (Fig. 3.31). Changes in the structure due to inorganic and organic coatings (ANT-XV/2 #65 and sediment trap material NB9) lead to a reactivity decrease in dissolution rate constants; it is more

3. Experimental results and discussion

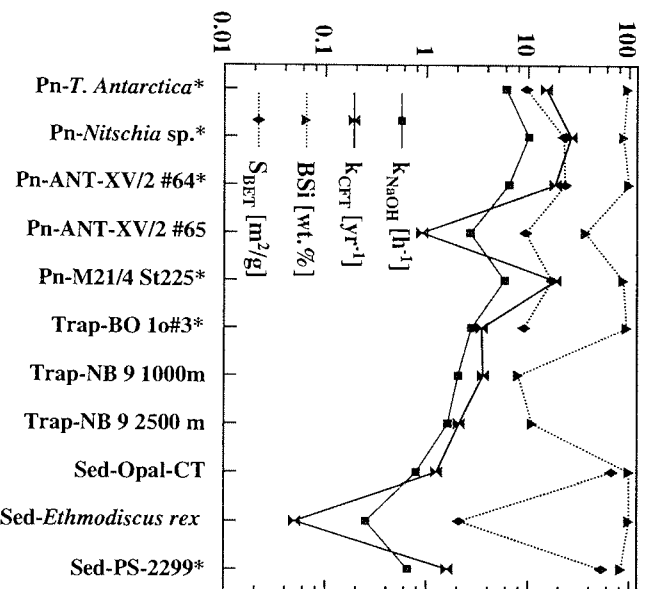


Fig. 3.35 Determination of reactive surface area of untreated or acid-cleaned (*) single biogenic opal samples (Pn Plankton, Trap Sediment trap material, Sed sedimentary opal) using different parameters which all represent parts of the reactive surface, i.e. the surface which will participate in the dissolution process (see text). Bold lines (k_{NaOH} alkaline leaching constant (85°C, pH 12.5, 0.32 N NaOH), k_{CFT} continuous flow-through rate constant (2°C, pH 8, seawater)), dashed lines (BSi [wt.%] biogenic silica content of sample (including 10% water according to MORTLOCK and FROELICH [1989]), S_{BET} [m²/g] specific surface area). Note that correlation is best between k_{CFT} and k_{NaOH} (see Fig. 3.36).

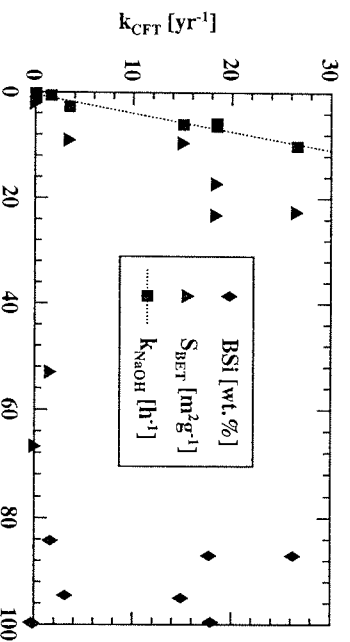


Fig. 3.36 Dissolution rate constant k_{CFT} derived from flow-through experiments performed or recalculated for pH 8 and $T = 2^\circ\text{C}$ in artificial seawater as a function of reactive surface area, approximated with (a) biogenic silica content (BSi), (b) nitrogen BET specific surface area (S_{BET}) or (c) alkaline reaction rate constant k_{NaOH} reveal best correlation between k_{CFT} and k_{NaOH} with a correlation coefficient $R^2 = 0.982$. Note that only data for nearly pure opal (acid-cleaned samples, *Ethmodiscus rex* and Opal-A/CT) (Fig. 3.35) are included.

pronounced in flow-through than in alkaline leaching experiments due to a lower sensitivity of the latter method (see discussion above).

Variations in the specific reactive surface area are in part matched by corresponding changes in nitrogen BET surface area measurements. Particularly when acid-cleaned samples are considered, large differences appear when organic coatings or diagenetically altered samples (Opal-A/CT, PS-2299) were included. Hence, the overall correlation between reaction rate constant k_{CFT} (Fig. 3.36) and nitrogen surface areas for nearly pure opal samples, excluding those samples with distinct surface coatings such as trap material (NB9) and ANT-XV/2 #65, underscores the fact that the N_2 BET surface area does not provide a satisfactory proxy for tracking the evolution of the reactive surface area of biogenic silica in the sediments [see also VAN CAPPELLEN, 1996, VAN CAPPELLEN and QIU, 1997b].

The kinetic equation most widely used in pore water modeling studies (Eq. 3.27) assumes that the reactive surface area is proportional to the amount of opal, implying that (a) the specific surface area of these particles does not change with depth, and (b) the total surface area is proportional to the concentration of biogenic silica in sediment [e.g., SCHINK et al., 1975; BOUDREAU, 1990; RABOUILLE and GAILLARD, 1990]. Figures 3.35 and 3.36 reveal that this is not even true for nearly pure opal samples from different origins. Without doubt, this correlation is very weak; in sediments this correlation is even more doubtful when plotting k_{CFT} and opal contents of sediments described in this thesis (not shown here). It suggests that only parts of biogenic silica - often referred to as "reactive fraction" [e.g., SCHINK et al., 1975; MCMANUS et al., 1995; RABOUILLE et al., 1997] of the total fraction - represent the overall reactive surface area which is actively involved in the overall dissolution process.

Finally, considering the extraordinarily good correlation of k_{NaOH} and k_{CFT} (Figs. 3.35 and 3.36) lends supports to the concept of using the alkaline rate constant as a rapidly determinable alternative when relative changes in the reactive surface area are to be determined. Given the empiric expression

$$k_{\text{CFT}} = a \cdot k_{\text{NaOH}} + b \quad (3.9)$$

with constants $a = 2.88 \text{ yr h}^{-1}$ and $b = -1.34 \text{ yr}^{-1}$ of the linear regression of k_{CFT} plotted versus k_{NaOH} , it is possible to determine reaction rates for acid-cleaned opal samples in seawater at 2°C while determining the opal content of the sample at 85°C and pH 12.5. The results can then be recalculated for ambient seawater temperatures and pressures. It is important to mention that only the leaching data base established for this thesis has been used to calculate the constants a and b . It should be mentioned that the above-mentioned expression is restricted to almost pure and/or acid-cleaned biogenic silica samples.

The enigma

Following the enigma is addressed (Chap. 1), i.e. the bimodal character of the relationship between surface water production and benthic accumulation. Published data summarized in NELSON et al. [1995] indicate that the bulk accumulation (15-25%) of biogenic silica appears in Southern Ocean regions in which only 10% of global production occurs. In oligotrophic gyres and other systems, in which the remaining 75-90% of biogenic silica is produced in surface waters, underlying sediments

3. Experimental results and discussion

accumulate only minor amounts of silica. Several mechanisms control the efficiency of opal preservation in the oceans in ways which may lead to the regional differences observed (Chap. 1).

The ocean is everywhere undersaturated with respect to biogenic silica (e.g., STUMM and MORGAN, 1981). Consequently, dissolution occurs at all depths as particles sink through the water column. Dissolution continues during burial until interstitial waters become saturated. Thus, a process which either lowers BSi dissolution rates during sedimentation and burial or decreases the time sediment particles are exposed to an undersaturated solution will increase the fraction of surface-produced opal preserved in sediments.

An elegant study by BIDDLE and AZAM [1999] provides further impulses. The overall dissolution process is of less importance as long as organic coatings are present and the breakdown of protective coatings is slowed in areas limited in dissolved iron [PAKULSKI, 1996]. Results from untreated and acid-cleaned phytoplankton samples from the North Atlantic and the Southern Ocean are presented here, but in all phytoplankton samples reaction rate constants yield no significant differences as long as acid-cleaned samples are considered. But reactivity decreases substantially by a factor of ~20 if organic coatings remain almost untreated (ANT-XV/2 #65). Indeed, silica shells can survive high surface water temperatures as well as an undersaturated water column as a whole if the hydrolytic attack of organic matter through bacterial assemblages is slowed. Given the results of the present thesis to explain the outlined discrepancy above, differences in dissolution kinetics of various biosiliceous species (Tab. 3.4) are only one aspect which must be regarded. Results from selected phytoplankton samples reveal no systematic differences in reaction rate constants when phytoplankton assemblages from the Norwegian Sea (M21/4, $k_{CFT} \sim 18(2) \text{ yr}^{-1}$) and the Bransfield Strait (ANT-XV/2 #64, $k_{CFT} \sim 18(2) \text{ yr}^{-1}$) are compared (Tab. 3.24, Fig. 3.35). According to Figures 3.35 and 3.36 k_{NaOH} yields the same systematic trend.

It is clear, then that all mechanisms active in preventing silica denuding must be considered first, since subsequent dissolution processes, which follow almost the same principles, are of minor importance as long as the organic coatings remain intact during settling of the biosiliceous assemblage to the seafloor. SMETACEK (1999) has summarized the information now available and concludes that this discrepancy can be explained by iron-limited diatoms (FALKOWSKI et al., 1998) which produce thicker shells *a priori* (HUTCHINS and BRULAND, 1998; TAKEDA, 1998), and also by a slower breakdown of protective protein (BIDDLE and AZAM, 1999) because bacterial growth may also be iron-limited (PAKULSKI, 1996). Thus, a larger percentage of shells produced in "high-nutrient, low-chlorophyll" (HNLC) regions survives and is buried.

Additionally, packaged diatom remains in fecal pellets [e.g., NELSON et al., 1995], which are intensified during blooms, together with the sedimentation of large aggregates [ALLDREDGE and GOTTSCHALK, 1989] may actually efficiently transport this material to the seafloor.

Once the silica shells are buried, apparent solubilities are reached most quickly in Southern Ocean regions, in which dissolution kinetics are less inhibited by secondary reactions which may slow down the time (depth) needed to build-up pore water asymptotic silicic acid values.

3. Experimental results and discussion

Overall rate constants k_B as a result from pore water fitting procedures have shown that efficiency in reaching the asymptotic silicic values, i.e. apparent solubilities, is highest in Southern Ocean sediments in which additional detrital contents are lowest (3.2.2.2). Thus, dissolution kinetics in sediments underlying low productivity regions (e.g., Southern Ocean) are additionally favored to prevent the dissolution of silica shells buried, because pore water more rapidly become saturated (Fig. 3.44, Sect. 3.2.2.3).

In summary, the flow-through experiments during which natural conditions were maintained provide useful information concerning the apparent solubilities (Fig. 3.12, Sect. 3.1.1.3.1) of sediment pore waters. This is possible since the experiments were carried out with natural seawater conditions and sediment samples were not pretreated. The effect of pretreatment which extremely enhances reactivity in terms of k_{CFR} due to the removal of organic coatings was demonstrated for phytoplankton and Southern Ocean sediments (Tab. 3.6, Fig. 3.33).

Furthermore, there is much evidence to support the conclusion that secondary precipitations similar to those found in natural environments may also occur in some flow-through experiments, since all sources for such precipitations are given: (a) silicic acid, (b) major cations from artificial seawater, (c) Al from detrital minerals present in the sediments studied. Such reprecipitation reactions are likely to be active in the removal of silicic acid from solution, either from inflow solution or from dissolving silica tests. This can result in a systematic lowering of the measured difference between outflow and inflow concentrations of silicic acid, yielding lower estimates of reaction rates. To which extent and from which undersaturation state a back-reaction should be taken into account is for heterogeneous sediment samples difficult to determine and requires further research. The appearance of such reprecipitations, however, has been documented during similar volcanic glass flow-through experiments in which reprecipitations visually occur [STRONCIK-TREUE, pers. comm.]. Those reprecipitation or reverse weathering reactions present a further important focus on research since they may represent an important sink for silicic acid in the global silica cycle. In Section 3.1.2.3.4 this topic will be discussed.

It is important to mention that experimental rates determined for sedimentary opal tend to reveal similar reactivity trends than those calculated from pore water modeling studies (3.2). Quantitative similarities, however, could not be achieved for reasons which are discussed in Section 3.2.3.3.2. CASEY et al. [1993] has summarized a comparison of laboratory and field studies and stated that it is unreasonable to expect quantitative similarity in reaction rates. The results of reactivities presented in this thesis confirm that laboratory weathering is restricted to the mere prediction of trends. In contrast, flow-through experiments revealed that apparent field solubilities, i.e. pore water asymptotic silicic acid values, can be reproduced (Fig. 3.12). These are needed for a reliable modeling study of the early diagenesis of biogenic silica (3.2.2). Furthermore, reaction rates determined in unnaturally high solid/fluid ratios have the advantage that they approximate the single dissolution process of the most reactive phase which may occur even in natural environments.

This single dissolution process, however, cannot be extracted from pore water modeling studies alone. Thus, these and other previous results [VAN CAPPELLEN and QIU, 1997a,b] are important steps forward towards a more reliable description of natural processes, in which the overall dissolution-reprecipitation process is described in

3. Experimental results and discussion

separate terms of dissolution and precipitation. In on-going research strategies it will be necessary to more reliably examine the counterpart reactions, namely precipitation reactions which occur naturally and may be responsible for smaller estimates of the kinetic constant of several orders of magnitude when modeling pore water profiles (3.2). k_B , derived from pore water modeling studies, must be treated as an overall reaction rate constant, i.e. a constant which is the product of both dissolution and reprecipitation reactions which actually occur in natural settings. This constant k_B , however, does not provide information about the single dissolution process of biogenic opal in natural environments. Accordingly, both laboratory and field experiments or measurements are needed for a holistic understanding of natural processes such as the dissolution kinetics of biogenic silica and reprecipitation reactions in marine environments (3.2.3.3.2).

Compared to flow-through dissolution experiments, adsorption methods (see above) or alkaline dissolution experiments have the advantage of being much faster and simpler to implement on a routine basis for providing first insights into depth-dependent changes in surface or overall reactivities. These methods, however, cannot replace flow-through experiments but must rather be treated as additional valuable tools to obtain more detailed insights into processes occurring in sediments, for example the influence of volcanic glasses in PS-2283-6 or easily soluble aluminosilicates in MC-1-3 or MC-145 (see above).

Flow-through experiments are still needed to study both dissolution and precipitation reaction under natural conditions and for the calibration of the adsorption measurements [VAN CAPPELLEN, 1996] as well as for rate constants k_{NaOH} .

3.1.2.3.4 Reverse weathering control on biogenic silica dissolution

The manifold phenomena of aluminum-silica interaction have led to intensive studies of dissolution kinetics of biogenic silica in the past [LEWIN, 1961; HURD, 1973; VAN BENNEKOM et al., 1991; VAN BENNEKOM et al., 1991; VAN BEUSEKOM, 1995; VAN CAPPELLEN and QIU, 1997a,b; DIXIT and VAN CAPPELLEN, 1998]. VAN BENNEKOM et al. [1991] and VAN BEUSEKOM [1995] discovered that the early incorporation of aluminum in silica shells in surface waters leads to extensive inhibition of the subsequent dissolution process and lowers solubility to values which, in some cases, are far below a silica solubility of $1000 \mu\text{M}$ at 4°C [HURD, 1973]. VAN CAPPELLEN and QIU [1997a] propose that apparent silica solubilities are strongly dependent on pore water aluminum concentrations in marine sediments.

In this thesis, it has been quantitatively shown that Al concentrations which do not exceed certain values ($\text{Al} > 650 \text{ nM}$) have no significant effect on silica dissolution rates in laboratory experiments (3.1.1.2.4, Fig. 3.6). Previous studies have not unambiguously shown how aluminum may reduce silica reactivity if it is present at concentrations far below the solubility of its oxyhydroxides and how minute aluminum adsorption may slow down the kinetics of silica dissolution [e.g., WILEY, 1975a; DOVE, 1994; Nelson et al., 1995]. If unnaturally high concentrations of Al are present in solution (i.e. restricted to laboratory experiments), aluminum sorbs/precipitates on SiO_2 surfaces as aluminum-oxyhydroxides [e.g., WILLEY, 1975; DOVE et al., 1994; DIXIT and VAN CAPPELLEN, 1998]. There is no evidence for unusually high concentrations of dissolved Al in most marine pore waters (for example Arabian Sea, Fig. 3.7), although reverse weathering reactions have been reported to occur in the literature [e.g., SILLÉN,

3. Experimental results and discussion

1961; MACKENZIE and GARRELS, 1965; MACKENZIE et al. 1967; HURD, 1973; LERMAN, 1973; STOFFYN-EGLI, 1982; MACKIN and ALLER, 1986; MACKIN and SWIDER, 1987; MICHALOPOULOS and ALLER, 1995] or have been experienced in laboratory studies with natural components occurring very rapidly if conditions are suitable [e.g., MACKIN, 1989; MICHALOPOULOS and ALLER, 1995].

The laboratory studies outlined here have provided some indications that formation of such authigenic phases may occur. The use of natural sediments of different compositions and artificial seawater, which provide the essential cations for subsequent precipitations, has apparently forced the system to precipitate silicic acid, which, in turn, is induced by the inflow solution or is provided by silicic acid release from biosiliceous assemblages present in the sediments under investigation. From negative differences between outflow and inflow solution, a stadium which occurs more quickly if detritus/opal contents increase (3.1.1.3.2, Fig. 3.18), it can be concluded that some reprecipitation reactions may begin in the reactor and may even begin before apparent solubility with respect to opal/detritus ratio is reached. Recent results from similar flow-through experiments [STRONCIK-TREUE, pers. comm.] deployed with volcanic glasses provide clear evidence that reprecipitation occurs in the reactor. Traces of newly-formed precipitates on both glass particles and reactor walls have been visually observed in the laboratory.

Reverse weathering reactions, nevertheless, require sources of both Al and Si. Flow-through experiments suggest that precipitation results are substantial, namely, in apparent solubility values measured in the laboratory or in pore waters of sediments with low opal/detritus ratios, far from saturation with respect to amorphous silica [1000 μM ; HURD, 1973]. This suggests that a balance between solubilities of both biogenous silica and non-biosiliceous phases exists. Such a balance shifted towards biogenic silica would result in higher apparent solubilities and reaction rates obtained in the uppermost centimetres of the core (Fig. 3.4), before moving towards apparent solubilities which are increasingly affected by the solubilities of additional detrital materials. Additionally, the decrease in reactivity or solubility may be caused by biogenic silica residuals already undergone substantial alteration through surface coatings, by reduced surface reactivities induced by a decreasing number of silanol groups on and/or the preferential dissolution of more reactive silica tests. From a thermodynamic point of view, biogenic silica is now far from being unaltered amorphous silica with respective properties such as a solubility of 1000 μM at pH 8 and 4°C [HURD, 1973].

Even in kinetics these altered silica tests do not behave as in the water column where highest reaction rates occur on silica surfaces which are continuously renewed through direct water contact. Reactivity is reduced and preservation is stronger the deeper the tests are buried and the further alteration has proceeded (Fig. 3.34).

Two sources are required, namely silicic acid from most soluble biogenic silica and Al, since both are needed to coprecipitate, including other cations (e.g., Na, K, Mg) from ambient pore water solution to form authigenic clays as surface precipitates [e.g., HURD, 1973]. From a thermodynamic point of view precipitation occurs when locally enhanced concentrations, for example in micropores, provide saturation with respect to secondary phases. This leads to the conclusion that once silicic acid concentrations increase, most reactive Al within the system is set free from unstable

3. Experimental results and discussion

amorphous Al oxides or highly weathered aluminosilicates, and may migrate only short distances to be immediately involved into near simultaneous dissolution-precipitation processes [MICHALOPOULOS and ALLER, 1995]. The commonly known immobility of Al concluded from barely measurable Al concentrations in pore waters does not preclude the involvement of Al in those more or less simultaneous dissolution-precipitation processes or its being the result of a high turnover rate.

The experiments described here yield strong evidence for such a mechanism, since all Al concentrations used in aluminum flow-through experiments (3.1.1.3.2) were too low to provide measurable Al concentrations in the outflow solution, even when highest Al concentrations were used. On the other hand, silicic acid was 'lost' during experiments in large amounts, making reprecipitation in the flow-reactor likely.

Nevertheless, aluminosilicates also form without the build-up of large Al pore water concentrations, for example in the presence of kaolinite [MICHALOPOULOS and ALLER, 1995], which at least requires the involvement of 'mobile' aluminum. Indeed, apart from a marked solubility decrease (Fig. 3.10) very low reaction rate constants (k_{CFT}) for biogenic silica in the presence of kaolinite (Fig. 3.32) were measured. Additionally, the lowest k_{NaOH} values obtained, values which are somewhat proportional to k_{CFT} values (Fig. 3.36), appear in different detritus/opal mixtures when kaolinite was applied. It seems reasonable to assume that high Al release during alkaline leaching procedures is a good indicator for reduced silica dissolution rates even under natural conditions since reprecipitation with silicic acid can either lower the measurable silicic acid release or lead to a subsequent lower dissolution rate of biogenic silica. The first answer appears to be most conclusive since the overall dissolution of BSi is faster under the extreme condition of alkaline leaching than the development of full coating, which may lower the dissolution rate of biogenic silica. k_{NaOH} is a useful indicator of reactive aluminosilicate phases in sediments, as in the case of the Pacific sediments (MC-145 and MC-1-3) such reactions are favored to occur since Al releases during the alkaline leaching procedures are by far greatest throughout the cores under investigation (Fig. 3.30). This possibility will again be discussed under consideration of calculated parameters from pore water modeling procedure (3.2.3.3.1).

Since other cations from the inflow solution are also present, other phases may form as well. For example, sepiolite formation involving Mg has been reported [e.g., CHRIST et al., 1973; GARRELS and CHRIST, 1965; BADAUT and RISACHER, 1983]. The experimental evidence summarized by results of this thesis takes into account previous [e.g., MACKIN, 1989; MICHALOPOULOS and ALLER, 1995; VAN CAPPELLEN and QIU, 1997a,b] and recent laboratory evidence [DIXIT and VAN CAPPELLEN, 1998; DIXIT, pers. comm.). The early diagenesis of biogenic silica in sediments involve reactions shown in Figure 3.37.

There is, however, a lack of direct evidence for the precipitation of such newly-formed aluminosilicate phases in flow-through experiments performed with biogenic silica embedded in heterogeneous sediment matrices, since XRD amorphous phases are barely distinguishable from existing phases in the heterogeneous sediment matrix. But, the unequivocal results of flow-through experiments with volcanic glasses [STRONCIK-TREUE, pers. comm.] are anticipated. Volcanic glasses, which also represent highly silicified amorphous phases have the advantage of not representing such a heterogeneous mixture as found in the sediments under investigation.

Early diagenetic reactions of biogenic silica in sediments

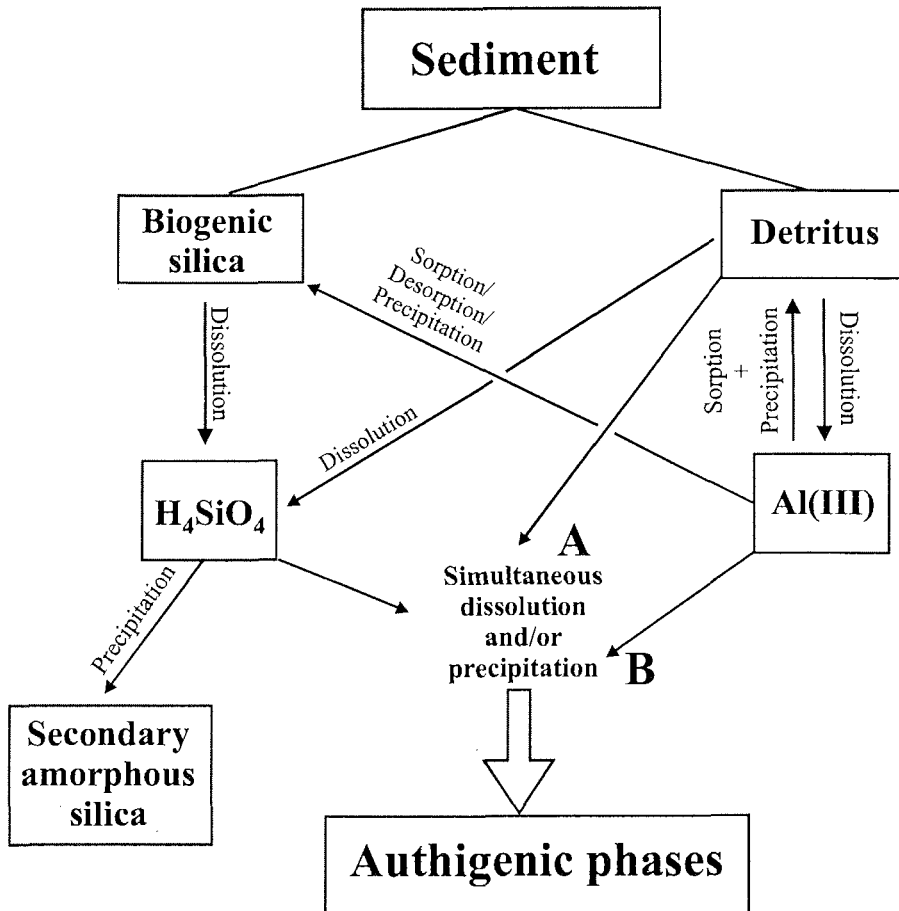


Fig. 3.37 Early diagenetic reactions of biogenic silica in sediments. Sediments of various compositions consist of both biogenic silica and detrital minerals, such as clays, quartz, feldspars or volcanic glasses and ashes in addition to carbonate or organic residues. Detrital clays and biogenic silica are important sources of Al or/and Si, which both appear in varied ratios in sediment pore water, to a large extent controlled by the logarithmic ratio of detrital/opal (Fig. 3.18). Silicic acid may adsorb onto detrital components, reprecipitate on biogenic silica shells to form less soluble siliceous coatings, or be involved in reverse weathering reactions with aluminum and other major cations to form authigenic clays. This formation is thought to take place: (A) through coprecipitation of soluble Si and Al as proposed by VAN CAPPELLEN and QIU [1997a] or (B) through near-simultaneous dissolution and reprecipitation of aluminum with silicic acid when pore water build-ups of Si stress the need for reprecipitation under involvement of Al and other cations present [MICHALOPOULOS and ALLER, 1995 and this thesis]. The concentration of dissolved silica observed in pore waters may, therefore, be a function of the availability of dissolved alumina and of the composition of siliceous phases.

3. Experimental results and discussion

The evolution of reprecipitates has been visually observed during the course of the experiment (see above). SEM studies [Stroncik-Treue, pers. comm.] give strong evidence for the evolution of secondary precipitates formed during flow-through experiments before apparent solubility with respect to the volcanic glass phase has been reached.

If such a controlling mechanism can be confirmed for sediments in which biogenic silica is embedded, this may result in the addition of reverse weathering reactions, i.e. the formation of authigenic clays, as an important sink for silicic acid, with corresponding implications for global controls of elemental cycling, in general, and for the silica cycle, in particular (Fig. 1).

3.1.2.3.5 Geochemical implications for early diagenetic modeling of biogenic silica dissolution

Non-linear dissolution rate law

The results of this study confirm results by VAN CAPPELLEN and QIU [1997a,b] which state that the dissolution rate of biogenic opal, at least for sedimentary opal samples (3.1.2.3.1), is strongly and non-linearly dependent on the degree of departure of seawater from saturation. In Section 3.2.3.3.1 a further incorporation of such a non-linear rate law (Eq. 3.22) with $m \neq 1$ instead of a linear rate law ($m = 1$) in existing diagenetic models for deep-sea sediments was investigated to determine whether it provides crucial improvements towards a more sophisticated description of pore water silicic acid profiles or fluxes through the sediment-water interface. As long as halfsaturation of apparent silica solubility is reached for most cores after a few millimetres in the sediment (Fig. 3.44 in Section 3.2.2.3) the use of a linear rate law at low temperatures ($\sim 2^\circ\text{C}$) to model pore water silicic acid values seems to be justified according to my and previous results [VAN CAPPELLEN and QIU, 1997 a,b].

An exponential increase in the biogenic silica dissolution rate at critical levels of undersaturation, however, would provide a better understanding of the efficient recycling of silicic acid in the ocean's surface waters. Dissolution in upper surface waters take place at extremely high degrees of undersaturation, i.e. a relative degree of undersaturation of > 0.99 considering surface water silicic acid concentrations of $< 10 \mu\text{M}$ and moderate temperatures, suggesting dissolution rates several orders of magnitude higher when non-linear dissolution kinetics can be applied. Laboratory results have not yet yielded similar trends for single opal species under investigation, but for sediment trap material from the Norwegian Sea such non-linear behavior has been observed (Fig. 3.20).

At high degrees of undersaturation (Eq. 2.13) a dissolution plateau [BURCH et al., 1993] is also likely to occur where the free energy term $f(\Delta G_r)$ (Eq. 2.2), hence the undersaturation term in Equation 2.13, can be neglected. This may put restrictions on endlessly high dissolution rates.

Incorporation of a depth-dependent reactivity constant

Neither the assumption of constant total reactive surface area in diagenetic models (dissolution rate laws contain no explicit surface area dependence) [e.g., EMERSON et al., 1984; MCMANUS et al., 1995] nor a variable surface area (by assuming that it is proportional to the concentration of biogenic silica) merits further justification [e.g., SCHINK et al., 1975; BOUDREAU, 1990]. This assumption also ignores reactive surface area changes, at least in sediments in which silica contents remain nearly constant with depth [VAN CAPPELLEN and QIU, 1997 b].

SCHINK et al. [1975] stated that a more sophisticated model would adopt a k_B , the dissolution rate constant of biogenic silica in a pore water sediment system, decreasing with depth because of the gradual formation of inorganic coatings on siliceous tests. BOUDREAU [1990] again emphasizes the incorporation of a depth-dependent reactivity constant. The surface coating model [KAMATANI et al., 1988; MCMANUS et al., 1995] assume that k_B dominates the down-core changes in reaction rate. Evidence found by VAN CAPPELLEN [1996] has led to investigations of depth-dependent reaction rates in modeling pore water silicic acid [RABOUILLE et al., 1997].

The results discussed in the previous section provide unequivocal evidence for the involvement of rate constants, which represent a decreasing tendency with depth as a first step. Going one step further, rate equations should involve two separate equations, the first which represents the dissolution of biogenic silica, the second which accounts for reprecipitation reactions occurring in sedimentary environments. Therefore, possible reprecipitation reactions occurring in sedimentary environments have to be identified and experimentally quantified by means of flow-through experiments [VAN CAPPELLEN and QIU, 1997 a,b; RABOUILLE et al., 1997].

Since no other constraints but, rather, only measurable parameters, have been placed on this pore water fitting procedure (3.2) to analytically achieve reaction rate constants $k_B(x)$, which are compared with the corresponding laboratory-derived dissolution rate constant k_{CFT} , and fluxes of silicic acid through the sediment-water interface, it is no coincidence that a depth-dependent reaction rate occurs in the modeling approach. Indeed, there is a certain amount of mechanistic or chemical rationale which has been discussed in the previous chapters. The formula Equation 3.22 has the advantage that it makes it possible to consider the bulk of biogenic silica as a single compound whose reactivity varies with depth; this reactivity decrease with depth is a forcing consequence from the laboratory results (Figs. 3.35 and 3.36).

Inflow of multiple opal types differing in solubility and reactivity constant values

There is no *a priori* reason to assume that the types of opal entering the sediment have the same solubility or reactivity. My results show that reaction rates differ from one species to another due to physical properties, for example $k_{CFT}(E. rex) = 0.052(6) \text{ yr}^{-1}$, $k_{CFT}(T. antarctica) = 15(1) \text{ yr}^{-1}$; $k_{CFT}(Nitschia \text{ sp.}) = 26(2) \text{ yr}^{-1}$ (Tab. 3.4). Corresponding surface areas are $\sim 2 \text{ m}^2/\text{g}(E. rex)$, $\sim 10 \text{ m}^2/\text{g}(T. antarctica)$, and $\sim 22 \text{ m}^2/\text{g}(Nitschia \text{ sp.})$ (Tab. 3.4).

In addition, the reactivity expressed by the reactivity constant may change with time (depth) due to the aging of the material, either through adsorption of inorganic cations or the decrease of organic coatings. This can also result in depth-dependent changes in solubility and reactivity, and is demonstrated when reactivity changes are compared

3. Experimental results and discussion

with depth (Fig. 3.34). These results clearly demonstrate that the surface reactivity of exposed biogenic silica decreases significantly on early diagenetic time-scales (VAN CAPPELLEN, 1996) (1.000-10.000 years). The dissolved silica equation must be modified to reflect multiple sources. Various species all represent individual dissolution kinetics. The following equation can account for the preferential dissolution of the most reactive fraction and would no longer produce reaction rate constants which solely represent the bulk behavior of a biosiliceous assemblage within a sediment core (3.2.3.3.1):

$$\frac{d}{dx} \left[\varphi(x) D_s \frac{dS_i}{dx} \right] + \varphi \sum_{i=1}^n R_i = 0 \quad (3.10)$$

(see BOUDREAU (1990) for further details, e.g. concerning conservation equations for each of the „n“ reactive solid types along with new boundary conditions). Overall, it is unlikely that this set of equations will be assessable through analytical methods. This will necessitate the use of a numerical method to gain a solution which is beyond the scope of this thesis.

3.1.2.4 Conclusion

- (1) The dissolution kinetics of sedimentary and single opal samples retrieved from various depth horizons of both the water column and sediments exhibit a partly linear dependence on the degree of undersaturation as long as low degrees of undersaturation are considered, but switches to an exponential dependence at higher degrees of undersaturation.
- (2) Results were fitted using a fully non-linear rate law, a rate law with a functional dependence on the relative degree of undersaturation:

$$R_{\text{diss}} = k_{\text{diss}} \left(1 - \frac{[\text{Si}]}{[\text{Si}]_{\text{eq}}} \right)^m$$

where R_{diss} is the dissolution rate measured in flow-through experiments. k_{diss} (or k_{CFT}) is the apparent rate constant which combines all non-determined properties of biosiliceous assemblages within individual sedimentary matrices. $[\text{Si}]$ is the concentration of silicic acid in solution and $[\text{Si}]_{\text{eq}}$ represents the apparent solubility value. m is a constant describing the deviation from linear dissolution behavior. m ranges from 1-3 for sediment samples and particle trap materials.

- (3) Biogenic silica dissolution in the water column can be described by an exponential increase of the dissolution rate, when a critical level of undersaturation is exceeded. This provide a better understanding of the efficient recycling of silicic acid in the oceans' surface waters. Sediment trap material (NB9 1000 m and 2000 m; Norwegian Sea), provided such a clear non-linear dissolution behavior ($m \sim 2.4$) with rate constants of $3.6(2) \text{ yr}^{-1}$ (1000m) and $2.1(1) \text{ yr}^{-1}$ (2500 m) for $T = 2^\circ\text{C}$ and pH 8, suggesting the preferential dissolution of a more soluble biosiliceous fraction during settling.
- (4) A steady decrease in reactivity of biosiliceous remains produced in the euphotic zone as they evolve, during their transfer to the sea floor and after deposition in various sedimentary environments was obtained. Dissolution rate constants

3. Experimental results and discussion

determined for 2°C and pH 8 or recalculated from flow-through experiments at 25°C (using $E_a = 60$ kJ/mol) decrease from ~ 27 yr⁻¹ for acid-cleaned phytoplankton, 2-4 yr⁻¹ for particle trap material to 0.05 and 0.36 yr⁻¹ for sediment material within the top 0-30 cm (time scales 1,000-10,000 years). The giant diatom *Ethmodiscus rex* reveals the smallest dissolution rate constant ($k_{\text{CFT}} = 0.05$ yr⁻¹) ever reported in literature.

- (5) Scotia Sea sediments in general exhibit practically no change in reactivity with increasing depth according to surface area and cobalt adsorption experiments or when applying an alkaline leaching procedure. Ash particles from the 1991 Mount Hudson eruption found in core PS-2283-6 is likely to cause a marked change in dissolution behavior from a solubility and reactivity point of view. While the ash content decreases with depth, apparent solubility values increase due to enhanced opal/detritus ratios whereas reactivity decreases, most probably from alteration by the ash.
- (6) Changes in reactivity throughout the remainder of the cores were characterized by flow-through experiments and are also fairly well represented by k_{NaOH} , the dissolution rate constant from opal leaching experiments. Compared to flow-through experiments, both adsorption methods for opal-rich and the use of k_{NaOH} have the advantage of being faster and simpler to implement on a routine basis, the latter without being restricted to opal-rich sediments. Flow-through experiments, however, are needed for the calibration of adsorption and alkaline measurements of reactivity and for kinetic and solubility measurements under natural conditions. None of the kinetic constants derived from flow-through experiments or from alkaline leaching procedures can define the extent to which a reactivity decrease is attributable to a decrease of surface reactivity or to the preferential dissolution of more soluble species within the sediments, since both methods quantify bulk reactivities and not reactive surface sites.
- (7) An empirical relationship established between k_{NaOH} and k_{CFT} values, provided the use of simple opal leaching techniques to gain reaction rate constants for seawater conditions. This expression, however, is restricted to acid-cleaned and nearly pure opal samples.
- (8) Neither surface areas gained through nitrogen BET specific surface areas nor the total biogenic silica content of sediments provide a reliable proxy for the surface area of a solid which is available for reaction in solution since neither parameter matches the variations in dissolution rate constants obtained in flow-through experiments or alkaline leaching procedures.
- (9) The geochemical implications of this study are the implementation of depth-dependent reaction rate constants, determined by flow-through experiments, alkaline leaching techniques or cobalt adsorption experiments.
- (10) Results obtained using these methods suggest that the formation of aluminosilicate minerals in marine sediments by reverse weathering reactions are likely to occur, indirect evidence for such a formation can be provided from the existing data set.

3. Experimental results and discussion

- (11) Pacific sediments MC-145 (Peru Basin) and MC-1-3 (Juan de Fuca Ridge) give strong evidence to easily soluble aluminosilicates which may be active in controlling pore water silicic acid values.
- (12) The results favor the assumption of the formation of authigenic aluminosilicates during the early diagenesis of biogenic silica in sediments. A closely coupled near-simultaneous dissolution-precipitation reaction between silicic acid derived from dissolution of biogenic silica and mobile Al escaping from relatively unstable Al oxides or highly weathered aluminosilicates is proposed. This mechanism requires no build-up of high aluminum concentrations in pore waters.
- (13) The productivity/burial ratio providing a large discrepancy between Northern and Southern Atlantic can be explained combining the information now available with laboratory results outlined here:

(a) Water column

Iron-limited diatoms make thicker shells, hence Southern Ocean shells are naturally thicker. Bacterial growth is also iron-limited. Thus, a larger percentage of shells in HNLC regions survive and is buried since organic coatings lower reactivity by at least a factor of ~ 20 and slow down dissolution in the water column.

(b) Sediment

Considering subsequent dissolution process in the sediment column, Southern Ocean species again are at advantage since the sediment structure (high opal/detritus ratios) benefits the dissolution process more readily towards apparent saturation values than does the sediment structure in the Northern Atlantic. There, high detrital contents favor adsorption and back-precipitation reactions and slow down the net dissolution process; thus shells remain longer in undersaturated pore waters. A preferential dissolution of more soluble silica remains occurs and leads to a further decrease in biogenic silica contents in Northern Atlantic sediments, whereas biogenic silica remains in the Southern Ocean, once surrounded by saturated pore water, survive.

3.2 Pore water modeling

3.2.1 Introduction

To quantify sedimentary fluxes and identify the processes controlling preservation and recycling efficiencies of biogenic silica, pore water profiles and solid phase silica distributions at 13 locations with different depositional environments, and, hence different opal/detritus ratios have been compared with laboratory results. The benthic silica cycle for 5 locations in the Arabian Sea was quantified using data derived from sediment trap studies in the Arabian Sea [HAAKE et al., 1993].

In particular, it is important in assessing dissolution of biogenic silica within sediments to evaluate whether laboratory conditions reliably reproduce the depth distribution of biogenic silica dissolution kinetics. The latter are directly related to the applicability of diagenetic equations [BERNER, 1980] fed with measurable parameters from sediments and pore waters. In general, diagnostic sediment models are used to simulate silicic acid and biogenic opal profiles [e.g., SCHINK et al., 1975; BERNER, 1980; BOUDREAU, 1990a,b; MCMANUS et al., 1995; RABOUILLE et al., 1997]. Despite strikingly different approaches [summarized in MCMANUS et al., 1995] these models all reproduce pore water silicic acid profiles. Modeling of pore water profiles alone, however, neither explains the factors and processes responsible for the preservation of biogenic opal and the large variations in asymptotic silicic acid values in the sediments nor the depth distributions of kinetic constants controlling dissolution of biogenic silica. Therefore, these were determined independently in laboratory flow-through experiments (3.1 and 3.2) to achieve the most reasonable model. Models, again, are useful for the analysis of experimental work on reaction terms for opal dissolution and the build-up of silicic acid concentration in pore water. Thus, a synthesis of modeling and laboratory experiments best interprets the processes occurring in natural marine environments.

Based on the laboratory results outlined in the previous sections, important implications for more realistic reaction terms have been described in Sections 3.1.1.3.3 and 3.1.2.3.5. It is beyond the scope of the present thesis to include all laboratory results in existing dynamic models of biogenic silica [e.g., SCHINK et al., 1975]. As a first step, an analytical approach using the one-dimensional diagenetic equation according to BERNER [1980] has been chosen, ignoring dynamics (i.e., advection and mixing of solid and liquid phases due to bioturbation or bioirrigation) and selecting observed properties (silicic acid, porosities, biogenic opal contents) as depth-dependent parameters to calculate reactivity constants $k_B(x)$ and fluxes of silicic acid through the sediment-water interface. Fluxes derived from gradients in the fitting procedure at $x = 0$ [e.g., SAYLES et al., 1996; WILLEY and SPIVACK, 1997; KONING et al., 1997] and calculated by two-point gradients [e.g., HENSEN et al., 1998] between bottom water and the first depth interval (bottom water and 0.25 or 0.5 cm) have been discussed. Laboratory results, such as non-linear dissolution kinetics according to Equation 2.13, have been exemplary integrated in this modeling procedure and the use of different fitting functions to reproduce silicic acid profiles more reliably has been discussed. Depth-dependent dissolution rate constant $k_B(x)$ were compared with those from much more simplified fitting procedures which derive k_B . Hereby porosities and biogenic silica contents within the sediment were chosen as constants throughout depth [e.g., HURD, 1973; ARCHER et al., 1993; SAYLES et al., 1996; KONING et al., 1998], an approach which

3. Experimental results and discussion

leaves out the observed reactivity decrease with depth (3.1.2.3.2 and 3.1.2.3.3). The exponential decrease constant α for silicic acid profiles is regarded as particularly suited to reflect the extent to which dissolution-precipitation reactions may act as inhibitors for sediment solution reactions reaching stable silicic acid values.

3.2.2 Results

3.2.2.1 Pore water modeling

Description of the model

The mass balance of material in a small box of sediment can be expressed simply as the difference between input and output flux and production and consumption. Three major processes result in silicic acid concentration at any given depth: diffusion, advection, and diagenetic reaction. For deep-sea sediments, the general diagenetic equation for the behavior of silicic acid per volume sediment is [BERNER, 1980]:

$$\frac{\partial(\phi(x)[\text{Si}])}{\partial t} = \frac{\partial}{\partial x} \left(\phi(x) D_s \frac{\partial[\text{Si}]}{\partial x} \right) + \frac{\partial(\omega \phi(x)[\text{Si}])}{\partial x} + \phi(x) R(x) \quad (3.11)$$

Rate
Diffusion
Advection
Reaction

[Si]	Concentration of silicic acid [$\mu\text{mol} (\text{cm}^{-3} \text{ pore water})$]
$\phi(x)$	Porosity, depth-dependent
D_s	Molecular diffusion coefficient, corrected for effect of tortuosity [$\text{cm}^2 \text{ yr}^{-1}$]
ω	Fluid advection velocity relative to sediment-water interface [cm yr^{-1}]
x	Depth relative to sediment-water interface [cm]
$R(x)$	Net opal dissolution rate, depth-dependent [$\mu\text{mol Si} (\text{cm}^{-3} \text{ pore water}) \text{ yr}^{-1}$]

This one-dimensional differential equation is valid if the sediment column is considered continuous, and it may be used if horizontal variations are negligible in comparison to vertical changes [BOUDREAU, 1986].

It has frequently been shown that deep-sea sedimentation rates are very slow compared with aqueous diffusion [e.g., HURD, 1973; BERNER, 1980]. Furthermore, in deep-sea sediments, the biodiffusion coefficient D_B has proved to be substantially smaller than the molecular diffusion coefficient D_s [BERNER, 1980]. In near-shore, organic-rich sediments ALLER [1977] and EMERSON et al. [1984] have shown that the irrigation coefficient D_I is much greater than D_s or D_B . The magnitude of D_I , in deep-sea sediments, however, has not yet been determined, and it needs to be demonstrated that D_I is in fact negligible compared to D_s . Therefore, advective transport due to burial and compaction and the transport of solutes via bioturbation and bioirrigation are not dealt with in the following approach. The agreement of fluxes derived from *in situ* benthic chamber measurements with pore water modeling supports this assumption [SAYLES et al., 1996; MCMANUS et al., 1995; KONING et al., 1997]. Assuming steady state conditions ($\partial[\text{Si}]/\partial t = 0$), the appropriate diagenetic equation for dissolved silica in deep-sea sediments is:

$$\frac{\partial}{\partial x} \left(\phi(x) D_s \frac{\partial [\text{Si}]}{\partial x} \right) + \phi(x) R(x) = 0 \quad (3.12)$$

The molecular diffusion coefficient D_s for silicic acid corrected for tortuosity according to ANDREWS and BENNETT [1981] is:

$$D_s = \frac{D_m}{\theta^2} = \frac{D_m}{\phi F} \quad (3.13)$$

According to WOLLAST and GARRELS [1971] the free solution molecular diffusion coefficient D_m in seawater at 25°C is $2.2 \times 10^{-5} \text{ cm}^2 \text{ s}^{-1}$. A temperature correction using the Stokes-Einstein relation [LI and GREGORY, 1974] results in a value of $5.5 \times 10^{-6} \text{ cm}^2 \text{ s}^{-1}$ ($173 \times 10^{-4} \text{ m}^2 \text{ yr}^{-1}$). The formation factor F includes the effect of tortuosity θ on diffusive transport and can be written as a function of porosity [ARCHIE, 1942]:

$$F = \phi^{-n} \quad (3.14)$$

ULLMAN and ALLER [1982] recommend $n = 2$ for compacted sediments ($\phi \leq 0.7$) and $n = 3$ for surface sediments with higher porosities ($\phi \geq 0.7$). BOUDREAU [1996] relate θ and ϕ through the simple relation of $\theta^2 = 1 - \ln(\phi^2)$. The first term of a Taylor series expansion produces $\theta^2 \approx \phi^{-2}$. This is Archie's Law [ARCHIE, 1942; LERMAN, 1979] with $n = 3$, i.e. a formation factor, F , which is equal to ϕ^{-3} . For flux and reactivity calculations emphasis has been placed on the top of surface sediments with porosities $\phi \geq 0.7$, where $n = 3$ [ULLMANN and ALLER, 1982]. Thus, Equation 3.13 reduces to

$$D_s = D_m \phi^2 \quad (3.15)$$

The flux of silicic acid from sediment $J(x)$ results from Fick's first law of diffusion:

$$J(x) = -\phi(x) D_s \frac{\partial [\text{Si}]}{\partial x} \quad (3.16)$$

The magnitude of the flux of silicic acid across the sediment-water interface and reaction rate constants of sedimentary biogenic silica were evaluated with an inverse modeling approach using exponential fit functions. With boundary conditions $[\text{Si}]_0 = \text{Si}_0$ and $[\text{Si}]_\infty = \text{Si}_{\text{sat}}$, pore water profiles were fitted to an exponential function [e.g., MCMANUS et al., 1995; SAYLES et al., 1996; KONING et al., 1997; RAGUENEAU et al., submitted)

$$\text{Si}(x) = \text{Si}_{\text{sat}} + (\text{Si}_0 - \text{Si}_{\text{sat}}) e^{-\alpha x} \quad (3.17)$$

where $\text{Si}(x)$, Si_0 and Si_{sat} are the concentration of silicic acid at depth x , zero and infinite depth; α is an exponential decrease constant for the concentration. The first condition $\text{Si}_0 = \text{Si}(x=0)$ implies that the diffusive sublayer [BOUDREAU and GUINASSO, 1982] has little influence on opal dissolution [ANDREWS and HARGRAVE, 1984; MCMANUS et al., 1995]. According to the solubility measurements presented here (3.1.1), it can be assumed that the asymptotic pore water silicic acid concentration at the bottom of the multicorer represents the apparent saturation value. Since most of the concentration changes occurred within 20-30 cm of surface sediments and apparent asymptotic silicic

3. Experimental results and discussion

acid values did not considerably change in underlying depths, as documented by results from retrieved gravity cores, a core length of 20-30 cm is sufficient for these studies.

If porosities have not been measured, a mean value of 0.8 has commonly been used as a first approximation [e.g., RABOUILLE and GAILLARD, 1990; SAYLES et al., 1996; WILLEY and SPIVACK, 1997; HENSEN et al., 1998]. This leads, however to large underestimations of the fluxes and dissolution rates as a function of depth (Tab. 3.8, Sect. 3.2.2.2). Therefore, porosity changes with depth $\phi(x)$ were considered to take into account the large porosity gradients near the sediment-water interface. Since the effective pore water diffusion coefficient of dissolved chemical constituents is, in part, a function of porosity (Eq. 2.20) and because the change in porosity also influences the curvature in the silicic acid profile due to changes in reaction rates [MCMANUS et al., 1995; RABOUILLE et al., 1997; WALLMANN, in prep.], this will in turn influence the value of the model parameters. This relationship is included in the formulation

$$\phi(x) = \phi_{\infty} + (\phi_0 - \phi_{\infty})e^{-px} \quad (3.18)$$

where $\phi(x)$ is porosity at depth x , ϕ_0 is porosity at first depth segment (0.25 or 0.5 cm), ϕ_{∞} is asymptotic porosity, and p is the exponential decrease constant for porosity. The asymptotic depth considered is the depth at which porosity tends to stabilize. Porosity at $x = 0$ is defined as ϕ_{\max} (Fig. 3.41) and determined by extrapolation of the fit function. Substituting Equations 3.15, 3.17 and 3.18 in 3.12 and differentiating 3.17 with respect to depth results in:

$$J(x) = D_m \left[\phi_{\infty} + (\phi_0 - \phi_{\infty})e^{-px} \right]^3 \alpha (Si_0 - Si_{\text{sat}}) e^{-\alpha x} \quad (3.19)$$

Benthic dissolution fluxes have been compared using either Equation 3.19, including the first derivative at $x = 0$ from the non-linear approximation of pore water silicic acid concentrations (Eq. 3.17) [e.g., SAYLES et al., 1995], or simply a linear two-point calculation based on silicic acid concentrations between bottom water and the first sampling interval in the sediment (i.e., 0.25 or 0.5 cm).

The depth-dependent reaction rate can be calculated according to Equation 3.12

$$R(x) = \frac{1}{\phi(x)} \frac{\partial J(x)}{\partial x} \quad (3.20)$$

Differentiation of Equation 3.19 and substitution in Equation 3.20 results in:

$$R(x) = -D_m \alpha (Si_0 - Si_{\text{sat}}) \phi(x) e^{-\alpha x} \left[3p(\phi(x) - \phi_{\infty}) + \alpha \phi(x) \right] \quad (3.21)$$

where the units are as follows: α and p in cm^{-1} , $(Si_0 - Si_{\infty})$ (in $\mu\text{mol cm}^{-3}$ pore waters) and D_m (in $\text{cm}^2\text{yr}^{-1}$); reaction rate $R(x)$ (in $\mu\text{mol yr}^{-1} \text{cm}^{-3}$ pore waters); ϕ is not technically without dimension if the volumes of water [cm^3 pore water] and sediment [cm^3 sediment] are separated.

Following the general rate law (Eq. 2.2), biogenic silica dissolution rates calculated from Equation 3.21 are related to the relative departure from equilibrium, the amount of opal in the sediments, and a kinetic constant [e.g., SCHINK et al., 1975; MCMANUS et al., 1995]:

$$R(x) = k_B(x) \frac{1 - \phi(x)}{\phi(x)} \text{BSi}(x) \frac{\delta_s}{M_{\text{BSi}}} \left(\frac{\text{Si}_{\text{sat}} - \text{Si}(x)}{\text{Si}_{\text{sat}}} \right)^m \quad (3.22)$$

$R(x)$	reaction rate, depth-dependent [$\mu\text{mol yr}^{-1} \text{cm}^{-3}$ (pore waters)] (Eq. 3.21)
$k_B(x)$	rate constant, depth-dependent [yr^{-1}]
$\phi(x)$	porosity, depth-dependent [cm^3 (pore waters)/ cm^3 (of sediment)]
$\text{BSi}(x)$	weight fraction of BSi in solids, depth-dependent
δ_s	grain density of solids [2.65 g cm^{-3}]
M_{BSi}	molecular weight of biogenic silica [$6.6 \cdot 10^{-5} \text{ g } \mu\text{mol}^{-1}$]
$\text{Si}(x)$	silicic acid concentration at depth [$\mu\text{mol cm}^{-3}$]
Si_{sat}	asymptotic silicic acid concentration [$\mu\text{mol cm}^{-3}$]
m	reaction order

$k_B(x)$ has been calculated for each depth interval using Equation 3.22, dividing $R(x)$ through the right-hand term here referred to as $S(x)$

$$S(x) = \frac{1 - \phi(x)}{\phi(x)} \text{BSi}(x) \frac{\delta_s}{M_{\text{BSi}}} \left(\frac{\text{Si}_{\text{sat}} - \text{Si}(x)}{\text{Si}_{\text{sat}}} \right)^m \quad (3.23)$$

BSi contents were also fitted, but not *a priori* using an e-type function such as Equation 3.17 or 3.18. Linear decrease functions or average BSi values were applied as well to fit measured depth-dependent BSi values within reason.

To compare the results derived from dissolution experiments with those from fitting pore water values, reaction rates $R(x)$ are expressed in the same units of [$\mu\text{mol H}_4\text{SiO}_4 \text{ g}^{-1} \text{Opal h}^{-1}$] or for brevity [$\mu\text{mol Si g}^{-1} \text{Opal h}^{-1}$]. Thus, we obtain $R(x)'$ from Equation 3.23:

$$R(x)' = \frac{1}{M_{\text{BSi}}} k_B(x) \left(\frac{\text{Si}_{\text{sat}} - \text{Si}}{\text{Si}_{\text{sat}}} \right)^m \quad (3.24)$$

with $k_B(x)' = k_B(x) / 8760 \text{ [h}^{-1}\text{]}$.

The rate expressions 3.23 or 3.24 are particularly useful in determining rate constants $k_B(x)$. $R(x)$ further considers the influence of changing opal contents with depth, decreasing porosities as well as an increasing saturation level of dissolved silica (3.2.3.3.1).

Finally, this depth-dependent kinetic constant was fitted to derive an exponential decrease constant κ , following the expression:

$$k_B(x) = k_{B,\infty} + (k_B^0 - k_{B,\infty}) e^{-\kappa x} \quad (3.25)$$

where k_B^0 is the kinetic constant at the sediment-water interface ($x = 0$) and $k_{B,\infty}$ is the kinetic constant at any given sediment depth. This equation has also been adopted by RABOUILLE et al. [1997] to describe the decreasing reactivity of bulk biogenic silica with depth. To demonstrate the significant difference between the constant approach (ϕ , BSi = const.) and resulting constants $k_{B, \text{const.}}$, depth-dependent kinetic constants $k_B(x)$ with $k_{B, \text{const.}}$ values were compared for each core (Fig. 3.42).

Equation 3.24 is an overall formulation which does not make any *a priori* assumptions about the processes which lower kinetic rates, except assuming that asymptotic silicic acid concentrations reflect an equilibrium value of biogenic silica in

3. Experimental results and discussion

its host sediment structure. This is supported by these laboratory results which treated pore water asymptotic silicic acid values as true equilibrium values (3.1.1.3.1 and Fig. 3.12).

Solubility changes throughout the core were excluded for a first approximation because of insufficient data points to fit a general trend. Nevertheless, for NAST (Arabian Sea) sediment the influence of a depth-dependent apparent solubility change on calculated kinetic constants is exemplarily demonstrated (3.2.3.3.1).

The dissolution kinetics represented by Equation 3.23 constitute a compromise among assumptions which have to be made in any model because of a lack of accessible parameters. The absolute reactive surface area of biogenic opal in a mixture of detrital components, for example, is still difficult to assess. Any clay minerals or oxides present will distort the results of reactive surface area by contributing large amounts of geometric or reactive surface area.

Nevertheless, cobalt (Co) adsorption experiments (3.1.2.2.3) [VAN CAPPELLEN and QIU, 1997b] provide a powerful tool to determine reactive surface areas in nearly pure opal sediments. Here, an alkaline extraction method has been applied to assess the change of reactivity with depth. A quantification of reactive surface area in terms of reactive sites per mass biogenic opal, however, is still lacking.

For this reason and to achieve consistency with previous studies [e.g., SCHINK et al., 1975; SCHINK and GUINASSO, 1980; RABOUILLE et al., 1997], the linear dependence of reaction rate on mass concentration of soluble opal has been adopted in this study. This appears adequate to my approach which considers the bulk of biogenic silica as a single compound whose reactivity, expressed by $k_B(x)$, changes with depth.

The dissolution rate of biogenic silica is a non-linear function of the degree of undersaturation [Eq. 2.13 ($m \neq 1$), Sect. 3.2; VAN CAPPELLEN and QIU, 1997a,b]. For *in situ* conditions ($T < 5^\circ\text{C}$), however, the degrees of undersaturation must usually exceed values of 0.8 to significantly deviate from a linear rate law. The dissolution of biogenic silica in pore waters usually occurs at undersaturation states significantly lower than the prescribed value of 0.8. Therefore, Equation 3.22 and a linear dependence of the dissolution rate of biogenic silica has been applied to the degree of undersaturation, i.e., $m = 1$, was applied to calculate depth-dependent reaction rate constants $k_B(x)$. These results have been compared with non-linearly fitted Equation 3.23 [$1 \leq m \leq 2$] between reaction rates and the degree of undersaturation of silicic acid.

It should be added that in the water column, in which degrees of undersaturation usually largely exceed values of 0.8, such non-linear dissolution rate behavior of dissolution rate need to be included to more reliably describe the dissolution behavior of BSi (Fig. 3.20).

3.2.2.2 Benthic dissolution fluxes

Silicic acid profiles

Concentration versus depth profiles from 8 of 13 sediment cores (Fig. 2.1 and Tab. 2.1, for data see A.2.1-A.2.6.4) as well as fitted profiles applying Equation 3.17 are shown in Figure 3.38. These reflect great regional differences in productivity and efficiency of opal burial from surface-produced biogenic silica. Generally, pore water concentrations of silicic acid increased from bottom water into the sediment due to the complex interplay of dissolution/precipitation processes of biogenic silica and non-

biosiliceous phases. Bottom water values range from 13 μM in the Norwegian Sea (M31/2) to 185 μM in the Northern Pacific (MC-1-3). Asymptotic silicic acid values $[\text{Si}]_{\text{sat}}$ display a range of ~ 100 μM (M31/2) to ~ 800 μM (PS-2312-1). Laboratory results from this study suggest that asymptotic silicic acid values measured in the field truly reflect the equilibrium between pore water and siliceous phases within sediments. This is an important constraint for subsequent pore water modeling to derive depth-dependent rate constants since $[\text{Si}]_{\text{sat}}$ in Equations 3.17 and 3.23 changes throughout the core and does not *a priori* equal 1000 μM (HURD, 1973; for $T = 4^\circ\text{C}$).

Benthic dissolution fluxes of silica

The fluxes were estimated according to Equation 3.19, using the first derivative of Equation 3.17 at $x = 0$ obtained by fitting the entire dissolved silica profile. These were compared with fluxes using the two-point concentration gradient between bottom water silicic acid concentrations and dissolved silica contents in the first depth segment (0.25 or 0.5 cm) (Fig. 3.39 and Tab. 3.7). The fitting routine used was that of OriginTM, based on the Levenbergh-Marquardt algorithm, and usually took data from the entire core length and bottom water silicic acid concentrations ($\text{Si}_{x=0}$). Input and output parameters are schematically illustrated in Figure 3.40. The entire core length has not been included for NAST, CAST and MC-1-3, because pore water profiles revealed a significant decrease with depth below first asymptotic silicic acid values. A relatively drastic change in opal/detritus ratios with depth seems to be attributable to decreases in silicic acid saturation values (cf. Sect. 3.1.1.3.2 or Figure 3.18). For MC-145 the fitting procedure has been restricted to depth interval 0-20.5 cm. Below that depth sediment structure changes significantly reflecting the transition from the Holocene to the last glacial period (HAECKEL, pers. comm.; Sect. 2.1.1.)

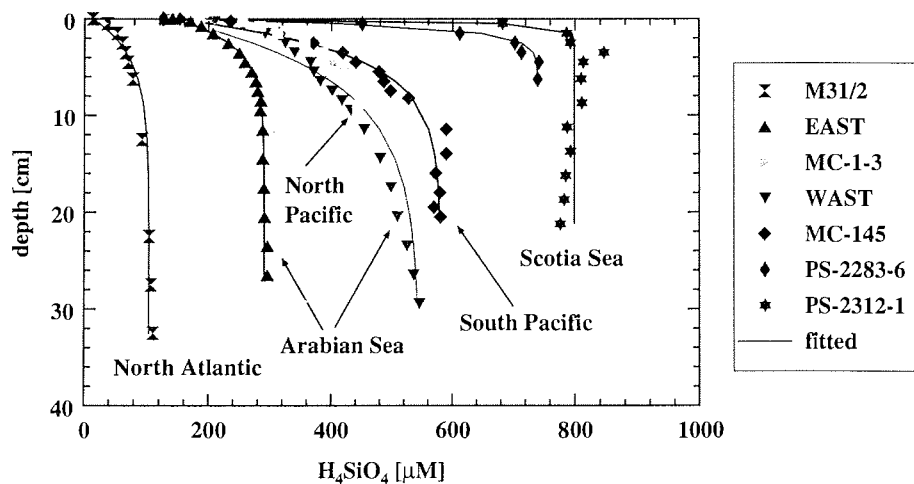


Fig. 3.38 Pore water silicic acid as a function of depth from squeezed cores of 8 selected stations (for locations see Fig. 2.1 and Tab. 2.1; data in A.2.1-A.2.6.4). Again, the discrepancy of pore water asymptotic silicic acid concentrations and the solubility of an acid-cleaned siliceous ooze (1000 μM at 4°C , HURD, 1973) must be mentioned (3.1.1.3.1).

3. Experimental results and discussion

Tab. 3.7 Comparison of benthic silicic acid fluxes from linear or non-linear gradients of silicic acid profiles near the sediment-water interface (same order as in Figure 3.39) for all cores studied. Si_0 bottom water silicic acid concentration; Si_{sat} modeled asymptotic silicic acid; α exponential decrease constant from non-linear fitting procedure of silicic acid versus depth profiles; fluxes (J) are in $mmol\ m^{-2}\ day^{-1}$. Station numbers follow those of Figure 2.1 and Table 2.1.

No/Station/ Core	Length _{fitted} [cm]	Si_0 [μM]	Si_{sat} [μM]	α [cm^{-1}]	J_{linear}	$J_{non-linear}$	J_{mean}
1 PS-2312-1	21.25	129	799	3.5	3.2	7.0	5(3)
1 PS-2314-1	18.75	126	686	2.3	2	3.6	3(1)
1 PS-2299	22.5	126	721	1.8	2.2	3.5	2.9(9)
1 PS-2283-6	6.3	126	740	1.3	1.8	2.7	2.3(6)
5 MC-145	20.5	153	580	0.27	1.3	0.45	0.9(6)
4 MC-1-3	9.5	185	444	0.47	1.0	0.44	0.7(4)
3 NAST	14.5	143	284	0.62	0.57	0.34	0.5(2)
3 CAST	12.5	143	324	0.51	0.59	0.30	0.5(2)
3 WAST	29.5	140	546	0.16	1.0	0.25	0.6(5)
2 MC#33	17.5	45	203	0.38	0.17	0.17	0.17
3 EAST	26.5	141	291	0.38	0.34	0.17	0.3(1)
3 SAST	29.5	134	267	0.15	0.31	0.15	0.2(1)
1 M31/2	32.5	13	108	0.26	0.085	0.042	0.06(3)

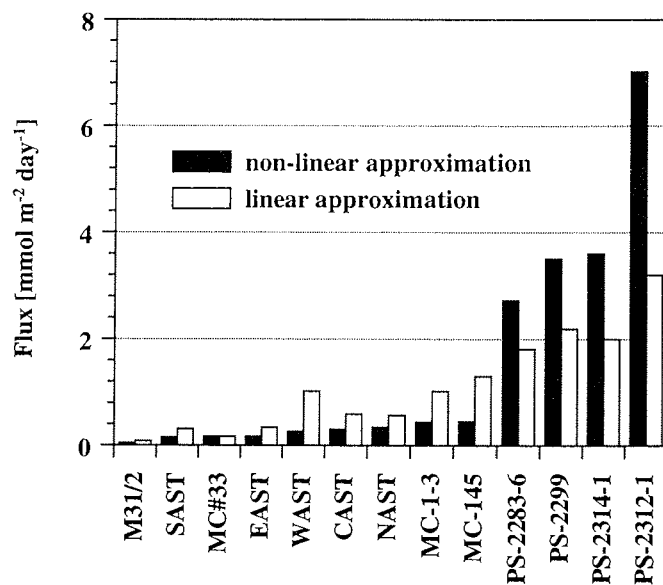


Fig. 3.39 Comparison of benthic silicic acid fluxes as determined from fitting the entire dissolved silica profile (dark columns) and those calculated from a linear approximation between bottom water dissolved silica and the concentration in the upper 0.25 or 0.5 cm core section. The Southern Ocean sediments yield systematically lower fluxes based on linear approximation, whereas sediments with lower BSI contents reveal systematically higher values. The complete data set is given in Table 3.7.

A further increase in opal content in the lower core section (> 20.5 cm) is attributed to different sedimentation behavior during the last glacial period (CaCO_3 contents also increase by an order of magnitude (2.1.1)) and its effect on early diagenetic reactions.

In summary, to compare calculated parameters among cores and steady state conditions, Equation 3.17 was used with a single variable and the fitting procedure was restricted to the first silicic acid values stabilized at a certain sediment depth. At first glance, data were reasonably well fitted by this approach ($R^2 \geq 0.9$) (Fig. 3.38).

A closer look at values near the sediment-water interface (0-2 cm), however, reveal major differences between the measured and fitted patterns applying the classical fitting expression (Eq. 3.17) [e.g., MCMANUS et al., 1995; SAYLES et al., 1995; HENSEN et al., 1998; RAGUENEAU et al., submitted] (3.2.3.2, Fig. 3.46). All profiles with high silica contents from the Scotia Sea (30-60 wt.%, A. 2.6.1 - A. 2.6.4) yield systematic lower flux values using a linear approximation of the gradient beneath the sediment-water interface, whereas those from other regions with much lower biogenic silica contents (1-20 wt.%, A. 2.1 - A. 2.5) yield systematically higher fluxes. MC#33 (BENGAL) is the only site with good agreement between fluxes estimated by either of the two methods (3.2.1.3).

Direct consequences of porosity increases towards sediment-water interface

Reliable porosities (2.4.6) are also of great importance for flux calculations. Equation 3.19 reveals $J(x) \propto \phi(x)^3$. Porosities significantly increase towards the sediment-water interface (Fig. 3.41, A.2.1 - A.2.6.4). Mean values for the whole core or *a priori* assumptions of 0.8 porosity [e.g., SCHINK and GUINASSO, 1980; RABOUILLE and GAILLARD, 1990; WILLEY and SPIVACK, 1997] result in significantly lower estimates of silicic acid fluxes.

To demonstrate the significant differences, fluxes were calculated using ϕ_{\max} , the porosity at the sediment-water interface and a whole core mean value ϕ_{mean} . Results using mean porosities are 50-100% lower than those estimated with changing porosities (Figure 3.42).

In Figure 3.41 and Table 3.8 striking differences in ϕ_{\max} , derived from extrapolating porosities to $x = 0$ using Equation 3.16, are obvious. M31/2, highly detrital but low clay mineral contents, has the smallest porosities, whereas those sediments with relatively high detrital clay contents (MC-145; MC-1-3; SAST) as well as those derived from WAST and NAST reveal porosities exceeding 0.9. Significant decreases in porosity within the top sections (0-10 cm) are obvious in PS-2283-6 ($p = 1.5$), sediments from the NAST site (Arabian Sea) ($p = 0.65$), and the Norwegian Sea (M31/2) ($p = 0.62$) (Tab. 3.8). A very small decrease in porosity with sediment depth were obtained in cores MC-145 (Peru Basin; $p = 0.05$) and MC-1-3 (Juan de Fuca Ridge; $p = 0.12$).

3. Experimental results and discussion

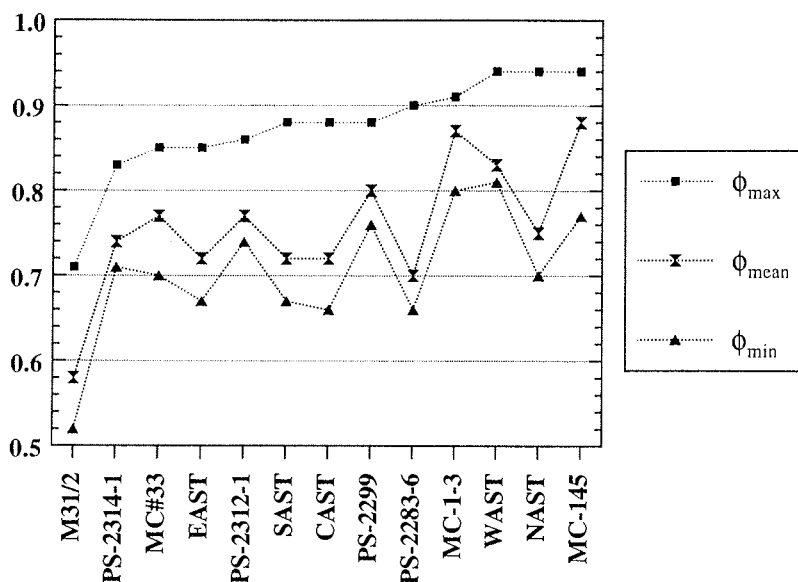


Fig. 3.40 Porosity differences among the cores at $x = 0$ (ϕ_{\max}), at final depth of fitting procedure (ϕ_{\min}) and as a mean value (ϕ_{mean}). Large differences between mean values and porosities near the sediment surface are obvious for cores NAST, PS-2283-6, CAST, SAST, EAST and M31/2. Distinct small changes over a great depth interval are shown by cores MC-145, MC-1-3 and WAST. These large porosity changes near the surface strongly influence flux and reactivity calculations (Fig. 3.41). For porosities see A.2.1-A.2.6.4 or Tab. 3.8.

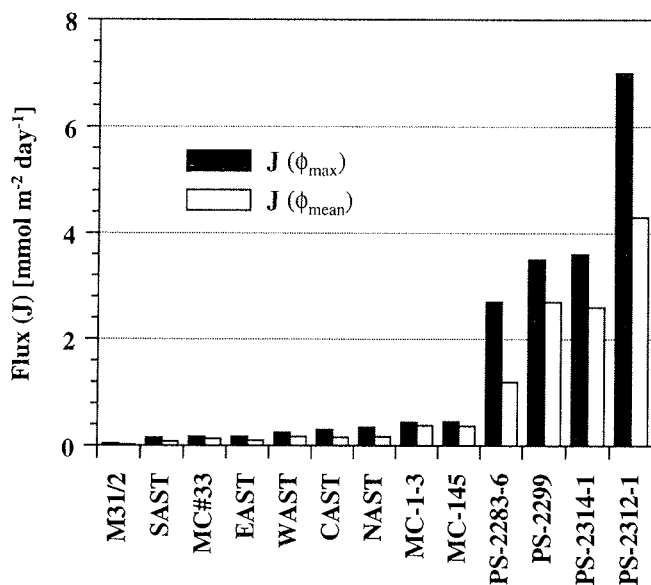


Fig. 3.41 Flux calculations using constant mean porosity (ϕ_{mean}) and ϕ_{\max} from direct measurements just beneath the sediment-water interface. Porosities are the source of large uncertainty for flux calculations from pore water silicic acid profiles. Data are listed in Tab. 3.8.

3. Experimental results and discussion

Tab. 3.8 Comparison of benthic silicic acid fluxes calculated from non-linear gradients near the sediment-water interface and fitted values of ϕ_{\max} or ϕ_{mean} for all cores studied. p is the exponential decrease constant for porosity from non-linear fitting procedure of porosity versus depth (Eq. 3.18); fluxes (J) are in $\text{mmol m}^{-2} \text{day}^{-1}$. Station numbers follow those of Figure 2.1 and Table 2.1.

No/Station/ Core	Length _{fitted} [cm]	$J(\phi_{\text{mean}})$	$J(\phi_{\text{max}})$	ϕ_{mean}	ϕ_{max}	ϕ_{min}	p
1 PS-2312-1	21.25	4.3	7	0.77	0.86	0.77	0.56
1 PS-2314-1	18.75	2.6	3.6	0.74	0.83	0.74	0.5
1 PS-2299	22.5	2.7	3.5	0.8	0.88	0.8	0.6
1 PS-2283-6	6.3	1.2	2.7	0.7	0.9	0.7	1.5
5 MC-145	20.5	0.37	0.45	0.88	0.94	0.88	0.05
4 MC-1-3	9.5	0.38	0.44	0.87	0.91	0.87	0.12
3 NAST	14.5	0.17	0.34	0.75	0.94	0.75	0.65
3 CAST	12.5	0.16	0.30	0.72	0.88	0.72	0.43
3 WAST	29.5	0.17	0.25	0.83	0.94	0.83	0.53
2 MC#33	17.5	0.13	0.17	0.77	0.85	0.77	0.23
3 EAST	26.5	0.10	0.17	0.72	0.85	0.72	0.23
3 SAST	29.5	0.08	0.15	0.72	0.88	0.72	0.44
1 M31/2	32.5	0.02	0.04	0.58	0.71	0.58	0.62

3.2.2.3 Depth-dependent reaction rate constants

Results assuming a near linear rate law

Apart from flux determinations, a second objective of this pore water fitting procedure has been to extract reaction rate constants from pore water silicic acid, BSi and porosity profiles, as illustrated in Figure 3.42 for NAST area sediments. Silicic acid versus depth profiles were fitted using Equation 3.17; bottom water and asymptotic silicic acid concentration have been predefined; or in the case of large scatter, both Si_{sat} and α were determined as described in Section 3.2.2.1. This profile and its parameters were combined with those of fitting porosities with depth (Eq. 3.18) in Equation 3.21. The dissolution rate of biogenic silica may in general be expressed after SCHINK et al. [1975] (Eq. 3.22; $m = 1$), adjusted to the volume of pore water and assuming first-order kinetics at the first step. The term $S(x)$ (Eq. 3.23) can be separated out from Equation 3.22. Combining reaction rates determined from pore water profiles with dependent variables of dissolution summarized in term $S(x)$ (Eq. 3.23) (using Si, BSi and porosity as input parameters) results in depth-dependent dissolution rate constants $k_B(x)$.

Applying a constant opal (and porosity) model, i.e., average porosities and opal contents [see BOUDREAU, 1990a], dissolution rate constant $k_{B,\text{const}}$ provides a significantly lower estimate of surface reactivity for biogenic silica (Fig. 3.42).

As mentioned, such a lower estimate was also found for flux calculations with constant porosities. Applying the fitting procedure with depth-dependent parameters, the rate constant drops by orders of magnitude between the interface and a depth of ~ 2 -3 cm (NAST, PS-2283-6; PS-2312-1, PS-2299, PS-2314-1), of ~ 3 -7 cm (CAST, SAST, EAST, WAST, MC-1-3, MC#33, M31/2) or of ~ 10 cm (MC-145) to reach an almost constant value $k_{B,\text{const}}$ ($k_B(x) \sim k_{B,\text{const}}$; Fig. 3.42 and Tab. 3.9). For a comparison Table 3.9 lists $k_{B,\text{max}}$ values, maximum reaction rate constants near the

3. Experimental results and discussion

sediment-water interface, and $k_{B, \text{const}}$ values. Table 3.9 gives further sediment depths where $k_B(x)$ and $k_{B, \text{const}}$ values converge.

It is noteworthy that $k_B(x)$ values do not necessarily converge exactly to the constant value $k_{B, \text{const}}$, but may be lower. This is explained by the fact that biogenic silica, $\text{BSi}(x)$, or porosity values ($\phi(x)$), exhibit lower than mean values at certain depths which consequently reduce values of either $S(x)$ (Eq. 3.23) or $R(x)$ (Eq. 3.21). Therefore, $k_B(x)$ approaches somewhat lower values than $k_{B, \text{const}}$, but is not essentially zero at depth as in the model presented by RABOUILLE et al. [1997] (see Section 3.2.3.3.1 for further discussion).

Iso-saturation lines (Fig. 3.44) demonstrate the striking differences in silicic acid profiles (Fig. 3.38). It should be further noted that in most cores the dissolution process follows $k_B(x)$ rather than $k_{B, \text{const}}$ when saturation does not exceed a value of 95%. Only M31/2 and WAST cores provided rather constant dissolution behavior immediately below ~ 4 cm sediment depth. In these cases agreement between the data and the model was less reliable than for other cores (Fig. 3.38). Depths of the lines were calculated from Equation 3.17 using parameters of fitted silicic acid profiles given in Table 3.7. In principle, a high density of iso-lines represents a rapid achievement of saturation with depth. Southern Ocean sediments most rapidly attain saturation, within 1-2 cm sediment depth; whereas sediments from the WAST site (Arabian Sea) and from the Norwegian Sea (M31/2) may not become saturated even at the end of the core, thus suggesting the possibility of slow dissolution and/or fast reprecipitation of non-biosiliceous phases or simply the exhaustion of solid phase SiO_2 .

Tab. 3.9 Depth-dependent reaction rate constants $k_B(x)$ calculated for $x = 0$ from Equations 3.22 and 3.23 of fitted profiles according to the modeling scheme (Fig. 3.42). Depth-independent reaction rate constant $k_{B, \text{const}}$ was calculated using the same fitting procedure with mean porosity and BSi contents [e.g., BOUDREAU, 1990a]. At depth where $k_B(x) \sim k_{B, \text{const}}$, both constants tend to converge (Fig. 3.42). For comparison calculated depth at which pore waters reveal 99% of apparent solubility ($[\text{Si}] = 0.99[\text{Si}]_{\text{sat}}$) was assumed as apparent saturation value (see Fig. 3.44). Station numbers follow those of Figure 2.1 and Table 2.1. Note: station/cores here reveal a different order than that of calculated fluxes in Table 3.7 and Table 3.8.

No/Station/ Core	Length _{fitted} [cm]	$k_B(x=0)$ [yr ⁻¹]	$k_{B, \text{const}}$ [yr ⁻¹]	Depth ($k_B(x) \sim k_{B, \text{const}}$) [cm]	Depth ($[\text{Si}] = 0.99[\text{Si}]_{\text{sat}}$) [cm]
3 NAST	14.5	0.407	0.049	2.5	6.3
1 PS-2283-6	6.3	0.39	0.016	2	3.5
1 PS-2312-1	21.25	0.319	0.136	2	1.3
1 PS-2314-1	18.75	0.18	0.061	3	1.9
1 PS-2299	22.5	0.151	0.053	2	2.4
3 CAST	12.5	0.119	0.027	3.5	7.9
3 SAST	29.5	0.066	0.011	4	10.7
3 EAST	26.5	0.047	0.014	6.5	10.3
4 MC-1-3	9.5	0.043	0.022	5.5	8.6
2 MC#33	17.5	0.043	0.018	4.5	11.5
3 WAST	29.5	0.035	0.0053	4	27.4
5 MC-145	20.5	0.013	0.0058	10	16.1
1 M31/2	32.5	0.01	0.0011	3.5	17.3

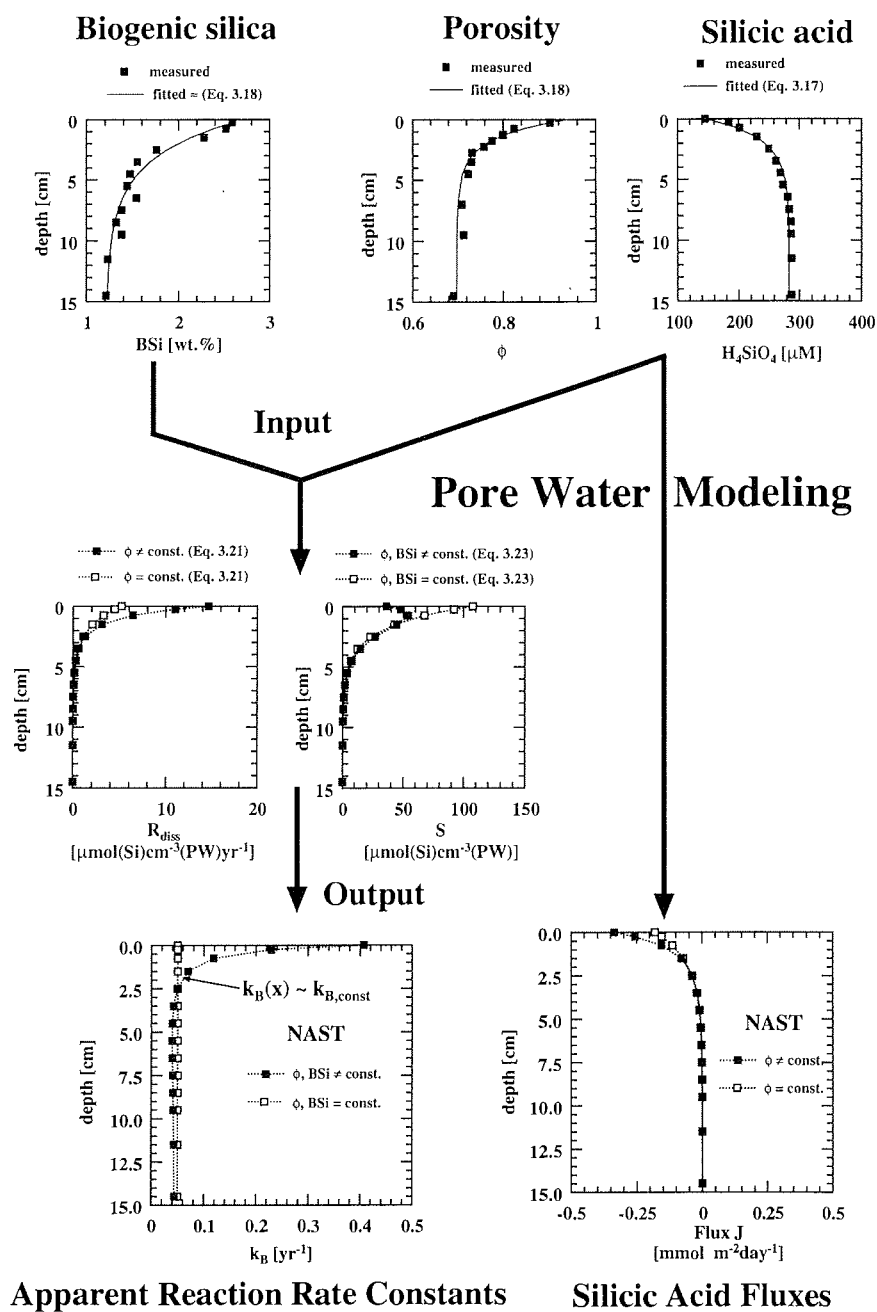


Fig. 3.42 Schematic illustration of pore water modeling (fitting) procedure. The depth distribution of BSi contents for NAST sediments were fitted using an expression according to Equation 3.18, i.e., BSi contents decrease exponentially with depth (depending on the typical shape of BSi versus depth pattern we also applied linear decreasing fit function or average values to fit the BSi profiles). In most cores $k_B(x)$ decreases by orders of magnitude between the sediment-water interface and a depth of ~ 2 -3 cm to stabilize where $k_B(x) \sim k_{B,\text{const}}$. $k_{B,\text{const}}$ was calculated using a constant opal and porosity model [discussed in BOUDREAU, 1990a].

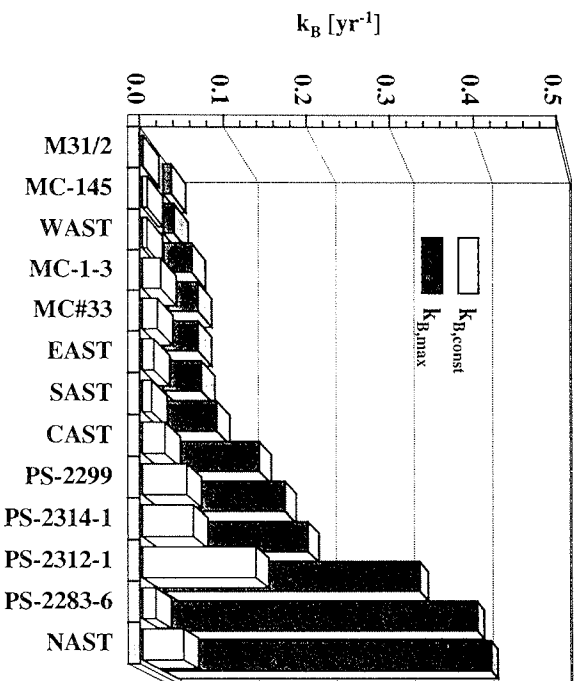


Fig. 3.43 Apparent reaction rate constants $k_B(x)$ and $k_{B,const}$ derived from pore water fitting procedure according to Figure 3.42. Data are given in Table 3.8.

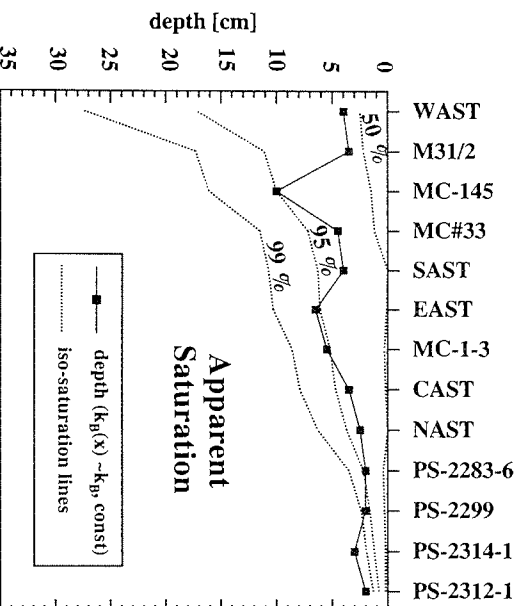


Fig. 3.44 Iso-saturation lines calculated from fitted silicic acid profiles show differences among the cores (see also Fig. 3.38). Within uncertainties saturation value of 99% is considered as apparent saturation at respective depth. Below that depth the net dissolution rate (Eq. 3.22) becomes zero with zero degree of undersaturation. Half saturation (50%) appears almost at or near the sediment surface, suggesting that non-linear dissolution kinetics may be of minor importance in sediments. Depth at which $k_B(x)$ reaches $k_{B,const}$ values (Tab. 3.9) are illustrated by filled squares.

Major factors which may contribute to observed profile shape are discussed in the following sections.

Also mentionable is the fact that for most of the cores the half-saturation depth appears within the first cm of sediment. A half-saturation depth is defined as the sediment depth [cm] at which silicic acid concentrations are equal to one-half their values at apparent saturation, i.e., the asymptotic silicic acid value. This suggests that, at least for sediment-pore water regimes, non-linear dissolution kinetics play a subordinate role. According to flow-through results, non-linear dissolution kinetics require degrees of undersaturation exceeding those of 0.5 at ambient temperature [Fig. 3.19, this study; Fig. 4, VAN CAPPELLEN and QIU, 1997b]. Except for the iso-saturation field one line represents the depth at which $k_B(x)$ tend to converge with $k_{B,const}$ values.

As described above (3.2.2.1) there are two sources of uncertainty in calculating benthic silicic acid fluxes in deep-sea sediments, that is the adjustment of both the asymptotic silicic acid concentration and the gradient at the interface (Eq. 3.17). This leads to an underestimation of the gradients and the subsequent flux calculations just beneath the sediment-water interface (for sediment derived from other than the Southern Ocean sites) compared with a linear adjustment of gradients via bottom water values and first depth intervals (Fig. 3.39). This underestimation is further included in the reaction rate constants for subsurface sediment sections.

Apart from these another source of uncertainty is the problem of lateral and temporal undersampling. In particular, temporal undersampling can result in major uncertainties when seasonal aspects are considered.

3.2.3 Discussion

3.2.3.1 Variations in benthic silicic acid fluxes

The flux of biogenic silica is highly variable in different pelagic areas, depending primarily on water depth and on the production of siliceous plankton in the surface layer. Pore water silicic acid profiles from all multicorers under investigation were modeled to calculate dissolution fluxes across the sediment-water interface (Eq. 3.19). Fitting the entire dissolved silica profile (Eq. 3.17) [e.g., SAYLES et al., 1995; MCMANUS et al., 1995; KONING et al., 1997; RAGUENEAU et al., submitted] was compared with fluxes calculated by a two-point concentration gradient.

The differences among the cores have already been mentioned for benthic dissolution fluxes of silicic acid through the sediment-water interface (3.2.2.2). Regional comparisons reveal that Scotia Sea sediments exhibit the largest mean fluxes among the cores (Tab. 3.7) with values of 2-5 $\text{mmol m}^{-2} \text{day}^{-1}$. SCHLÜTER et al. [1998] report values of 2-4 $\text{mmol m}^{-2} \text{day}^{-1}$ for Scotia Sea sediments. Their calculations resulted in somewhat lower estimates (Fig. 3.39) as compared with sediments from other regions in which the linear approach yielded strikingly higher fluxes (Fig. 3.39).

The sediments from the Peru Basin or Juan de Fuca Ridge reveal mean flux estimates of 0.7-0.9 $\text{mmol m}^{-2} \text{day}^{-1}$. These fluxes are lower than fluxes reported from the Equatorial Pacific [1-1.9 $\text{mmol m}^{-2} \text{day}^{-1}$, MCMANUS et al., 1995] by a factor of two.

Arabian Sea surface sediments which have not been studied extensively in the past provide benthic silicic acid fluxes in the range of 0.2-0.5 $\text{mmol m}^{-2} \text{day}^{-1}$. KONING et al. [1997] reported on benthic silicic acid fluxes which were determined during shipboard incubation or by modeling of pore water silicic acid profiles taken during a transect

3. Experimental results and discussion

from the Somali Coast (565 m) to the Somali Basin at 10°N and 51°34'E-53°33'E. Their deep-sea sediment station 915 (4059 m) was latitudinally comparable to the southernmost core described in this study (SAST, 10°N 65°E, Tab. 2.1, Fig. 2.1) but differed in longitude. Pore water modeling gave a flux of $0.76 \pm 0.03 \text{ mmol m}^{-2} \text{ day}^{-1}$, shipboard incubations reveal comparable results of $0.71 \text{ mmol m}^{-2} \text{ day}^{-1}$. Thus, the mean flux estimates reported here are somewhat lower than those reported by KONING et al. [1997] for the Somali Basin, which is not surprising since our stations are further away from the influence of coastal upwelling. They measured fluxes ranging from 0.5-2.7 $\text{mmol m}^{-2} \text{ day}^{-1}$ on that transect with highest values obtained in the westernmost location at 565 m water depth.

At the BENGAL site, a mean flux of $0.17 \text{ mmol m}^{-2} \text{ day}^{-1}$ was calculated from both the linear and non-linear approximations of the gradient beneath the sediment-water interface. This flux is comparable to the values reported by RAGUENEAU et al. [submitted] from 7 cruises to the BENGAL site which incorporate seasonal variations. Fluxes of silicic acid, estimated from pore water gradients as well as from deployments of several benthic chambers were reported to reveal a similar mean recycling flux of the same value suggesting that *ex situ* flux estimations are indeed reliable.

Norwegian Sea sediments (M31/2) revealed similar low asymptotic silicic acid values ($\sim 100 \mu\text{M}$) and corresponding low silicic acid fluxes ($0.06 \text{ mmol m}^{-2} \text{ day}^{-1}$) [SCHLÜTER and SAUTER, submitted] compared with those reported from SAYLES et al. [1996] for the BATS site (Bermuda Atlantic Time Series) ($31^{\circ}50'N$, $64^{\circ}10'W$). Benthic dissolution fluxes ($0.047 \text{ mmol m}^{-2} \text{ day}^{-1}$) at the BATS site were measured *in situ* with chambers several times a year. The small amount of opal ($\sim 1 \text{ wt.}\%$) and a nearly constant distribution of BSi in Norwegian Sea surface sediments suggests that only relatively dissolution-resistant siliceous components reach the seafloor and are buried in the sediment. SEM photomicrographs of the deeper sections of the core (30-35 cm) reveal only single fragments (spicules) of siliceous sponges and single diatoms within the fine-grained sediment structure of lowest porosity ($\phi = 0.5-0.7$ within the top 10 cm).

3.2.3.2 Initial silicic acid enrichment: Sampling artefact or rapidly dissolving BSi ?

A thorough fit of the dissolved silica gradient at the interface and asymptotic concentrations is aimed at to determine benthic dissolution fluxes and reaction rates. Both values and the exponential decrease constant α for silicic acid are important constraints in calculating the flux according to Equation 3.19 as well as porosity changes and reaction rate constants (3.2.2.2).

A frequent, but usually neglected, phenomenon is explained by the difficulties in sequential pore water sampling [Sect. 2.1.2.1 and WILLEY and SPIVACK, 1997] and the inability of the non-linear fitting Equation 3.17 to represent both the asymptotic silicic acid value and the gradient just beneath the sediment-water interface with a single parameter α , the exponential decrease constant for silicic acid. Consequently, there were large uncertainties when comparing fluxes at $x = 0$ by taking gradients from the pore water fitting procedure of silicic acid (Eq. 2.22) or gradients between bottom water and the first depth interval (bottom water and 0.25 or 0.5 cm) were determined.

Since neither benthic chamber measurements [e.g., SAYLES et al., 1995; MCMANUS et al., 1995; KONING et al., 1997; RAGUENEAU et al., submitted] nor an entire core

squeezing technique [e.g., SAYLES et al., 1995; MCMANUS et al., 1995] have been deployed to consider whether these steeper subsurface increases in cores of low biogenic silica contents are indeed reasonable, a further discussion remains speculation. Nevertheless, the limitations in flux calculations and mechanisms which may be due to stronger gradients beneath the sediment-water interface are discussed in the following section.

Limitations of flux calculations

(1) Seasonality

In the major part of the study areas, flux measurements are the result of single cruises and single multicorer deployments. If seasonality is the reason for subsurface maxima in nutrients and silicic acid, fluctuations cannot be ruled out when considering nutrient recycling within the top sediment sections [HENSEN et al., 1998] and resulting flux calculations by either method.

RAGUENEAU et al. [submitted] conclude from similar comparisons of gradients taken from linear or non-linear approaches (and 30-50% lower estimates) that fitting according to Equation 3.17 gives more reliable results, and in accord with benthic chamber measurements. This is somewhat surprising since both methods (linear and non-linear gradient approaches) exhibit the same fluxes in my study. RAGUENEAU et al., however, added that the fluxes estimated using pore water gradients display a seasonal trend: During spring, dissolved silica concentrations in the top cm exhibit values lower (60-80 μM) than those obtained during summer and fall (70-100 μM). SAYLES et al. [1996] reported no seasonality in opal-poor sediments.

This observation may, in fact, give a reasonable explanation for the observed surface maxima. A rapid dissolution caused by enhanced benthic biological activity due to freshly deposited organic matter surrounding partly siliceous cells [SMITH et al., 1993] and enhanced enzymatic or bacterial hydrolytic attack on diatom cell walls [SMITH et al., 1992; BIDDLE and AZAM, 1999] which would denude biogenic silica of its organic coating and hasten its subsequent dissolution. A higher temporal resolution is needed to prove whether subsurface maxima vary indeed significantly with seasonal events apart from the limitations which are reported below (2-5).

(2) Spatial variations due to natural patchiness

(3) Vertical resolution

Vertical resolution of samples is a major constraint for flux calculations, both for fitting an entire profile and for the gradient at the sediment-water interface based on single point estimates.

(4) Effects due to recovery and processing

Multicorer recovery and pore water sampling is a source of large uncertainty. It cannot be ruled out that sampling sediments from the first depth segment with overlying bottom water may result in somewhat higher silicic acid values in the topmost section [Sect. 2.1.2.1 and WILLEY and SPIVACK, 1997].

3. Experimental results and discussion

(5) Sampling artefact

SAYLES et al. [1996] propose that uniform compaction may express pore fluid or shift the profile upward toward the interface. In any case, the gradient between the uppermost sample and bottom water would be enhanced.

(6) Porosity estimations

Porosity assumptions are large sources of uncertainties (Fig. 3.42, Tab. 3.8). A reliable estimation of surface porosities is essential since $J(x) \propto \phi^3$.

A two-layer model (fitting procedure) to account for subsurface maxima

There is strong evidence for near-surface enhanced dissolution rates of biogenic silica in all cores, apart from MC#33 and, to a lesser extent in Scotia Sea sediments. Recent publications reveal the same [e.g., KONING et al., 1997, sample 905 and 915; HENSEN et al., 1998, Fig. 1 GeoB 1413 and GeoB 2717; RAGUENEAU et al., submitted], but apart from Ragueneau et al. [submitted] this phenomenon is not further discussed. In Southern Ocean sediments it is less striking probably for reasons of reduced sensitivity. This topic has been discussed as part of the explanation for the reduced sensitivity of k_{NaOH} , the alkaline reactivity rate constant, which was less developed in Southern Ocean sediments but highly developed in silica-poor sediments (3.1.2.2.4). The effect of a seasonal imprint on the calculated dissolution rate of BSi dissolution in silica-rich sediments may be greatly overlapped by a strong dissolution background signal, which appears throughout the year, yielding 99% saturation in those sediments even below 2 cm sediment depth (see iso-saturation lines in Fig. 3.44). As a consequence, k_{NaOH} and silica contents in silica-rich sediments are almost constant (A. 2.6.1-2.6.4) and seasonally stronger gradients near the sediment-water interface may be rejected.

Since the fitting procedure referred to here as the “classical model” is not the best choice to reliably represent both strong subsurface gradients and asymptotic silicic acid values, a two-layer model is proposed to calculate fluxes from the first derivative of the first layer fitting function at $x = 0$.

Finding the two-layer-model parameters

The need to fit both the subsurface gradient and asymptotic silicic acid concentration with one expression (Eq. 3.17) was approached using the same expression in two layers; to express the fitting procedure a mean silicic acid versus depth profile SAST (Arabian Sea) (Fig. 3.45) has been selected. Layer I represents the sediment section at which a rapid dissolving process may appear [$0 \text{ cm} \leq x \leq 0.25$ or 0.5 cm]. For layer (I) care was taken to fit the dissolved silicic acid gradient at the sediment-water interface and the asymptotic concentration as closely as possible. This was done using bottom water silicic acid concentrations of Si_{01} in Equation 3.17, and asymptotic silicic acid concentration Si_{satI} taken from fitting interval II. The exponential decrease constant α , in the first layer referred to as α_1 , was adjusted to fit silicic acid concentrations directly below the sediment-water interface (0.25 cm or 0.5 cm depending on sampling intervals taken at the surface). As a matter of fact, the asymptotic silicic acid values and the subsurface gradients from bottom water to the first depth segment, very large in most of the cores and linearly approximated [e.g., HENSEN et al., 1998; SCHLÜTER et al., 1998] are also well represented by this surface model. Values measured between the

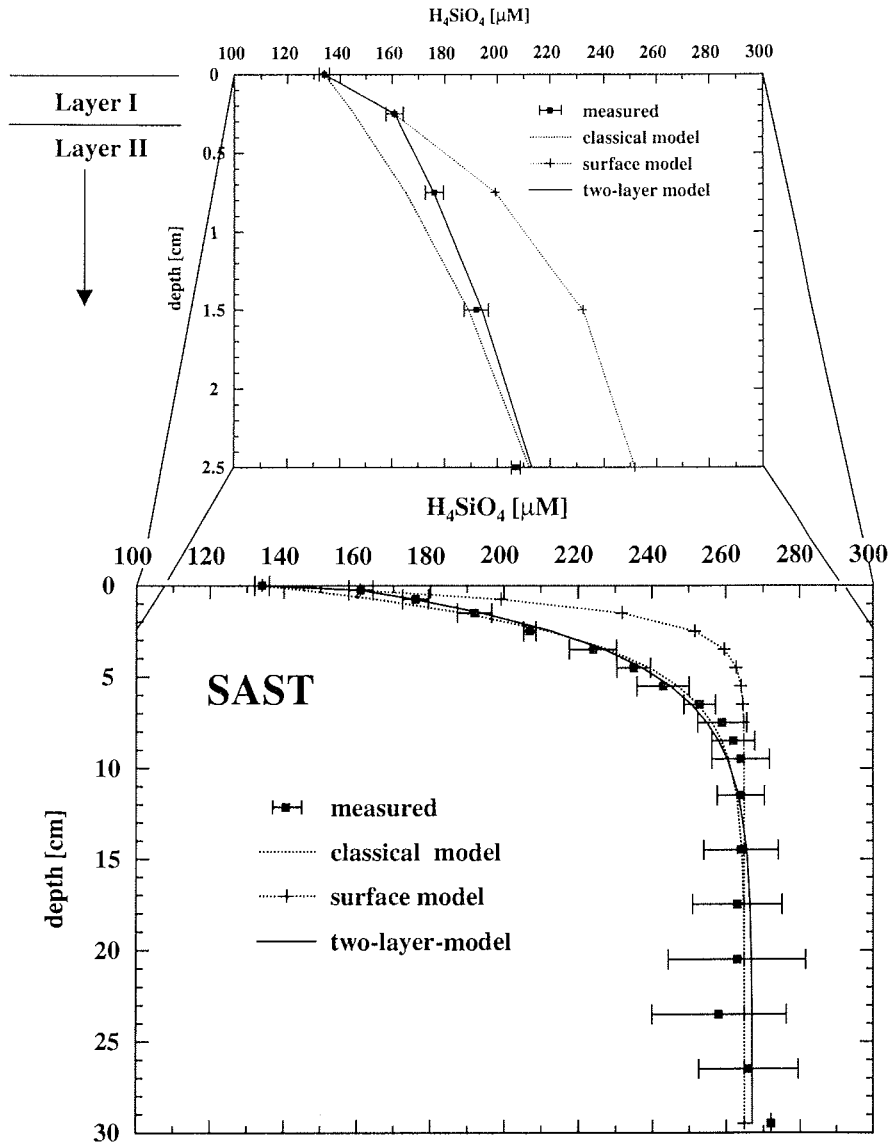


Fig. 3.45 Benthic dissolution fluxes and reaction rates from (A) classical pore water fitting procedure [e.g., SAYLES et al., 1996; KONING et al., 1997] using the derivative of Equation 3.17 at $x = 0$ in Equation 3.16 or (B) the slope between bottom water value and value at first depth segment. The results differ greatly. To minimize the spread between measured and fitted points in (A) a two-layer model (fitting procedure) is proposed which produces a larger gradient (α_1) in the first depth interval (0-0.5 cm) and much lower gradients ($\alpha_2 < \alpha_1$) further below.

3. Experimental results and discussion

Tab. 3.10 Pore water silicic acid and two-layer model fitting parameters. Units for the fluxes are $\text{mmol m}^{-2} \text{day}^{-1}$ and α are cm^{-1} . A comparison of fluxes according to classically non-linear, linear and two-layer fit of silicic acid is shown in Figure 3.46. For station No. see Table 2.1 and Figure 2.1.

No./Station/ Core	$[0 \leq x \leq 0.25 \text{ or } 0.5]$		$[0.25 \text{ or } 0.5 \leq x]$		$\text{Si}_{\text{sat}} [\mu\text{M}]$	$J_{\text{two-layer}}(x=0)$
	$\text{Si}_{01} [\mu\text{M}]$	α_{01}	$\text{Si}_{02} [\mu\text{M}]$	α_{02}		
2 MC#33 ¹	45	0.38			203	0.17
1 M31/2	13	0.57	37	0.15	108	0.097
3 WAST	140	0.75	209	0.13	546	1.2
5 MC-145	153	0.84	236	0.21	591	1.44
3 EAST	141	0.85	170	0.31	293	1.17
3 SAST	134	0.91	161	0.30	267	0.39
3 CAST	143	1.18	191	0.36	331	0.71
4 MC-1-3	185	1.25	255	0.35	448	1.17
3 NAST	145	1.31	184	0.43	288	0.73
6 PS-2283-6	126	1.48	450	0.84	746	3.2
6 PS-2299 ¹	126	1.81			721	3.5
6 PS-2314-1 ¹	126	2.35			686	3.6
6 PS-2312-1 ¹	129	3.49			799	7.0

¹No adjustment according to the two-layer model performed, since classical fit (Eq. 3.17) reliably represents measured data.

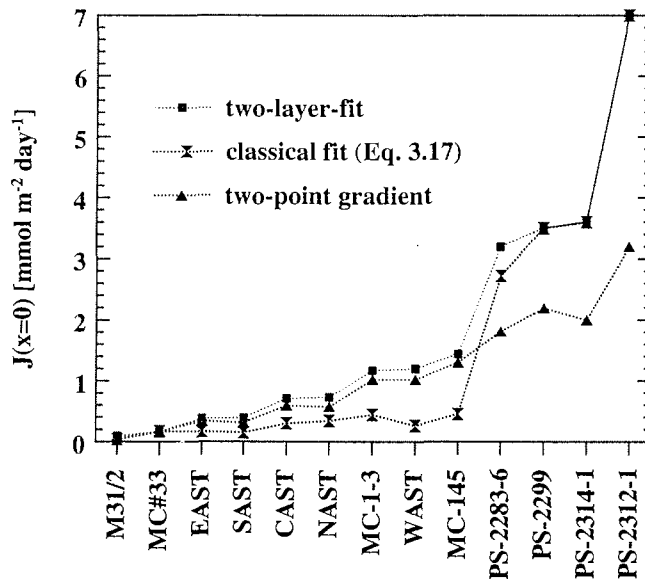


Fig. 3.46 Flux calculation using 3 fitting procedures. (A) Classical non-linear fitting procedure (Eq. 3.17) (double-triangle); (B) gradient estimate using a two-point approximation between bottom water and the first depth segment (triangles); (C) two-layer model (squares) (see text); note, MC#33, PS-2299, PS-2312-1 and PS-2314-1 need not be adjusted since the classical fit reliably represents silicic acid concentrations in the first depth segment.

respective point and asymptotic silicic acid value, however, are only poorly represented by this “surface model” adjusted for layer I, resulting in an “overshoot” (see crosses in Fig. 3.45).

The fitting procedure for the remainder of the core, layer II (bottom layer) [0.25 or 0.5 cm $\leq x$] was performed using again Equation 3.17. Varying boundary conditions for Si_0 , which was now represented by silicic acid concentrations at 0.25 or 0.5 cm, were chosen; for Si_{sat} a mean asymptotic silicic acid concentration was taken for the first fitting routine, an adjustment which provides Si_{sat} and α_2 as output parameters followed the Origin™ fitting routine using the Levenberg-Marquarth algorithm. The decrease constant α_2 describes the shape of the curve in layer II, and its value is somewhat lower than that given for the classical fitting procedure (dotted line without symbols). Table 3.10 summarizes the results in terms of boundary conditions, resulting exponential decrease constants α_1 and α_2 , and silicic acid fluxes. In Table 3.11 the reaction rate constants $k_B(x = 0)_{max}$ and $k_B(x = 0.25$ or 0.5 cm) from both fitting intervals are given, since the slope at $x = 0.25$ or 0.5 cm does not have a unique solution.

In Section 3.2.2.2 differences in flux calculations according to the linear and non-linear approximation were discussed. The relatively poor agreement between the classical model and data for subsurface concentrations gave impetus to develop a fitting procedure based on the concept of a two-layer model. The result is a combination of the rapid change of concentrations at the sediment-water interface, perhaps attributed to rapid dissolving BSi assemblages, and slower changes in concentration below due to enhanced reprecipitation reactions. The adjustment of the first “fit” was made by “eye-fitting”. Care was taken to fit the dissolved silica gradient at the interface and asymptotic concentrations as closely as possible. The exponential decreasing constant α_2 is, thus a measure for subsurface gradients, but this fit only poorly represents data points at the sediment-water interface. Within boundary conditions, however, both fits give more reliable results than a single fit according to Equation 3.17. The overall description of silicic acid concentrations based on the two-layer model, however, is mathematically discontinuous at 0.25 or 0.5 cm.

In summary, two different methods were tried to fit the slope of the interfacial gradient: The asymptotic silicic acid value and the subsurface concentration increase from the first depth segment towards the asymptotic silicic acid value. Given the limitations of both methods a two-layer model was then proposed from which recycling fluxes were calculated. The following methods were discussed regarding the interfacial gradient:

- (A) Linear approximation
- (B) Classical non-linear fitting (Eq. 3.17)
- (C) Two-layer model using the classical fitting function (Eq. 3.17) over two depth intervals:
 - Layer I (interface layer) [0 cm $\leq x \leq 0.25$ or 0.5 cm],
 - Layer II (bottom layer) [0.25 or 0.5 cm $\leq x$]

The linear approach or the two-layer model can be favored for flux calculations, although a two-point regression constitutes a source of large uncertainties due to sample

3. Experimental results and discussion

processing. Nevertheless, it more reliably reflect the recycling flux which actually occurs near the sediment-water interface, including possible seasonal imprints.

Using Equation 3.17 and a single variable (α) was not the best choice for large variations in the upper part of the sediment column, where seasonal imprints occur and neither fit the measured profile in general nor large subsurface gradients in particular. As an alternative the two-layer model was proposed which uses the non-linear fitting procedure twice. A first decreasing constant α_1 accomodated the strong gradient in the interface interval, whereas α_2 fit the rest of the profile, beginning with a silicic acid concentration of the first depth segment. It remains unclear whether the interface gradients for ($x \rightarrow 0$) are indeed linear or non-linear. The large discrepancy for Scotia Sea sediments between fluxes based on linear fits and non-linear fits (Fig. 3.46) stems from the mathematical difference calculating a slope with the first derivative at $x = 0$ or via a two-point gradient.

A more detailed data analysis is necessary to determine whether method (1) or (2) or the two-layer model (3) is most applicable for describing flux across the sediment-water interface. A higher sediment-depth resolution near the interface, plus systematic comparisons of *ex situ* and *in situ* measurements of pore water profiles under seasonal and spatial variations are required.

3.2.3.3 A comparison of dissolution rate constants: Laboratory and field rates

3.2.3.3.1 Dissolution rates as a function of depth

For determining depth-dependent apparent rate constants from pore water profiles, the fitting procedure shown in Figure 3.42 was applied. Again, the question arises which of the three proposed methods is best for representing the *depth-distribution* of dissolved silicic acid. Summarizing the previous section (3.2.3.2), it is most important for flux calculations that values representing the *interface gradient* are best fitted. It is less important to represent the entire profile by the method of choice. Accordingly, flux calculations must be based on the linear two-point estimation of the subsurface gradient or the non-linear approximation of the subsurface gradient according to the two-layer model.

Now, reactivity trends over the entire core length are to be extracted from the pore water fitting procedure of choice, rather than just representing single points. The non-linear pore water fitting procedure according to Equation 3.17 was favored [e.g., SAYLES et al., 1996; WILLEY et al., 1997; KONING et al., 1997; RAGUENEAU, submitted]. This procedure estimates gradients on a number of measured points, rather than applying a two-point fit. Thus, Equation 3.17 minimizes the influence of unrecognized errors (2.1.2.1) within single samples particularly those from the first depth interval. Nevertheless, laboratory rate constants were compared with both results in terms of surface dissolution rate constants $k_B(x = 0)$ derived from the classical fitting procedure (Eq. 3.17) and from a stronger gradient at the sediment-water interface based on the two-layer model.

An important difference with the classic SCHINK & GUINASSO (S & G) model (SCHINK et al., 1975) is the output in terms of depth-dependent apparent rate constants. This is supported by my own laboratory results and those of VAN CAPPELLEN and QIU [1997a,b] and WILLEY and SPIVACK [1997]. RABOUILLE et al. [1997] took the results by VAN CAPPELLEN and QIU [1997 a,b] and first introduced a depth-dependent dissolution

3. Experimental results and discussion

Tab. 3.11 Depth-dependent kinetic “constants” $k_B(x)$ derived from classical fitting procedure according to Equation 3.17 (3.2.2.3, Tab. 3.9) and those from the two-layer model (3.2.3.2). I indicates the first non-linear fit within the two-layer procedure describing the surface layer (parameters (Tab. 3.10): Si_{01} , Si_{sat} , α_1); II indicates the second (bottom) layer with parameters Si_{02} , Si_{sat} , α_2 (Tab. 3.10).

No./ Station/Core	Two-layer fit				Classical fit (Eq. 3.17)		
	k_B^0 (two-layer) [yr ⁻¹]	$k_{B,x=0.25}^I$ [yr ⁻¹]	$k_{B,x=0.25}^{II}$ [yr ⁻¹]	$k_{B, const}^{II}$ [yr ⁻¹]	k_B^0 [yr ⁻¹]	$k_B(x=0.25)$ [yr ⁻¹]	$k_{B, const}$ [yr ⁻¹]
1 M31/2	0.033	0.02	0.006	0.0004	0.010	0.006	0.001
2 MC#33 ^I	0.043			0.018	0.043	0.039	0.018
5 MC-145	0.12	0.12	0.008	0.0035	0.013	0.013	0.006
6 PS-2299 ^I	0.15			0.053	0.15	0.092	0.053
6 PS-2314-1 ^I	0.18			0.061	0.18	0.13	0.061
3 EAST	0.20	0.18	0.028	0.0087	0.048	0.043	0.014
4 MC-1-3	0.28	0.27	0.023	0.012	0.043	0.041	0.022
3 SAST	0.30	0.24	0.036	0.0073	0.066	0.051	0.011
6 PS-2312-1 ^I	0.32			0.14	0.32	0.23	0.14
3 WAST	0.42	0.31	0.017	0.0034	0.035	0.025	0.005
6 PS-2283-6	0.50	0.13	0.023	0.0047	0.39	0.068	0.016
3 CAST	0.51	0.40	0.050	0.014	0.12	0.094	0.027
3 NAST	1.4	0.80	0.12	0.022	0.41	0.23	0.049

^INo adjustment according to the two-layer model performed; classical fit (Eq. 3.17) reliably represents measured data.

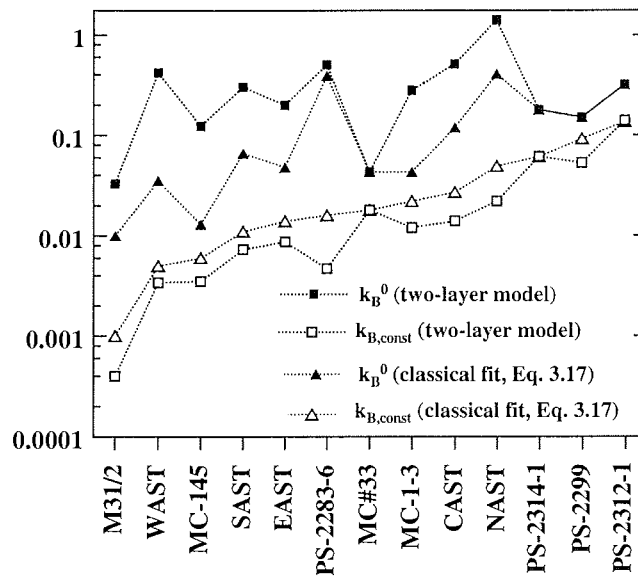


Fig. 3.47 Dissolution rate constants from pore water modeling procedures according to Figure 3.42 using the classical fitting procedure for silicic acid (Eq. 3.17) or the two-layer model (3.3.2). Results are strikingly different, assuming a surface fit (Fig. 3.45), with α_2 which is two to three times higher than α_2 or α in the case of the classical fit to describe the slope of the interfacial gradient.

3. Experimental results and discussion

kinetic constant in the S & G model. The kinetic constant was set to vary exponentially with depth and was expressed by a similar relationship, used for the description of the decrease of porosities (Eq. 3.18). In contrast to the results outlined here, the kinetic constant described by RABOUILLE et al. [1997] was essentially zero with depth. A similar description was provided by MCMANUS et al. [1995] for the surface coating model, where $k_B(x)$ dominates down-core changes in reaction rates, which become essentially zero when asymptotic silicic acid value is reached in pore water. In this formulation, the decrease of the kinetic constant is at first a mathematical consequence. However, it also reflects some mechanistic or chemical rationale (see below).

The fitting parameters were combined in Equations 3.22 and 3.23 to provide analytical solutions for the decrease of reaction rate with depth ($k_B(x)$). Assuming constant porosities and biogenic silica contents with depth results in a reaction rate constant $k_{B, \text{const}}$ which may represent a kinetic constant at saturation depth. $k_B(x)$ values at saturation depth are always lower than prescribed values since actual porosities and biogenic silica contents at depth are still somewhat lower than the average value. The depth at which $k_B(x)$ approach $k_{B, \text{const}}$ values, the kinetic constants k_B^0 ($x = 0$), a maximum reactivity value for biogenic silica in respective cores, and $k_{B, \text{const}}$ values are shown in Fig. 3.45. The constant dissolution behavior in most cores begins at ~ 95% saturation (Fig. 3.45).

The exponential decrease of the net dissolution rate $R(x)$ (Eqs. 3.21 and 3.22) may result from three independent mechanisms:

- (1) The dissolution rate may be determined by a departure from saturation. The saturating phase may be biogenic silica, but is more likely a heterogeneous mixture of siliceous phases (3.1.1.3.1).
- (2) A second key mechanism is the gradual decrease in reactivity due to a decrease in reactive sites [e.g., VAN CAPPELLEN and QIU, 1997b] as outlined by k_{NaOH} decreases with depth or by decreasing dissolution rate constants determined in flow-through experiments.
- (3) Reprecipitation of silicic acid and Al occurs on biogenic silica assemblages in the presence of clay minerals and other aluminosilicates. These either release Al into solution (mechanism A in Figure 3.37) or constitute a source for Al which contribute to simultaneous dissolution and precipitation reactions (mechanism B in Figure 3.37).

What does the fitting procedure tell us about the dissolution kinetics of biogenic silica in various sediment columns ?

Figure 3.47 and Table 3.11 show major differences in subsurface kinetic constants by comparing results of the classical fit of silicic acid versus depth (Eq. 3.17) with those from the two-layer fitting procedure (3.2.3.2) for sediments with opal contents < 20 wt.% as well as slight differences for PS-2283-6. With a mean porosity and biogenic silica value throughout the cores, the classical fitting procedure provides somewhat larger $k_{B, \text{const}}$ values than the two-layer model did. The differences are usually smaller (factor 1-2) than for values at $x = 0$ (factor 5-10). Considering k_B^0 (two-layer) values as apparent rate constants and the upper limit of reactivity among the cores, they may be divided into three distinct groups:

- I. Highly reactive [$1 \text{ yr}^{-1} < k_B < 2 \text{ yr}^{-1}$]
NAST (Arabian Sea)
- II. Reactive [$0.1 \text{ yr}^{-1} < k_B < 1 \text{ yr}^{-1}$]
MC-145, MC-1-3 (Pacific Ocean)
PS-2283-6, PS-2299, PS-2312-1, PS-2314-1 (Scotia Sea)
EAST, SAST, WAST, CAST (Arabian Sea)
- III. Poorly reactive [$0.01 \text{ yr}^{-1} < k_B < 0.1 \text{ yr}^{-1}$]
MC#33, M31/2 (North Atlantic)

Considering results from the classical fitting procedure the following division into two groups seems reasonable:

- I.' Highly reactive [$0.1 \text{ yr}^{-1} < k_B < 0.5 \text{ yr}^{-1}$]
NAST, CAST (Arabian Sea)
PS-2283-6, PS-2299, PS-2312-1, PS-2314-1
- II.' Poorly reactive [$0.01 \text{ yr}^{-1} < k_B < 0.1 \text{ yr}^{-1}$]
MC-145, MC-1-3 (Pacific Ocean)
EAST, SAST, WAST (Arabian Sea)
MC#33, M31/2

In the literature, k_B values from modeling pore water silicic acid have been reported of between 0.02 to 0.3 yr^{-1} in the Indian sector of the Southern Ocean [RABOUILLE et al., 1997], 0.05 - 0.27 yr^{-1} for a reactive sediment fraction and 0.0006 yr^{-1} for an unreactive sediment fraction in the Equatorial Pacific [MCMANUS et al., 1995]. SCHINK and GUINASSO [1980] have discussed results for calculations with k_B equal to 0.01 and 0.1 yr^{-1} . SCHINK et al. [1975] commonly use a value of 0.03 yr^{-1} . SCHINK and GUINASSO [1980], however, have also discussed the possibility that k_B may be as small as 0.002 yr^{-1} . These literature data using constant estimates are comparable with either of the two approximations; the kinetic constants of the two-layer model clearly tend to provide higher estimates.

More quantitative research in this field is needed to show whether subsurface maxima in kinetic constants and silicic acid fluxes (3.2.3.2) are indeed related to the enhanced enzymatic degradation of organic matter as described for the water column [e.g., BIDDLE and AZAM, 1999] resulting from biogenic silica shells during enhanced productivity, or if it is simply a sampling artefact. The latter, however, is difficult to believe since pore waters in the Arabian Sea were normally taken from more than three replicate multicorer tubes and processed individually (2.1.1). Subsurface maxima are, however, reproduceable. In the following section considerations were restricted to results derived from the classical fitting procedure, which can be treated as the lower estimate of possibly enhanced subsurface dissolution.

Dissolution rate as a function of depth

In the fitting procedure the depth-dependent rate constant was obtained as output from fitting silicic acid (Eq. 3.17), porosities (Eq. 3.18), biogenic silica contents with depth (3.2.2.1) and applying the diagenetic equation according to BERNER [1980] under steady state conditions. The procedure is illustrated in Figure 3.42 for NAST sediments. In Figure 3.48 the results are given for selected cores (cf. Fig. 3.38). To quantify the extent of reactivity decrease with depth κ , the exponential decrease for kinetic constant

3. Experimental results and discussion

with depth (Fig. 3.49) was chosen as a result of fitting output parameter $k_B(x)$ with depth according to Equation 3.25.

The decreasing constant κ (Fig. 3.49) is again a mathematical consequence of measured parameters, assuming that the classical diagenetic Equation 3.11 [BERNER, 1980] describes biogenic silica diagenesis as a whole. Both $k_B(x)$ and κ are useful for comparisons with laboratory results to understand the underlying processes.

To determine the parameters which are responsible for a reactivity decrease in different sediments, combined effect of the three input parameters (silicic acid, porosity and BSi at respective depth) since the diffusion, counterbalancing silica dissolution within the modeling study was involved in the formulation with a constant diffusion coefficient D_S (Eq. 3.15). Although the fitting procedure seems rather straightforward, since silicic acid fluxes and depth-dependent kinetic constants were retrieved, it is not possible to satisfactorily resolve the key controls on biogenic silica behavior during early diagenesis.

Recently, MCMANUS et al. [1995] have shown that modeling based on completely different assumptions is equally successful when reproducing measured pore water profiles. These authors have reviewed three published models:

(1) *The equilibrium model* [ARCHER et al., 1993]

Asymptotic silicic acid concentration [Si_{sat}] is regulated by the solubility of opal in sediment.

(2) *The reactive opal model* [SCHINK et al., 1975]

Opal is assumed to have two fractions, from which the unreactive is the one buried. In this model [Si_{sat}] depends on the availability of soluble opal and the sediment mixing rate.

(3) *The surface coating model* [LUCE et al., 1972; KAMATANI, et al., 1988]

In this model [Si_{sat}] is kinetically controlled by the balance between a very slow dissolution process through a surface layer coating the opal and the precipitation of a less soluble phase containing silica [MACKIN, 1987].

Given the three choices, the preferred explanation by MCMANUS et al. [1995] is derived from independent storage experiments involving surface aging or poisoning processes. Therefore, extensive laboratory studies were undertaken to decipher single key mechanisms which may explain the rapid decrease of the kinetic rate constant (Figs. 3.48 and 3.49) observed in Scotia Sea sediment PS-2283-6. Given the kinetic rate constants derived from flow-through experiments (k_{CFT}) (Fig. 3.31) the reactivity decrease was also observed, albeit to a much lesser extent. Given the values in Table 3.11 the reaction rate constant decreases by 1-2 orders of magnitude, depending on which of the two proposed fitting procedures (classical and two-layer model) is applied. Reactivity decrease represented by constant k_{CFT} is by a factor of 2-3. In Section 3.1.2.2.4 the role of volcanic ash has been discussed as a source of kinetic inhibition for the dissolution of biogenic opal.

Figure 3.48 shows that sediments from the Juan de Fuca Ridge (MC-1-3) and the Peru Basin (MC-145) show different behavior than the sediments from the other cores. This is indicated by k_B values which do not change by orders of magnitude. With regard to the input parameter, a striking difference is obvious from porosity versus depth behavior.

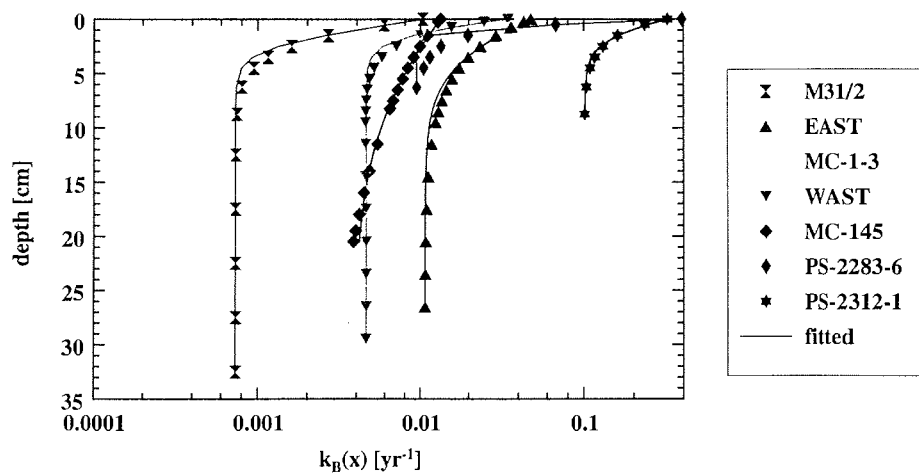


Fig. 3.48 Dissolution rate constant as output parameter $k_B(x)$ from pore water fitting procedure described in Section 3.2.2.1 and illustrated in Figure 3.42. To calculate the attenuation coefficient for the depth-dependent kinetic constant values from different depth intervals have been fitted using Equation 3.25.

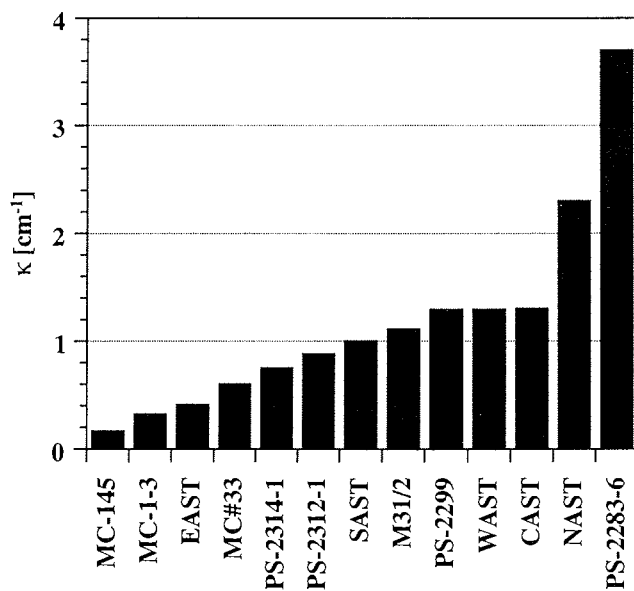


Fig. 3.49 Attenuation coefficient κ as a function of depth for sediments of study. κ was calculated from fitting model output parameter $k_B(x)$ versus depth according to Equation 3.25.

3. Experimental results and discussion

Porosity decrease constants (Tab. 3.8) are very small for MC-1-3 and MC-145. This is illustrated in Figure 3.40 when comparing $\Delta(\phi_{\max}-\phi_{\text{mean}})$ values. This difference is quite small for MC-1-3 and MC-145. Consequently, porosities are high even at depth ($\phi_{\min} \sim 0.88$) compared with the other cores in which porosities ϕ_{\min} are often far below 0.8 and decrease rapidly within the first centimeters. This is a driving force in Equation 3.21 when considering the reactivity decrease $k_B(x)$ with depth observed throughout the cores. On the other hand, reactivity in terms of silicic acid release is not great compared with the opal content actually present in these cores. Figure 3.38 reveals an overall flat increase in pore water silicic acid in MC-145 and MC-1-3, as well as for WAST or EAST sediments. Assuming a fast silicic acid release at the sediment-water interface in the two-layer model, α_2 values describing the increase of silicic acid with depth, are relatively small compared with cores containing far less opal (e.g., NAST, CAST, SAST) which are equal or even higher than with MC-1-3 and MC-145 cores. The half-saturation depth for MC-145 is ~ 2 -3 cm, (Fig. 3.44), which again reveals that the dissolving process is inhibited in Pacific Ocean cores, to a lesser extent in MC-1-3 but much more in MC-145. In both cores the existence of highly soluble aluminosilicates must be considered when interpreting results from flow-through and alkaline leaching experiments as well as silicic acid versus depth profiles (3.1.2.2.4). The pronounced flat pattern of reaction rates versus silicic acid concentration measured in flow-through experiments (Fig. 3.2) also seems to be a result of the interaction of dissolving biogenic silica and reprecipitation of a less soluble phase.

To summarize the discussion in Section 3.1.2.2.4, there is evidence that, particularly in these sediment types, unidentified reverse weathering reactions may be active in the presence of easily soluble aluminosilicates and regulate the somewhat slower build-up of pore water silicic acid towards the apparent solubility of biogenic silica in the presence of non-biosiliceous phases. Such a mechanism may also explain the slow increase of silicic acid in WAST sediments; another explanation may be the extraordinarily high content of organic matter throughout the core (A. 2.3.1).

Somewhat surprising, however, is the high reactivity in the topmost section of NAST surface sediments; this is underscored by the highest k_B^0 values of all cores studied (Tab. 3.11) and a subsequent reactivity decrease with depth represented by the high decreasing constant κ in Figure 3.49 (see also Fig. 3.42). Such a reactivity decrease is also supported by flow-through experiments (Fig. 3.31), but again to a much smaller degree. This is at least in part attributable to easily soluble biogenic silica present in the topmost sections of the sediments and is perhaps enhanced by intensive benthic degradation of organic matter. Another explanation is an overestimation of $k_B(x)$ due to an underestimation of apparent biogenic silica solubility in the surface sections when applying the asymptotic silicic acid value as apparent solubility for the entire core (3.2.3.3.2).

Results for changing saturation values

Flow-through studies have been focussed on the comparison of solubility and reactivity between cores derived from various environmental settings. Depth-distribution is limited to 2-3 depth horizons per sediment core. Nevertheless, enough information was available to elucidate the key mechanisms which control the build-up of pore water silicic acid with depth and between different cores. The NAST sediment

core (Arabian Sea) was selected (Fig. 3.50) to demonstrate the changes in apparent rate constant (Eq. 3.23) when variations in apparent solubility values within the sediments are included.

From flow-through experiments carried out at 25°C a change of apparent solubility from $\sim 600 \mu\text{M}$ at depth 0.25 cm, $\sim 560 \mu\text{M}$ at 3.5 cm to $\sim 300 \mu\text{M}$ at 26.5 cm depth (A.3.3.2) was observed. A linear temperature-solubility relationship has been chosen as a first attempt to estimate solubilities for *in situ* temperatures, assuming that pore water silicic acid concentrations at depth represent apparent solubility value at *in situ* temperatures ($\sim 2^\circ\text{C}$). According to this value, apparent solubilities for further depth intervals and *in situ* temperature are $\sim 500 \mu\text{M}$ (3.5 cm) and $\sim 530 \mu\text{M}$ (0-0.5 cm). With the solubility value of $530 \mu\text{M}$ at depth $x = 0$ a kinetic constant for the classical model of $k_B^0 \sim 0.15 \text{ yr}^{-1}$ was calculated. This is 2-3-times lower than the previous assumption (Tab. 3.11). The kinetic constant at the sediment-water interface for a two-layer model correspondingly decreases from 1.4 to 0.5 yr^{-1} . Again, flow-through experiments are useful for identifying apparent solubility changes with depth, even in those sediment sections where pore water profiles are not able to reach an asymptotic silicic acid value due to transport-reaction interplay. To avoid time-intensive flow-through experiments for the determination of solubility distribution with depth, empirical relationships (3.2 and 3.3) may be applied as a first estimate for solubility changes due to opal/detritus changes.

Solubility changes $[\text{Si}]_{\text{sat}}$ must be included in pore water modeling studies if solubility changes are measured in flow-through experiments or expected from a drastic change in the logarithmic detritus/opal ratio (Fig. 3.18) within the sediment core.

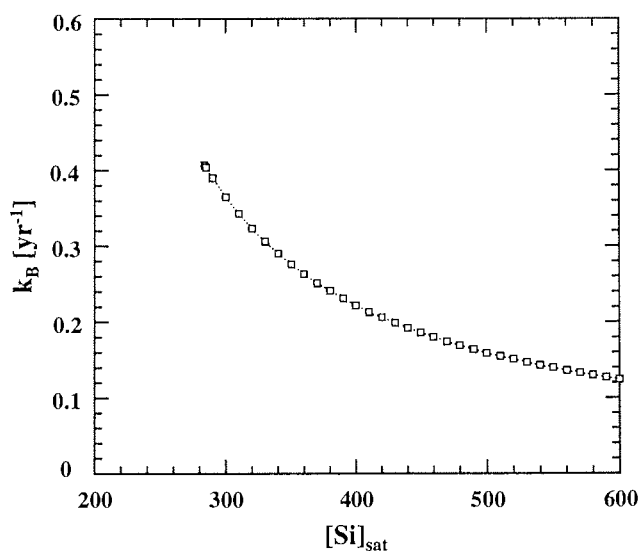


Fig. 3.50 Pore water fitting procedure (Fig. 3.42). Within this formulation reaction rate constant from NAST sediment decreases as a result of increasing apparent solubility. This must be considered in early diagenetic modeling of silicic acid in sediments.

3. Experimental results and discussion

Results with non-linear dissolution kinetics

Flow-through experiments were carried out with biogenic silica embedded in various sediment regimes to discover whether a transition from linear to non-linear dissolution kinetics [VAN CAPPELLEN and QIU, 1997a,b] could also be observed in deep-sea sediments with a low biogenic silica content (Fig. 3.22). An overall non-linear rate equation was chosen to fit experimental rate versus degree of undersaturation data (Eq. 3.13). Reaction order m usually ranges from 1-2 at 25°C (A. 3.11). The transition from an almost linear to an exponential increase appears when the degree of undersaturation exceeds a critical level. Results by VAN CAPPELLEN and QIU [1997 a,b] gained at *in situ* temperature have revealed that the rate increase in the fast kinetics regime was less pronounced than the one observed at higher temperatures. Deviation from linearity at *in situ* conditions usually requires degrees of undersaturation greater than 0.8. Thus, for a first approximation such a non-linear behavior is negligible at depth exceeding at least half-saturation (Fig. 3.44). In the previously described pore water fitting procedure, the complicating effects of non-linear kinetics were ignored which is reasonable since dissolution in most cores appeared at degrees of undersaturation ($\ll 0.8$). Half-saturation for most cores appeared within 0-2 cm of the sediment (Fig. 3.44).

Nevertheless, the “linear” rate constants obtained from the fitting procedure do not provide a useful tool to describe the dissolution process of siliceous skeletons in the overlying water column where a critical degree of undersaturation is fulfilled throughout depth [VAN CAPPELLEN and QIU, 1997b]. Furthermore, the skeletons have not yet undergone intensive aging processes, so they are likely to follow the non-linear kinetics of dissolution observed for sediments under the highest degrees of undersaturation (3.1.2.3.1).

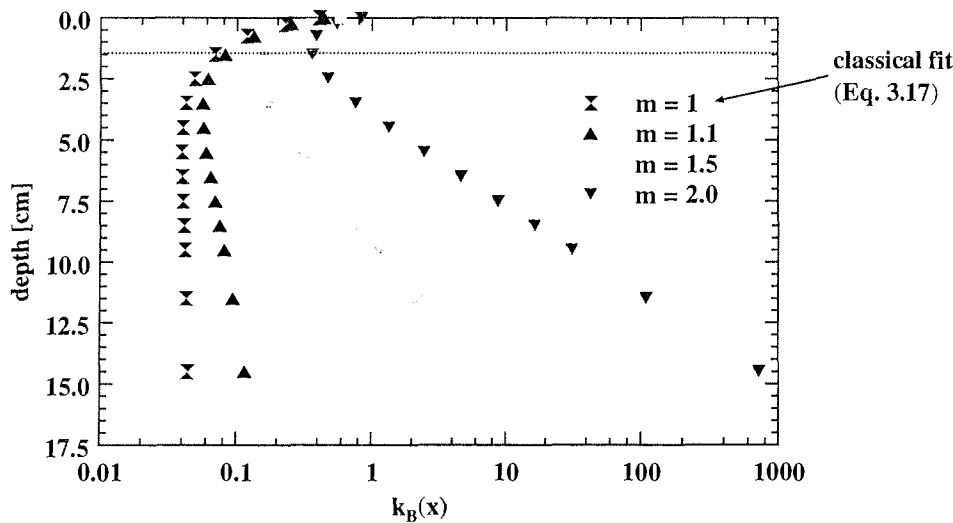


Fig. 3.51 Applying non-linear dissolution kinetics ($m \neq 1$ in Equation 3.23) in the classical fitting procedure yield somewhat arbitrary results when exceeding certain depths (dotted line). In principle, with increasing non-linearity in Equation 3.23 kinetic constants k_B^0 increases. Below that line k_B values for $m > 1$ again tend to increase rapidly. This is a matter of that mathematical procedure which has no physico-chemical rationale.

Since the phytoplankton experiments have not reached the transition towards non-linearity due to insufficient undersaturation, such a non-linearity remains unproven for acid-cleaned phytoplankton. Further flow-through experiments are needed at highest degrees of undersaturation to discover whether the dissolution kinetics of biogenic silica in the water column indeed follow non-linear kinetics.

For comparative purposes and to demonstrate that ignoring a possible non-linear dissolution kinetics may be responsible for underestimating rate constants nearest to the sediment-water interface dissolution rate constants from NAST pore water were plotted versus the degree of undersaturation with increasing non-linearities (Fig. 3.51).

Figure 3.51 shows that an increasing reaction order m with respect to the degree of undersaturation produces a large increase in kinetic constant $k_B(x)$. k_B^0 increases from $\sim 0.4 \text{ yr}^{-1}$ (with $m = 1$) towards $\sim 0.8 \text{ yr}^{-1}$ (with $m = 2$). Thus, ignoring non-linear dissolution kinetics may additionally add a factor of ~ 2 uncertainty when estimating apparent rate constant from pore water profiles at $x = 0$. Nevertheless, these uncertainties do decrease rapidly in a few mm beneath the sediment-water interface within the sediment matrix with respect to undersaturation state because the dissolution process follows that linear rate law at degrees of undersaturation < 0.8 [Fig. 3.20, this thesis; VAN CAPPELLEN and QIU, 1997a,b].

3.2.3.3.2 What do dissolution experiments tell us about natural weathering ?

A comparison of laboratory and field rates

The rate distribution predicted from k_{CFT} the reaction rate constant derived from flow-through experiments, or k_{NaOH} , the reaction rate constant determined in alkaline solution (Fig. 3.31), are in generally good agreement with $k_B(x)$ values obtained from fitting an early diagenetic transport-reaction model [BERNER, 1980] (Fig. 3.52). However, as usually reported from laboratory-based studies [e.g., HURD, 1973; PACES, 1983; VELBEL, 1985; DAHMKE, 1988; CASEY et al., 1993; DOVE, 1995; VAN CAPPELLEN and QIU, 1997a,b; RAGUENEAU et al., submitted] it is evident that laboratory-based k_{CFT} values differ systematically by 1-2 orders of magnitude compared with values obtained from the fitting procedure. Nevertheless, values from the two-layer model taken from the gradient just beneath the sediment water interface, do fall in the same order of magnitude.

More research on processes just beneath the sediment-water interface is needed, since the increase of silicic acid that appears in the first depth segment, 0-1 cm beneath the sediment-water interface, is not the only striking observation but is accompanied by enhanced bacterial activities. Maxima in dissolved aluminum and dissolved organic carbon in Indian Ocean sediments correlate well with the nutrient maxima and provide evidence for a common underlying process (Fig. 3.9 and Sect. 3.1.1.2.3). In deep-sea sediments, bacterial enzymes are the primary agents of the early diagenesis of organic matter. Most enzymes measured during cruises in the Arabian Sea displayed the highest activities in the first cm of the cores [PFANNKUCHE, pers. comm.]. Therefore, it is quite reasonable that subsurface maxima in nutrients such as nitrite, nitrate, phosphate and ammonia may be direct products of organic matter remineralization (Fig. 3.9).

3. Experimental results and discussion

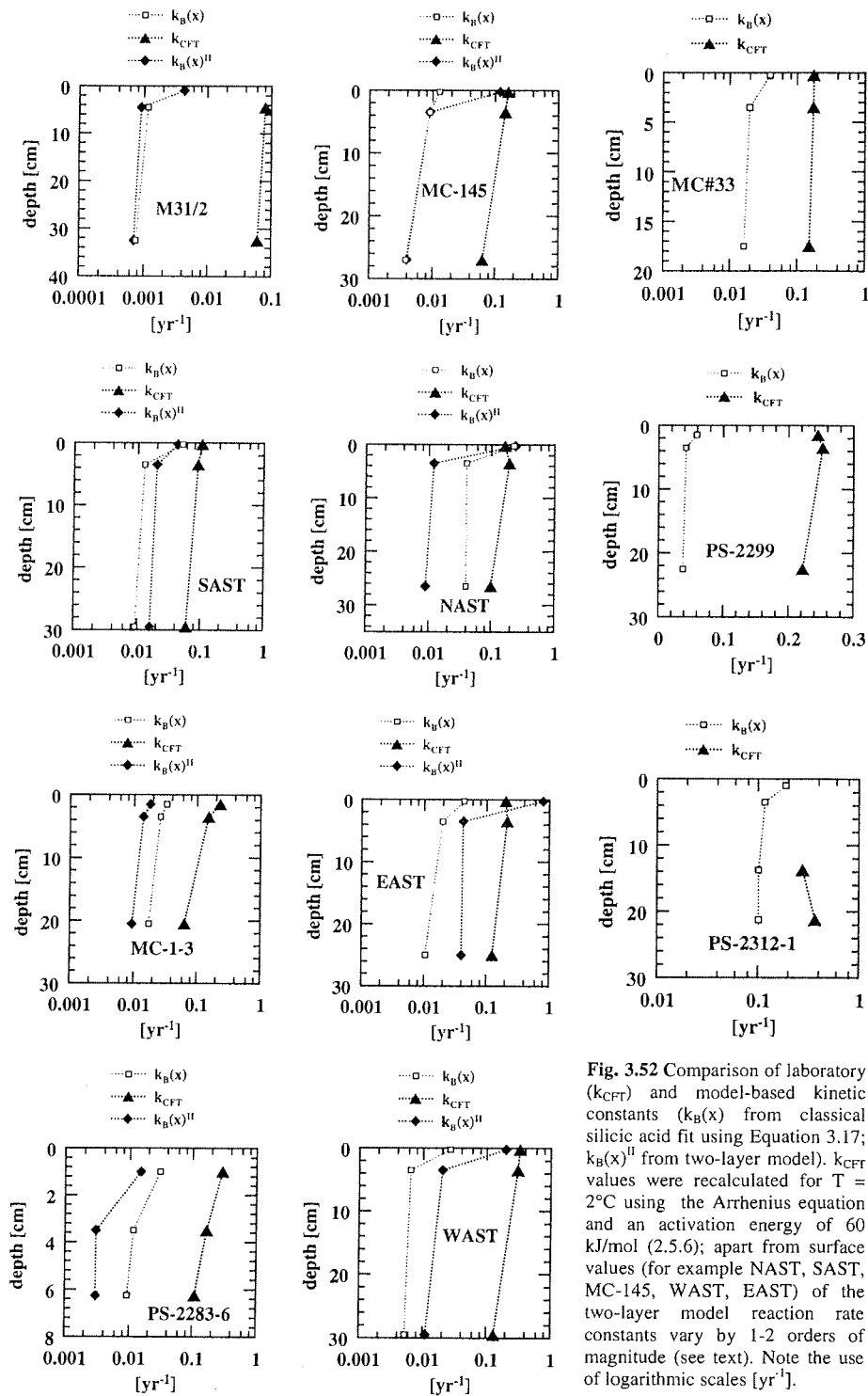


Fig. 3.52 Comparison of laboratory (k_{CFT}) and model-based kinetic constants ($k_B(x)$) from classical silicic acid fit using Equation 3.17; $k_B(x)^{II}$ from two-layer model). k_{CFT} values were recalculated for $T = 2^\circ C$ using the Arrhenius equation and an activation energy of 60 kJ/mol (2.5.6); apart from surface values (for example NAST, SAST, MC-145, WAST, EAST) of the two-layer model reaction rate constants vary by 1-2 orders of magnitude (see text). Note the use of logarithmic scales [yr^{-1}].

Which factors are responsible for systematic differences when comparing laboratory and modeling results ?

Laboratory results from flow-through experiments (or k_{NaOH} values) and results from batch experiments (Fig. 3.22) reveal the same principle rate distributions. For k_{NaOH} and k_{CFT} values a different sensitivity behavior was mentioned (Sect. 3.1.2.2.4, Fig. 3.31). Nevertheless, a systematic inaccuracy remains unresolved. Field and laboratory results reveal that understanding of natural processes in terms of kinetics differs from understanding the thermodynamics, which could be reproduced in laboratory flow-through experiments (3.1).

Considering the general rate law for dissolution and precipitation (LASAGA et al., 1994; Eq. 2.2 in Section 2.5.1) previous estimates [e.g., HURD, 1973; PACES, 1983; VELBEL, 1985; DAHMKE, 1988; CASEY et al., 1993; DOVE, 1995; VAN CAPPELLEN and QIU, 1997a,b; RAGUENEAU et al., submitted] and my own laboratory results differ from those of modeling pore water distributions; this is not surprising since

- (1) laboratory experiments are still unable to reproduce reactive surface areas in sedimentary environments and
- (2) determination of the reactive surface area which is involved in a dissolution process in sediments is still lacking which leaves high uncertainties in both laboratory and field rates.
- (3) pore water modeling procedures yield kinetic constants for the overall process of silicic acid release through dissolution of the most soluble phase within the sediments (i.e., biogenic silica) and subsequent consumption of silicic acid through reprecipitation reactions.

Kinetic constants derived from flow-through experiments, however, characterize the dissolution behavior of the most soluble fraction within the sediments and prevent reprecipitation reactions (For heterogeneous sediments this seems to be only partly fulfilled (3.1.2.3.4)).

Thus, these constants are *a priori* not comparable (see below) since both represent different reactions.

To understand the strategies of different experimental approaches and the output variables (k_{CFT} , k_{NaOH} , k_{Batch}) in contrast to k_{B} from pore water modeling the principles of flow-through experiments in contrast to batch experiments should again be taken into account.

Advantages of mixed-flow reactors in geochemical kinetics

Much information about the earliest stages of weathering comes from laboratory experiments where the mineral surface chemistry is rigorously controlled and the solution composition can be maintained even far from equilibrium. Mixed flow-through systems [e.g., WOLLAST and CHOU, 1985; DOVE and CRERAR, 1990; NAGY et al., 1990, 1991; NAGY and LASAGA, 1992; BURCH et al., 1993; VAN CAPPELLEN and QIU, 1997a,b] have major advantages over the conventional batch systems used in past kinetic studies. Batch results were restricted in the present thesis to a descriptive level and were used for additional information whenever results of flow-through experiments were unavailable. The major advantages of flow-through compared with batch experiments are:

3. Experimental results and discussion

- (1) Flow-through experiments are expected to be able to avoid diffusion limited conditions as well as those limited by secondary precipitates. These may be active in natural pore water systems as well as in batch reactors. Reaction rate constants from pore water modeling $k_B(x)$ reflect overall rate constants; these include dissolution and reprecipitation reactions occurring in natural systems. A direct comparison with k_{CFT} , then, is strictly speaking not permissible assuming that reprecipitations in flow-through systems can really be avoided (see above and Section 3.1.2.3.4). Dissolution rate constants from batch experiments have similar low reaction rate constants as those derived from pore water modeling. This suggests that batch experiments are more likely to represent the overall process which actually occurs in natural environments. The rate constant, k_{Batch} [RICKERT, unpublished results], however, is a value that summarizes the information of dissolution and reprecipitation simultaneously occurring in these closed systems. A more process orientated approach should include two rate expressions, one representing the dissolution of biogenic silica, and a counterbalancing rate expression accounting for silicic acid precipitation. Neither fitting a pore water profile nor conducting a batch experiment provides information about a single dissolution process. Thus, flow-through experiments are required to study both processes independently.
- (2) Reaction rates in flow-through systems are readily measured at steady state conditions without fitting concentrations versus time (batch) or depth (pore water). The system is capable of measuring reaction rates directly since the fluid composition is uniform throughout the vessel, and at steady state (3.1.1.2.1). The reaction is measured at constant chemical under- or oversaturation state. Concentration gradients which occur in natural environments are avoided through continuous stirring. Hence, the reaction term within a complex sedimentary matrix is separated to obtain reaction rate constants which are unaffected by transport processes.

In summary, the use of batch experiments or pore water fitting procedures enables us to measure overall rate constants for biogenic silica dissolution involving secondary processes in different sedimentary matrices which may be useful to describe individual sites and their diagenetic history. Yet, since a system put more than one additional constraint on the dissolution kinetics of biogenic silica, it remains impossible to transfer these individual field constants from one site to another site.

Reaction rate constants gained from flow-through experiments are clearly higher than those from the pore water fitting procedures or batch experiments since they ideally provide a single dissolution process for most soluble phases and suppress reprecipitation reactions which are likely to occur in natural environments (3.1.2.3.3 and 3.1.2.3.4) [SILLÉN, 1961; MACKENZIE and GARRELS, 1965; MACKENZIE et al. 1967; HURD, 1973; LERMAN, 1973; STOFFYN-EGLI, 1982; MACKIN and ALLER, 1986; MACKIN and SWIDER, 1987; MICHALOPOULOS and ALLER, 1995].

Reprecipitation reactions may be inevitable, however, even in flow-through reactors when deploying a heterogeneous sediment matrix including biogenic opal and inflow solutions which provide all essential cations for possible reprecipitation reactions

3. Experimental results and discussion

(3.1.2.3.4). Volcanic glass flow-through experiments, deployed in a similar fashion [STRONCIK-TREUE, pers. comm.] revealed that dissolution/reprecipitation reactions occur even in flow-through reactors.

Thus, much more detailed experiments are needed to quantify precipitation reactions that may act in natural environments or in closed batch experiments as a counterpart for dissolution of biogenic silica; thereby lowering the overall reaction rates maybe by up to two times compared with those measured in open flow-through reactors. These and other gaps in our quantitative understanding, for example the role of sorbed organic and inorganic constituents on silica reactivity within the sediments and the impossibility of determining surface areas of biogenic opal within a complex sediment matrix (see above), will continue to limit our ability to compare laboratory and field reactivities in general and dissolution and precipitation of biogenic silica in sedimentary matrices in particular.

3.2.3.4 The benthic silica cycle in the Arabian Sea: A mass balance

Within the multidisciplinary deep-sea program BIGSET (Chap. 1), several cruises were carried out to quantify the flux and turnover of material in the benthic boundary layer at 5 locations in the northern (NAST), western (WAST), central (CAST), eastern (EAST) and southern (SAST) Arabian Sea.

Tab. 3.12 Benthic silica cycles at 5 stations in the Arabian Sea. Opal rain rates (RR) measured in sediment traps [HAAKE et al., 1993]² deployed at 3000 m or by steady state mass balance calculation. Water depths¹ are given in Table 1. Sedimentation rates were taken from SIROCKO [1989]³ based on $\delta^{18}\text{O}$ measurements. Depth-dependent opal accumulation rates [Opal-AR] were calculated according to Equation 3.25; BE burial efficiencies based on recalculated rain rates; J pore water efflux of silicic acid (Tab. 3.8). The inventory of biogenic silica between 0 and 11.5 cm of the sediment column was estimated to derive mean residence of BSi in the sediment column. Burial time is the reciprocal value of sedimentation rate. All fluxes are given in $\text{mol Si m}^{-2} \text{yr}^{-1}$. The whole benthic cycles for the 5 locations are given in Figure 3.53. Uncertainties (see Figs. 3.53a-c) are given in brackets.

Properties	NAST	WAST	CAST	EAST	SAST
Water depth [m] ¹	3190	4030	3950	3840	4430
Trap depth [m] ²	---	3030	2950	2830	---
RR _{3000m} ²	---	0.2(1)	0.055(24)	0.08(3)	---
RR _{calculated}	0.13(1)	0.11(1)	0.12(1)	0.074(4)	0.067(4)
SR [cm kyr ⁻¹] ³	6.2	6.5	6.6	6.6	6.0
Opal-AR	0.010(2)	0.017(3)	0.012(2)	0.012(2)	0.012(2)
BE [%]	7.3	15	9.9	16	17
J(x = 0) _{classical fit}	0.12(1)	0.09(1)	0.11(1)	0.062(3)	0.055(4)
Inventory (0-11.5 cm) [mol _{Opal} m ⁻² _{Sed}]	21(2)	35(4)	23(2)	25(3)	27(3)
residence time [yr]	170	290	220	400	480
Burial time [yr]	1855	1764	1740	1742	1914

³Opal accumulation rates were calculated based on $\delta^{18}\text{O}$ stratigraphy values from 6 (2 cores were chosen at NAST) sediment cores [SIROCKO, 1989] taken at or as close as possible to the sediment trap stations [HAAKE et al., 1993] or to the sediment locations used in this study (Tab. 2.1). NAST: KL64 19°05'N 64°41' E and SK232 21°47'N 64°36' E; WAST: KL71 16°14'N 60°15' E; CAST: KL26 15°31'N 68°46' E; EAST: KL26 15°31'N 68°46' E; SAST: KL87 10°30'N 57°44' E.

3. Experimental results and discussion

Due to strong seasonal and regional variations in vertical particle fluxes [HAAKE et al., 1993], which is strongly driven by monsoons, it is expected that the seasonality can be traced to the benthic activities and turnover rates. A substantial data base gathered over several years by sediment trap investigations is available for three locations in this region (WAST, CAST, EAST) [HAAKE et al., 1993] and facilitates the assessment of interannual variabilities and their dependence on climatic processes.

The benthic silica cycle starting with fluxes at 1000 m above the seafloor (water depth ~ 3000 m) and the subsequent incorporation and remineralization in the sediments follows the flux and dissolution rate constant calculation as described in Section 3.2.2.2. Biogenic silica [wt.%] decreases from typically 2-3 wt.% (NAST, EAST, CAST, SAST) or 5-6 wt.% (WAST) down to < 1.5 or 3 wt.%, respectively. Methods used to determine benthic silicic acid fluxes were outlined in Section 3.2.2.2. A linear approximation used between the bottom water silicic acid concentration and the concentration in the first sampling interval (0.25 cm) or a whole core fitting procedure (Eq. 3.17) were compared. Fluxes calculated from the linear approximation were systematically higher by a factor of 1-4 than those derived from the whole core fitting procedure. This is due to a strong gradient near the sediment-water interface; the implications of such a strong increase in silicic acid were likewise discussed above (3.2.3.2). Given the pattern and calculations (Tab. 3.9) of pore water silicic acid data (Figs. 3.38 and 3.42), most of the dissolution process of biogenic silica occurs in the top 10 cm of the core. Subsequent calculations are based on the deposit of biogenic silica within the top 13 cm of the sediment and on fluxes derived from the classical fitting procedure (Tab. 3.7). Therefore, results should be treated as a low estimate for benthic fluxes (3.2.3.2). It will be demonstrated, however, that applying even such a low estimate for benthic recycling pore water efflux as a counterpart to opal rain rate from the water column (e.g., 3000 m) to the seafloor may result in putting too much emphasis on trap data [HAAKE et al., 1993].

In addition to the estimation of the recycling dissolved silica flux, depth-dependent biogenic silica accumulation rates based on Equation 2.25 were calculated:

$$\text{Opal} - \text{AR} = [1 - \phi(x)] \delta_s \text{SR BSi}(x)/100 \quad (2.25)$$

Opal-AR	opal accumulation rate [mol m ⁻² yr ⁻¹]
$\phi(x)$	porosity (depth-dependent)
δ_s	sediment density [2.65 g/cm ³]
SR	sedimentation rate [cm/1000 yr]
BSi(x)	biogenic silica content (depth-dependent)

Depth-dependent accumulation rates have been calculated using sedimentation rates (SR) based on $\delta^{18}\text{O}$ stratigraphies of sediment cores which have been taken in the vicinity of the multicorer casts [SIROCKO, 1989].

In Equation 3.25, the product $[1 - \phi(x)] \delta_s$ represents dry bulk density. Mean values were applied which are quite similar throughout most of the cores (0.010(2) - 0.012(2) mol m⁻² yr⁻¹) except for WAST, where significantly higher accumulation rates (0.017(3) mol m⁻² yr⁻¹) were determined. The standard deviation (given in brackets) from average values is ~ 20%. Assuming steady state and that the benthic silicic acid flux is mainly induced by biogenic silica dissolution with a negligible influence of silicate minerals,

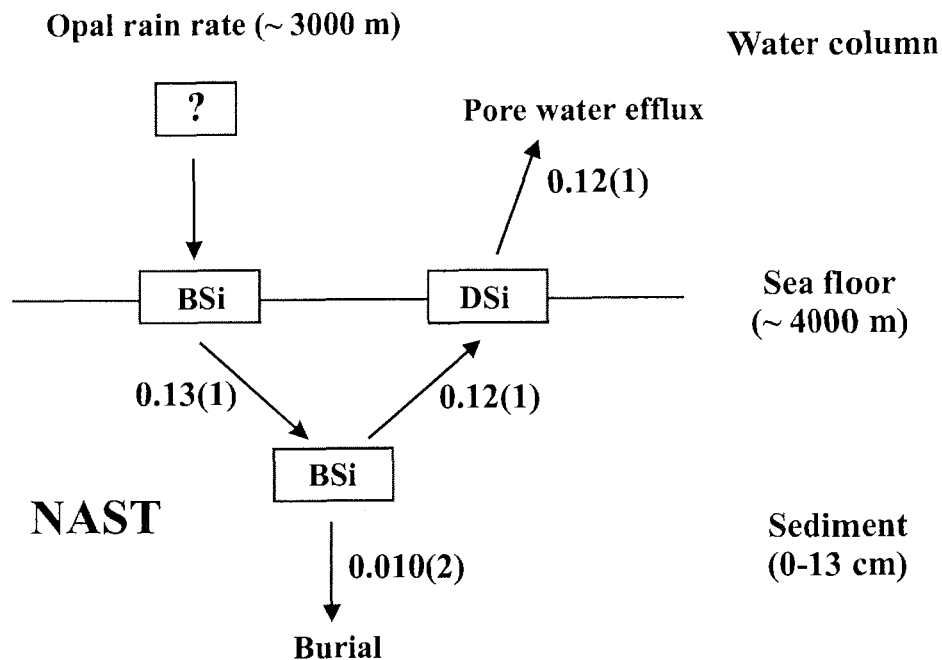


Fig. 3.54a Mass balance for NAST (Arabian Sea) [$\text{mol m}^{-2} \text{yr}^{-1}$]. Rain rates were recalculated by a steady state mass balance calculation (see text). Burial efficiency based on this recalculated rain rates is $\sim 7.3\%$ (Tab. 3.12).

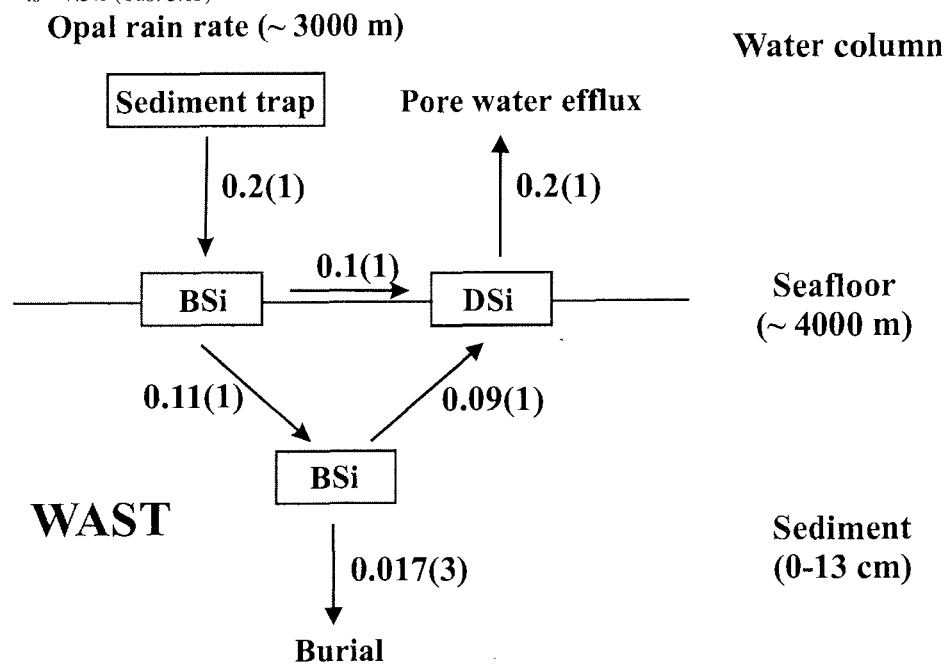


Fig. 3.54b Mass balance for WAST [$\text{mol m}^{-2} \text{yr}^{-1}$]. Rain rates were measured in sediment traps [HAAKE et al., 1993] and recalculated by a steady state mass balance calculation (see text). Burial efficiency based on this recalculated rain rates is $\sim 15\%$ (Tab. 3.12).

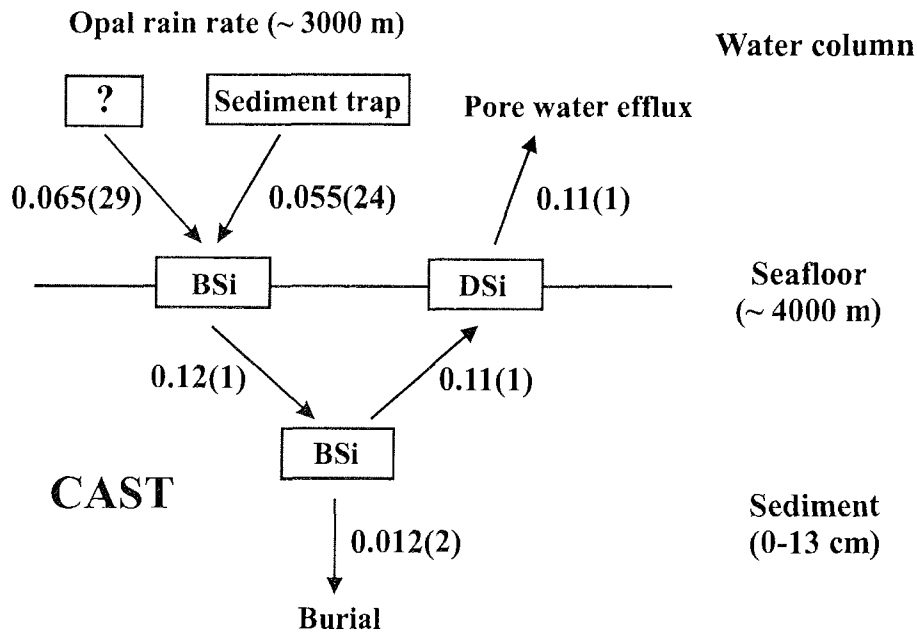


Fig. 3.54c Mass balance for CAST [$\text{mol m}^{-2} \text{yr}^{-1}$]. Rain rates were measured in sediment traps [HAAKE et al., 1993] and recalculated by a steady state mass balance calculation (see text). Burial efficiency based on this recalculated rain rates is ~ 9.9% (Tab. 3.12).

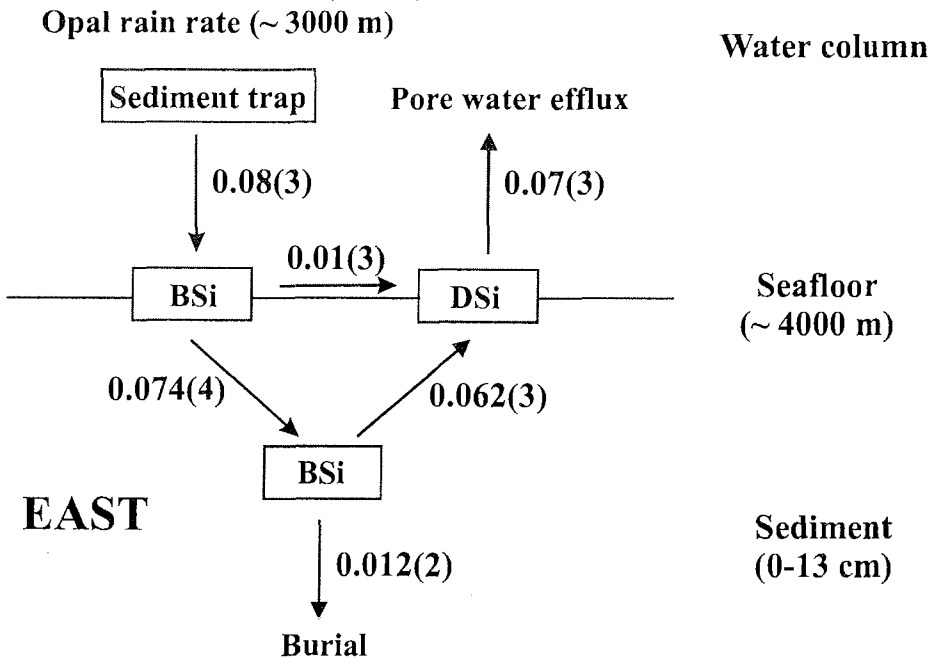


Fig. 3.54d Mass balance for EAST [$\text{mol m}^{-2} \text{yr}^{-1}$]. Rain rates were measured in sediment traps [HAAKE et al., 1993] and recalculated by a steady state mass balance calculation (see text). Burial efficiency based on this recalculated rain rates is ~ 16% (Tab. 3.12).

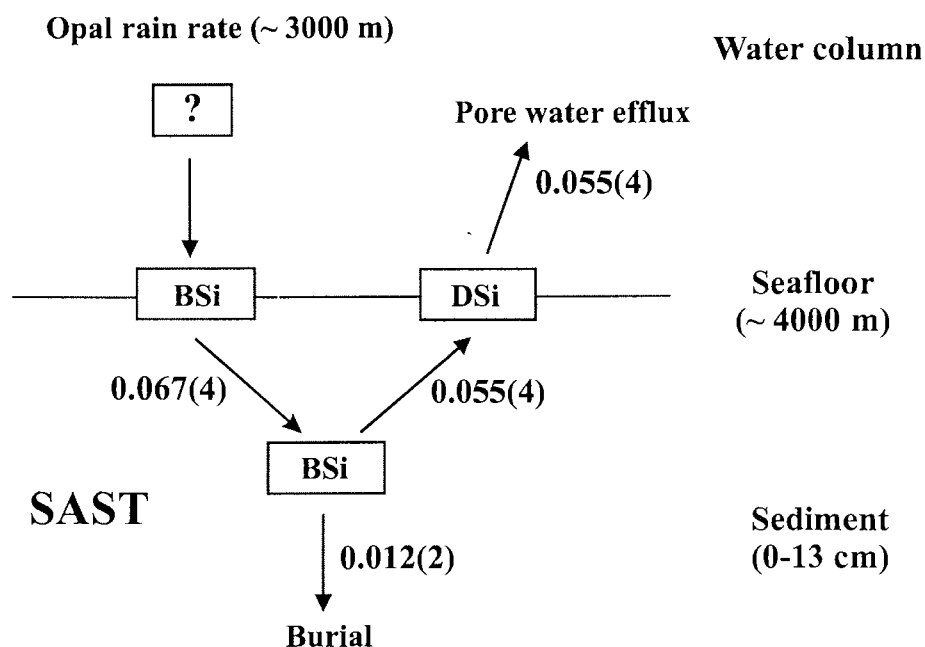


Fig. 3.54e Mass balance for SAST (Arabian Sea) [$\text{mol m}^{-2} \text{yr}^{-1}$]. Rain rates were recalculated by a steady state mass balance calculation (see text). Burial efficiency based on this recalculated rain rates is $\sim 17\%$ (Tab. 3.12).

the biogenic silica rain rate needed to close the benthic silica cycle were calculated by summing the benthic recycling flux of silicic acid and mean accumulation rates [e.g., KONING et al., 1997; RAGUENEAU et al., submitted]. The rain rate ($RR_{\text{calculated}}$) required can thus be estimated. According to these estimates, NAST sediments require the largest rain rates ($0.13(1) \text{ mol m}^{-2} \text{yr}^{-1}$) followed by CAST ($0.012(1) \text{ mol m}^{-2} \text{yr}^{-1}$) and WAST ($0.011(1) \text{ mol m}^{-2} \text{yr}^{-1}$); half of this rain rate is needed to close the silica cycle at SAST and EAST sites (Tab. 3.12). Comparing these recalculated rates with actual trap data [HAAKE et al., 1993] from $\sim 1000 \text{ m}$ above the seafloor, consistency within uncertainties ($\sim 30\text{-}50\%$) based on seasonal variations over a couple of years [HAAKE et al., 1993] was only observed at EAST site. At CAST, trap data reveal only $\sim 50\%$ of the rain rate that was recalculated whereas at the WAST trap, pore water efflux and burial flux together do not completely balance the particle fluxes from the trap.

For all stations, particulate biogenic silica fluxes, recycling fluxes from the sediment and burial fluxes were compared to calculate a mass balance for each site (Figs. 3.54 a-e). Assuming that the balance may be erroneous due to underestimations derived from sediment traps, an additional box was created (Figs. 3.54 a-e, box signed with a question mark) to demonstrate that the cycle would be balanced with an additional biogenic silica tool. This is only one explanation for the imbalance of the silica cycle at CAST. Another explanation may be the overestimation of diffusive flux due to sediment compaction during multicorer deployment. This may be responsible for getting larger gradients at the sediment-water interface [SAYLES et al., 1996]. Lateral transport is another explanation, however the opposite seems more to the point and may

3. Experimental results and discussion

explain the imbalance at WAST. According to the classical fitting procedure, the measured data points in the first 5 cm are only poorly represented (Fig. 3.38), resulting in large underestimations of the recycling flux of silicic acid from pore waters (Tab. 3.7). Assuming an average value between both estimates (linear or non-linear fitting procedure), the recycling flux is doubled and can balance the particle rain documented by sediment trap data. This is one explanation for the excess $0.8 \text{ mmol m}^{-2} \text{ yr}^{-1}$ calculated from the imbalance between particle fluxes from the trap and recycling effluxes and the burial rate. Another explanation is the dissolution of a major part of biogenic silica present in the trap but already lacking in the top of the core and/or the additional efflux from a thin, extremely reactive layer just below the sediment-water interface not sampled in the profiles, or it may be caused by bioturbation [KONING et al., 1997]. For NAST and SAST, no trap data were available, therefore input fluxes (Figs. 3.54 a-e) are only calculated based on the formalism described above.

Burial efficiencies are in the range of 7-17%, based on recalculated fluxes, as 83-93% of the rain rate reaching the seabed is assumed to get recycled in the top 13 cm of the sediment column. Generally, this is in good agreement with a compilation of silica recycling and burial data for many deep-sea sites showing that $\sim 90\%$ of the biogenic silica arriving at the sediment-water interface (the opal rain rate) dissolve prior to burial [RAGUENEAU et al., submitted]. HAAKE et al. [1993] reported somewhat higher burial efficiencies (15-25%) based on trap data and total accumulation rates taken from SIROCKO and SARNTHEIN [1989] and SIROCKO [1989]. It should be added that opal contents also appeared below 13 cm sediment-depth, but due to saturation of silicic acid this inventory is at first approximation no longer involved in dissolution processes.

Particulate fluxes reported from the Somali Slope and Somali Basin [KONING et al., 1997] are distinctly higher than the recalculated rain rates due to a higher productivity in the vicinity of the Somali Coast. Burial efficiencies, however, are distinctly lower (6-8%) [KONING et al., 1997].

A residence time estimate for biogenic silica in the top 13 cm of the sediment, where most of the dissolution process occurs, can be obtained for the opal inventory estimated for each station. Dividing the inventory of biogenic silica by the recycling silicic acid flux, estimated from the classical non-linear approach, yields residence times for biogenic silica within the 'dissolution-zone' (0-13 cm).

The opal inventory was calculated on the basis of opal content profiles (A. 2.3.1. - A. 2.3.5), porosity profiles (A. 2.3.1 - A. 2.3.5), assuming a sediment density of 2.65 g cm^{-3} . This yields a profile of BSi (wt.%) expressed in $\text{mol SiO}_2 \text{ cm}^{-3}$ of sediment, taking into account the molecular weight of biogenic silica of 66 g/mol (assuming an average water content of 10% for biogenic opal [MORTLOCK and FROELICH, 1989]). Integration over the first 13 cm of the sediments provides an inventory estimation in the range of 21(2) - 35(4) $\text{mol}_{\text{Opal}} \text{ m}^{-2}_{\text{Sed}}$ with highest values at WAST (3.2.3.4). Residence times of between 170 and 480 years were calculated based on these inventories (3.2.3.4). These values are in the range of those reported by SAYLES et al. [1996] in deep-sea sediments of the Western Atlantic (~ 100 -350 years). Similar values can also be calculated from the invariable rate constant $k_{B,\text{const}}$ which lies in the range of 0.011 yr^{-1} and 0.027 yr^{-1} and yields residence times of 20-90 years (Tab. 3.9).

Constants obtained from $k_B(x)$ values of the first depth interval provide even higher values and consequently lower mean residence times, for example opal particles at

CAST with k_B values of 0.1 yr^{-1} at $x = 0$ have mean lifetimes of only 10 years. Considering the time it would take for a silica particle to get buried below the dissolution zone (assuming a sedimentation rate of 6 cm kyr^{-1} this is some 2000 years burial time, Tab. 3.12), no BSi should be accumulating in these sediments. In fact, however, biogenic silica contents were observed at even lower depth. Burial efficiencies of up to 20% were calculated. This has something to do with the fact that implicit to the estimates and pore water fitting procedure the assumption is that all opal measured in the sediment is reactive; this was induced by the assumption that the reaction rate is proportional to the bulk silica content in Equation 3.22. Indeed, the calculations show large uncertainties considering the individual calculations. Nevertheless, kinetic constants of at least 2 orders of magnitude lower than those estimated by the pore water silicic acid fitting procedure have to be assumed to enable silica particles to get buried below dissolution depth.

In summary, it could be revealed that treating biogenic silica inventories as a single pool with the same reactivity is a too simplified assumption. In fact, residence times in the mixed layer, say ~ 400 years for 2 cm of mixed surface sediment, largely exceeded my estimate of mean lifetimes based on rate constant $k_{B,\text{const.}}$ (~ 20 -90 years in surface sediments). This consideration and the results of the flow-through experiments supported a general decrease of reactivity and apparent solubilities from surface waters towards deep buried single diatom species (*Ethmodiscus rex*) (Fig. 3.4, Sect. 3.1.1.2.2; Fig. 3.34, Sect. 3.1.2.3.2). This is consistent with the idea of the preferential dissolution of a more soluble phase starting in the water column where slightly silicified species most readily dissolve during settling and when reaching the sediment. Most recently, BIDDLE and AZAM [1999] reported bacteria-mediated acceleration of silica dissolution by a rapid degradation of the organic matrix which protects siliceous species from dissolution. Being buried, this preferential depletion of the opal inventory by more easily dissolving species most probably occurs since they provide the lowest activation energies concerning the dissolution process. This results in kinetic constants which are inherent to those most soluble opal species but do not account for the opal inventory as a whole. Preferential dissolution experiments are required [MIKKELSEN, 1980; SHEMESH et al., 1989] to explain these lower kinetic constants which in turn may result in more realistic estimates of residence times of opal species within the bulk opal pool. This idea has already been proposed earlier [e.g., HURD, 1973; SCHINK et al., 1975; MIKKELSEN, 1980; SHEMESH et al., 1989; McManus et al., 1995; WILLEY et al., 1997] but has not yet been quantified over such a broad range of natural conditions as presented in this study by means of flow-through experiments.

As a consequence, the estimates of k_B must be divided in a reactive and an unreactive constant for a reactive and an unreactive fraction of biogenic silica. This is part of the reactive opal model proposed by SCHINK et al. [1975]. In this model the reactive component of total opal dominates the down-core change in reaction. Because solid phase measurement techniques cannot distinguish between reactive and unreactive opal, this fraction can only be calculated [e.g., SCHINK et al., 1975; BOUDREAU, 1990a, McMANUS et al., 1995]. The input of multiple opal types differing in solubility and reactivity constants in numerical modeling studies was proposed in Section 3.1.2.3.5. This was suggested to account for the reactivity decrease caused by aging effects

3. Experimental results and discussion

through adsorption of inorganic cations or organic matter, or by reduced silica diversity in favor of species of high silicification or lower reactivity.

3.2.4 Conclusion

- (1) Pore water data, biogenic silica profiles and porosity distributions from surface sediments at 13 locations were selected to quantify sedimentary fluxes and to identify the processes controlling preservation and recycling efficiencies of biogenic silica within different sediment matrices.
- (2) A simplified steady state model based on the one-dimensional diagenetic equation using fitting routines which ignore advection and the dynamics of solids, is useful to reproduce natural distributions for all 13 stations (silicic acid, biogenic silica concentrations and porosity versus depth); benthic dissolution fluxes at the sediment-water interface and depth-dependent reactivity constants $k_B(x)$ could then be extracted with analytical solutions which provide higher values in depth intervals near the sediment-water interface and approach lower values with increasing depth.
- (3) Asymptotic silicic acid values display a range between $\sim 100 \mu\text{M}$ measured in North Atlantic sediments and $800 \mu\text{M}$ in Scotia Sea sediments; benthic recycling fluxes vary accordingly between 0.05 and $7 \text{ mmol m}^{-2} \text{ day}^{-1}$.
- (4) Benthic dissolution fluxes calculated from subsurface gradients by the classical fitting procedure were compared with fluxes gained from a linear estimate of the subsurface gradient of silicic acid profiles to reveal that major differences in flux calculation depend on the procedure applied. Results provide systematic lower fluxes by a factor of 2-4 in sediments of low BSi contents ($< 20\%$), whereas in the siliceous oozes of the Scotia Sea ($\sim 60\%$ BSi) the linear approach results in systematically lower estimates by a factor of ~ 2 .
- (5) The benthic silica cycle has been studied at 5 deep-sea localities (NAST, WAST, CAST, EAST, SAST) in the Arabian Sea. Mean benthic silicic acid fluxes based on the classical fitting procedure for each site range between $0.055(4)$ (SAST) and $0.12(1)$ (NAST) $\text{mol m}^{-2} \text{ yr}^{-1}$. Assuming steady state and that all benthic recycling effluxes of silicic acid stem from the dissolution of biogenic silica, the rain rate reaching the seabed was estimated summing up the average accumulation rates of biogenic silica and the recycling fluxes. The average accumulation rates were estimated to be in the range of 0.010 and $0.017 \text{ mol m}^{-2} \text{ yr}^{-1}$. Based on the opal inventory in 0-13 cm of sediments ($21(2) - 35(4) \text{ mol}_{\text{Opal}} \text{ m}^{-2}_{\text{Sed}}$), mean residence times of biogenic silica were estimated at 170 to 480 years. This is far below the time it would take for a silica particle to become buried below the dissolution zone ($\sim 0-13 \text{ cm}$) which lies in the range of $\sim 2000 \text{ yr}$. Hence, opal should not accumulate, but indeed, burial efficiencies range from 7 to 17%. This suggests that kinetic constants which have been estimated from flow-through experiments (see 9) and also estimates from pore water modeling procedure (see 8), which yield significantly lower lifetimes of BSi within the dissolution zone, are in fact estimates representing the most soluble species within the sediment column. This suggests that a non-reactive fraction with distinctly slower dissolution kinetics gets buried.

- (6) Evidence of a seasonal imprint within the sediment-water interface were discussed and a two-layer model was proposed to more reliably fit large gradients within the first half centimetre of the sediment as well as the rest of the profile.
- (7) Depth-dependent apparent rate constants from the classical fitting procedure provide significantly lower estimates than those which were determined by flow-through experiments for respective sediments and depths. These values, however, re-reflect the dissolution rate of the most soluble fraction within the accumulated opal.
- (8) Given the results of this thesis and earlier laboratory kinetic studies, the appropriate level of comparison of field and laboratory dissolution rates is at the scale of reactivity trends. Aqueous dissolution experiments are not directly applicable to natural weathering due to unnaturally high fluid/mineral ratios, where the mineral surface chemistry is precisely controlled and the formation of secondary minerals is suppressed to a large extent (3.1.2.3). Kinetic constants derived from pore water modeling in contrast represent the overall dissolution-precipitation process occurring in the sediment column. Therefore, these constants are not directly comparable.
- (9) Although experimental studies in water-rich systems are not yet applicable to natural weathering on an absolute scale due to still unaccessible parameters, the results and distribution within the sediment column of both estimates have provided a qualitative consistency.

In summary, future research strategies should focus on early diagenetic models of biogenic silica in deep-sea sediments including two rate expressions. One should account for the dissolution process and release of silicic acid, the other for its reprecipitation. Neither processes is extractable from pore water modeling alone. Therefore, it is important to emphasize that laboratory flow-through experiments as provided in my thesis should further be deployed as an important approach for a complete understanding of natural processes. Research strategies which account for the reprecipitation reactions occurring in natural environments must be developed.

4. Summary and general conclusions

Controls on the recycling and preservation of biogenic silica in marine environments

In this thesis, a better understanding of biogenic silica dissolution in both the field and laboratory settings has been achieved which in turn provides answers to important questions which puzzle biogeochemists working on the early diagenesis of biogenic silica:

- (1) Dissolution experiments were carried out to examine the decrease in reactivity of biosiliceous remains produced in the euphotic zone, transferred to the sea floor and deposited in various sedimentary environments. A stirred-flow-through reactor technique was used to determine silica solubilities in eleven cores collected in changing sedimentary regimes providing different opal/detritus ratios. Apparent solubilities of biogenic silica in the deepest sections of the cores exhibited a relative order of values which is similar to variations in asymptotic pore water concentrations observed in the field.
- (2) Single acid-cleaned, nearly pure opal samples collected from various locations in surface waters, in the water column (450 m, 1000 m, 2500 m), and from different sediment depths show only slight solubility differences (1000-1200 μM at 2°C and pH 8).
- (3) The variability of apparent solubilities or, for that matter, pore water asymptotic silicic acid values, is best explained by the dilution of biogenic silica due to various detrital contents rather than solubility differences of siliceous skeletons produced in the water column. Detrital material controlling the pore water build-up of silicic acid was emphasized as the main environmental factor. This was shown by flow-through experiments carried out with opal/clay mixtures. Biogenic silica revealed a significant drop in apparent solubility when detrital clays were present in solution. Kaolinite, followed by montmorillonite and illite, was most effective in preventing biogenic silica from reaching solubility values similar to those observed for pure acid-cleaned silica samples.
- (4) Laboratory experiments and field observations yielded no evidence for aluminum concentrations which would lead to a possible interaction with dissolved silica.
- (5) A mechanism of closely coupled dissolution and reprecipitation reactions which control the build-up of pore water silicic acid values was proposed. These "reverse weathering" reactions do not preclude the involvement of aluminum in these nearly simultaneous dissolution-reprecipitation processes, but do not necessitate highly dissolved aluminum intermediates either.
- (6) Flow-through experiments revealed that extremely high concentrations of magnesium (~ 5.5 M) control the preservation of opal in hypersaline brines.
- (7) The dissolution rate of sedimentary and single opal samples switches from a linear to an exponential dependence on the degree of undersaturation with increasing distance from equilibrium. This disagrees with the most widely used linear rate law that form the basis of nearly all diagenetic models of biogenic silica. The exponential increase of the dissolution rate when a critical level of undersaturation is exceeded elucidates a better understanding of the efficient recycling of silicic acid in surface water of the oceans, but may, in a first estimate, be negligible for

4. Summary and general conclusions

the early diagenesis of biogenic silica in sediments where silicic acid concentrations often exceed the essential critical undersaturation within a few millimetres of the sediment column.

- (8) The kinetic measurements revealed a steady decrease in biosiliceous reactivity from surface waters through the water column to near-surface sediments and a further decrease within the sediment-column with advancing early diagenesis. Dissolution rate constants determined for 2°C and pH 8 or recalculated from flow-through experiments at 25°C (using $E_a = 60$ kJ/mol) decrease from ~ 27 yr⁻¹ for acid-cleaned phytoplankton, 2-4 yr⁻¹ for untreated or acid-cleaned sediment trap material to 0.05-0.36 yr⁻¹ within the sediment column. The giant diatom *Ethmodiscus rex* is notable because it exhibits the lowest dissolution rate constant ($k_{\text{CFR}} = 0.05$ yr⁻¹) ever reported in the literature.
- (9) The reactivity decreases both in the water and the sediment column do not correlate with the measured N₂-BET surface area, or with the bulk concentration of extractable biogenic silica. Neither the flow-through nor the alkaline leaching experiments provide an answer to the question as to which extent the reactivity decrease is a result of a decrease in surface reactivity or of the deposition of a more reactive silica fraction, since both methods do not quantify specific reactive surface sites but represent bulk reactivities. Cobalt adsorption experiments carried out with Scotia Sea siliceous oozes to quantify surface site densities of silanol groups, however, do not suggest a significant decrease in surface reactivity during early diagenesis.
- (10) By comparing dissolution rates of untreated phytoplankton samples and those of samples which were peroxide- and acid-cleaned, it was verified that the formation of organic layers may also be responsible for the observed decrease in reactivity by a factor of ~ 20 .
- (11) The appropriate level of a comparison of laboratory dissolution rate constants with depth-dependent kinetic constants gained from fitting pore water silicic acid, biogenic silica and porosity profiles to a one-dimensional diagenetic equation at steady state is at the scale of reactivity trends. A positive relationship between reactivities determined by means of flow-through experiments and alkaline leaching experiments was observed, suggesting the use of alkaline leaching experiments as a relative measure for reactivity variations in sediments. Compared with flow-through experiments, both the adsorption method and the use of alkaline leaching constants have the advantage of being much faster and simpler to implement on a routine basis to gain reactivity variations throughout the core.
- (12) Kinetic constants derived from pore water modeling represent the overall dissolution-precipitation process occurring in the sediment column. Therefore, these constants are not directly comparable to dissolution rate constants determined in flow-through experiments which more likely represent the dissolution behavior of the most soluble biogenic silica fraction. Future research strategies should, hence, focus on early diagenetic models of biogenic silica in deep-sea sediments including two rate expressions. One rate expression should account for the dissolution process and release of silicic acid, the other for its

4. Summary and general conclusions

reprecipitation. Thus, further flow-through experiments are needed to cope with these reprecipitation reactions as an important approach for a complete understanding of the early diagenesis of biogenic silica in natural environments.

- (13) Based on the opal inventory ($21\text{-}35 \text{ mol}_{\text{Opal}} \text{ m}^{-2}_{\text{Sed}}$) within the dissolution zone of sediments ($\sim 0\text{-}13 \text{ cm}$) from 5 deep-sea localities in the Arabian Sea and mean benthic recycling fluxes ($0.06\text{-}0.12 \text{ mol m}^{-2} \text{ yr}^{-1}$), mean residence times of biogenic silica of 170-480 years were estimated. No opal is expected to accumulate, considering the time it would take for a silica particle to become buried below 13 cm (~ 2000 years). In contrast, burial efficiencies range from 7 to 17%. This suggests that kinetic constants based on bulk concentrations of biogenic opal within the sediments are indeed mean values, representing at least two fractions, from which one is more reactive and preferentially dissolves within the sediment column and in flow-through experiments and a second, non-reactive fraction with distinctly slower dissolution kinetics becomes buried.
- (14) Combining literature data with these laboratory results, a high efficiency of biogenic silica recycling is favored in the Northern Atlantic compared with the Southern Ocean. A larger percentage of silica shells in HNLC regions survive and is subsequently buried because diatoms with a priori thicker shells evolve in iron-limited regions. Additionally, as a consequence of iron-limited bacterial growth the effective removal of organic coatings is reduced, which, in turn, slows down dissolution in the water column by a factor of at least ~ 20 . Considering the subsequent dissolution process in the sediment column, Southern Ocean species again have the advantage of escaping further dissolution since the sediment structure of high opal/detritus ratios benefits the dissolution process towards apparent saturation values to a larger extent than the sediment structure in the Northern Atlantic. Accordingly, pore waters in Southern Ocean sediments most rapidly become saturated, i.e., biogenic silica buried in these sediments escape further dissolution within 1-2 cm sediment depth. In contrast, pore waters of sediments underlying HNLC regions usually become saturated in significantly greater sediment depths; thereby opal skeletons dissolve to a great extent.

References

- Aargaard P. and Helgeson H. C. (1982) Thermodynamic and kinetic constraints on reaction rates among minerals and aqueous solutions. I. Theoretical considerations. *Am. J. Sci.* **282**, 237-285.
- Abelmann A., Gersonde R., and Spiess V. (1988) Pliocene-Pleistocene paleoceanography in the Weddell Sea - Siliceous microfossil evidence. In *Geological history of the polar oceans: Arctic versus Antarctic* (eds. U. Bleil and J. Thiede), pp. 729-759. Kluwer.
- Alldredge A. L. and Gottschalk C. C. (1989) Direct observations of the mass flocculation of diatom blooms: characteristics, settling velocities and formation of diatom aggregates. *Deep-Sea Res.* **36**, 159-171.
- Aller R. C. and Benninger L. K. (1981) Spatial and temporal patterns of dissolved ammonium, manganese, and silica fluxes from bottom sediments of Long Island Sound. *US J. Marine Res.* **39**, 295-314.
- Anders, T. (1997) *Stabile Sauerstoffisotope in marinen Diatomeen: Isotopenfraktionierung und palaeozeanographische Anwendung*. Dissertation, Christian-Albrechts-Universität zu Kiel.
- Anderson G. F., Hall P. O. J., Rutgers v.d. Loeff M. M., Sundby B., and Westerlund S. F. G. (1986) Benthic respiration measured by total carbonate production. *Limnol. Oceanogr.* **31** (2), 319-329.
- Andrews D. and Bennett, A. (1981) Measurements of diffusivity near the sediment-water interface with a finescale resistivity probe. *Geochim. Cosmochim. Acta* **45**, 2157-2169.
- Andrews D. and Hargrave B. T. (1984) Close interval sampling of interstitial silicate and porosity in marine sediments. *Geochim. Cosmochim. Acta* **48**, 711-722.
- Anikouchine W. A. (1967) Dissolved chemical substances in compacting marine sediments. *J. Geophys. Res.* **72**, 505-509.
- Archer D., Lyle M., Rodgers K., and Froelich P. (1993) What controls opal preservation in tropical deep-sea sediments? *Paleoceanography* **8**, 7-21.
- Archie G. E. (1942) The electrical resistivity log as an aid in determining some reservoir characteristics. *Petrol. Tech.* **1**, 55-62.
- Badaut D. and Risacher F. (1983) Authigenic smectite on diatom frustules in Bolivian saline lakes. *Geochim. Cosmochim. Acta* **47**, 363-375.
- Baes Jr. C. F. and Mesmer R. E. (1976) *The hydrolysis of cations*. Wiley and Sons.
- Barker P., Gasse F., Fontes J.-C., and Druart J.-C. (1994) Experimental dissolution of diatom silica in concentrated salt solutions and implications for paleoenvironmental reconstruction. *Limnol. Oceanogr.* **39**, 99-110.
- Belvayeva T. V. (1968) Range and numbers of diatoms of the genus *Ethmodiscus* (Castr) in Pacific plankton and sediments. *Oceanology* **8**, 79-85.
- Bender M. L., Martin W., Hess J., Sayles F., Ball L. and C. Lambert (1987) A whole-core squeezer for interstitial pore-water sampling. *Limnol. Oceanogr.* **32**, 1214-1225.

References

- Berelson W. M., Hammond D. E., and Cutter G. A. (1990) *In situ* measurements of calcium carbonate dissolution rates in deep-sea sediments. *Geochim. Cosmochim. Acta* **54**, 3013-3020.
- Berger W. H. and Herguera J. C. (1992) Reading the sedimentary record of the ocean's productivity. In *Primary Productivity and Biogeochemical Cycles in the Sea* (ed. P.G. Falkowski and A.D. Woodhead), pp. 455-486. Plenum Press.
- Berger G., Cadore E., Schott J., and Dove P. M. (1994) Dissolution rate of quartz in lead and sodium electrolyte solutions between 25 and 300° C: Effect of the nature of surface complexes and reaction affinity. *Geochim. Cosmochim. Acta* **58**, 541-551.
- Berner R. A. (1974) Kinetic models for the early diagenesis of nitrogen, phosphorus, and silicon in anoxic marine sediments. In *The Sea, Marine Chemistry*, Vol. 5 (ed. E. D. Goldberg), pp. 427-450. John Wiley.
- Berner R. A. (1980) *Early Diagenesis - A Theoretical Approach*. Princeton University Press.
- Bidle K. D. and Azam F. (1999) Accelerated dissolution of diatom silica by marine bacterial assemblages. *Nature* **397**, 508-512.
- Biebow N. (1991) *Methoden zur quantitativen Aufbereitung von Radiolarien und Diatomeen an zwei holozänen Sedimentkernen südwestlich von Spitzbergen*. Diplomarbeit, Christian-Albrechts-Universität zu Kiel.
- Blum A. E. and Lasaga A. C. (1987) Monte Carlo simulation of surfaces reaction rate laws. In *Aquatic Surface Chemistry: Chemical Processes at the Particle-Water Interface* (ed. W. Stumm), pp. 255-292. Wiley.
- Bohrmann G., Abelmann A., Gersonde R., Hubberten H., and Kuhn G. (1994) Pure siliceous ooze, a diagenetic environment for early chert formation. *Geology* **22**, 207-210.
- Bonatti E. and Nayudu Y. R. (1965) The origin of manganese nodules on the ocean floor. *Am. J. Sci.* **263**, 77-139.
- Boudreau B. P. (1986) Mathematics of tracer mixing in sediments: I. spatially-dependent, diffusive mixing. *Am. J. Sci.* **286**, 161-198.
- Boudreau B. P. (1990a) Asymptotic forms and solutions of the model for silica-opal diagenesis in bioturbated sediments. *J. Geophys. Res.* **95**, 7367-7379.
- Boudreau B. P. (1990b) Modelling early diagenesis of silica in non-mixed sediments. *Deep-Sea Res.* **37**, 1543-1567.
- Boudreau B. P. (1996) The diffusive tortuosity of fine-grained unlithified sediments. *Geochim. Cosmochim. Acta* **60(16)**, 3139-3142.
- Boudreau B. P. and Guinasso Jr. N. L. (1982) *The influence of a diffusive sublayer on accretion, dissolution, and diagenesis at the sea floor*. Lexington Books.
- Brack K. (1997) *Eine verbesserte Aufschlußmethode zur Messung von biogenem Opal in marinen Sedimenten*. Diplomarbeit, Christian-Albrechts-Universität zu Kiel.
- Brady P. V. and Walther J. V. (1990) Kinetics of quartz dissolution at low temperatures. *Chem. Geol.* **82**, 253-264.
- Broecker W. S. and Peng T.-H. (1982) *Tracers in the Sea*. Eldigio Press.

- Brunauer S., Emmett P. H., and Teller E. (1938) Adsorption of gases in multimolecular layers. *J. Am. Chem. Soc.* **60**, 309-319.
- Buesseler K. O. (1998) Understanding the coupling between primary production and particulate export in the upper ocean. *EOS transactions, American Geophysical Union* **79**(1), 95.
- Burch T. E., Nagy K. L., and Lasaga A. C. (1993) Free energy dependence of albite dissolution kinetics at 80°C and pH 8.8. *Chem. Geol.* **105**, 137-162.
- Burton W. K., Cabrera N. and Frank F. C. (1951) The growth of crystals and the equilibrium structure of their surfaces. *Philos. Trans. R. Soc. London, Series A* **243**, 299-358.
- Caddée G. C. and Laane R. W. P. M. (1983) Behaviour of POC, DOC, and fluorescence in the freshwater compartment of the river EMS. In *Transport of Carbon and minerals in major world rivers*, Part 2 (ed. E. T. Degens, S. Kempe, and H. Soliman), 331-342.
- Calvert S. E. (1971) Composition and origin of North Atlantic deep sea cherts. *Contrib. Mineral Petrol.* **33**, 273-288.
- Carroll S., Mroczek E., Alai M., and Ebert M. (1998) Amorphous silica precipitation (60 to 120°C): Comparison of laboratory and field rates. *Geochim. Cosmochim. Acta* **62**, 1379-1396.
- Casey H. W., Banfield J. F., Westrich H. R. and McLaughlin L. (1993) What do dissolution experiments tell us about natural weathering? *Chem. Geol.* **105**, 1-15.
- Casey W. H., Westrich H. R., Banfield J. F., Ferruzzi G., and Arnold G. W. (1993) Leaching and reconstruction at the surface of dissolving chain-silicate minerals. *Nature* **366**, 253-256.
- Chamley, H. (1989) *Clay Sedimentology*. 623 pp. Springer.
- Chen C.-T., A. and Marshall W. L. (1982) Amorphous silica solubilities- IV. Behaviour in pure water and aqueous sodium chloride, sodium sulfate, magnesium chloride, and magnesium sulfate solutions up to 350 °C. *Geochim. Cosmochim. Acta* **46**, 279-287.
- Chester R. and Elderfield H. (1968) The infrared determination of opal in siliceous deep-sea sediments. *Geochim. Cosmochim. Acta* **32**, 1128-1140.
- Chisholm-Brause C. J., O'Day P. A., Brown G. E., and Parks G. A. (1990) Evidence for multinuclear metal-ion complexes at solid/water interfaces by X-ray absorption spectroscopy. *Nature* **348**, 4147-4156.
- Chou L. and Wollast R. (1984) Study of the weathering of albite at room temperature and pressure with a fluidized bed reactor. *Geochim. Cosmochim. Acta* **48**, 2205-2217.
- Chou L. and Wollast R. (1985) Steady-state kinetics and dissolution mechanisms of albite. *Am. J. Sci.* **285**, 963-993.
- Christ C. L., Hostezler, P. B., Siebert, R. M. (1973) Studies in the system MgO-SiO₂-CO₂-H₂O (III): The activity-product constant of sepiolite. *Am. J. Sci.* **273**, 65-83.
- Conley D. J. (1998) An interlaboratory comparison for the measurement of biogenic silica in sediments. *Mar. Chem.* **63**, 39-48.

References

- Dahmke A. (1988) Lösungskinetik von feldspat-reichen Gesteinen und deren Bezug zu Verwitterung und Porenwasser-Chemie natürlicher Sander-Sedimente. *Reports Geol.-Paläontol. Inst. Univ. Kiel*. **20**, 168 pp.
- DeMaster D. J. (1981) The supply and accumulation of silica in the marine environment. *Geochim. Cosmochim. Acta* **45**, 1715-1732.
- DeMaster D. J. (1991) Measuring biogenic silica in marine sediments and suspended matter. In *Marine particles: analysis and characterization* (eds. D. C. Hurd and D. W. Spencer). *Geophysical Monograph* 63, American Geophysical Union, pp. 363-367.
- DeMaster D. J., Smith W. O. J., Nelson D. M., and Aller J. Y. (1996) Biogeochemical processes in Amazon shelf waters: Chemical distributions and uptake rates of silicon, carbon and nitrogen. *Cont. Shelf Res.* **16**, 617-643.
- Dickson A. G. (1993) The measurement of sea water pH. *Mar. Chem.* **44**, 131-142.
- DIN (1975) Bestimmung der spezifischen Oberfläche von Feststoffen durch Stickstoff-adsorption, 152-156.
- Dixit S. and Van Cappellen P. (1998) Interactions between biogenic silica and aluminum: Implications for the oceanic silica cycle. *EOS Transactions, Am. Geophys. Union, 1998 Fall Meeting* **79 (45)**, 447.
- Dove P. M. (1995) Kinetic and thermodynamic controls on silica reactivity in weathering environments. *Reviews in Mineralogy* **31**, 235-290.
- Dove P. M. and Crerar D. A. (1990) Kinetics of quartz dissolution in electrolyte solutions using a hydrothermal mixed flow reactor. *Geochim. Cosmochim. Acta* **54**, 955-969.
- Dove P. M. and Elston S. F. (1992) Dissolution kinetics of quartz in sodium chloride solutions: Analysis of existing data and a rate model for 25° C. *Geochim. Cosmochim. Acta* **56**, 4147-4156.
- Dove P. M., Krishnan V., and Murovitz J. R. (1994) Controls on the surface reactivity of silica: The effect of aluminum on the kinetics of quartz dissolution. *Geol. Soc. Am. Abstr.* **26**, A-110.
- Dove P. M. and Rimstidt J. D. (1994) Silica-water interaction. In *Silica. Physical behavior, geochemistry and materials applications.*, Vol. 29 (eds. P. J. Heaney, C. T. Prewitt, and G. V. Gibbs), pp. 259-308.
- Drever J. I. (1997) *The geochemistry of natural waters. Surface and groundwater environments*. Prentice-Hall, Inc. Simon & Schuster / A Viacom Company.
- Dugger D. L., Stanton, J. H., Irby, B. N., McConnell, B. L., Cummings, W. W., Maatman, R. W. (1964) The exchange of twenty metal ions with the weakly acidic silanol group of silica gel. *J. Phys. Chem.* **68**, 656-760.
- Eggimann D. W., Manheim F. T., and Betzer P. R. (1980) Dissolution and analysis of amorphous silica in marine sediments. *J. Sediment. Petrol.* **50**, 215-225.
- Eisma D. and van der Gaast S. J. (1971) Determination of opal in marine sediments by X-ray diffraction. *Neth. J. Sea Res.* **5**, 382-389.
- Emerson S., Jahnke R., and Heggie D. (1984) Sediment-water exchange in shallow water estuarine sediments. *J. Mar. Res.* **42**, 709-730.

- Erez J., Takahashi K., and Honjo S. (1982) *In situ* dissolution experiment of Radiolaria in the central North Pacific Ocean. *Earth and Planetary Science Letters* **59**, 245-254.
- Ewald W. (1995) *Die Zugänglichkeit von Schichtzwischenräumen bei der Gasadsorption*. Dissertation, Christian-Albrechts-Universität zu Kiel.
- Falkowski P. G., Barber R. T., and Smetacek V. (1998) Biogeochemical controls and feedbacks on ocean primary production. *Science* **281**, 200-206.
- Fanning K. A. and Pilson M. E. Q. (1971) Interstitial silica and pH in marine sediments: Some effects of sampling procedures. *Science* **173**, 1228-1231.
- Fleming B. A. (1986) Kinetics of reaction between silicic acid and amorphous silica surfaces in NaCl solutions. *Journal of Colloid and Interface Science* **110**, 40-64.
- Fowler S. W. and Small L. F. (1972) Sinking rates of euphausiid fecal pellets. *Limnol. Oceanogr.* **27**, 293-296.
- Fritz B., Zins-Pawlas M.-P., and Gueddari M. (1987) Geochemistry of silica rich brines from lake Natron (Tanzania). *Sci. Geol. Bull.* **40**, 97-110.
- Garrels R. M. and Christ C. L. (1965) *Solutions, minerals and equilibria*. Freeman.
- Gehlen M., van Raaphorst W., and Wollast R. (1993) Kinetics of silica sorption on North Sea sediments. *Chem. Geol.* **107**, 359-361.
- Gifford R. O. and Frugoli D. M. (1964) Silica source in soil solutions. *Science* **145**, 386-388.
- Glud R. N., Gundersen J. K., Jørgensen B. B., Revsbech N. P., and Schulz H.-D. (1994) Diffusive and total oxygen uptake of deep-sea sediments in the eastern South Atlantic Ocean: *in situ* and laboratory measurements. *Deep-Sea Res.* **41**, 1767-1788.
- Govindaraju, K. (1994) Compilation of working values and sample descriptions for 383 geostandards. *Geostandards Newsletter (Spec. Issue)* **18**, 1-158.
- Grasshoff K., Ehrhardt M., and Kremling K. (1983) *Methods of Seawater Analysis*. Verlag Chemie.
- Haake B., Ittekkot V., Rixen T., Ramaswamy V., Nair R. R., and Curry W. B. (1993) Seasonality and interannual variability of particle fluxes to the deep Arabian Sea. *Deep-Sea Res.* **40**, 1323-1344.
- Haeckel M., König I., Riech V., Weber M., and Suess E. (submitted) Pore water profiles and numerical modelling of Peru Basin deep-sea sediments. *Deep-Sea Res.*
- Hathaway B. J. and Lewis C. E. (1969) Electronic properties of transition-metal complex ions adsorbed on silica gel. II. Cobalt (II) and cobalt (III). *J. Chem. Soc. (A)*, 1183-1188.
- Haul R. and Dümbgen G. (1960) Vereinfachte Methode zur Messung von Oberflächengrößen durch Gasadsorption. *Chem.-Ing.-Techn.* **32**, 349-354.
- Haul R. and Dümbgen G. (1963) Vereinfachte Methode zur Messung von Oberflächengrößen durch Gasadsorption. 2. *Mitteilung Chem.-Ing.-Techn.* **35**, 586-589.

References

- Hensen C., Landenberger H., Zabel M., and Schulz H. D. (1998) Quantification of diffusive benthic fluxes of nitrate, phosphate, and silicate in the southern Atlantic Ocean. *Global Biogeochem. Cycles* **12**(3), 193-210.
- Hesse R. (1988) Diagenesis #13. Origin of chert: Diagenesis of biogenic siliceous sediments. *Geoscience Canada* **15**, 171-192.
- Hurd D. C. (1972) Factors affecting solution rate of biogenic opal in seawater. *Earth and Planetary Science Letters* **15**, 411-417.
- Hurd D. C. (1973) Interactions of biogenic opal, sediment and seawater in the Central Equatorial Pacific. *Geochim. Cosmochim. Acta* **37**, 2257-2282.
- Hurd D. C., Pankratz H. S., Asper V., Fugate J., and Morrow H. (1981) Changes in the physical and chemical properties of biogenic silica from the Central Equatorial Pacific: Pt. III, Specific pore volume, mean ore size, and skeletal ultrastructure of acid-cleaned samples. *Am. J. Sci.* **281**, 833-895.
- Hurd D. C. and Birdwhistell S. (1983) On producing a more general model for biogenic silica dissolution. *Am. J. Sci.* **283**, 1-28.
- Hutchins, D. A. and Bruland K.W. (1998) Iron-limited diatom growth and Si:N uptake ratios in a coastal upwelling regime. *Nature* **393**, 561-564.
- Hydes D. J. and Liss, P.S. (1976) Fluorimetric method for the determination of low concentrations of dissolved aluminium in natural waters. *Analyst* **101**, 922-931.
- Iler R. K. (1973) Effect of adsorbed Alumina on the solubility of amorphous silica in water. *Journal of Colloid and Interface Science* **43**, 399-408.
- Iler R. K. (1979) *The Chemistry of Silica*. Wiley and Sons.
- Jahnke R. A., Emerson S. R., Cochran J. K., and Hirschberg D. J. (1986) Fine scale distributions of porosity and particulate excess ^{210}Pb , organic carbon and CaCO_3 in surface sediments of the deep equatorial Pacific. *Earth and Planetary Science Letters* **77**, 59-69.
- Juillet-Leclerc A. (1984) Cleaning process for diatomaceous samples. *8th Diatom-Symposium*, 733-736.
- Kamatani A. (1969) Regeneration of inorganic nutrients from diatom decomposition. *J. Oceanogr. Soc. Japan* **25**, 63-74.
- Kamatani A. (1982) Dissolution rates of silica from diatoms decomposing at various temperatures. *Marine Biol.* **68**, 91-96.
- Kamatani A. and Riley J. P. (1979) Rates of dissolution of diatom silica walls in seawater. *Marine Biol.* **55**, 29-35.
- Kamatani A., Ehri N., and Tréguer P. (1988) The dissolution kinetics of diatom ooze from the Antarctic area. *Deep-Sea Res.* **35**, 1195-1203.
- Kastner M., Keene J. B., and Gieskes J. M. (1977) Diagenesis of siliceous oozes, I. Chemical controls on the rate of opal-A to opal-CT transformation-an experimental study. *Geochim. Cosmochim. Acta* **41**, 1041-1059.
- Keir R. S. (1980) The dissolution kinetics of biogenic calcium carbonates in seawater. *Geochim. Cosmochim. Acta* **44**, 241-252.
- Keller W. D. (1970) Environmental aspects of clay minerals. *J. Sediment. Petrol.* **40**, 788-854.

- Kent D. B. and Kastner M. (1985) Mg^{2+} removal in the system Mg^{2+} -amorphous SiO_2 - H_2O by adsorption and Mg-hydroxysilicate precipitation. *Geochim. Cosmochim. Acta* **49**, 1123-1136.
- Kohly A. (1998) Diatom flux and species composition in the Greenland Sea and the Norwegian Sea in 1991-1992. *Mar. Geology* **145**, 293-312.
- Kolla V., Henderson L., and Biscaye P. E. (1976) Clay mineralogy and sedimentation in the western Indian Ocean. *Deep-Sea Res.* **23**, 949-961.
- Koning E., Brummer G.-J., Van Raaphorst W., Van Bennekom J., Helder W., and Van Ipperen J. (1997) Settling, dissolution and burial of biogenic silica in the sediments of Somalia (northwestern Indian Ocean). *Deep-Sea Res.* **II 44**, 1341-1360.
- Lampitt R. S., Noji T., and von Bodungen B. (1990) What happens to zooplankton fecal pellets ? Implications for material flux. *Mar. Biol.* **104**, 15-23.
- Landén A., Holby O., and Hall P. O. (1996) Determination of biogenic silica in marine sediments - selection of pretreatment method and effect of sample size. *Vatten* **52**, 85-92.
- Lasaga A. C. (1981a) Rate laws of chemical reactions. In *Kinetics of geochemical processes*, **8** (ed. A. C. Lasaga, Kirkpatrick, R. J.), 1-169. Mineral. Soc. Am.
- Lasaga A. C. (1981b) Transition state theory. In *Kinetics of geochemical processes* **8** (ed. A. C. Lasaga, Kirkpatrick, R. J.), 135-169. Mineral. Soc. Am.
- Lasaga A. C. (1984) Chemical kinetics of water-rock interactions. *J. Geophys. Res.* **89** (B6), 4009-4025.
- Lasaga A. C., and Gibbs, G. V. (1990) Ab-initio quantum mechanical calculations of water- rock interactions: adsorption and hydrolysis reactions. *Am. J. Sci.* **290**, 263-295.
- Lasaga A. C., Soler J. M., Ganor J., Burch T. E., and Nagy K. L. (1994) Chemical weathering rate laws and global geochemical cycles. *Geochim. Cosmochim. Acta* **58** (10), 2361-2386.
- Lasaga, A. C. (1995) Fundamental approaches in describing mineral dissolution and precipitation rates. *Reviews in Mineralogy* **31**, 23-86.
- Lawson D. S., Hurd D. C., and Pankratz H. S. (1978) Silica dissolution rates of decomposing phytoplankton assemblages at various temperatures. *Am. J. Sci.* **278**, 1373-1393.
- Leinen M. (1977) A normative calculation technique for determining opal in deep-sea sediments. *Geochim. Cosmochim. Acta* **41**, 671-676.
- Leinen M. (1985) Techniques for determining opal in deep-sea sediments: a comparison of radiolarian counts and X-ray diffraction data. *Marine Micropaleontol.* **9**, 375-383.
- Lerman, A. (1979) *Geochemical Processes - Water and Sediment Environments*. 481 pp. Wiley.
- Lewin J. C. (1961) The dissolution of silica from diatom walls. *Geochim. Cosmochim. Acta* **21**, 182-198.
- Lisitzin A. P. (1985) The silica cycle during the last ice age. *Palaeogeogr., Palaeoclim., Palaeoecol.* **50**, 241-270.

References

- Li Y.-H. and Gregory S. (1974) Diffusion of ions in sea water and in deep-sea sediment. *Geochim. Cosmochim. Acta* **38**, 703-714.
- Luce R. W., Bartlette R. W., and Parks G. A. (1972) Dissolution kinetics of magnesium silicates. *Geochim. Cosmochim. Acta* **36**, 35-50.
- Mackenzie F. T. and Garrels R. M. (1965) Silicates: Reactivity with sea water. *Science* **150**, 57-58.
- Mackenzie F. T. and Garrels R. M. (1966) Chemical mass balance between rivers and oceans. *Am. J. Sci.* **261**, 507-521.
- Mackenzie F. T., Garrels R. M., Bricker O. P., and Bickley F. (1967) Silica in sea water: Control by silica minerals. *Science* **155**, 1404-1405.
- Mackin J. E. (1987) Boron and silica behaviour in salt-marsh sediments: Implications for paleo-boron distributions and the early diagenesis of silica. *Am. J. Sci.* **287**, 197-241.
- Mackin J. E. (1989) Relationships between Si, Al, and Fe deposited on filter-covered glass substrates in marine sediments and in suspensions of sediments and standard clays. *Marine Chem.* **26**, 101-117.
- Mackin J. E. and Aller R. C. (1983) The infinite dilution diffusion coefficient for $\text{Al}(\text{OH})_4^-$ at 25°C. *Geochim. Cosmochim. Acta* **47**, 959-961.
- Mackin J. E. and Aller R. C. (1984) Dissolved Al in sediments and waters of the East China Sea: Implications for authigenic mineral formation. *Geochim. Cosmochim. Acta* **48**, 281-297.
- Mackin J. E. and Aller R. C. (1986) The effects of clay mineral reactions on dissolved Al distributions in sediment and waters of the Amazon continental shelf. *Continental Shelf Research* **6(12)**, 245-262.
- Mackin J. E. and Swider K. T. (1987) Modelling the dissolution behaviour of standard clays in seawater. *Geochim. Cosmochim. Acta* **51**, 2947-2964.
- Mackin J. E. (1989) Relationships between Si, Al, and Fe deposited on filter-covered glass substrates in marine sediments and in suspensions of sediments and standard clays. *Marine Chemistry* **26**, 101-117.
- Marshall W. L. (1980) Amorphous silica solubilities. 1. Behaviour in aqueous sodium nitrate solutions. *Geochim. Cosmochim. Acta* **44**, 907-913.
- Marshall W. L. and Warakowski J. M. (1980) Amorphous silica solubilities. 2. Effect of aqueous salt solutions at 25°C. *Geochim. Cosmochim. Acta* **44**, 915-924.
- Martin W. R., Bender M., Leinen M., and Orchardo J. (1991) Benthic organic carbon degradation and biogenic silica dissolution in the central equatorial Pacific. *Deep-Sea Res.* **38**, 1481-1516.
- Mathias J. and Wannemacher G. (1988) Basic characteristics and applications of Aerosil 30. The chemistry and physics of the Aerosil surface. *Journal of Colloid and Interface Science* **125**, 61-68.
- McKeague J. A. and Cline M. G. (1963) Silica in soil solution. *Can. J. Soil Sci.* **43**, 70-96.
- McManus J., Hammond D. E., Berelson W. M., Kilgore T. E., Demaster D. J., Ragueneau O. G., and Collier R. W. (1995) Early diagenesis of biogenic opal:

- Dissolution rates, kinetics, and paleoceanographic implications. *Deep-Sea Res.* **42**, 871-903.
- Measures C. I. and Edmond J. M. (1990) Aluminum in the South Atlantic: Steady state distribution of a short residence-time element. *J. Geophys. Res.* **95**, 5331-5340.
- MEDRIFFF-Consortium (1995) Three brine lakes discovered in the seafloor of the eastern Mediterranean. *EOS* **76** (33), 313.
- Michalopoulos P. and Aller R. C. (1995) Rapid Clay Mineral Formation in Amazon Delta Sediments: Reverse Weathering and Oceanic Elemental Cycles. *Science* **270**, 614-617.
- Mikkelsen N. (1979) Diatoms of equatorial deep-sea sediments: Sedimentation and dissolution over the last 20,000 years. *Nova Hedwiga* **64**, 489-502.
- Moran S. B., Moore R. M., and Westerlund S. (1992) Dissolved aluminium in the Weddell Sea. *Deep-Sea Res.* **39**, 537-547.
- Morgenstein M. (1967) Authigenic cementation of scoriaceous deep-sea sediments west of the Society Ridge. *Sedimentology* **9**, 105-118.
- Morse J. W. (1983) The kinetics of calcium carbonate dissolution and precipitation. In *Carbonates: Mineralogy and Chemistry* (ed. R. J. Reeder), *Mineral. Soc. Am., Rev. Mineral.* **11**, 227-264.
- Mortlock R. A. and Froelich P. N. (1989) A simple method for the rapid determination of biogenic opal in pelagic marine sediment. *Deep-Sea Res.* **36**, 1415-1426.
- Müller G. (1967) Methods in sedimentary petrology. In *Sedimentary Petrology*, Part 3. W. von Engelhardt & G. Müller Schweizbart'sche Verlagsbuchhandlung.
- Müller P. J. and Schneider R. (1993) An automated leaching method for the determination of opal in sediments and particulate matter. *Deep-Sea Res.* **40**, 425-444.
- Nagy K. L., Steefel C. I., Blum A. E. and Lasaga A. C. (1990) Dissolution and precipitation kinetics of kaolinite: Initial results at 80°C with application to porosity evolution in a sandstone. In *Prediction of Reservoir Quality through Chemical Modeling* (eds. I. D. Meshir and P. J. Ortoleva), *Am. Soc. Geol. Mem.* **49**, pp. 85-101.
- Nagy K. L., Blum A. E. and Lasaga A. C. (1991) Dissolution and precipitation kinetics of kaolinite at 80°C and pH 3. The dependence on solution saturation state. *Am J. Sci.* **291**, 649-686.
- Nagy K. L. and Lasaga A. C. (1992) Dissolution and precipitation kinetics of gibbsite at 80°C and pH 3: The dependence on solution saturation state. *Geochim. Cosmochim. Acta* **56**, 3093-3111.
- Nair R. R., Ittekkot V., Manganini S. J., Ramaswamy E. T., Haake B., Degens E. T., Desai B. N., and Honjo S. (1989) Increased particle flux to the deep ocean related to monsoons. *Nature* **338**, 749-751.
- Nelson D. M., Tréguer P., Brzezinski M. A., Leynaert A., and Quéguiner B. (1995) Production and dissolution of biogenic silica in the ocean: Revised global estimates, comparison with regional data and relationship to biogenic sedimentation. *Global Biogeochem. Cycle* **9**, 359-372.

References

- Newton P. P. and Boyd P. W. (1998) Does planktonic community structure determine downward particulate organic carbon flux in different oceanic provinces ? *EOS transactions, American Geophysical Union* **79**(1), 95.
- O'Connor T. L. and Greenberg S. A. (1958) The kinetics for the solution of silica in aqueous solution. *J. Phys. Chem.* **62**, 1195-1198.
- Oelkers E. H. and Schott J. (1995) Experimental study of anorthite dissolution and the relative mechanism of feldspar hydrolysis. *Geochim. Cosmochim. Acta* **59**, 5039-5053.
- Okamoto G., Okura T. and Goto K. (1957) Properties of silica in water. *Geochim. Cosmochim. Acta*, **12**, 123-132.
- Olafsson J. (1983) Mercury concentrations in the North Atlantic in relation to cadmium, aluminium and oceanographic parameters. In *Trace metals in sea water* (eds. C. S. Wong, E. Boyle, K. W. Bruland, J. D. Burton and E. D. Goldberg), *NATO Conference Series*, Plenum, 475-485.
- Orians K. J. and Bruland K. W. (1986) The biogeochemistry of aluminum in the Pacific Ocean. *Earth Planet. Sci. Lett.* **78**, 397-410.
- Pacés T. (1983) Rate constants of dissolution derived from measurements of mass balance in hydrological catchments. *Geochim. Cosmochim. Acta* **47**, 1855- 1863.
- Pakulski, J. D. (1996) *Nature* **383**, 133-134.
- Pichon J. J., Bareille G., Labracherie M., Labeyrie L. D., Baudrimont A., and Turon J. L. (1992) Quantification of the biogenic silica dissolution in Southern Ocean sediments. *Quaternary Research* **37**, 361-378.
- Press R. and Siever R. (1986) *Earth*. W.H. Freeman and Company.
- Rabouille C. and Gaillard J. F. (1990) The validity of steady-state flux calculations in early diagenesis: a computer simulation of deep-sea silica diagenesis. *Deep-Sea Res.* **37**, 625-646.
- Rabouille C., Gaillard J.-F., Tréguer P., and Vincendeau M.-A. (1997) Biogenic silica recycling in surficial sediments across the Polar Front of the Southern Ocean (Indian Sector). *Deep-Sea Res. II* **44**, 1151-1176.
- Ragueneau O., DeMaster D. J. and McManus J. (1996) Controls on biogenic opal preservation in sediments: from Equatorial Pacific data to global relationships. In *OPALEO: On the use of opal as a paleoproductivity proxy*. Minutes of the workshop, Brest, France, pp. 62-67.
- Ragueneau O., Tréguer P., Anderson R. F., Brzezinski M. A., DeMaster D. J., Dugdale R. C., Dymond J., Fischer G., Francois R., Heinze C., Leynaert A., Maier-Reimer E., Martin-Jézéquel V., Nelson D. M., and Quéguiner B. (submitted) Understanding the Si cycle in the modern ocean: a pre-requisite for the use of biogenic opal as a paleoproductivity proxy. *Global and Planetary Change*.
- Ragueneau O., Gallinari M., Stahl H., Tengberg A., Grandel S., Lampitt R., Witbaard R., Hall, P., Rickert D. and Hauvespre A. (submitted) The benthic silica cycle in the northeast Atlantic : seasonality, annual mass balance and preservation mechanisms. *Progress in oceanography*.

- Reimers C. E., Jahnke R. A., and McCorkle D. C. (1992) Carbon fluxes and burial rates over the continental slope and rise off Central California with implications for the global carbon cycle. *Global Biogeochem. Cycles* **6**, 199-224.
- Riedel W. R. and Aberdeen E. (1957) In: *Treatise on Marine Ecology and Paleoecology* (ed. J. W. Hedgepeth), *Mem. Geol. Soc. Amer.* **67**, pp. 1067-1072.
- Rimstidt J. D. and Barnes H. L. (1980) The kinetics of silica-water reactions. *Geochim. Cosmochim. Acta* **44**, 1683-1699.
- Sackett W. and G. Arrhenius (1962) Distribution of aluminum species in the hydrosphere - I Aluminum in the ocean. *Geochim. Cosmochim. Acta* **26**, 955-968.
- Savrda C. E. and Bottjer D. D. (1987) The exaerobic zone, a new oxygen-deficient marine biofacies. *Nature* **327**, 54-56.
- Sayles F. L., Deuser W. G., Goudreau J. E., Dickinson W. H., Jickells T. D., and King P. (1996) The benthic cycle of biogenic opal at the Bermuda Atlantic Time Series site. *Deep-Sea Res.* **42**, 383-409.
- Scasso R. A., Corbell H., and Tiberi T. (1994) Sedimentological analysis of the tephra from the 12-15 August 1991 eruption of Hudson volcano. *Bull. Volcanol.* **56**, 121-133.
- Schink D. R., Fanning K. A., and Piety J. (1974) Dissolved silica in the upper pore waters of the Atlantic Ocean floor. *J. Geophys. Res.* **15**, 2243-2250.
- Schink D. R., N. L. Guinasso J., and Fanning K. A. (1975) Processes Affecting the Concentration of Silica at the Sediment-Water Interface of the Atlantic Ocean. *J. Geophys. Res.* **80** (21), 3013-3031.
- Schink D. R. and Guinasso Jr. N. L. (1980) Processes affecting silica at the abyssal sediment-water interface. *Biogéochimie de la Matière Organique à l'Interface Eau-Sédiment Marin, Colloq. Int. du CNRS* 293, 81-92.
- Schlüter M. (1990) Zur Frühdiagenese von organischem Kohlenstoff und Opal in Sedimenten des südlichen und östlichen Weddellmeeres. Geochemische Analyse und Modellierung. Alfred-Wegener-Institut für Polar- und Meeresforschung.
- Schlüter M. and Rickert D. (1998) Effect of pH on the measurement of biogenic silica. *Mar. Chem.* **63**, 81-92.
- Schlüter M., Rutgers van der Loeff M., Holby O. and Kuhn G. (1998) Silica cycle in surface sediments of the South Atlantic. *Deep-Sea Res. I* **45**, 1085-1109.
- Schlüter M., Sauter E. J., Schulz-Bull D., Balzer W. and Suess E. (submitted) Organic carbon and biogenic silica cycle of surface sediments: A comparison of high northern and southern latitudes of the Atlantic Ocean. In *North Atlantic: A Changing Environment* (eds. Schäfer, P., Ritzrau, W., Schlüter, M. & Thiede, J.). Springer.
- Schlüter, M. and Sauter E. (submitted) Biogenic silica cycle in surface sediments of the Greenland Sea. *J. Mar. Systems*.
- Schmidt M., Botz R., Stoffers P., Anders T. and Bohrmann G. (1997) Oxygen isotopes in marine diatoms: A comparative study of analytical techniques and new results on the isotope composition of recent marine diatoms. *Geochim. Cosmochim. Acta* **61** (11), 2275-2280.

References

- Shemesh A., Burckle L. H., and Froelich P. N. (1989) Dissolution and preservation of Antarctic diatoms and the effect on sediment Thanatocenoses. *Quat. Res.* **31**, 288-308.
- Shemesh A., Burckle L. H., and Hays J. D. (1995) Late pleistocene oxygen isotope records of biogenic silica from the Atlantic sector of the Southern Ocean. *Paleoceanography* **10**, 179-196.
- Siever R. and Woodford N. (1973) Sorption of silica by clay minerals. *Geochim. Cosmochim. Acta* **37**, 1851-1880.
- Sillén L. G. (1967) The ocean as a chemical system. *Science* **156**, 1189-1197.
- Sirocko F. (1989) Zur Akkumulation von Staubsedimenten im nördlichen Indischen Ozean; Anzeiger der Klimageschichte Arabiens und Indiens. *Reports Geol.-Paläontol. Inst. Univ. Kiel.* **27**, 185 pp.
- Sirocko, F. and Sarnthein M. (1989) Wind-borne deposits in the Northwestern Indian Ocean: record of Holocene sediments versus modern satellite data. In *Paleoclimatology and paleometeorology: moderns and past patterns global atmospheric transport* (eds. M. Leinen and M. Sarnthein). *NATO ASI Series C* **282**, 401-433.
- Smetacek V. S. (1985) Role of sinking in diatom life-history cycles: Ecological, evolutionary, and geological significance. *Mar. Biol. Berlin* **84**, 239-251.
- Smetacek V. (1999) Bacteria and silica cycling. *Nature* **397**, 475-476.
- Smith C. R., Pope R. H., Demaster D. J., and Magaard L. (1993) Age-dependent mixing of deep-sea sediments. *Geochim. Cosmochim. Acta* **57**, 1473-1488.
- Smith K. L. (1992) Benthic boundary layer communities and carbon cycling at abyssal depths in the central North Pacific. *Limnol. Oceanogr.* **37**(5), 1034-1056.
- Stoffyn-Egli P. (1982) Dissolved aluminium in interstitial waters of recent terrigenous marine sediments from the North Atlantic Ocean. *Geochim. Cosmochim. Acta* **46**, 1345-1352.
- Stumm W. and Morgan J. J. (1981) *Aquatic Chemistry*. Wiley – Interscience.
- Stumm W. and Wieland, E. (1990) Dissolution of oxide and silicate minerals: Rates depend on surface speciation. In *Aquatic chemical kinetics* (ed. W. Stumm), pp. 367-400. John Wiley & Sons.
- Takeda, S. (1998) Influence of iron availability on nutrient consumption ratio of diatoms on oceanic waters. *Nature* **393**, 774-777.
- Tréguer P., Nelson D. M., Van Bennekom A. J., DeMaster D. J., Leynaert A., and Quéguiner B. (1995) The silica balance in the world ocean: A reestimate. *Science* **268** (21), 375-379.
- Tsunogai S., Shinichiso N., Harada K., and Kurosaki T. (1986) Large but variable particulate flux in the Antarctic Ocean and its significance for the chemistry of Antarctic water. *J. Oceanol. Soc. Jap.* **42**, 83-90.
- Turner J. T. and Ferrante J. G. (1979) Zooplankton fecal pellets in aquatic systems. *BioScience* **29**, 670-677.
- Ullman W. J. and Aller R. C. (1982) Diffusion coefficients in near-shore sediments. *Limnol. Oceanogr.* **27**, 552- 556.

- Van Bennekom A. J. (1980) On the role of aluminium on the dissolution kinetics of diatom frustules. In *Proceedings* (ed. R. Ross), pp. 445-454. Otto Koeltz Science Publishers.
- Van Bennekom A. J. (1981) The role of aluminium on the dissolution kinetics of diatom frustules. In *Proc. 6th Diatom Symp. 1980* (ed. R. Ross), 445-454. Otto Koeltz Science Publishers.
- Van Bennekom A. J., Berger G. W., van der Gaast S. J., and de Vries R. T. P. (1988) Primary productivity and the silica cycle in the Southern Ocean (Atlantic sector). *Paleoceanography, Paleoclimatology, Paleoecology* **67**, 19-30.
- Van Bennekom A. J., Jansen J. H. F., van der Gaast S. J., van Iperen J. M., and Pieters J. (1989) Aluminium-rich opal: An intermediate in the preservation of biogenic silica in the Zaire (Congo) deep-sea fan. *Deep-Sea Res.* **36**, 173-190.
- Van Bennekom A. J., Buma A. G. J., and Nolting R. F. (1991) Dissolved aluminium in the Wedell-Scotia Confluence and effect of Al on the dissolution kinetics of biogenic silica. *Mar. Chem.* **35**, 423-434.
- Van Beusekom J. E. E. (1991) *Wechselwirkungen zwischen gelöstem Aluminium und Phytoplankton in marinen Gewässern*. Dissertation, University of Hamburg, 164 pp.
- Van Beusekom J. E. E., van Bennekom A. J., Tréguer P., and Motvan J. (1997) Aluminium and silicic acid in water and sediments of the Enderby and Crozet Basins. *Deep-Sea Res. II* **44**, 987-1003.
- Van Cappellen P. (1996) Reactive surface area control of the dissolution kinetics of biogenic silica in deep-sea sediments. *Chem. Geol.* **132**, 125-130.
- Van Cappellen P. and Qiu L. (1997a) Biogenic silica dissolution in sediments of the Southern Ocean. I. Solubility. *Deep-Sea Res.* **44**, 1109-1128.
- Van Cappellen P. and Qiu L. (1997b) Biogenic silica dissolution in sediments of the Southern Ocean. II. Kinetics. *Deep-Sea Res.* **44**, 1129-1149.
- Van Lier J. A., deBruyn P. L., and Overbeek J. T. G. (1960) The solubility of quartz. *J. Phys. Chem.* **64**, 1675-1682.
- Velbel M. A. (1985) Geochemical mass balances and weathering rates in forested watersheds of the southern Blue Ridge. *Am. J. Sci.* **285**, 904-930.
- Von Bodungen B., Antia A., Bauerfeind E., Haupt O., Koeve W., Peeken I., Peinert R., Reitmeier S., Thomsen C., Voss M., Wunsch M., Zeller U., and Zeitschel B. (1995) Pelagic processes and vertical flux of particles: an overview over a long-term comparative study in the Norwegian Sea and Greenland Sea. *Geol. Rdsch.* **84**, 11-27.
- Von Bodungen B., Smetacek V. S., Tilzer M. M., and Zeitschel B. (1986) Primary production and sedimentation during spring in the Antarctic Peninsula Region. *Deep-Sea Res., Part A* **33**, 177-194.
- Wallmann K., Aghib F. S., Castradori D., M. B. Cita, Suess E., Greinert J., and Rickert D. (submitted) Sedimentation and formation of secondary minerals in the hypersaline Discovery Basin, eastern Mediterranean. *Marine Geol.*

References

- Wallmann K., Suess E., Westbrook G. H., Winckler G., Cita M. B. and the MEDRIF consortium (1997) Salty brines on the Mediterranean sea floor. *Nature* **387**, 31-32.
- Wey R. and B. Siffert (1961) Reactions de la silice monomoléculaire en solution avec les ions Al^{3+} et Mg^{2+} . *Coll. Int. C.N.R.S.* **105**, 11-23.
- Willey J. D. (1974) The effect of pressure on the solubility of silica in seawater at 0°C. *Mar. Chem.* **2**, 239-250.
- Willey J. D. (1975a) Silica-alumina interactions in seawater. *Mar. Chem.* **3**, 241-251.
- Willey J. D. (1975b) Reactions which remove dissolved alumina from seawater. *Mar. Chem.* **3**, 227-240.
- Willey J. D. (1980) Effects of aging on silica solubility: a laboratory study. *Geochim. Cosmochim. Acta* **44**, 573-578.
- Willey J. D. and Spivack A. J. (1997) Dissolved silica concentrations and reactions in pore waters from continental slope sediments offshore from Cape Hatteras, North Carolina, USA. *Mar. Chem.* **56**, 227-238.
- Williams L. A. and Crerar D. A. (1985) Silica diagenesis, II. General mechanisms. *J. Sediment. Petrol.* **55**, 312-321.
- Williams L. A., Parks G. A., and Crerar D. A. (1985) Silica diagenesis, I. Solubility controls. *J. Sediment. Petrol.* **55**, 301-311.
- Windom H. L. (1976) Lithogenous material in marine sediments. In *Chemical Oceanography* **5** (ed. J. P. Riley and R. Chester), pp. 105-135. Academic Press.
- Wirth G. S. and Gieskes J. M. (1979) The initial kinetics of the dissolution of vitreous silica in aqueous media. *Journal of Colloid and Interface Science* **68**, 492-500.
- Wollast R. (1967) Kinetics of the alteration of K-feldspar in buffered solutions at low temperature. *Geochim. Cosmochim. Acta* **31**, 635-648.
- Wollast R. (1974) The silica problem. In *The Sea*, Vol. 5 (ed. E. D. Goldberg), 359-392. John Wiley.
- Wollast R. and Garrels R. M. (1971) Diffusion coefficient of silica in sea water. *Nature Phys. Sci.* **229**, 94.
- Wong G. T. F. and Grosch C. E. (1978) A mathematical model for the distribution of dissolved silicon in interstitial waters-an analytical approach. *J. Mar. Res.* **36**, 735-750.
- Zhang J. W. and Nancollas G. H. (1990) Mechanisms of growth and dissolution of sparingly soluble salts. In *Mineral-Water Interface Geochemistry* (eds. M. F. Hochella Jr. and A. F. White), *Reviews in Mineralogy* **23**, 365-396.

APPENDIX

A.1 XRF-Chemical bulk analysis of Na-montmorillonite (purified from Ca-montmorillonite M50 (Milos, Greece)), kaolinite (China Clay; Frantz Company, Bonn: no speciation), and illite (Massif Central, Le Puy) used for opal (PS-2314-1 10-12.5 cm)/clay mixtures in Section 3.1.1.2.3.

Elements	Unit	Na-Montmorillonite	Illite	Kaolinite
SiO ₂	%	60.85	51.04	45.32
Al ₂ O ₃	%	18.10	20.94	38.16
MnO	%	< 0.01	0.05	< 0.01
MgO	%	4.91	4.22	0.24
Na ₂ O	%	4.42	0.20	0.09
CaO	%	0.06	0.75	0.06
TiO ₂	%	0.29	0.74	0.03
P ₂ O ₅	%	0.03	0.12	0.09
K ₂ O	%	0.16	7.96	0.78
Fe ₂ O ₃	%	3.62	7.38	0.58
Ba	ppm	26	278	69
Co	ppm	17	24	12
Cr	ppm	36	< 18	< 18
Ce	ppm	36	< 2	20
La	ppm	< 14	< 14	< 14
Nb	ppm	14	21	17
Ga	ppm	16	41	74
Pb	ppm	30	39	27
Pr	ppm	< 8	< 8	< 8
Rb	ppm	14	600	92
Sr	ppm	9	139	89
Th	ppm	23	8	21
V	ppm	42	81	18
Y	ppm	15	21	29
Zr	ppm	144	48	83
Zn	ppm	55	168	30
H ₂ O	%	7.04	6.96	11.95
CO ₂	%	0.15	0.14	0.08
Σ	%	99.70	100.64	97.44

Appendix

A.2.1 Average composition of Norwegian Sea (Fig. 2.1) sediment (ARK-X/1: M31/2). Note, detrital [wt.%] content is a vertical overall mean value; large uncertainties in brackets assign large compositional variations throughout the core. Here, CaCO₃ varies from ~ 80% at the top and ~ 6% below 4 cm. For detrital contents in Table 2.4, we assume 6% CaCO₃ and 94% detritus below 8 cm. BW bottom water.

depth [cm] ¹	CaCO ₃ [%] ²	C _{org} [%] ²	N _{org} [%] ²	C/N	Opal [%] ³	Detritus [%]	O/D	H ₄ SiO ₄ [μM] ²	φ ²
BW								13	
0.1	77.25	0.61	0.1	6.1		21 ⁴	0.056		0.710
0.3	50	0.54	0.13	4.2		48 ⁴	0.024		0.663
0.5	52.43	0.52	0.2	2.6	1.1	46	0.024	36.6	0.649
0.7	50.85	0.61	0.16	3.8		47 ⁴	0.025		0.641
0.9	43.41	0.57	0.16	3.6		56 ⁴	0.021		0.641
1.1									0.616
1.3									0.628
1.5								52.7	0.611
1.7	46.31	0.56	0.11	5.1	1.3	52	0.025		0.598
1.9	27.92	0.32	0.11	2.9		70 ⁴	0.017		0.591
2.1									0.577
2.3									0.551
2.5								60.6	0.560
2.7									0.556
2.9	19.88	0.41	0.19	2.2	1.2	78	0.015		0.552
3.25	26.55	0.32	0.13	2.5		72 ⁴	0.016		0.544
3.5					1.0			65.9	0.539
3.75	9.75	0.23	0.2	1.2		89	0.012		0.521
4.25	6.06	0.26	0.11	2.4		94 ⁴	0.013		0.520
4.5					1.5			70.6	
4.75	5.87	0.22	0.19	1.2		92	0.016		0.545
5.25	6.12	0.19	0.2	1.0		93 ⁴	0.013		0.542
5.75	5.73	0.16	0.22	0.7		93 ⁴	0.013		0.536
6.25	6.04	0.16	0.12	1.3	1.2	93	0.013	77.5	0.535
6.75	5.88	0.19	0.12	1.6		94 ⁴	0.013		0.526
7.25	6.65	0.12	0.15	0.8	1.1	92	0.012		0.510
7.75	6.03	0.2	0.18	1.1		94 ⁴	0.013		0.504
8.75					1.0				0.508
12.5					1.2			92.6	
17.5					1.0				
22.5					1.0			104.4	
27.5					1.1			107.5	
32.5					1.6			110.1	
Mean ⁵	25(23)	0.3(2)	0.15(4)	2(2)	1.2(2)	73(23)	0.02(1)		0.57(5)

¹Different sampling intervals were taken for porosity and other determinations.

²Data kindly provided by M. Schlüter (SCHLÜTER and SAUTER, submitted).

³Relative precision was generally better than 10%.

⁴Detrital contents were calculated using an overall average content of BSi (1.2 wt.%).

⁵Note, vertical overall mean values are not normalized to 100%. Uncertainties given in brackets display vertical variations.

A.2.2 Average composition of BENGAL (Fig. 2.1) sediments (M36/6: MC#33, 34), mean pore water silicic acid concentrations (M36/6: MC#33, 34, 36), and porosity data (M36/6: MC#33); BW bottom water. Standard deviations are given in brackets.

depth [cm] ¹	CaCO ₃ [%]	C _{org} [%]	N _{org} [%]	C/N	Opal [%] ²	Detritus [%]	O/D	H ₄ SiO ₄ [μM]	φ ³
BW								45(4)	
0.25	66(1)	0.44(7)	0.06(2)	7.3	1.6	32	0.050	60(4)	0.841
0.75	65.6(6)	0.5(2)	0.06(3)	7.9	1.6	32	0.049	89(17)	0.808
1.25									0.797
1.5	66.0(7)	0.4(1)	0.05(2)	7.2	1.4	32	0.042	106(11)	
1.75									0.790
2.25									0.784
2.5	66.36(8)	0.30(5)	0.047(6)	6.3	1.5	32	0.046	140(26)	
2.75									0.780
3.5	65.9(2)	0.27(1)	0.045(8)	5.9	1.5	32	0.048	146(36)	0.771
4.5	66.2(3)	0.24(2)	0.045(7)	5.3	1.4	32	0.044	173(21)	0.748
5.5	66.7(3)	0.22(3)	0.042(5)	5.4	1.4	32	0.043	192(19)	
6.5	66.2(8)	0.22(2)	0.040(1)	5.5	1.4	32	0.044	197(16)	
7									0.746
7.5	63.12	0.20(3)	0.032(4)	6.3	1.4	35	0.040	200(17)	
8.5	63(2)	0.18(2)	0.032(1)	5.6	1.3	35	0.036	207(23)	
9.5	61(2)	0.18(1)	0.031(1)	5.9	1.1	38	0.028	208(34)	0.720
11.5	51(3)	0.16(0)	0.032(4)	5.1	1.1	48	0.022	196(21)	
14.5	44.0(7)	0.15(2)	0.027(3)	5.6	1.0	55	0.018	190(24)	0.716
17.5	41.6(2)	0.15(2)	0.027(3)	5.6	1.0	57	0.017	203(8)	
19.5									0.699
24.5									0.687
29.5									0.725
Mean ⁴	61(9)	0.2(1)	0.04(1)	6.0(8)	1.3(2)	38(9)	0.04(1)		0.75(4)

¹Different sampling intervals were taken.

²Relative precision was generally better than 10%.

³Kindly provided by O. Pfannkuche.

⁴Note, *vertical* overall mean values are not normalized to 100%. Uncertainties given in brackets display vertical variations.

Appendix

A.2.3.1 Average composition of WAST (Fig. 2.1) sediments (SO118: MC#10, 16, 31, 50, 53), mean pore water silicic acid concentrations (SO118: MC#10, 16, 31, 50, 53; SO129: MC#3^{A1}, MC#3-p, MC#36), and porosity data (M31/3: MC#7; M33/1: MC#8, 12; SO118: MC#10, 30); BW bottom water. Standard deviations of mean values are given in brackets.

depth [cm] ¹	CaCO ₃ [%]	C _{org} [%]	N _{org} [%]	C/N	Opal [%] ²	Detritus [%]	O/D	H ₄ SiO ₄ [μM]	Al [nM] ⁴	DOC [rel. units] ⁵	φ ⁶
BW								140(4)	25.2(5)	10.05	
0.25	44(2)	1.5(1)	0.22(4)	6.8	5.6	49	0.115	209(16)	41.0	11.68	0.924(7)
0.5											0.90(1)
0.75	45(6)	1.2(1)	0.20(7)	6.0	4.8	49	0.098	256(23)	30.7	12.85	0.884(1)
1.25											0.874(3)
1.5	43(3)	1.2(1)	0.18(7)	6.7	5.2	50	0.103	292(26)	29.3(1)	12.47	0.861(7)
1.75											0.861(0)
2.25											0.852(4)
2.5	45(3)	1.5(1)	0.2(1)	7.5	4.7	48	0.097	325(23)	30(2)	12.61	0.84(1)
2.75											0.843(6)
3.5	48(1)	1.8(2)	0.21(6)	8.6	4.2	46	0.091	340(26)	30.3	12.44	0.831(8)
4.5	49(2)	2.0(0)	0.25(9)	8.0	4.0	45	0.089	366(24)	27.9(3)	12.00	0.821(9)
5.5	50(2)	2.1(3)	0.27(7)	7.8	3.5	44	0.080	371(22)	31.6	11.59	0.82(1)
6.5	51(2)	2.3(1)	0.25(5)	9.2	3.4	44	0.078	382(25)	29.3(1)	11.42	0.81(2)
7											0.808(0)
7.5	53(2)	2.2(1)	0.30(8)	7.3	3.8	41	0.093	401(26)	28.5	11.46	0.80(2)
8.5	52.1(9)	2.3(1)	0.28(5)	8.2	3.8	42	0.091	417(24)	25.9(3)	11.33	
9.5	52(2)	2.18(9)	0.25(4)	8.7	3.6	42	0.086	432(24)	26.7	11.44	0.80(2)
11					3.4				27.8(9)	11.55	
11.5	53(1)	2.24(7)	0.25(6)	9.0		41 ³	0.085	454(22)			
12.5											0.80(2)
13					3.6				27.8		
14.5	54(2)	2.32(7)	0.25(6)	9.3		40 ³	0.087	480(20)			0.810(3)
15					3.4				25.8(8)	11.56	
15.5											0.80(1)
17					3.3						
17.5	53(2)	2.4(2)	0.28(6)	8.6		41 ³	0.086	498(23)	27.3	11.76	
18.5											0.82(1)
19					3.6						
19.5											0.811(6)
20.5	53(2)	2.40(8)	0.26(4)	9.2		41 ³	0.086	509(27)	22.9	11.76	0.80(1)
21					3.5						
21.5											0.810(8)
23					3.5						
23.5	54.3(2)	2.31(8)	0.27(4)	8.6		40 ³	0.088	525(20)	24.9	11.82	
24.5											0.808(8)
25.0					3.5						
26.5	51(2)	2.3(3)	0.27(7)	8.5		42 ³	0.083	536(16)	26.3	12.38	
27.0					3.4						
29.0					3.6						
29.5	52.5	2.4(1)	0.24(6)	10		41 ³	0.085	546(20)	24.5	12.38	0.81(1)
31					3.4						
32.5	52.6	2.42(9)	0.3(1)	8.1		42 ³	0.072	556(14)			
35.5	52.8	2.39(4)	0.24(5)	10		41 ³	0.085	561(19)			
38.5	54.0	2.2(2)	0.24(5)	9.2		40 ³	0.087	565(1)			
41.5	55.2	2.2	0.21	11		39 ³	0.090	579			
Mean ⁷	51(3)	2.1(4)	0.25(3)	8.4	3.9(6)	43(3)	0.088(7)		28(2)	11.8(6)	0.83(3)

¹Different sampling intervals were taken for porosity and other determinations.

²Relative precision was generally better than 10%.

³Detrital contents were calculated using an average content of BSi (3.5 wt.%) from 9.5-41.5 cm.

⁴Relative precision is usually better than +/- 3nM.

⁵Nat. fluorescence (excitation: λ = 465 nm, emission: λ = 555 nm) of sample [rel. units] ∝ DOC [CADDÉE and LAANE, 1983].

⁶Kindly provided by O. Pfannkuche.

⁷Note, vertical overall mean values are not normalized to 100%. Uncertainties given in brackets display vertical variations.

Appendix

A.2.3.2 Average composition of NAST (Fig. 2.1) sediments (SO118: MC#41, 45), mean pore water silicic acid concentrations (SO129: MC#39-p, 39^{Al}, 42), and porosity data (SO118: MC#43, 44, 45); BW bottom water. Standard deviations of mean values are given in brackets.

depth [cm] ¹	CaCO ₃ [%]	C _{org} [%]	N _{org} [%]	C/N	Opal [%] ²	Detritus [%]	O/D	H ₄ SiO ₄ [μ M]	Al [nM] ³	ϕ ⁴
BW								145(2)		
0.25	46(1)	0.46(3)	0.09	5.1	2.8	51	0.056	184(7)		0.90(2)
0.5										
0.75	47.6(2)	0.45(5)	0.08	5.6	2.8	49	0.056	201(13)		0.824(8)
1.25										0.80(1)
1.5	48	0.42(3)	0.08	5.3	2.5	49	0.051	230(13)		
1.75										0.78(1)
2.25										0.76(2)
2.5	48.9(5)	0.5(1)	0.07	7.1	1.9	49	0.040	251(13)		
2.75										0.73(2)
3.5	49.8(6)	0.31(0)	0.07	4.4	1.7	48	0.035	263(19)		0.73(2)
4.5	50.6(3)	0.30(4)	0.08	3.8	1.6	47	0.034	270(15)		0.724(7)
5.5	52(1)	0.32(1)	0.07	4.6	1.6	46	0.035	274(18)		
6.5	53.3(1)	0.31(3)	0.08	3.9	1.7	45	0.038	282(14)		
7					1.5					0.71(1)
7.5	53	0.414(4)	0.08	5.2	1.5	45	0.032			
8.5	54.0(4)	0.36(2)	0.07	5.1	1.5	44	0.034	384(14)		
9.5	55(1)	0.31(4)	0.06	5.2				287(13)		0.71(3)
11.5	58(1)	0.28(3)	0.07	4.0	1.4	41	0.033	288(13)		
12.5	58(1)									
14.5	62.4(9)	0.24	0.06	4.0	1.3	36	0.037	288(14)		0.70(2)
17.5	63(1)	0.24(5)	0.05	4.8	1.1	36	0.031	278(9)		
19										
19.5										0.69(2)
20.5	55	0.17(2)	0.05	3.4	0.9	44	0.020	270		
21.5										
22.5										
23.5	60.5(5)	0.32(8)	0.05	6.4	1.0	38	0.027	266		
24.5										0.692(8)
26.5	60(3)	0.50(6)	0.06	8.3	0.8	39	0.020	263		
29.5	55.0	0.25	0.06	4.2	0.8	44	0.018			0.68(2)
Mean ⁵	54(5)	0.3(1)	0.07(1)	5(1)	1.6(6)	44(5)	0.04(1)			0.74(6)

¹Different sampling intervals were taken for porosity and the other determinations.

²The relative precision was generally better than 10%.

³Al could not be detected due to contamination of the PW.

⁴Kindly provided by O. Pfannkuche.

⁵Note, *vertical* overall mean values are not normalized to 100%. Uncertainties given in brackets display vertical variations.

Appendix

A. 2.3.3 Average composition of EAST (Fig. 2.1) sediments (M33/1: MC#22, 27, 28; SO129: MC#24^{Al}), mean pore water silicic acid concentrations (SO129: MC#24-p-g; MC#24^{Al}), and porosity data (M33/1: MC#22); BW bottom water. Standard deviations of mean values are given in brackets.

depth [cm] ¹	CaCO ₃ [%]	C _{org} [%]	N _{org} [%]	C/N	Opal [%] ³	Detritus [%]	O/D	H ₄ SiO ₄ [μ M]	Al [nM] ^{5,6}	DOC [rel. units] ⁷	ϕ ⁸
BW								141(3)	17	10.19	
0.25	49(2) ²	0.7(1)	0.087(5)	8.0	2.5	53	0.053	170(6)	38	15.02	
0.5											0.84
0.75	47.0(1) ²	0.6(2)	0.07(2)	8.6	2.3	56	0.047	188(2)	30	12.33	
1.5	47.1(1) ²	0.6(2)	0.068(9)	8.8	2.4	55	0.047	207(6)	23	12.25	0.78
2.5	47.6(0) ²	0.7(3)	0.08(2)	8.8	1.9	55	0.039	232(8)	29	11.27	0.76
3.5	48.4(0) ²	0.7(3)	0.09(4)	7.8	1.9	54	0.039	250(6)	25	11.16	0.76
4.5	48.3(4) ²	0.6(1)	0.068(9)	8.8	2.0	52	0.040	259(7)	28	11.07	0.74
5.5	48.8(4)	0.46(7)	0.080(4)	5.8	1.7	49	0.035	270(5)	23	11.08	0.74
6.5	49.2(3)	0.39(7)	0.07(2)	5.6	1.7	49	0.036	277(5)	26	11.08	0.71
7.5	48.8(8)	0.42(7)	0.06(2)	7.0	1.7	49	0.034	280(1)	23	11.08	0.71
8.5	48(2)	0.42(5)	0.06(1)	7.0	1.7	50	0.034	285(5)	23	11.08	0.69
9.5	49.2(7)	0.38(4)	0.07(2)	5.4	1.3	49	0.027	284(5)	23	11.08	0.68
11	53(5)	0.41(2)	0.06(2)	6.8		45 ⁴	0.031				
11.5					1.2			288(3)	18	11.08	
12.5											0.67
13	56(6)	0.38(3)	0.043(6)	8.8		42 ⁴	0.033				
14.5					1.5			288(2)	17	11.05	
15	56(6)	0.36(4)	0.04(1)	9.0		43 ⁴	0.033				
15.5											
17	59(3)	0.36(4)	0.06(2)	6.0		39 ⁴	0.036				0.70
17.5					1.5			290(4)	20	10.98	
18.5											0.68
19	59(2)	0.35(6)	0.057(2)	6.1		40 ⁴	0.035				
20.5					1.4			291(4)	14	10.98	
21	59(2)	0.36(8)	0.05(2)	7.2		39 ⁴	0.036				
21.5											0.66
23	57(3)	0.40(8)	0.041(1)	9.8		41 ⁴	0.034				
23.5					1.3			296	17	11.00	
25	49(4)	0.3(1)	0.039	7.7		50 ⁴	0.028				0.65
26.5					1.4			296	14	11.00	
27	49	0.29(5)	0.053	5.5		49 ⁴	0.029				
Mean ⁹	51(4)	0.5(1)	0.06(2)	7(1)	1.7(4)	46(4)	0.036(7)				0.72(5)

¹Different sampling intervals were taken during M33/1 in comparison to SO118 and SO129 and for porosity determinations.

²Carbonate data from MC#22 neglected due to significant analytical uncertainties.

³Relative precision was generally better than 10%.

⁴Detrital contents were calculated using an average content of BSi (1.4 wt.%) from 9.5-27 cm.

⁵Al data from MC#24^{Al} (SO129).

⁶Relative precision is usually better than +/- 3nM.

⁷Nat. fluorescence (excitation: $\lambda = 465$ nm, emission: $\lambda = 555$ nm) of sample [rel. units] \propto DOC [CADDÉE and LAANE, 1983].

⁸Kindly provided by O. Pfannkuche; mean porosity values measured on 9 multicorer tubes during SO129 are in markedly good agreement with our porosities measured during M33/1 (considering uncertainties < 5 %).

⁹Note, vertical overall mean values are not normalized to 100%. Uncertainties display vertical variations.

Appendix

A. 2.3.4 Average composition of CAST (Fig. 2.1) sediments (M33/1: MC#17, 18; SO118: MC#35, 40; SO129: MC#29^{Al}), mean pore water silicic acid values (SO129: MC#29^{Al}, MC#30-p,-g, MC#30^{Al}), and porosity data (M33/1: MC#18; SO118: MC#35, 37, 39); BW bottom water. Standard deviations of mean values are given in brackets.

depth [cm] ¹	CaCO ₃ [%]	C _{org} [%]	N _{org} [%]	C/N	Opal [%] ²	Detritus [%]	O/D	H ₄ SiO ₄ [μ M]	Al [nM] ^{4,5}	DOC [rel. units] ⁶	ϕ ⁷
BW								143(2)	31	9.61	
0.25	67(2)	0.47(3)	0.07(2)	6.7	2.7	29	0.090	191(13)	41	12.18	0.86(2)
0.5	68(1)	0.43(7)	0.06(2)	7.2				208(11)	45	11.71	0.80
0.75	68.6(4)	0.34(2)	0.04(2)	8.5	2.4	29	0.082	240(10)	37	10.94	0.791(7)
1.25											0.770(1)
1.5	68.3(6)	0.36(1)	0.04(1)	9.0	2.5	29	0.088	268(13)	36	10.67	0.743
1.75											0.752(7)
2.25											0.74(1)
2.5	68.5(7)	0.35(2)	0.04(1)	8.8	2.7	28	0.095	282(10)	38	10.58	0.722
2.75											0.73(1)
3.5	69(1)	0.35(4)	0.05(1)	7.0	1.6	29	0.057	308(11)	38	10.40	0.725(9)
4.5	69.9(9)	0.37(4)	0.04(1)	9.3	1.8	28	0.066	313(8)	38	10.35	0.732(9)
5.5	70.1(2)	0.34(2)	0.05(1)	6.8	2.1	27	0.077	321(9)	38	10.34	0.695
6.5	71(1)	0.41(6)	0.046(5)	8.9	1.5	27	0.056	321(9)	38	10.34	0.681
7											0.69(1)
7.5	71.2(9)	0.36(5)	0.054(5)	6.7	1.4	27	0.053	325(9)	38	10.34	0.673
8.5	72(1)	0.29(1)	0.050(8)	5.8	1.4	26	0.054	326(8)	41	10.34	0.666
9.5	72.6	0.29	0.04(1)	7.3	1.4	26	0.055				0.668(3)
11.5	75.5	0.27	0.04	6.8	1.1	23	0.049	322(1)	40	10.30	0.663
12.5								321	39	10.25	0.660
13											
14.5	74.5	0.19	0.03	6.3	0.7	25	0.028		40	10.20	0.664(1)
15											
15.5	69.5	0.18	0.03	6.0		30 ³	0.024				
17											
17.5	69.5	0.18	0.03	6.0	0.8	30	0.024	310	39	10.00	
19											
19.5											0.676(2)
20.5	65.2	0.18	0.03	6.0		34 ³	0.021				
21											
21.5	62.2	0.12	0.02	6.0		37 ³	0.019				
22.5					0.7			294	40		
23											
23.5	62.2	0.12	0.02	6.0		37 ³	0.019				0.680
24.5											0.678
25											
27	57.5	0.17	0.02	8.5		42 ³	0.017				
27.5					0.6				42		
29.5	57.5	0.17	0.02	8.5		42 ³	0.017	306			0.659(3)
Mean ⁸	69(4)	0.3(1)	0.04(1)	7(1)	1.6(7)	30(5)	0.05(3)		39(2)	10.5(6)	0.71(4)

¹Different sampling intervals were taken during M33/1 in comparison to SO118 and SO129 and for porosity determinations.

²Relative precision was generally better than 10%.

³Detrital contents were calculated using an average content of BSi (0.7 wt.%) from 14.5-29.5 cm.

⁴Al data from MC#29^{Al} (SO129).

⁵Relative precision is usually better than +/- 3 nM.

⁶Nat. fluorescence (excitation: $\lambda = 465$ nm, emission: $\lambda = 555$ nm) of sample [rel. units] \propto DOC [CADDÉE and LAANE, 1983].

⁷Kindly provided by O. Pfannkuche.

⁸Note, vertical overall mean values are not normalized to 100%. Uncertainties display vertical variations.

Appendix

A.2.3.5 Average composition of SAST (Fig. 2.1) sediments (M33/1: MC#30, 32), mean pore water silicic acid concentrations (SO129: MC#14-p,-g; MC#14^{A1}); porosity data (SO118: MC#19, 22); BW bottom water. Standard deviations of mean values are given in brackets.

depth [cm] ¹	CaCO ₃ [%]	C _{org} [%]	N _{org} [%]	C/N	Opal [%] ²	Detritus [%]	O/D	H ₄ SiO ₄ [μM]	Al ^{4,5} [nM]	DOC [rel. units] ⁶	ϕ ⁷
BW								134(2)	29	10.03	
0.25	41(2)	0.27(4)	0.06(1)	4.5	2.3	56	0.041	161(3)	29	11.95	0.85(1)
0.75	40.4(5)	0.23(2)	0.060(4)	3.8	2.1	57	0.036	176(3)	45	10.60	0.799(4)
1.25											0.783(6)
1.5	41.2(5)	0.21(3)	0.041(3)	5.1	2.2	56	0.039	192(5)	49	10.36	
1.75											0.759(5)
2.25											0.75(1)
2.5	41.9(5)	0.19(1)	0.042(3)	4.5	2.3	56	0.042	207(2)	50	10.37	
2.75											0.74(1)
3.5	42.4(3)	0.22(2)	0.05(2)	4.4	2.2	55	0.040	224(6)	38	10.30	0.717(5)
4.5	43(2)	0.21(3)	0.041(4)	5.1	1.9	55	0.034	235(5)	39	10.30	0.712(4)
5.5	43.5(5)	0.17(1)	0.038(5)	4.5	1.3	55	0.024	243(7)	33	10.30	
6.5	45(1)	0.17(4)	0.05(1)	3.4	1.6	53	0.029	253(4)	27	10.30	
7											0.684(5)
7.5	44.4(6)	0.17(2)	0.040(4)	4.3	1.7	54	0.031	259(7)	28	10.30	
8.5	45(1)	0.15(2)	0.037(4)	4.1	1.8	53	0.034	262(6)	31	10.33	
9.5	45(1)	0.14(3)	0.04(3)	3.5	1.3	53	0.024	264(8)	26	10.27	0.669(4)
11	45.7(9)	0.16(4)	0.033(8)	4.8		53 ³	0.029				
11.5					1.8			264(6)	24	10.28	
13	45(3)	0.10(1)	0.034	2.9		54 ³	0.028				
14.5					1.5			264(10)	23	10.26	0.667(3)
15	44(2)	0.08(2)	0.038(4)	2.1		54 ³	0.028				
17	38(1)	0.08	0.035(8)	2.3		60 ³	0.025				
17.5					1.6			263(12)	23	10.21	0.669(5)
19	38(1)	0.09(1)	0.04(2)	2.3		60 ³	0.025				
19.5											
20.5					1.2			263(19)	25	10.25	
21	35(1)	0.07(1)	0.024(4)	2.9		64 ³	0.023				
23	37(5)	0.09(0)	0.027(5)	3.3		61 ³	0.025				
23.5					1.8			258(18)	20	10.16	
24.5											0.676(4)
25	34(2)	0.10(1)	0.032(1)	3.1		65 ³	0.023				
26.5					1.5			266(13)	23	10.18	
27	33(0)	0.11(1)	0.028(6)	3.9		65 ³	0.023				
29	33(2)	0.09(1)	0.05(4)	1.8		66 ³	0.023				
29.5					1.7			272(0)	24	10.20	0.667(5)
31	33.6	0.08(1)	0.025(1)	3.2		65 ³	0.023				
Mean ⁸	40(5)	0.14(6)	0.04(1)	4(1)	1.8(3)	58(5)	0.029(7)		31(9)	10.4(4)	0.72(6)

¹Different intervals were taken during M33/1 compared to SO118 and SO129 and for porosity determinations.

²Relative precision was generally better than 10%.

³Detrital contents were calculated using an average content of BSi (1.5 ± 0.2 wt.%) from 9.5-31 cm.

⁴Al data from MC#14^{A1} (SO129).

⁵Relative precision is usually better than ± 3nM.

⁶Nat. fluorescence (excitation: λ = 465 nm, emission: λ = 555 nm) of sample [rel. units] ∝ DOC [CADDÉE and LAANE, 1983].

⁷Kindly provided by O. Pfannkuche.

⁸Note, vertical overall mean values are not normalized to 100%. Uncertainties display vertical variations.

A.2.4 Average composition of Juan de Fuca Ridge (Fig. 2.1) sediment (MC-1-3). BW bottom water.

depth [cm] ¹	CaCO ₃ [%]	C _{org} [%]	N _{org} [%] ²	C/N	Opal [%] ³	Detritus [%] ⁴	O/D	H ₄ SiO ₄ [μM]	φ
BW								185	
0.25	0	1.176						255	
0.5									0.905
0.75	0	1.08			9.3	90	0.104	284	0.892
1.5	0	1.01			8.8	90	0.097	312	0.886
2.5	0	0.99			9.3	90	0.104	356	0.869
3.5	0	1.09			9.2	90	0.103	386	0.860
4.5	0	1.21			9.4	89	0.106	402	0.860
5.5	0.68	1.17			9.4	89	0.106	421	0.850
6.5	2.24	1.22			9.4	87	0.109	432	0.850
7.5	3.30	1.10			9.7	86	0.113	447	0.843
8.5	2.23	1.06			9.5	87	0.109	448	0.835
9.5	0.82	1.16			9.7	88	0.110	443	0.836
11.5	0.73	1.04			8.8	89	0.099	444	0.841
12.5									0.832
13.5									0.821
14.5	2.18	0.96			7.1	90	0.080	449	0.815
15.5									0.819
16.5									0.803
17.5	1.98	0.91			6.5	91	0.071	435	0.816
18.5									0.803
19.5									0.803
20.5	1.61	0.93			5.6	92	0.061	414	0.825
21.5									0.820
Mean ⁵	1(1)	1.1(1)			9(1)	89(2)	0.10(2)		0.83(2)

¹Different sampling intervals were taken for porosity determinations.

²Not determined.

³Relative precision was generally better than 10%.

⁴Detrital contents were calculated including organic nitrogen calculated from Redfield ratio (C/N = 8; N ~ 0.1).

⁵Note, *vertical* overall mean values are not normalized to 100%. Uncertainties given in brackets display vertical variations.

Appendix

A.2.5 Average composition of Peru Basin (Fig. 2.1) sediment (SO106: MC-145), pore water silicic acid concentrations (SO106: MC-145), and porosity data (SO106: MC-145,-155). BW bottom water. Uncertainties of mean values are given in brackets.

depth [cm] ¹	CaCO ₃ [%] ²	C _{org} [%] ²	N _{org} [%] ³	C/N	Opal [%] ⁴	Detritus [%] ⁵	O/D	H ₄ SiO ₄ [μ M]	ϕ^2
BW								153	
0.25	6.48	0.75			20(1)	73	0.270	236	0.935(8)
0.75	3.93	0.76			19(1)	76	0.256		0.920(1)
1.5	4.15	0.68			18(1)	77	0.239	315	0.907(9)
2.5	3.43	0.72			18(1)	78	0.233	370	0.908(9)
3.5	5.01	0.67			17(1)	77	0.221	418	0.90(1)
4.5	5.23	0.69			18(1)	76	0.242	440	0.895(7)
5.5	5.23	0.66						478	0.89(1)
6.5	5.32	0.69			16(1)	78	0.206	486	0.89(2)
7.5	5.91	0.80			18(1)	75	0.238	497	0.89(1)
8.25	8.51	0.78						527	
8.5									0.88(3)
8.75	9.36	0.88			15(1)	75	0.199		
9.25	12.43	0.78							
9.5									0.87(2)
9.75	16.34	0.77			16(1)	67	0.240		
10.25	17.62	0.73							
10.75	19.12	0.80							
11									0.87(2)
11.5	19.26	0.96			14(1)	65	0.220	590	
12.5	22.97	1.03							
13									0.84(4)
14	23.74	0.79						590	
15									0.84(3)
16	27.09	0.65			15(1)	57	0.265	572	
17									0.83(1)
18	23.71	1.05						579	
19									0.825(1)
19.5	24.09	1.00						569	
20.5								580	
20.75	24.88	0.97							
21									0.823(6)
21.25	20.07	1.43						557	
22	26.53	0.95							
22.25	26.96	1.14			16(1)	56	0.279	599	
22.75								609	
23	24.22	1.34							0.83(2)
23.25	26.22	1.14						620	
24	25.94	1.12			15(1)	58	0.260	613	0.82(2)
25	28.37	1.02			16(1)	54	0.302		
26	25.51	1.31			21(1)	53	0.391	614	
27	22.68	1.33			17(1)	59	0.295		0.82(2)
28	22.47	1.21			21(1)	55	0.386	591	
29	27.05	1.12						590	0.824(0)
30	26.35	1.38			19(1)	53	0.359	584	
Mean ⁶	17(9)	0.9(2)			18(2)	66(1)	0.27(6)		0.86(4)

¹Different sampling intervals were taken for porosity and other determinations.

²HAECKEL et al. [submitted].

³Not determined.

⁴Relative precision was generally better than 5%.

⁵Detrital contents were calculated including organic nitrogen calculated from Redfield ratio (C/N = 8; N ~ 0.1).

⁶Note, vertical overall mean values are not normalized to 100%. Uncertainties given in brackets display vertical variations.

A.2.6.1 Average composition of Scotia Sea (Fig. 2.1) sediment (ANT-X/5; PS-2283-6). BW bottom water.

depth [cm] ¹	CaCO ₃ [%] ²	C _{org} [%] ²	N _{org} [%] ²	C/N	Opal [%] ³	Detritus [%]	O/D	H ₄ SiO ₄ [μM] ²	φ ²
BW								126	
0.1	0	0.63	0.11	5.7					0.869
0.3	0	0.51	0.07	7.3					0.888
0.5	0	0.47	0.07	6.7	23	76	0.307	450	0.773
0.7	0	0.36	0.05	7.2					0.716
0.9	0	0.40	0.06	6.7					0.709
1.1	0	0.35	0.05	7.0					0.680
1.3	0	0.38	0.05	7.6					0.689
1.5	0	0.41	0.06	6.8	27	72	0.374	611	0.685
1.7	0	1.03	0.20	5.2					0.695
1.9	0	0.38	0.05	7.6					0.685
2.1	0	0.72	0.13	5.5					0.680
2.3	0	0.34	0.05	6.8					0.666
2.5	0	0.37	0.05	7.4	34	66	0.516	703	0.656
2.7	0	0.31	0.05	6.2					0.628
2.9	0	0.32	0.04	8.0					0.617
3.25	0	0.34	0.05	6.8					0.667
3.5					38	62 ⁴	0.610	713	0.683
3.75	0	0.40	0.06	6.7					0.691
4.25	0	0.41	0.05	8.2					
4.5					41	59 ⁴	0.701	742	0.675
4.75	0	0.36	0.05	7.2					0.659
5.25	0	0.28	0.04	7.0					0.660
5.75	0	0.37	0.06	6.2					0.673
6.25	0	0.38	0.05	7.6	44	56	0.792	740	0.694
6.75	0	0.51	0.08	6.4					0.666
7.25	0	0.39	0.05	7.8					0.639
7.75	0	0.31	0.05	6.2					0.639
8.25	0	0.28	0.04	7.0					0.622
8.75	0	0.25	0.04	6.3					
Mean ⁴	0	0.4(2)	0.06(3)	6.9(7)	35(8)	64(7)	0.5(2)		0.68(5)

¹Different sampling intervals were taken for porosity and other determinations.

²SCHLÜTER et al. [1998].

³Relative precision was generally better than 5%.

⁴Values were calculated assuming mean C_{org} = 0.4% and N_{org} = 0.06%.

⁵Note, *vertical* overall mean values are not normalized to 100%. Uncertainties given in brackets display vertical variations.

Appendix

A.2.6.2 Average composition of Scotia Sea (Fig. 2.1) sediment (ANT-X/5; PS-2299). BW bottom water.

depth [cm] ¹	CaCO ₃ [%] ²	C _{org} [%] ²	N _{org} [%] ²	C/N	Opal [%] ³	Detritus [%]	O/D	H ₄ SiO ₄ [μM] ²	φ ²
BW								126	
0.1	0	0.79	0.1	7.9					0.874
0.3	0	0.79	0.08	9.9					0.847
0.5	0	0.79	0.09	8.8	51	48	1.06	480	0.813
0.7	0	0.77	0.09	8.6					0.830
0.9	0	0.78	0.08	9.8					0.820
1.1	0	0.73	0.08	9.1					0.832
1.3	0	0.79	0.09	8.8					0.815
1.5	0	0.75	0.08	9.4	53	46	1.15	675	0.802
1.7	0	0.79	0.09	8.8					0.826
1.9	0	0.81	0.09	9.0					0.794
2.1	0	0.8	0.09	8.9					0.846
2.3	0	0.79	0.09	8.8					0.814
2.5	0	0.81	0.08	10.1	54	45	1.21	733	0.781
2.7	0	0.74	0.07	10.6					0.794
2.9	0	0.74	0.09	8.2					0.777
3.25	0	0.64	0.07	9.1					0.769
3.5					53	47	1.12	756	
3.75	0	0.67	0.07	9.6					0.782
4.25	0	0.68	0.08	8.5					0.768
4.5					52	48	1.08	752	
4.75	0	0.64	0.06	10.7					0.758
5.25	0	0.66	0.07	9.4					0.783
5.75	0	0.64	0.06	10.7					0.755
6.25					53	47 ⁴	1.12	729	
6.75									
7.25									
7.75									
8.25									
8.75					51	49 ⁴	1.04	721	
9.25									
9.75									
11.25					49	50 ⁴	0.97	725	
13.75					50	49 ⁴	1.01	718	
16.25					49	50 ⁴	0.98	702	
18.75					48	51 ⁴	0.93	693	
22.5					48	51 ⁴	0.94	681	
Mean ⁵	0	0.74(6)	0.08(1)	9.3(7)	51(2)	49(2)	1.05(9)		0.80(3)

¹Different sampling intervals were taken for porosity and other determinations.

²SCHLÜTER et al. [1998].

³Relative precision was generally better than 3%.

⁴Values were calculated [%Detritus = 100% - %CaCO₃ - %C_{org} - %N_{org} - %Opal], assuming C = 0.6, N = 0.06.

⁵Note, *vertical* overall mean values are not normalized to 100%. Uncertainties given in brackets display vertical variations.

A.2.6.3 Average composition of Scotia Sea (Fig. 2.1) sediment (ANT-X/5: PS-2312-1). BW bottom water.

depth [cm] ¹	CaCO ₃ [%] ²	C _{org} [%] ²	N _{org} [%] ²	C/N	Opal [%] ³	Detritus [%]	O/D	H ₄ SiO ₄ [μM] ²	φ ²
BW								129	
0.1	0	0.96	0.1	9.6					0.852
0.3	0	1.01	0.11	9.2					0.814
0.5	0	0.95	0.1	9.5	60	39	1.54	682	0.800
0.7	0	0.9	0.1	9.0					0.797
0.9	0	0.9	0.1	9.0					0.804
1.1	0	0.9	0.09	10.0					0.806
1.3	0	0.89	0.09	9.9					0.783
1.5	0	0.91	0.09	10.1	65	34	1.92	787	0.801
1.7	0	0.95	0.1	9.5					0.799
1.9	0	0.9	0.1	9.0					0.757
2.1	0	0.92	0.1	9.2					0.779
2.3	0	0.88	0.09	9.8					0.799
2.5	0	0.94	0.09	10.4	62	37	1.68	793	0.764
2.7	0	0.94	0.1	9.4					0.773
2.9	0	0.93	0.09	10.3					0.748
3.25	0	0.95	0.1	9.5					0.760
3.75	0	1.01	0.1	10.1	63	36	1.74	846	0.759
4.25	0	1.02	0.11	9.3					0.732
4.75	0	1	0.1	10.0	60	39	1.54		0.757
5.25	0	1.03	0.11	9.4				814	0.762
5.75	0	1.04	0.1	10.4					0.757
6.25	0	1.03	0.11	9.4	63	36	1.76		0.742
6.75	0	1	0.1	10.0					0.745
7.25	0	0.99	0.09	11.0				810	0.737
7.75	0	0.99	0.09	11.0					0.731
8.25	0	0.96	0.09	10.7					0.719
8.75	0	0.97	0.09	10.8	61	38	1.62		0.729
9.25	0	0.84	0.08	10.5					0.728
9.75	0							811	
11.25	0				63	36 ⁴	1.75	788	
13.75	0				65	34 ⁴	1.92	793	
16.25	0				65	34 ⁴	1.88	785	
18.75	0				67	32 ⁴	2.09	782	
21.25	0				63	36 ⁴	1.73	776	
Mean ⁵	0	0.93(6)	0.093(9)	9.9(6)	63(2)	36(2)	1.8(2)		0.77(3)

¹Different sampling intervals were taken for porosity and other determinations.

²SCHLÜTER et al. [1998].

³Relative precision was generally better than 3%.

⁴Values were calculated [%Detritus = 100% - %CaCO₃ - %C_{org} - %N_{org} - %Opal], assuming C = 0.9, N = 0.09.

⁵Note, *vertical* overall mean values are not normalized to 100%. Uncertainties given in brackets display vertical variations.

Appendix

A.2.6.4 Average composition of Scotia Sea (Fig. 2.1) sediment (ANT-X/5; PS-2314-1). BW bottom water.

depth [cm] ¹	CaCO ₃ [%] ²	C _{org} [%] ²	N _{org} [%] ²	C/N	Opal [%] ³	Detritus [%]	O/D	H ₄ SiO ₄ [μ M] ²	ϕ ²
BW								126	
0.1	0	0.8	0.09	8.9					0.852
0.3	0	0.87	0.1	8.7					0.814
0.5	0	0.85	0.1	8.5	48	51	0.94	508	0.800
0.7	0	0.85	0.11	7.7					0.797
0.9	0	0.8	0.09	8.9					0.804
1.1	0	0.88	0.09	9.8					0.806
1.3	0	0.83	0.1	8.3					0.783
1.5	0	0.85	0.1	8.5	48	51	0.93	678	0.801
1.7	0	0.83	0.09	9.2					0.799
1.9	0	0.82	0.09	9.1					0.757
2.1	0	0.83	0.09	9.2					0.779
2.3	0	0.81	0.1	8.1					0.799
2.5	0	0.79	0.09	8.8	48	51	0.93	719	0.764
2.7	0	0.82	0.1	8.2					0.773
2.9	0	0.8	0.09	8.9					0.748
3.25	0	0.84	0.09	9.3					0.760
3.75	0	0.87	0.1	8.7	48	51	0.93	708	0.759
4.25	0	0.88	0.1	8.8					0.732
4.75	0	0.87	0.1	8.7	51	48	1.06	679	0.757
5.25	0	0.9	0.1	9.0					0.762
5.75	0	0.87	0.09	9.7					0.757
6.25	0	0.86	0.09	9.6	51	48	1.05	643	0.742
6.75	0	0.86	0.09	9.6					0.745
7.25	0	0.86	0.09	9.6					0.737
7.75	0	0.9	0.09	10.0					0.731
8.25	0	0.88	0.09	9.8					0.719
8.75					48	52	0.93	665	0.729
9.25									0.728
9.75									
11.25					54	45	1.22	676	
13.75					54	45	1.19	710	
16.25					52	47	1.12	676	
18.75					52	47	1.12	687	
21.25					56	43	1.31		
Mean ⁵	0	0.85(3)	0.095(6)	9.0(6)	51(3)	48(3)	1.1(1)		0.77(3)

¹Different sampling intervals were taken for porosity and other determinations.

²SCHLÜTER et al. [1998].

³Relative precision was generally better than 3%.

⁴Values were calculated [%Detritus = 100% - %CaCO₃ - %C_{org} - %N_{org} - %Opal], assuming C = 0.9, N = 0.09.

⁵Note, vertical overall mean values are not normalized to 100%. Uncertainties given in brackets display vertical variations.

Appendix

A. 2.7 Pore water silicic acid, aluminum, and relative DOC concentrations of three locations in the Arabian Sea determined during cruise SO129; BW bottom water.

Station	WAST-TOP			EAST-CAST			SAST-EAST		
Sample	MC#35 ^{Al}			MC#26 ^{Al}			MC#20 ^{Al}		
Location	16°10'N 59°46'E			15°02'N 64°34'E			12°51'N 66°48'E		
Water depth [m]	1910			3920			4140		
depth [cm]	H ₄ SiO ₄ [μ M]	Al [nM]	DOC [rel. units] ¹	H ₄ SiO ₄ [μ M]	Al [nM]	DOC [rel. units] ¹	H ₄ SiO ₄ [μ M]	Al [nM]	DOC [rel. units] ¹
BW	131	32	9.565	138	32	9.624	136	13	9.981
0.25	191	78	14.25	176	33	11.86	185	29	13.80
0.75	236	45	12.12	197	35	11.02	210	44	11.61
1.5	279	30	11.34	216	36	10.90	227	32	10.93
2.5	313	25	11.35	237	33	10.78	246	33	10.83
3.5	338	27	11.20	253	34	10.66	254	35	10.75
4.5	361	38	11.11	264	31	10.43	266	33	10.79
5.5	378	33	11.13	270	34	10.28	265	30	10.73
6.5	394	30	11.27	269	35	10.31	274	33	10.76
7.5	403	31	11.30	276	35	10.30	277	28	10.82
8.5	420	28	11.50	276	34	10.30	280	31	10.74
9.5	426	27	11.50	277	36	10.30	280	33	10.70
11.5	432	28	11.46	280	36	10.30	277	30	10.65
14.5	443	26	11.50	277	33	10.30	276	28	10.60
17.5	440	33	11.58	275	35	10.28	276	27	10.55
20.5				273	33	10.24	272	28	10.55
23.5				271	34	10.25	268	26	10.53
26.5				266	34	10.29	253	29	10.50
29.5				266	36	10.38	249	28	10.19
Mean	34(13)	11.5(9)		34(1)	10.5(5)		31(11)	10.9(9)	

¹Nat. fluorescence (excitation: $\lambda = 465$ nm, emission: $\lambda = 555$ nm) of sample [rel. units] \propto DOC [CADDÉE and LAANE, 1983].

A.3.1/A.3.2 Silicic acid concentration as a function of time and depth (M31/2 and MC#33). Steady state was assumed if 4-5 subsequent samples show variations $< \pm 5\%$. Note that not all samples taken (1 sample day⁻¹) were measured; frequency was enhanced at the end of the run. In each experiment, 0.5 g sediment was used. Opal contents are listed in A.2.3.3.

M31/2		4-5 cm						
t [h]	11	12	13	14	15	16	17	
0	35.2	74.2	145	296	376	622	750	
24	54.4	84.8	147	280	334	554	657	
49.5	51.7							
72	48.9	80.1	148	277	336	535	652	
94.25	46.7							
120.75	45.8	81	156	280	340	551	654	
144.75	43.3							
168.5	42.1	85.1	147	284	347	540	657	
194	42.7							
217.25	41.2	77.5	147	286	353	583	673	
239.5	42.4							
266	40.7	78.7	146	290	350	554	668	
288.25	39.2	75.9	145	291	351	556	668	
310.75	39.7	76.3	146	290	358	556	667	
362	39.7	77.6	145	289	360	559	673	
408	41.1	75.7	145	291	356	564	618	
455.25	41.2	76.8	146	288	359	585	689	
Si _{in} [μM]	40.7	76.9	146	289	354	558	670	
R [$\mu\text{mol g}^{-1} \text{h}^{-1}$]	0.49	0.25	0.05	-0.31	-0.49	-0.93	-1.2	

MC#33		0-0.5 cm						
t [h]	11	12	13	14	15	16	17	
0	39.2	71.6	141	289	354	565	695	
20.25	77.3	117	166	310	367	601	667	
44.5	71.4							
67	66.6							
115	58.8	88.3	157	302	358	554	659	
139.5	54.8	86.1	155	297	357	552	661	
164.25	54.4	84.3	156	296	355	554	656	
187.5	53.2	82.9	155	294	353	553	662	
209	50.9	82.3	155	293	360	549	655	
281.5	49.4	81.2	153	292	357	555	656	
286.75	50.2	80	154	293	351	551	660	
304.75	49.4		292	354	549	659		
Si _{in} [μM]	50	81.2	154	293	356	551	658	
R [$\mu\text{mol g}^{-1} \text{h}^{-1}$]	1.9	1.7	1.2	0.36	0.08	-0.46	-1.2	

30-35 cm								
t [h]	11	12	13	14	15	16		
0	34.5	68.4	144	285	589	750		
24	53.6	69.9	121	222	428	558		
49.5								
72	47.3	77.5	126	231	424	524		
94.25								
120.75	43.7	70.2	132	243	424	541		
144.75								
168.5	41.5	66.7	135	255	446	548		
194								
217.25	41	68	139	261	454	567		
239.5		68						
266	39	67.4	141	259	453	592		
288.25		77.7	137	265	460	637		
310.75	39.2	69.9	138	267	475	608		
362	37.8	72.8	137	268	477	609		
408	38.6	68.4	145	266	488	632		
455.25	38.7	47.2	140	275	490	632		
Si _{in} [μM]	39.1	70.3	140	266	483	624		
R [$\mu\text{mol g}^{-1} \text{h}^{-1}$]	0.44	0.19	-0.20	-0.96	-1.7	-2.0		

3-4 cm								
t [h]	11	12	13	14	15	16	17	
0	35.7	68.6	141	289	367	547	661	
19.5	76.2	101	170	311	375	555	640	
44	69.4							
67.5	63.4							
93	57.6	86.8	162	299	367	533	631	
117.25	52							
141	50.3							
163.25	48.7	79.5	155	295	366	534	632	
189.25	47.9							
203.75	47.1							
237	45.5							
262	45.1	76.9	152	291	362	532	636	
286.25	44.6	76.5	150	293	364	534	635	
307.25	44.6	77.2	149	294	362	536	640	
320	43.9	76.5	151	292	361	536	639	
331	43.3	76	150	289	363	534	639	
358.5	43.4	74.7	148	291	362	530	640	
378.25	43.1	75	150	288	362	532	636	
Si _{out} [μM]	45.6	76.5	151	290	362	533	637	
R [$\mu\text{mol g}^{-1} \text{h}^{-1}$]	1.9	1.5	1.0	0.13	-0.24	-0.44	-0.78	

16-19 cm								
t [h]	11	12	13	14	15	16		
0	35.5	63.8	139	292	537	657		
19.5	91.9	102	180	304	542	650		
44								
67.5								
93	61.0	81	166	297	521	643		
117.25								
141								
163.25	-46.3	72.2	155	295	526	642		
189.25								
203.75								
237								
262	43.2	68.3	148	294	527	638		
286.25	41.8	68.9	146	293	531	640		
307.25	41.7	72.9	147	296	535	639.2		
320	40.9	67.4	145	294	532	638.5		
331	41.5	67.6	144	294	528	638.2		
358.5	40.1	67.5	145	294	528	639.2		
378.25	40.7	67.3	144	294	529	639.2		
Si _{in} [μM]	42.0	69	147	294	530	639		
R [$\mu\text{mol g}^{-1} \text{h}^{-1}$]	1.8	1.5	1.2	0.43	-0.38	-0.99		

A.3.3.1/A.3.3.2 Silicic acid concentration as a function of time and depth (WAST MC#53 and NAST MC#45). Steady state was assumed if 4-5 subsequent samples show variations $< \pm 5\%$. Note that not all samples taken (1 sample day⁻¹) were measured; frequency was enhanced at the end of the run. In each experiment, 0.5 g sediment was used. Opal contents are listed in A.2.3.3. Rate constants (k_{eff}), reaction orders (m) and apparent solubilities are given in A.3.1.1.

199

MC#53		0-0.5 cm							
t [h]	11	12	13	14	15	16	17	18	
0	33.8	70.1	144	289	504	656	884	1163	
25	144	175	244	345	528	637	870	1080	
51			260	359	536	642	875	1070	
70.5									
101.5	180	201	269	364	551	642	878	1080	
127.5									
145.5									
172	185	204	273	372	563	666	880	1080	
194									
218.5									
242	184	203	268	378	571	679	884	1080	
270									
337.5	183	208	273	389	587	703	884	1110	
360.5	184	210	276	394	587	713	885	1120	
384.5	181	205	270	390	593	725	886	1120	
410.5	177	200	266	381	588	714	886	1130	
461.5	163	187	253	372	576	709	887	1120	
482.5	156	180	249	370	561	721	885	1120	
495	153	178	245	367	564	716	884	1110	
$S_{\text{tot}} [\mu\text{M}]$	157	182	249	375	567	705	885	1117	
$R [\mu\text{mol g}^{-1} \text{h}^{-1}]$	3.3	3.0	2.8	2.3	0.99	0.44	0.01	-0.39	

MC#45		0-0.5 cm						
t [h]	11	12	13	14	15	16	17	
0	30.7	66.6	134	271	344	548	684	
22	85.3	118	182	304	368	559	661	
48	77.5							
72	67.5							
118.75	56.3							
144.5	52							
168.75	51	86.1	162	290	364	565	665	
196.5	49	85.2	166	288	366	561	675	
216	48.5	83.9	163	284	361	560	680	
241.25	48.2	83.4	161	285	360	561	675	
289.25	48.2	81.9	157	283	362	555	681	
310.75	47.6	80.7	154	281	357	552	681	
323	47.5					553		
337.25	47.3	81.1	154	280	360	554	683	
$S_{\text{tot}} [\mu\text{M}]$	48.4	83.2	160	284	361	554	677	
$R [\mu\text{mol g}^{-1} \text{h}^{-1}]$	1.8	1.7	1.4	0.73	0.52	0.10	-0.12	

3-4 cm									
t [h]	11	12	13	14	15	16	17	18	
0	32.7	34.7	68.0	208	349	512	647	1180	
31.5	122	136	146	258	393	554	691	1170	
74									
98									
121.5	106	153	125	246	382	539	687	1180	
147									
169.5									
197									
224.5	90.2	153	121	238	373	536	653	1150	
245.5									
267	85.1	152	118	239	371	531	655	1140	
316	80	150	114	233	364	529	653	1140	
341									
364	79.5	153	110	236	367	529	660	1140	
385									
411	77	144	0	233	368	529	648	1120	
436	76.8	142	108	232	368	525	654	1130	
459.5	75.6	141	106	234	367	521		1130	
484	77.9	145	104	236	363	526		1120	
$S_{\text{tot}} [\mu\text{M}]$	80.0	147	111	235	367	528	657	1120	
$R [\mu\text{mol g}^{-1} \text{h}^{-1}]$	3.4	2.6	3.1	2.0	1.3	0.64	0.23	-1.1	

3-4 cm							
t [h]	11	12	13	14	15	16	
0	28.6	63.5	139	277	575	716	
22	78.1	107	175	308	714	701	
48							
72							
118.75							
144.5							
168.75	43.3	77.3	161	290.3	579	700	
196.5	43.7	79	158	287	584	702	
216	41.8	76.2	158	286.4	572	695	
241.25	41.4	75	154	286.3	572	693	
289.25	41.1	73.2	154	284	578	702	
310.75	42.1	74.1	152	285	576	700	
323	41.5						
337.25	41.3	72.8	148	283	581	701	
$S_{\text{tot}} [\mu\text{M}]$	42.0	75.8	156	287	577	699	
$R [\mu\text{mol g}^{-1} \text{h}^{-1}]$	2.2	2.1	1.5	0.91	0.05	-0.52	

28-31 cm									
t [h]	11	12	13	14	15	16	17	18	
0	35.4	71.3	143	287	479	635	1180		
25	82.5	114	177	296	497	670	1130		
51	83.9	114	0	300	497	669	1140		
70.5									
101.5	77.5	108	168	295	495	665	1150		
127.5									
145.5									
172	72	102	161	294	493	650	1150		
194									
218.5									
242	67.3	98.3	162	294	495	640	1160		
270									
337.5	66.1	97.2	161	293	489	638	1160		
360.5	67.4	98	160	292	485	634	1150		
384.5	68.3	95.1	160	291	480	631	1150		
410.5	65.3	94.8	160	293	481	628	1150		
461.5	63.2	93.2	155	293	477	629	1140		
482.5	64.8	92.1	154	294	477	632	1150		
495	60.1	92.2	153	295	475	630	1160		
$S_{\text{tot}} [\mu\text{M}]$	65.0	94.7	158	293	485	632	1151		
$R [\mu\text{mol g}^{-1} \text{h}^{-1}]$	1.3	0.98	0.67	0.27	0.13	-0.01	-0.41		

28-31 cm								
t [h]	11	12	13	14	15	16	17	
0	29.8	61.9	139	272	551	674	1388	
19	59.6	92	149	292	545	652	1290	
45.75								
67.75								
90.5								
117.5								
164	37.6	70.4	146	273	542	673	1290	
189	35.6	67.7	150	274	538	652	1280	
211.25		71.3	154	274	562	642	1270	
236.5	35.9		154	273	563	671	1250	
262.75	35.1	66.6		272	569	644	1340	
290.5	32.3		145	273	520	662	1350	
331.25	34.4	64.2	142	274	563	662	1360	
345.5	32.8	64	138	273	514	659	1310	
388	33.3	64.9	142	274	547	660	1320	
$S_{\text{tot}} [\mu\text{M}]$	33.2	64.4	142	273	536	657	1343	
$R [\mu\text{mol g}^{-1} \text{h}^{-1}]$	1.2	0.89	0.61	0.21	-0.86	-1.1	-3.8	

Appendix

A.3.3.3/A.3.3.4 Silicic acid concentration as a function of time and depth (EAST MC#28 and SAST MC#14). Steady state was assumed if 4-5 subsequent samples show variations $\leq \pm 5\%$. Note that not all samples taken (1 sample day⁻¹) were measured; frequency was enhanced at the end of the run. In each experiment, 0.5 g sediment was used. Opal contents are listed in A.2.3.3. Rate constants (k_{1-7}), reaction orders (m) and apparent solubilities are given in A.3.11.

200

MC#28 0-0.5 cm							
t [h]	11	12	13	14	15	16	
0	31.9	63.8	132	271	561	695	
24.5	91.3	147	199	310	539	714	
48.5							
72							
96.75							
121.5							
151	56.9	88.5	167	297	578	683	
169	54.9	85.4	163	291	559	674	
192.75	56	83	162	290	576	682	
216.75	52.8	81.7		287	565		
241	54.2	81.5	158			702	
264.25	52.6	82	160	287	563	679	
290							
314.5	50.3	80.4	158	290	561	708	
336							
360	49.6			291	560	678	
384.75							
405.75							
448.75							
$S_{i_{\text{app}}} [\mu\text{M}]$	53.4	83.2	161	290	566	687	
$R [\mu\text{mol g}^{-1} \text{h}^{-1}]$	2.4	2.2	2.0	1.3	0.10	-0.17	

MC#14 0-0.5 cm								
t [h]	11	12	13	14	15	16	17	
0	35.4	69.6	139	283	353	571	707	
22.75	45.3	100	162	289	352	549	686	
70.75	45.6							
96.75	46.8							
118.25	49.3			283	350	547	674	
144	51.4	80.4	150	284	350	546	678	
165.75	56.5	79.1	149	285	350	549	672	
192	70.4	77.5	149	283	351	548	679	
204.25	45.2	77.3						
216.25	45.2	75.7	147	286	350	551	679	
266	43.5	79.8	148	282	354	554	682	
285.25	43.9	75.9	147	285	349	556	690	
311.5	43.5	74.9	147	282	351	551	684	

3-4 cm							
t [h]	11	12	13	14	15	16	
0	64.6	134	276	349.8	562	707.3	
24.5	142	182	318	412	550	724	
48.5							
72							
96.75							
121.5							
151	82.6	161	293	362	555	690	
169	82.1	160	290	363		685	
192.75		166	290		557	680	
216.75		154	285	365	556	679	
241			288	360		681	
264.25	80.4	152	287	357	557	680	
290	77.6						
314.5	79.2	150	285	353	556	684	
336	76.2						
360		149	285	351	558	679	
384.75	76.3						
405.75							
448.75	75.9						
$S_{i_{\text{app}}} [\mu\text{M}]$	78.8	156	288	359	557	682	
$R [\mu\text{mol g}^{-1} \text{h}^{-1}]$	2.2	1.7	0.94	0.37	-0.13	-0.66	

3-4 cm							
t [h]	11	12	13	14	15	16	
0	36.5	70.0	140	288	576	713	
22.75	52.6	105	170	299	551	666	
70.75							
96.75							
118.25		82.2	159	290	552	670	
144	50	78.6	154	289	551	669	
165.75	47.4	79.7	153	286	554	678	
192	46	75.3	149	286	557	658	
204.25							
216.25	44.7	76.7	146	287	554	675	
266	43.9	74.8	146	288	555	683	
285.25	43.2	73.8	147	288	558	681	
311.5	42.2	74.3	144	286	560	690	

24-26 cm							
t [h]	11	12	13	14	15	16	
0	29.9	63.5	134	277	562	706	
24.25	71.5	97.6	166	290	557	695	
48.75							
74.75							
99							
117.25							
141.25	41.8	73.2	146	279	546	698	
164.75	38.8	69.3	144	278	551	692	
172.75	38.3	70.3	142	277	554	686	
189	37	69.7	140	276		693	
212.75	35.9	69.1	140	283	554	696	
253.25	35.3	68.1	140	279	553	696	
$S_{i_{\text{app}}} [\mu\text{M}]$	36.6	69.3	141	279	554	693	
$R [\mu\text{mol g}^{-1} \text{h}^{-1}]$	1.4	1.2	0.72	0.17	-0.28	-0.49	

24-26 cm								
t [h]	11	12	13	14	15	16	17	
0	31.8	64.5	137	280	357	568	696	
19	74.2	100	168	288	361			
45.75	63.3							
67.75	56							
90.5	50.8							
117.5	46.5							
164	41.6	73.3	148	282	353	558		
189	38.4	69.5	143	280	355	555		
211.25	54.7	79.5	159	298	363	556	664	
236.5	45.7	76.1	157	306	358	556		
262.75	51.3	67.5	141	303	351	556	669	
290.5	37.7	69.6	141	277	357	554	669	
331.25	34.7	0	141	285	359	555	666	
345.5	35.4	66.4	140	281	350	553		
358	34.8	67	140	279	355	554		

Appendix

A.3.4/A.3.5 Silicic acid concentration as a function of time and depth (MC-1-3 and MC-145). Steady state was assumed if 4-5 subsequent samples show variations $\leq 5\%$. Note that not all samples taken were measured; frequency was enhanced at the end of the run. In each experiment of MC-1-3, 1 g sediment was used. Opal contents are listed in A.2.3.3. Rate constants (k_{rr}), reaction orders (m) and apparent solubilities are given in A.3.1.1.

MC-1-3 0-0.5 cm																	
t [h]	11	12	13	14	15	16	17	18									
0	34.2	66.2	140	288	362	523	654	1270									
22.5	188	213	277	397	467	601	665	1180									
51.5	168																
68	156																
92.5	139																
143.5	122																
165	114	140	233	354	451	601	665	1190									
190	117	142	235	358	457	605	677	1200									
213.5	118	141	232	357	451	596	673	1200									
241	115	140	232	349	452	597	675	1210									
261	114	137	231	347	446	592	676	1230									
313	111	135	230	346	447	589	671	1250									
333.5	109	133	229	343	438	589	675	1230									
356.5	107	131	232	345	440	584	673	1240									
367.5	106	129	242	342	440	586	673	1230									
379.5	106	130	256	338	441	584	666	1230									
404.5	104																
427.5	104	128	274	337	579	648	1230										
S_{lim} [μM]	111	135	236	346	444	590	673	1228									
R [$\mu mol g^{-1} h^{-1}$]	2.3	2.1	1.6	0.93	0.68	0.33	0.10	-0.22									
MC-1-3 3-4 cm																	
t [h]	11	12	13	14	15	16	17	18									
0	34.0	67.8	139	294	613	700	1400										
20.25	193	228	282	372	652	731	1290										
44.5																	
67																	
115	124	141	248	345	622	687	1250										
139.5	113	131	239	345	629	687	1270										
164.25	107	128	233	337	626	677	1280										
187.5	101	123	225	338	629	685	1280										
209	97.1	119	222	335	625	677	1290										
281.5	86.3	111	207	327	619	680	1290										
286.75	85.3	111	205	327	621	678	1300										
304.75	85.2	112	201	331	622	681											
S_{lim} [μM]	85.6	113.3	208.8	330.0	621.8	679.0	1293										
R [$\mu mol g^{-1} h^{-1}$]	1.6	1.4	1.1	0.59	0.05	-0.11	-0.62										
MC-1-3 19-22 cm																	
t [h]	11	12	13	14	15	16	17										
0	34.4	69.5	141	288	550	654	1280										
22.3	133	161	234	342	549	646	1240										
51.5																	
68																	
92.5																	
143.5																	
165	70.8	99.2	197	315	544	652	1210										
190	70	100	194	315	546	640	1230										
213.5	68	98.9	191	311	546	638	1230										
241	66.1	96.7	188	311	547	642											
261	65	95.6	187	309	544	641	1230										
313	62.5	92.4	183	306	546	646	1250										
333.5	61.2	91.4	181	307	543	643	1250										
356.5	60.8	91.5	178	306	545	647	1260										
367.5	59.8	92.9	177	304	540	648	1240										
379.5	59.8	93.8	176	302													
404.5																	
427.5	58.4																
S_{lim} [μM]	78.8	156	288	359	557	682	1293										
R [$\mu mol g^{-1} h^{-1}$]	2.2	1.7	0.94	0.37	-0.13	-0.66	-3.3										
MC-145 0-0.5 cm																	
t [h]	11	12	13	14	15	16	17	18									
0	31.1	69.0	140	286	363	593	736	1510									
19.5	207	230	323	422	500	667	779	1360									
45.75	169																
73.25	139																
98.5																	
117.75	119																
142.5	115	142	239	351	461	656	774	1390									
165.25	109	138	234	351	452	655	778	1400									
189.5	108	135	228	346	453	647	763	1410									
216.25	101	130	221	340	446	647	763	1410									
241.75	101	129	224	338	444	648	759	1390									
268	99.2	127	215	337	434	643	763	1390									
285.25	100	127	217	335	437	650	763	1410									
MC-145 3-4 cm																	
t [h]	11	12	13	14	15	16	17										
0	36.5	72.1	146	284	584	718	1470										
19.5	212	228	326	407	662	764	1330										
45.75																	
73.25																	
98.5																	
117.75																	
142.5	110	137	253	350	655	755	1360										
165.25	107	133	246	342	651	758	1370										
189.5	104	131	240	343	640	756	1380										
216.25	98.1	116	229	329	638	748	1380										
241.75	99.4	117	226	334	643	752	1380										
268	96.5	117	218	326	637	742	1360										
285.25	97.1	125	218	326	637	742	1360										
MC-145 26-28 cm																	
t [h]	11	12	13	14	15	16	17	18									
0	37.2	69.9	140	277	346	570	693	1430									
24.25	149	174	238	352	421	620	710	1280									
48.75	135																
74.75	117																
99	106																
117.25	99																
141.25	91.6	124	198	328	410	621	711	1270									
164.75	90.3	120	200	322	410	616	711	1270									
172.75	87.7	119	196	319	408	617	701	1300									
189	84.2	117	196	320	409	615	705	1300									
212.75	83.1	114	192	319	404	617	704	1310									
253.25	79.9	111	186	311	398	607	701	1310									

A.3.6.1/A.3.6.2 Silicic acid concentration as a function of time and depth (PS-2283-6 & PS-2299). Steady state was assumed if 4-5 subsequent samples show variations $\pm 5\%$. Note that not all samples taken (1 sample day⁻¹) were measured; frequency was enhanced at the end of the run. In each experiment 0.5 g sediment was used. Opal contents are listed in A.2.3.3. Rate constants (k_{FF}), reaction orders (m) and apparent solubilities are given in A.3.11.

PS-2283-6 1-2 cm									3-4 cm								5-7.5 cm									
t [h]	11	12	13	14	15	16	17	18	t [h]	11	12	13	14	15	16	17	18	t [h]	11	12	13	14	15	16	17	18
0	31.5	136	271	358	541	673	965	1380	0	31.8	67.0	143.8	295.5	569.5	714.5	1370	0	27.4	62	136.8	286.5	545.3	664.0	996.3	1385	
24	110	204		432	633	700	970	1300	24	100	129	374	342	616	724	1360	16.5	79.1	112	195	331	597	811	1000	1330	
45.5	110	201		422	629	699	975	1340	45.5	97.4	125	233	334	613	730	1360	41	70.5	101	188	323	610	718	998	1350	
92.5	119	203	311	428	594	694	973	1360	92.5	93	113	187	330	609	740	1380	73	67.8	93.7	186	320	598	704	995	1360	
113.5	111	195	310		579	690	969	1350	113.5	88.2	122	204	326	605	733	1380	97.5	65.8	96	184	320	579	700	996	1370	
148	105	195	305	424	592	695	960	1350	148	90	122	203	324	603	726	1370	114.5	63.3	94.1	186	314	592	708	995		
169	102	191	301	420	589	694	955	1350	169	86.2	119	195	324	596	724	1370	137	65	92.3	184	316	596		994		
193	100	189	303	414	582	692	950	1330	193	85.1	117	195	326	590	721	1340	164.5	57.9	87.5	179	310	584	686	992	1340	
219.5	97	185	305	416	584	693	940	1320	219.5	85.2	117	193	322	587		1340	187	56.4	86.6	184	316	585	698	994	1350	
242.5	94.1	190	305	405	573	685	930	1310	242.5	85.4	113	181	320	588	720	1350	209.75	54	84.5	181	314	599	691	992	1350	
259.5	91.5	185	301	400	572	676	926	1310	259.5	86.4	111	183	317	587	714	1350	232.5	54.8	86.5	182	313	584	689	991	1340	
281.5	89.5	180	303	404	579	676	927	1310	281.5		114	184	319	589	712	1360	282.5	50.4		173	310	600	698	992	1340	
306	90.3	182	300	401	571	678	928	1280	306		110	180	318	592	710	1350	306.5	49.3		167	312	588	683	990	1330	
Si_{out} [μM]	98.8	189	304	412	577	683	940	1323	Si_{out} [μM]	85.7	113.7	182	322	593	721	1358		Si_{out} [μM]	51.5	86.5	174	313.1	591	693.3	991	1337
R [$\mu mol g^{-1} h^{-1}$]	3.2	2.7	1.8	1.5	0.61	0.20	-0.44	-1.0	R [$\mu mol g^{-1} h^{-1}$]	1.9	1.7	1.4	1.1	0.29	0.09	-0.16		R [$\mu mol g^{-1} h^{-1}$]	1.3	1.4	1.1	0.82	0.47	0.31	-0.06	-0.50

PS-2299 1-2 cm									3-4 cm									20-25 cm								
t [h]	11	12	13	14	15	16	17	18	t [h]	11	12	13	14	15	16	17	18	t [h]	11	12	13	14	15	16	17	18
0	67.9	137	283	348	505	640	1030	1340	0	34.8	70.1	145	286	528	650	1028	1355	0	67.0	137	282	366	516	633	1300	1693
21	221	265	376	477	650	730	1000	1240	21	171	195	232	367	613	698	1000	1280	16.5	229	279	380	462	583	681	1250	1620
46									46									41	249	258	365	453	570	673	1270	1630
70									70	170								73	191	246	360	452	560	673	1280	1620
92.5	203	265	371	481	656	729	1040	1320	92.5		191	264	368	616	695	1010	1290	97.5	175	247	355	449	557	667	1270	1630
120.5									120.5									114.5	0	243	345	445	556	628	1270	1640
143	177	235	365	477	627	727	1000	1300	143	147	171	236	349	608	690	1020	1300	137	140	243	340	443	559	668	1260	1640
165	171	230	340	451	612	712			165	143	165	224	342	600	687	1010	1310	164.5	121	239	337	440	583	665	1270	1650
189.5	175	227	352	456	615	714	1010	1270	189.5	147	168	233	341	604	685	1010	1310	187	110	234	335	439	575	661	1260	1640
212.5	171	222	352	449	609	697	1020	1300	212.5	140	162	228	337	605	680	995	1310	209.75	105	223	330	438	588	652	1260	1640
237	164	218	340	439	590	693	1020	1290	237	146	160	210	334	599	678	1000	1310	232.5	106	211	332	436	553	653	1270	1650
261	163	213	334	425	587	669	1020	1290	261	145	155	208	332	595	676	1000	1310	282.5	103	208	334	438	555	652	1270	1640
																		306.5	100	204	335	435	564	652	1280	1640

A.3.6.3 Silicic acid concentration as a function of time and depth (PS-2312-1). Steady state was assumed if 4-5 subsequent samples show variations $\leq 5\%$. Note that not all samples taken (1 sample day⁻¹) were measured; frequency was enhanced at the end of the run. In each experiment, 0.5 g sediment was used. Opal contents are listed in A.2.3.3. Rate constants (k_{app}), reaction orders (m) and apparent solubilities are given in A.3.11.

PS-2312-1 12.5-15 cm							
t [h]	11	12	13	14	15	16	17
0	33.7	66.9	130	299	570	1080	1670
1	93.2	114	170	326	586	1120	1680
25	136	168	214	354	597		
49	151	179	220	356	616	1110	1660
77	160	193	235		609		1640
97	195	201	264	370	629	1100	
124	200	230	221		632	1090	1620
148	189			386	592	1070	
192.5	200	237	279	384	628	1070	
215	182	236	278	380	599	1070	1630
237	185		272	379	587	1090	1610
261	209	239	273	380	612	1070	1620
288	195		272	384	606	1070	1620
313	197	226	271	380	616	1080	1600
Si_{out} [μM]	195	234	274	382	612	1079	1620
R [$\mu mol g^{-1} h^{-1}$]	2.1	2.2	1.8	1.1	0.54	-0.04	-0.66

20-22.5 cm								
t [h]	11	12	13	14	15	16	17	18
0	38.0	39.1	294	357	529	714	1139	1425
24	139	158	349	407	598	753	1150	1330
48.5	149	179	360	413	575	772	1136	1350
69.5	172	209	374	403	580	768	1158	1360
88.5	183	229	382	418	591	777	1160	1360
115.5	204	240	395	416	0	776	1160	1370
138.5	214	263	396	437	601	782	1164	1350
163	246	290	400	446	619	788	1148	1360
214	249	318	403		600		1166	1370
236.5	264	339	402		608	796	1160	1380
261.5	240	325	400	462	600	785		1380
285	231	311	395	455	590	762	1158	1390
306.5	236	313	392	459	605	782	1144	1390
332	249	334	389	459	597	789	1142	1380
379.5	241	331	387	445	617	772	1140	1380
Si_{out} [μM]	245	324	396	452	602	782	1142	1381
R [$\mu mol g^{-1} h^{-1}$]	2.4	1.7	1.4	1.1	0.50	0.26	0.01	-0.20

Appendix

A.3.7 Opal dissolution experiments (O1-O11, Tab. 2.2: PS-2299, 12.5-15 cm) . Si_{out} [μM] as a function of time [h] and weight [mg]. Start time and silicic acid concentration of new input solutions (bold). Some experimental problems caused loss of data.

weight [mg]	100	100	100	100	250	100	400	150	500	500	200
t [h]	O1	O2	O3	O4	O5	O6	O7	O8	O9	O10	O11
0	1860	1830	1830	1870	1820	1810	1810	1820	1830		1840
23.5	1820	1850	1850	1860	1820	1820	1560	1780	1750		1790
46	1820	1840	1860	1870	1820	1820	1590	1800	1750		1770
70.5	1820	1840	1860	1850	1820	1820	1610	1800	1740		1750
94.25	1820	1800	1820	1860	1800	1800	1620	1780	1760		1720
121.5	1810	1750	1850	1850	1780	1810	1610	1790	1760		1740
152	1810	1740	1820	1850	1760	1800	1610	1800	1760		1720
168.5	1790	1740	1810	1860	1780	1780	1610	1790	1760		1730
194	1810	1710	1790	1850	1760	1780	1610	1800	1750		1730
242.5	1800	1700	1770	1860	1760	1770	1630	1790	1760		1730
265.5	1810	1700	1780	1860	1730	1760	1630	1780	1750		1740
288.75	1800	1710	1800	1860	1730	1750	1620	1790	1770		1760
304	1790	1720	1790	1860	1730	1750	1630	1790	1780		1740
340.5	1490	1510	1490	1500	1490	1510	1530	1540	1550	1520	1520
343.75	1500	1520	1480	1500	1490	1500	1550	1560	1580	1360	1530
360.75	1470	1510	1470	1510	1440	1490	1530	1550	1560	1300	1500
382.5	1470	1510	1470	1510	1440	1500	1540	1560	1540	1290	1480
407.5	1440	1500	1470	1500	1440	1490	1520	1560	1550	1290	1510
431.5	1480	1490	1470	1500	1460	1500	1510	1530	1530	1280	1500
458.5	1460	1490	1480	1500	1440	1490	1490	1540	1530	1290	1500
479.75	1450	1500	1440	1470	1440	1470	1500	1520	1520	1260	1490
509	1150	1190	1170	1100	1210	1140	1180	1150	1140	1120	1140
513	1110	1090	1080	1110	1100	1110	1130	1140	1240	1130	1130
528	1110	1110	1100	1120	1090	1120	1130	1120	1240	1130	1130
550	1130	1140	1140	1100	1130	1140	1120	1140	1220	1190	1150
579	1140	1160	1140	1110	1170	1120	1160	1150	1170	1180	1140
600.5	1130	1180	1160	1110	1190	1120	1170	1130	1150	1170	1160
627	1150	1180	1170	1110	1210	1120	1160	1140	1130	1150	1150
652.75	1150	1180	1170	1080	1220	1130	1170	1140	1140	1150	1150
673.25	1150	1190	1170	1070	1210	1130	1160	1140	1120	1140	1150
715.5	877	878	881	885	878	876	923	899	883	875	896
718.5	953	943	913	885	1120	1010	929	916	939	1100	944
745.5	969	947	943	881	1010	900	922	907	922	978	925
769	988	976	965	880	1030	901	934	911	925	977	909
796.5	1000	992	989	878	1050	908	931	905	915	968	919
821	1020	1000	1020	885	1060	903	933	904	919	965	923
841.5	1040	1010	1040	886	1060	907	930	898	914	965	920
863	1030	1020	1050	890	1080	901	925	901	914	963	921
883.75	1020	1020	1040	895	1080	905	927	905	906	968	918
922	740	747	746	752	744	732	750	752	747	749	741
933	827	894	1146	756	882	776	771	775	775	869	767
959.5	863	996	1018	759	995	792	778	772	777	861	775
984.25	888	980	990	754	1010	787	772	774	768	866	782
1007.25	902	960	972	753	1010	796	785	762	771	839	779
1030	909	950	970	752	1040	790	784	760	762	840	791
1054	875	940	965	754	960	770	775	753	762	835	789
1059	736	737	736	740	738	732	753	762	736	739	735
1079.5	921	1000	1014	759	999	810	771	764	769	867	770
1098	862	873	926	741	954	781	772	760	756	821	753
1128	848	893	916	740	950	772	758	768	746	809	753
1152	847	909	919	741	897	771	763	765	745	799	751
1179.5	592	591	595	592	597	591	588	583	594	592	589
1196	791	848	854	606	904	650	606	603	636	710	634
1220.25	807	798	850	583	893	668	607	591	624	709	634
1245	789	823	827	597	871	656	602	586	610	692	625
1269	801	834	831	593	873	653	601	590	610	691	620
1293.75	792	835	834	593	982	651	596	587	605	695	615
1315.5	788	840	838	593	879	658	589	591	603	690	613
1340.5	290	287	288	289	288	289	280	280	289	288	277
1365.5	652	769	720	295	834	395	329	301	365	534	328
1391.5	622	732	658	281	810	394	317	298	336	497	314
1413.5	603	709	648	310	801	389	313	293	322	481	322
1440.5	582	670	644	294	670	381	309	294	315	465	312
1463.5	571	652	641	294	678	375	307	292	312	458	311
1485.25	556	660	643	292	680	375	307	288	307	450	316
1513	35.1			34.7	35.5		34.5	34.3		34.7	
1531.5	470			48.8	709		99.1	67.0		327	
1557	443			48.8	663		94.8	63.4		340	
1581	422			46.4	652		92.5	63.1		302	
1604.5	400			46.5	613		91.0	63.0		279	
1631.25	394			48.2	584		93.0	63.5		239	
1653.25	384			46.4	557		91.0	63.8		240	
1655.25				35.2							
1679				44.3							
1700.75				43.1							
1727.5				42.7							
1752.25				43.2							
1776.25				42.7							
1799.25				43.3							
1823.75				42.1							
1848.25				41.3							

A.3.8 Aluminum flow-through experiments (3.1.1.2.3). 0.5 g Siliceous ooze sample PS-2312-1 (10-12.5 cm) was rinsed with various concentrations of aluminum $[Al]_{in}$ in artificial seawater with almost constant silicic acid $[Si]_{in}$ concentrations. Experiments were performed in 4 (A/A'-D/D') times 3 (Run #1-#3) duplicate runs with changing Al input solutions using the same sediment throughout the time of duration. Reaction rates $[\mu mol g^{-1} h^{-1}]$ for all runs are given at the end. Experiments #3 D/D' (results are indicated by a question mark) provide large uncertainties due to coprecipitation of Si and Al in input solution during the course of an experiment (3.1.1.2.3). A and A' were conducted without addition of Al.

	A	A'	B	B'	C	C'	D	D'	
Run#1	$[Si]_{in} [\mu M]$	298	296	300	297	298	298	298	299
	$[Al]_{in} [\mu M]$	0	0	0.092	0.083	0.192	0.193	0.653	0.651
Run#2	$[Si]_{in} [\mu M]$	314	311	314	302	297	296		
	$[Al]_{in} [\mu M]$	0	0	1.84	1.90	2.55	2.53		
Run#3	$[Si]_{in} [\mu M]$	295	288	285	285	291	291		
	$[Al]_{in} [\mu M]$	0	0	36	36.2	273	273		
	time [h]	$[Si]_A [\mu M]$	$[Si]_{A'} [\mu M]$	$[Si]_B [\mu M]$	$[Si]_{B'} [\mu M]$	$[Si]_C [\mu M]$	$[Si]_{C'} [\mu M]$	$[Si]_D [\mu M]$	$[Si]_{D'} [\mu M]$
Run#1	0	298	296	300	297	298	298	298	299
	↓ 19	390	386	384	386	384	393	386	396
	42.25	410	396	395	400	380	392	392	408
	92.25	422	425	414	409	393	388	401	415
	116.75	430	420	424	419	388	396	404	424
	143.5	427	421	420	422	396	404	409	427
	164	445	428	423	414	406	411	416	433
	187.25	444	444	436	433	415	414	422	437
	209.75	449	436	433	429	421	417	428	442
	237	445	443	439	428	426	423	432	445
	260.5	444	436	437	430	425	423	432	448
	292.5	442	431	417	429	413	405	418	425
	311.25	446	433	422	413	408	407	415	426
	337.75	436	423	412	417	409	403	419	406
	355	429	413	408	400	399	394	407	394
	379.25	428	421	407	422	404	399	409	407
	403.75	421	417	403	414	401	394	401	406
Run#2	430.5	419	423	406	416	393	387		
	↓ 454	420	420	415	415	396	398		
	482.5	421	421	402	398	387	392		
	500	419	423	390	396	380	384		
	524	416	416	387	390	370	375		
	546	416	419	383	389	368	371		
	571.75	420	419	380	384	361	366		
	594.75	418	422	379	381	357	359		
	625	419	423	379	380	359	358		
Run#3	649	408	423	362	359	301	304		
	↓ 670.75	410	425	351	347	274	278		
	696.75	408	422	350	343	257	268		
	720.5	415	423	333	341	239	245		
	751.5	418	428	331	335	226	224		
	774.75	410	421	333	338	210	217		
	795	412	417	326	331	206	217		
	817.25	408	423	328	333	204	213		
Run#1	$[Si]_{out} [\mu M]$	434	423	412	416	406	400	412	411
	$[Al]_{out} [\mu M]$	0	0	0	0	0	0	0	0
	Rate #1 $[\mu mol g^{-1} h^{-1}]$	1.1	1.1	0.95	0.99	0.93	0.88	0.97	0.97
Run#2	$[Si]_{out} [\mu M]$	419	421	383	387	363	366		
	$[Al]_{out} [\mu M]$	0	0	0	0	0	0		
	Rate #2 $[\mu mol g^{-1} h^{-1}]$	1.0	1.1	0.70	0.75	0.57	0.60		
Run#3	$[Si]_{out} [\mu M]$	411	423	330	336	212	218		
	$[Al]_{out} [\mu M]$	0	0	0	0	0	0		
	Rate #3 $[\mu mol g^{-1} h^{-1}]$	0.97	1.1	0.39	0.37	-0.70(?)	-0.62(?)		

A.3.9 Magnesium flow-through experiments (3.1.1.2.3). 0.5 g Siliceous ooze sample PS-2312-1 (10-12.5 cm) was rinsed with increasing concentrations of magnesium $[Mg]_{in}$ in artificial seawater with changing silicic acid $[Si]_{in}$ levels. Experiments were performed in 9 parallel runs, two but the last one were run in duplicate. Reaction rates $[\mu mol g^{-1} h^{-1}]$ for all runs are given at the end. A and A' were conducted without addition of Al. Prior to various $[Mg]_{in}$ (start after sample No. 8 (188 h)) sediments were allowed to equilibrate with artificial seawater containing 300 μM silicic acid and 57 mM magnesium.

		E	E'	F	F'	G	G'	H	H'	I
Mg-spike	$[Si]_{in}$ [μM]	298	298	298	298	267	265	219	228	139
	$[Mg]_{in}$ [mM]	56.8	56.8	230	229	917	918	1820	1830	3540
	time [h]	$[Si]_E$ [μM]	$[Si]_{E'}$ [μM]	$[Si]_F$ [μM]	$[Si]_{F'}$ [μM]	$[Si]_G$ [μM]	$[Si]_{G'}$ [μM]	$[Si]_H$ [μM]	$[Si]_{H'}$ [μM]	$[Si]_I$ [μM]
Equilibration	0	298	298	298	298	298	298	298	298	298
	↓									
	23.5	368	354	370	368	375	363	353	382	365
	47									
	69									
	95									
	118									
	142									
	168									
Mg-spike	188	435	427	448	425	445	433	427	412	445
	↓									
	210	435	434	412	378	340	341	279	273	165
	234.5	446	428	373	375	315	308	236	238	119
	256	436	418	364	375	303	296	223	219	108
	283.5	422	415	358	364	285	304	230	233	106
	306.25	435	421	349	352	289	301	235	228	111
	331.25	436	407	358	366	291	297	225	223	115
	352									116
	374.25									121
397.25									126	
Mg-spike	$[Si]_{out}$ [μM]	427	421	361	366	297	301	230	228	115
	$[Mg]_{out}$ [mM]	56.8	57.2	228	228	909	911	1800	1810	3520
	Rate [$\mu mol g^{-1} h^{-1}$]	1.1	1.0	0.54	0.58	0.26	0.32	0.10	0.00	-0.18

A.3.10 Flow-through experiments with opal/detrital clay mixtures (3.1.1.2.3) at T = 25 °C. 0.5 g mixed sediment samples PS-2312-1 (12.5-15 cm)/detrital clay (ratio 1:15) were rinsed with artificial sea water spiked with various silicic acid $[\text{Si}]_{\text{in}}$ levels. Reaction rates $[\mu\text{mol g}^{-1}\text{h}^{-1}]$ are given at the end. K Kaolinite, M Montmorillonite, I Illite.

time [h]	M#1	M#2	M#3	M#4	M#5	M#6	I#1	I#2	I#3	I#4	I#5	K#1	K#2	K#3	K#4	K#5	K#6
0	35	71	139	283	572	729	69.4	140	288	595	760	36	73	143	287	595	766
19.75	90.0	108	162	231	500	567	94.5	147	280	503	647	40.0	61.0	117	239	546	656
42.25	85.0	101	155	235	490	566	93.0	155	275	506	649	39.8	62.0	120	245	507	655
68.5	78.8	103	149	242	479	565	91.4	161	269	509	651	39.5	64.5	123	254		653
92.5	68.9	87.2	147	247	484	570	91.2	161	275	512	653	39.0	66.0	126	260	533	660
114.5	60.4	83.6	145	251	479	574	91.2	161	278	523	654	38.5	67.9	129	262		666
143	50.8	80.7	143	255	490	584	85.4	162	280	535	660	38.2	69.3	133	262	542	670
187	48.9	77.3	140	263	494	598	81.6	160	283	542	670	38.0	71.2	135	264		683
213.25	46.8	76.3	142	265	499	604	81.3	158	286	547	673	37.8	71.0	135	265	545	684
241	45.6	75.0	138	258	507	610	81.0	155	288	555	672	37.9	72.7	135	267	547	698
264.75	41.5	73.7	138	255	511	621	79.8	153	291	550	683	37.5	73.3	138	265	549	697
317	41.0	73.5	137	258	507	627	78.4	152	286	560	691	37.0	72.2	137	273	551	695
337	40.5	73.4	137	260	508	641	77.3	152	286	558	681	37.2	72.0	137	261	543	693
356	39.8	73.0	136	265	515	637	76.5	151	281	572	687	36.8	72.4	138	271	550	700
384.75	40.2	73.8	136	263	515	639	75.9	151	282	562	686	36.8	73.4	140	274	555	701
$[\text{Si}]_{\text{out}} [\mu\text{M}]$	41	73	137	260	511	633	79.0	152	285	560	686	37	73	138	269	550	697
Rate $[\mu\text{mol g}^{-1}\text{h}^{-1}]$	0.40	0.19	-0.08	-0.77	-1.1	-1.1	0.68	0.41	-0.11	-0.65	-0.89	0.10	-0.03	-0.20	-0.61	-0.80	-0.80

Appendix

A.3.11 Results of depth-dependent sediment flow-through experiments. Rate constants (k_{CFT}), reaction orders (m) and apparent solubilities were determined as described in Section 3.1.1.2.1. k_{CFT} and m_{CFT} are fitted parameters of measured steady state dissolution rates versus the relative degree of undersaturation (Eq. 3.13). Uncertainties from fitting procedures are given in brackets.

Station	Sample designation	Depth [cm]	Apparent solubility [$\pm 10\%$]	m_{CFT}	k_{CFT} [yr^{-1}]
Norwegian Sea	M31/2	4.5	107	1.85(0)	0.61(5)
		32.5	168	1.9(3)	0.46(6)
BENGAL	MC#33	0.25	380	1.39(4)	1.34(1)
		3.5	322	1.38(9)	1.33(3)
		17.5	398	1.2(1)	1.15(4)
WAST	MC#53	0.25	913	1.4(1)	2.5(1)
		3.5	753	1.7(2)	2.32(6)
		29.5	635	3.1(4)	0.98(6)
NAST	MC#45	0.25	611	1.60(9)	1.24(3)
		3.5	565	1.5(1)	1.46(5)
		26.5	319	1.1(3)	0.75(6)
EAST	MC#28	0.25	610	1.06(8)	1.53(3)
		3.5	488	1.3(1)	1.62(1)
		25	383	1.8(1)	0.95(3)
SAST	MC#14	0.25	306	1.44(7)	0.79(2)
		3.5	315	2.03(4)	0.68(1)
		29.5	312	1.59(4)	0.46(1)
Juan de Fuca	MC-1-3	1.5	716	1.6(1)	1.74(6)
		3.5	631	1.5(1)	1.15(4)
		20.5	601	1.4(2)	0.49(3)
Peru Basin	MC-145	0.25	887	2.2(3)	1.22(6)
		3.5	900	2.0(4)	1.1(1)
		27	784	1.8(3)	0.48(4)
Scotia Sea	PS-2283-6	1	762	1.29(7)	2.20(6)
		3.5	735	1.3(1)	1.26(5)
		6.25	945	1.2(1)	0.82(3)
Scotia Sea	PS-2299	1.5	1008	1.5(1)	1.85(6)
		3.5	915	1.7(1)	1.91(6)
		22.5	899	1.9(1)	1.68(6)
Scotia Sea	PS-2312-1	13.75	1056	2.4(4)	2.1(2)
		21.25	1132	3.0(2)	2.8(2)

A.3.12 BET-surface areas of untreated ($S_{\text{untreated}}$) and acid-cleaned ($S_{\text{acid-cleaned}}$) sediments in the Scotia Sea. Results of depth-dependent cobalt (Co) adsorption experiments (3.1.2.2.3) with acid-cleaned sediments PS-2299 and PS-2314-1.

Depth [cm]	PS-2299			PS-2314-1			PS-2312-1
	$S_{\text{untreated}}$ [$\text{m}^2 \text{g}^{-1}$]	$S_{\text{acid-cleaned}}$ [$\text{m}^2 \text{g}^{-1}$]	Co [$\mu\text{mol/g}$]	$S_{\text{untreated}}$ [$\text{m}^2 \text{g}^{-1}$]	$S_{\text{acid-cleaned}}$ [$\text{m}^2 \text{g}^{-1}$]	Co [$\mu\text{mol/g}$]	
0.5	22	51		16	56		11
1.5	18	51		15	56	6.2	12
2.5	18	51	6.6	13	58	5.8	13
3.5	19	51	6.1		54	5.3	13
4.5	22	52	6.1	15	51	5.8	11
6.25	20	53	5.4	16	54	5.9	11
8.75	21	51	4.8	14	50	5	12
11.25	23	53	5.4	17	48	4.9	12
13.75	25	53	5.5	16	49	4	12
16.25	19	53	5.7	13	42	4.7	11
18.75	18	54		14	45	5.4	11
21.25	22			17	45	4.2	11
22.5	21	54	4.5				

A.3.13 Alkaline leaching experiments with opal (PS-2312-1 12.5-15 cm)/clay (see A.1) (CaCO_3) mixtures (3.1.2.2.3). BSi [wt.%]: Opal content (including 10% H_2O after MORTLOCK and FROELICH, 1989); Al_2O_3 [wt.%]: Al release (given as Al_2O_3) during the first 4 h of opal dissolution; k_{NaOH} : alkaline reactivity rate constant, b_{NaOH} non-biosiliceous rate constant (Eq. 3.15, Sect. 2.5.4.3).

Opal/Clay(CaCO_3) mixture	BSi [wt.%]	Al_2O_3 [wt.%]	k_{NaOH}	b_{NaOH}
Opal PS-2312-1 12.5-15 cm	66	0.13	0.96	
Kaolinite-Opal (1:1)	35	0.45	0.90	0.09
Kaolinite -Opal (3:1)	17	1.2	0.71	0.03
Kaolinite -Opal (7:1)	11	1.2	0.41	0.05
Kaolinite -Opal (15:1)	6.3	2.0	0.32	
Kaolinite	6.0	4.0	0.13	0.07
Opal PS-2312-1 12.5-15 cm	66	0.13	0.96	
Montmorillonite-Opal (1:1)	35	0.62	0.80	0.08
Montmorillonite -Opal (3:1)	20	0.85	0.75	0.05
Montmorillonite -Opal (7:1)	9.8	0.81	0.59	0.06
Montmorillonite -Opal (15:1)	7.3	0.95	0.64	0.10
Montmorillonite	3.1	2.9	0.59	0.09
Opal PS-2312-1 12.5-15 cm	66	0.13	0.96	
Illite-Opal (1:1)	34	0.45	0.85	0.04
Illite-Opal (3:1)	19	0.85	0.75	0.08
Illite-Opal (7:1)	8.9	0.57	0.61	0.06
Illite-Opal (15:1)	5.1	0.64	0.61	0.08
Illite	1.4	0.83	0.54	0.06
Opal PS2312-1 12.5-15 cm	66	0.13	0.96	
Opal- CaCO_3 (1:3)	17	0.07	0.86	
Opal- CaCO_3 (1:15)	3.3	0.00	0.81	

A.3.14 Results from alkaline leaching experiments (0.032 N NaOH, T = 85°C). BSI [%]: Opal content (including 10 wt% H₂O after MORTLOCK and FROELICH, 1989); Al₂O₃ [%]: Al release (given as Al₂O₃) release during the first 4 h of opal dissolution; k = k_{NaOH}: alkaline reactivity rate constant; b = b_{NaOH}: non-biotite rate constant (Eq. 3.15, Sect. 2.5.4.3). For locations see Fig. 2.1, Tab. 2.1.

1. M31/2 (Norwegian Sea)			
BSI [%]	Al ₂ O ₃ [%]	k [h ⁻¹]	b [h ⁻¹]
0.5	1.1	0.53	0.64
1.5	1.3	0.58	0.41
2.5	1.2	0.50	0.34
3.5	1.0	0.44	0.56
4.5	1.5	0.43	0.28
6.25	1.2	0.45	0.37
8.75	1.0	0.41	0.43
12.5	1.2	0.28	0.18
17.5	1.0	0.36	0.3
22.5	1.0	0.43	0.63
27.5	1.1	0.28	0.27
32.5	1.6	0.43	0.22

2. MC#33 (BENGAL)			
BSI [%]	Al ₂ O ₃ [%]	k [h ⁻¹]	b [h ⁻¹]
0.25	1.8	0.69	1.8
0.75	1.7	0.72	1.9
1.5	1.5	0.68	2.0
2.5	1.6	0.64	1.5
3.5	1.7	0.70	1.5
4.5	1.6	0.68	1.6
5.5	1.5	0.57	1.6
6.5	1.5	0.58	1.3
7.5	1.6	0.71	1.3
8.5	1.4	0.63	1.1
9.5	1.2	0.50	1.2
11.5	1.2	0.61	0.65
14.5	1.1	0.55	0.70
17.5	1.1	0.67	0.74

3.1 WAST (MC#53, Arabian Sea)			
BSI [%]	Al ₂ O ₃ [%]	k [h ⁻¹]	b [h ⁻¹]
0.25	5.7	0.50	1.6
0.75	4.6	0.60	1.7
1.5	5.4	0.59	1.6
2.5	5.1	0.43	1.4
3.5	4.1	0.38	1.8
4.5	4.2	0.46	1.3
5.5	3.4	0.42	1.3
6.5	3.2	0.45	1.3
7.5	3.9	0.36	1.2
8.5	3.7	0.40	1.6
9.5	3.7	0.36	1.6
11	3.5	0.40	1.2
13	3.5	0.35	1.4
15	3.4	0.30	1.4
17	3.1	0.35	1.6
19	3.4	0.37	1.2
21	3.4	0.43	1.1
23	3.5	0.38	1.3
25	3.4	0.37	1.2
27	3.4	0.40	1.1
29	3.6	0.37	1.4
31	3.4	1.3	0.08

3.2 NAST (MC#39 ^A , Arabian Sea)			
BSI [%]	Al ₂ O ₃ [%]	k [h ⁻¹]	b [h ⁻¹]
0.25	2.8	0.63	1.1
0.75	2.8	0.69	0.98
1.5	2.5	0.58	0.88
2.5	1.9	0.48	0.87
3.5	1.7	0.43	1.3
4.5	1.6	0.42	0.98
5.5	1.6	0.42	0.92
6.5	1.7	0.43	0.91
7.5	1.5	0.36	0.93
8.5	1.5	0.34	0.91
9.5	1.5	0.35	0.75
11.5	1.4	0.35	0.86
14.5	1.3	0.30	0.69
17.5	1.1	0.29	0.92
20.5	0.9	0.30	1.0
23.5	1.0	0.31	0.77
26.5	0.8	0.32	0.92

3.3 EAST (MC#24 ^A , Arabian Sea)			
BSI [%]	Al ₂ O ₃ [%]	k [h ⁻¹]	b [h ⁻¹]
0.25	2.5	0.47	0.72
0.75	2.3	0.58	0.98
1.5	2.4	0.55	0.83
2.5	1.9	0.46	0.80
3.5	1.9	0.46	0.77
4.5	2.0	0.46	0.79
5.5	1.7	0.40	0.80
6.5	1.7	0.38	0.81
7.5	1.7	0.37	0.84
8.5	1.7	0.36	0.85
9.5	1.3	0.21	0.46
11.5	1.2	0.19	0.32
14.5	1.5	0.29	0.34
17.5	1.5	0.28	0.33
20.5	1.4	0.25	0.36
23.5	1.3	0.23	0.37
26.5	1.4	0.16	0.35

3.4 CAST (MC#29 ^A , Arabian Sea)			
BSI [%]	Al ₂ O ₃ [%]	k [h ⁻¹]	b [h ⁻¹]
0.25	2.7	0.47	1.97
0.75	2.4	0.57	1.69
1.5	2.5	0.57	1.66
2.5	2.7	0.49	1.35
3.5	1.6	0.40	1.54
4.5	1.8	0.45	1.32
5.5	2.1	0.40	1.09
6.5	1.5	0.37	1.50
7.5	1.4	0.35	1.33
8.5	1.4	0.36	1.44
9.5	1.4	0.33	1.44
11.5	1.1	0.31	1.26
14.5	0.8	0.24	1.24
17.5	0.8	0.24	0.85
22.5	0.7	0.24	0.48
27.5	0.7	0.30	0.44

A.3.14 Results from alkaline leaching experiments (0.032 N NaOH, T = 85°C). BSi [%]: Opal content (including 10 wt% H₂O after MORTLOCK and FROELICH, 1989); Al₂O₃ [%]: Al release (given as Al₂O₃ release during the first 4 h of opal dissolution; k = k_{NaOH}: alkaline reactivity rate constant, b = b_{NaOH}: non-biosiliceous rate constant (Eq. 3.15, Sect. 2.5.4.3). For locations see Figure 2.1 and Table. 2.1.

3.5 SAST (MC#14^{Al}, Arabian Sea)

	BSi [wt.%]	Al ₂ O ₃ [wt.%]	k [h ⁻¹]	b [h ⁻¹]
0.25	2.3	0.63	0.49	0.09
0.75	2.1	0.62	0.44	0.07
1.5	2.2	0.57	0.38	0.06
2.5	2.3	0.53	0.32	0.06
3.5	2.2	0.54	0.30	0.06
4.5	1.9	0.54	0.41	0.07
5.5	1.3	0.49	0.52	0.09
6.5	1.6	0.45	0.37	0.08
7.5	1.7	0.43	0.30	0.07
8.5	1.8	0.43	0.26	0.07
9.5	1.3	0.38	0.42	0.06
11.5	1.8	0.37	0.24	0.06
14.5	1.5	0.36	0.36	0.07
17.5	1.6	0.36	0.32	0.06
20.5	1.2	0.36	0.38	0.08
23.5	1.8	0.46	0.33	0.08
26.5	1.5	0.40	0.37	0.08
29.5	1.7	0.41	0.34	0.07

4. MC-1-3 (Juan de Fuca Ridge)

	BSi [wt.%]	Al ₂ O ₃ [wt.%]	k [h ⁻¹]	b [h ⁻¹]
0.25	9.9	1.5	3.3	0.14
0.75	9.3	1.5	2.9	0.13
1.5	8.8	1.5	3.1	0.15
2.5	9.3	1.5	2.6	0.16
3.5	9.2	1.4	2.5	0.17
4.5	9.4	1.4	2.9	0.15
5.5	9.4	1.4	2.9	0.15
6.5	9.4	1.4	2.8	0.15
7.5	9.7	1.4	2.8	0.16
8.5	9.5	1.5	2.7	0.15
9.5	9.7	1.3	2.9	0.17
11.5	8.8	1.3	2.8	0.15
14.5	7.1	1.1	2.7	0.14
17.5	6.5	1.1	2.1	0.13
20.5	5.6	1.1	1.8	0.13
423	1.9	0.94	1.0	0.12

6.1. PS-2283-6 (Scotia Sea)

	BSi [wt.%]	Al ₂ O ₃ [wt.%]	k [h ⁻¹]	b [h ⁻¹]
0.5	23	0.55	0.91	0.31
1.5	27	0.50	1.1	0.30
2.5	34	0.60	1.0	0.26
3.5	39	0.59	0.94	0.30
4.5	41	0.43	1.0	0.33
6.25	44	0.38	0.98	0.32

5. MC-145 (Juan de Fuca Ridge)

	BSi [wt.%]	Al ₂ O ₃ [wt.%]	k [h ⁻¹]	b [h ⁻¹]
0.25	20	2.5	2.4	0.25
0.75	19	2.6	2.8	0.28
1.5	18	2.6	2.9	0.25
2.5	18	2.6	2.5	0.25
3.5	17	2.3	2.4	0.22
4.5	18	2.5	2.5	0.29
6.5	16	2.0	1.6	0.25
7.5	18	2.3	2.5	0.27
8.75	15	2.1	1.8	0.25
9.75	16	2.0	2.5	0.24
11.5	14	1.7	2.4	0.20
16	15		2.3	0.20
22	16	1.4	2.0	0.21
24	15	1.4	1.4	0.19
25	16		1.2	0.18
26	21	1.3	0.96	0.15
27	17	1.2	1.0	0.18
28	21	1.2	0.86	0.14
30	24	1.2	1.1	0.19

6. 2. PS-2299, untreated (Scotia Sea)

	BSi [wt.%]	Al ₂ O ₃ [wt.%]	k [h ⁻¹]	b [h ⁻¹]
0.5	51.1	0.72	0.95	0.12
1.5	48.2	0.61	0.91	0.07
2.5	54.2	0.71	0.89	0.03
3.5	52.8	0.67	0.89	0.04
4.5	52.0	0.63	0.94	0.07
6.25	52.6	0.69	0.82	0.03
8.75	50.7	0.71	0.83	0.05
11.25	48.9	0.68	0.76	0.00
13.75	49.9	0.76	0.79	0.08
16.25	49.3	0.72	0.79	0.06
18.75	47.9	0.82	0.77	0.10
22.5	48.0	0.86	0.74	0.09

PS-2299, acid-cleaned (Scotia Sea)

0.5	66.3		1.46	0.18
1.5				
2.5	65.8		1.54	0.15
3.5	70.5		1.56	0.24
4.5	72.7		1.27	0.13
6.25	68.1		1.53	0.16
8.75	69.0		1.35	0.18
11.25	67.4		1.31	0.17
13.75	69.3		1.54	0.17
16.25	67.9		1.27	0.16
18.75	68.1		1.42	0.24
22.5	65.1		1.46	0.28

6.3. PS-2312-1 (Scotia Sea)

	BSi [wt.%]	Al ₂ O ₃ [wt.%]	k [h ⁻¹]	b [h ⁻¹]
0.5	59.9		1.2	0.02
1.5	65.1		1.3	0.08
2.5	62.1		1.4	0.12
3.5	62.8		1.4	0.13
4.5	59.9		1.3	0.07
6.25	63.1		1.2	0.15
8.75	61.1		1.2	0.15
11.25	63.0		1.2	0.12
13.75	65.1		1.2	0.16
16.25	64.7		1.2	0.05
18.75	66.9		1.1	0.05
21.25	62.7		1.0	0.15

6.4. PS-2314-1, untreated (Scotia Sea)

	BSi [wt.%]	Al ₂ O ₃ [wt.%]	k [h ⁻¹]	b [h ⁻¹]
0.5	48.1	0.51	0.97	0.08
1.5	47.9	0.46	0.98	0.06
2.5	47.9	0.52	0.98	0.14
3.5	47.7	0.44	0.97	0.05
4.5	50.8	0.48	1.00	0.12
6.25	50.8	0.48	0.93	0.08
8.75	48.1	0.49	0.93	0.07
11.25	54.4	0.51	1.00	0.07
13.75	53.8	0.49	0.88	0.04
16.25	52.3	0.49	0.81	0.07
18.75	52.4	0.43	0.86	0.06
22.5	56.1	0.50	0.75	0.03

PS-2314-1, acid-cleaned (Scotia Sea)

0.5	68.5		1.55	0.25
1.5	69.1		1.44	0.19
2.5	65.0		1.50	0.27
3.5	65.9		1.53	0.23
4.5	70.0		1.43	0.15
6.25	63.9		1.48	0.20
8.75	71.7		1.43	0.16
11.25	70.3		1.79	0.21
13.75	71.3		1.47	0.22
16.25	71.1		1.34	0.19
18.75	69.9		1.40	0.19
22.5	67.1		1.34	0.12

Folgende Hefte der Reihe „Berichte zur Polarforschung“ sind bisher erschienen:

- **Sonderheft Nr. 1/1981** – „Die Antarktis und ihr Lebensraum“
Eine Einführung für Besucher – Herausgegeben im Auftrag von SCAR
- **Heft Nr. 1/1982** – „Die Filchner-Schelfeis-Expedition 1980/81“
zusammengestellt von Heinz Köhnen
- **Heft Nr. 2/1982** – „Deutsche Antarktis-Expedition 1980/81 mit FS ‚Meteor‘“
First International BIOMASS Experiment (FIBEX) – Liste der Zooplankton- und Mikronektonnetzfüänge
zusammengestellt von Norbert Klages
- **Heft Nr. 3/1982** – „Digitale und analoge Krill-Echolot-Rohdatenerfassung an Bord des Forschungsschiffes ‚Meteor‘“ (im Rahmen von FIBEX 1980/81, Fahrtrabschnitt ANT III), von Bodo Morgenstern
- **Heft Nr. 4/1982** – „Filchner-Schelfeis-Expedition 1980/81“
Liste der Planktonfänge und Lichtstärkemessungen
zusammengestellt von Gerd Hubold und H. Eberhard Drescher
- **Heft Nr. 5/1982** – „Joint Biological Expedition on RRS ‚John Biscoe‘, February 1982“
by G. Hempel and R. B. Heywood
- **Heft Nr. 6/1982** – „Antarktis-Expedition 1981/82 (Unternehmen ‚Eiswarte‘)“
zusammengestellt von Gode Gravenhorst
- **Heft Nr. 7/1982** – „Marin-Biologisches Begleitprogramm zur Standorterkundung 1979/80 mit MS ‚Polarstern‘ (Pre-Site Survey)“ – Stationslisten der Mikronekton- und Zooplanktonfänge sowie der Bodenfischerei
zusammengestellt von R. Schneppenheim
- **Heft Nr. 8/1983** – „The Post-Fibex Data Interpretation Workshop“
by D. L. Cram and J.-C. Freytag with the collaboration of J. W. Schmidt, M. Mall, R. Kresse, T. Schwinghammer
- **Heft Nr. 9/1983** – „Distribution of some groups of zooplankton in the inner Weddell Sea in summer 1979/80“
by I. Hempel, G. Hubold, B. Kaczmaruk, R. Keller, R. Weigmann-Haass
- **Heft Nr. 10/1983** – „Fluor im antarktischen Ökosystem“ – DFG-Symposium November 1982
zusammengestellt von Dieter Adelung
- **Heft Nr. 11/1983** – „Joint Biological Expedition on RRS ‚John Biscoe‘, February 1982 (II)“
Data of micronekton and zooplankton hauls, by Uwe Piatkowski
- **Heft Nr. 12/1983** – „Das biologische Programm der ANTARKTIS-I-Expedition 1983 mit FS ‚Polarstern‘“
Stationslisten der Plankton-, Benthos- und Grundschleppnetzfüänge und Liste der Probenahme an Robben und Vögeln, von H. E. Drescher, G. Hubold, U. Piatkowski, J. Plötz und J. Vofß
- **Heft Nr. 13/1983** – „Die Antarktis-Expedition von MS ‚Polarbjörn‘ 1982/83“ (Sommerkampagne zur Atka-Bucht und zu den Kraul-Bergen), zusammengestellt von Heinz Köhnen
- **Sonderheft Nr. 2/1983** – „Die erste Antarktis-Expedition von FS ‚Polarstern‘ (Kapstadt, 20. Januar 1983 – Rio de Janeiro, 25. März 1983)“, Bericht des Fahrtleiters Prof. Dr. Gotthilf Hempel
- **Sonderheft Nr. 3/1983** – „Sicherheit und Überleben bei Polarexpeditionen“
zusammengestellt von Heinz Köhnen
- **Heft Nr. 14/1983** – „Die erste Antarktis-Expedition (ANTARKTIS I) von FS ‚Polarstern‘ 1982/83“
herausgegeben von Gotthilf Hempel
- **Sonderheft Nr. 4/1983** – „On the Biology of Krill *Euphausia superba*“ – Proceedings of the Seminar and Report of the Krill Ecology Group, Bremerhaven 12. - 16. May 1983, edited by S. B. Schnack
- **Heft Nr. 15/1983** – „German Antarctic Expedition 1980/81 with FRV ‚Walther Herwig‘ and RV ‚Meteor‘“ – First International BIOMASS Experiment (FIBEX) – Data of micronekton and zooplankton hauls
by Uwe Piatkowski and Norbert Klages
- **Sonderheft Nr. 5/1984** – „The observatories of the Georg von Neumayer Station“, by Ernst Augstein
- **Heft Nr. 16/1984** – „FIBEX cruise zooplankton data“
by U. Piatkowski, I. Hempel and S. Rakusa-Suszczewski
- **Heft Nr. 17/1984** – Fahrtbericht (cruise report) der ‚Polarstern‘-Reise ARKTIS I, 1983“
von E. Augstein, G. Hempel und J. Thiede
- **Heft Nr. 18/1984** – „Die Expedition ANTARKTIS II mit FS ‚Polarstern‘ 1983/84“,
Bericht von den Fahrtrabschnitten 1, 2 und 3, herausgegeben von D. Fütterer
- **Heft Nr. 19/1984** – „Die Expedition ANTARKTIS II mit FS ‚Polarstern‘ 1983/84“,
Bericht vom Fahrtrabschnitt 4, Punta Arenas-Kapstadt (Ant-II/4), herausgegeben von H. Köhnen
- **Heft Nr. 20/1984** – „Die Expedition ARKTIS II des FS ‚Polarstern‘ 1984, mit Beiträgen des FS ‚Valdivia‘ und des Forschungslugzeuges ‚Falcon 20‘ zum Marginal Ice Zone Experiment 1984 (MIZEX)“
von E. Augstein, G. Hempel, J. Schwarz, J. Thiede und W. Weigel
- **Heft Nr. 21/1985** – „Euphausiid larvae in plankton from the vicinity of the Antarctic Peninsula, February 1982“ by Sigrid Marschall and Elke Mizdalski
- **Heft Nr. 22/1985** – „Maps of the geographical distribution of macrozooplankton in the Atlantic sector of the Southern Ocean“ by Uwe Piatkowski
- **Heft Nr. 23/1985** – „Untersuchungen zur Funktionsmorphologie und Nahrungsaufnahme der Larven des Antarktischen Krills *Euphausia superba* Dana“ von Hans-Peter Marschall

- Heft Nr. 24/1985** – „Untersuchungen zum Periglazial auf der König-Georg-Insel Südshetlandinseln/ Antarktika. Deutsche physiogeographische Forschungen in der Antarktis. – Bericht über die Kampagne 1983/84“ von Dietrich Barsch, Wolf-Dieter Blümel, Wolfgang Flügel, Roland Mäusbacher, Gerhard Stäblein, Wolfgang Zick
- **Heft Nr. 25/1985** – „Die Expedition ANTARKTIS III mit FS ‚Polarstern‘ 1984/1985“ herausgegeben von Gotthilf Hempel.
 - **Heft Nr. 26/1985** – “The Southern Ocean”; A survey of oceanographic and marine meteorological research work by Hellmer et al.
 - **Heft Nr. 27/1986** – „Spätpleistozäne Sedimentationsprozesse am antarktischen Kontinentalhang vor Kapp Norvegia, östliche Weddell-See“ von Hannes Grobe
 - Heft Nr. 28/1986** – „Die Expedition ARKTIS III mit ‚Polarstern‘ 1985 mit Beiträgen der Fahrtteilnehmer, herausgegeben von Rainer Gersonde
 - **Heft Nr. 29/1986** – „5 Jahre Schwerpunktprogramm ‚Antarktisforschung‘ der Deutschen Forschungsgemeinschaft.“ Rückblick und Ausblick. Zusammenge stellt von Gotthilf Hempel, Sprecher des Schwerpunktprogramms
 - Heft Nr. 30/1986** – “The Meteorological Data of the Georg-von-Neumayer-Station for 1981 and 1982” by Marianne Gube and Friedrich Obleitner
 - **Heft Nr. 31/1986** – „Zur Biologie der Jugendstadien der Notothenioidei (Pisces) an der Antarktischen Halbinsel“ von A. Kellermann
 - **Heft Nr. 32/1986** – „Die Expedition ANTARKTIS IV mit FS ‚Polarstern‘ 1985/86“ mit Beiträgen der Fahrtteilnehmer, herausgegeben von Dieter Fütterer
 - Heft Nr. 33/1987** – „Die Expedition ANTARKTIS-IV mit FS ‚Polarstern‘ 1985/86 – Bericht zu den Fahrtabschnitten ANT-IV/3-4“ von Dieter Karl Fütterer
 - Heft Nr. 34/1987** – „Zoogeographische Untersuchungen und Gemeinschaftsanalysen an antarktischen Makroplankton“ von U. Piatkowski
 - Heft Nr. 35/1987** – „Zur Verbreitung des Meso- und Makrozooplanktons in Oberflächenwasser der Weddell See (Antarktis)“ von E. Boysen-Ennen
 - Heft Nr. 36/1987** – „Zur Nahrungs- und Bewegungsphysiologie von *Salpa thompsoni* und *Salpa fusiformis*“ von M. Reinke
 - Heft Nr. 37/1987** – “The Eastern Weddell Sea Drifting Buoy Data Set of the Winter Weddell Sea Project (WWSP)” 1986 by Heinrich Hoerber und Marianne Gube-Lehnhardt
 - Heft Nr. 38/1987** – “The Meteorological Data of the Georg von Neumayer Station for 1983 and 1984” by M. Gube-Lehnhardt
 - Heft Nr. 39/1987** – „Die Winter-Expedition mit FS ‚Polarstern‘ in die Antarktis (ANT V/1-3)“ herausgegeben von Sigrud Schnack-Schiel
 - Heft Nr. 40/1987** – “Weather and Synoptic Situation during Winter Weddell Sea Project 1986 (ANT V/2) July 16 - September 10, 1986” by Werner Rabe
 - Heft Nr. 41/1988** – „Zur Verbreitung und Ökologie der Seegurken im Weddellmeer (Antarktis)“ von Julian Gut
 - Heft Nr. 42/1988** – “The zooplankton community in the deep bathyal and abyssal zones of the eastern North Atlantic” by Werner Beckmann
 - **Heft Nr. 43/1988** – “Scientific cruise report of Arctic Expedition ARK IV/3” Wissenschaftlicher Fahrtbericht der Arktis-Expedition ARK IV/3, compiled by Jörn Thiede
 - **Heft Nr. 44/1988** – “Data Report for FV ‘Polarstern’ Cruise ARK IV/1, 1987 to the Arctic and Polar Fronts” by Hans-Jürgen Hirche
 - Heft Nr. 45/1988** – „Zoogeographie und Gemeinschaftsanalyse des Makrozoobenthos des Weddellmeeres (Antarktis)“ von Joachim Voß
 - Heft Nr. 46/1988** – “Meteorological and Oceanographic Data of the Winter-Weddell-Sea Project 1986 (ANT V/3)“ by Eberhard Fahrback
 - Heft Nr. 47/1988** – „Verteilung und Herkunft glazial-mariner Gerölle am Antarktischen Kontinentalrand des östlichen Weddellmeeres“ von Wolfgang Oskierski
 - Heft Nr. 48/1988** – „Variationen des Erdmagnetfeldes an der GvN-Station“ von Arnold Brodscholl
 - **Heft Nr. 49/1988** – „Zur Bedeutung der Lipide im antarktischen Zooplankton“ von Wilhelm Hagen
 - **Heft Nr. 50/1988** – „Die gezeitenbedingte Dynamik des Ekström-Schelfeises, Antarktis“ von Wolfgang Kobarg
 - Heft Nr. 51/1988** – „Ökomorphologie nototheniider Fische aus dem Weddellmeer, Antarktis“ von Werner Ekau
 - Heft Nr. 52/1988** – „Zusammensetzung der Bodenfauna in der westlichen Fram-Straße“ von Dieter Piepenburg
 - **Heft Nr. 53/1988** – „Untersuchungen zur Ökologie des Phytoplanktons im südöstlichen Weddellmeer (Antarktis) im Jan./Febr. 1985“ von Eva-Maria Nöthig
 - Heft Nr. 54/1988** – „Die Fischfauna des östlichen und südlichen Weddellmeeres: geographische Verbreitung, Nahrung und trophische Stellung der Fischarten“ von Wiebke Schwarzbach
 - Heft Nr. 55/1988** – “Weight and length data of zooplankton in the Weddell Sea in austral spring 1986 (Ant. V/3)“ by Elke Mizdalski
 - Heft Nr. 56/1989** – “Scientific cruise report of Arctic expeditions ARK IV/1, 2 & 3” by G. Krause, J. Meinke und J. Thiede

- Heft Nr. 57/1989** – „Die Expedition ANTARKTIS V mit FS ‚Polarstern‘ 1986/87“
Bericht von den Fahrtabschnitten ANT V/4-5 von H. Miller und H. Oerter
- **Heft Nr. 58/1989** – „Die Expedition ANTARKTIS VI mit FS ‚Polarstern‘ 1987/88“
von D. K. Fütterer
 - Heft Nr. 59/1989** – „Die Expedition ARKTIS V/1a, 1b und 2 mit FS ‚Polarstern‘ 1988“
von M. Spindler
 - Heft Nr. 60/1989** – „Ein zweidimensionales Modell zur thermohalinen Zirkulation unter dem Schelfeis“
von H. H. Hellmer
 - Heft Nr. 61/1989** – „Die Vulkanite im westlichen und mittleren Neuschwabenland,
Vestjella und Ahlmannryggen, Antarktika“ von M. Peters
 - **Heft Nr. 62/1989** – „The Expedition ANTARKTIS VII/1 and 2 (EPOS I) of RV ‚Polarstern‘
in 1988/89“, by I. Hempel
 - Heft Nr. 63/1989** – „Die Eisalgenflora des Weddellmeeres (Antarktis): Artenzusammensetzung und Biomasse
sowie Ökophysiologie ausgewählter Arten“ von Annette Bartsch
 - Heft Nr. 64/1989** – „Meteorological Data of the G.-v.-Neumayer-Station (Antarctica)“ by L. Helmes
 - Heft Nr. 65/1989** – „Expedition Antarktis VII/3 in 1988/89“ by I. Hempel, P. H. Schalk, V. Smetacek
 - Heft Nr. 66/1989** – „Geomorphologisch-glaziologische Detailkartierung
des arid-hochpolaren Borgmassivet, Neuschwabenland, Antarktika“ von Karsten Brunk
 - Heft Nr. 67/1990** – „Identification key and catalogue of larval Antarctic fishes“,
edited by Adolf Kellermann
 - Heft Nr. 68/1990** – „The Expedition Antarktis VII/4 (Epos leg 3) and VII/5 of RV ‚Polarstern‘ in 1989“,
edited by W. Arntz, W. Ernst, I. Hempel
 - Heft Nr. 69/1990** – „Abhängigkeiten elastischer und rheologischer Eigenschaften des Meereises vom
Eisgefüge“, von Harald Hellmann
 - **Heft Nr. 70/1990** – „Die besetzten benthischen Mollusken (Gastropoda und Bivalvia) des
Weddellmeeres, Antarktis“, von Stefan Hain
 - Heft Nr. 71/1990** – „Sedimentologie und Paläomagnetik an Sedimenten der Maudkuppe (Nordöstliches
Weddellmeer)“, von Dieter Cordes
 - Heft Nr. 72/1990** – „Distribution and abundance of planktonic copepods (Crustacea) in the Weddell Sea
in summer 1980/81“, by F. Kurbjweit and S. Ali-Khan
 - Heft Nr. 73/1990** – „Zur Frühdiagenese von organischem Kohlenstoff und Opal in Sedimenten des südlichen
und östlichen Weddellmeeres“, von M. Schlüter
 - Heft Nr. 74/1990** – „Expeditionen ANTARKTIS-VIII/3 und VIII/4 mit FS ‚Polarstern‘ 1989“
von Rainer Gersonde und Gotthilf Hempel
 - Heft Nr. 75/1991** – „Quartäre Sedimentationsprozesse am Kontinentalhang des Süd-Orkey-Plateaus im
nordwestlichen Weddellmeer (Antarktis)“, von Sigrun Grünig
 - Heft Nr. 76/1990** – „Ergebnisse der faunistischen Arbeiten im Benthal von King George Island
(Südshetlandinseln, Antarktis)“, von Martin Rauschert
 - Heft Nr. 77/1990** – „Verteilung von Mikroplankton-Organismen nordwestlich der Antarktischen Halbinsel
unter dem Einfluß sich ändernder Umweltbedingungen im Herbst“, von Heinz Klöser
 - Heft Nr. 78/1991** – „Hochauflösende Magnetostratigraphie spätquartärer Sedimente arktischer
Meeresgebiete“, von Norbert R. Nowaczyk
 - Heft Nr. 79/1991** – „Ökophysiologische Untersuchungen zur Salinitäts- und Temperaturtoleranz
antarktischer Grünalgen unter besonderer Berücksichtigung des β -Dimethylsulfoniumpropionat
(DMSP) - Stoffwechsels“, von Ulf Karsten
 - Heft Nr. 80/1991** – „Die Expedition ARKTIS VII/1 mit FS ‚Polarstern‘ 1990“,
herausgegeben von Jörn Thiede und Gotthilf Hempel
 - Heft Nr. 81/1991** – „Paläoglaziologie und Paläozeanographie im Spätquartär am Kontinentalrand des
südlichen Weddellmeeres, Antarktis“, von Martin Melles
 - Heft Nr. 82/1991** – „Quantifizierung von Meeresseigenschaften: Automatische Bildanalyse von
Dünnschnitten und Parametrisierung von Chlorophyll- und Salzgehaltsverteilungen“, von Hajo Eicken
 - Heft Nr. 83/1991** – „Das Fließen von Schelfeisen - numerische Simulationen
mit der Methode der finiten Differenzen“, von Jürgen Determann
 - Heft Nr. 84/1991** – „Die Expedition ANTARKTIS-VIII/1-2, 1989 mit der Winter Weddell Gyre Study
der Forschungsschiffe ‚Polarstern‘ und ‚Akademik Fedorov‘“, von Ernst Augstein,
Nikolai Bagriantsev und Hans Werner Schenke
 - Heft Nr. 85/1991** – „Zur Entstehung von Unterwassereis und das Wachstum und die Energiebilanz
des Meereises in der Atka Bucht, Antarktis“, von Josef Kipfstuhl
 - **Heft Nr. 86/1991** – „Die Expedition ANTARKTIS-VIII mit FS ‚Polarstern‘ 1989/90. Bericht vom
Fahrtabschnitt ANT-VIII/5“, von Heinz Miller und Hans Oerter
 - Heft Nr. 87/1991** – „Scientific cruise reports of Arctic expeditions ARK VI/1-4 of RV ‚Polarstern‘
in 1989“, edited by G. Krause, J. Meincke & H. J. Schwarz
 - Heft Nr. 88/1991** – „Zur Lebensgeschichte dominanter Copepodenarten (*Calanus finmarchicus*,
C. glacialis, *C. hyperboreus*, *Metridia longa*) in der Framstraße“, von Sabine Diel

- Heft Nr. 89/1991** – „Detaillierte seismische Untersuchungen am östlichen Kontinentalrand des Weddell-Meeress vor Kapp Norvegia, Antarktis“, von Norbert E. Kaul
- Heft Nr. 90/1991** – „Die Expedition ANTARKTIS-VIII mit FS ‚Polarstern‘ 1989/90. Bericht von den Fahrtabschnitten ANT-VIII/6-7“, herausgegeben von Dieter Karl Fütterer und Otto Schrems
- Heft Nr. 91/1991** – „Blood physiology and ecological consequences in Weddell Sea fishes (Antarctica)“, by Andreas Kunzmann
- Heft Nr. 92/1991** – „Zur sommerlichen Verteilung des Mesozooplanktons im Nansen-Becken, Nordpolarmeer“, von Nicolai Mumm
- Heft Nr. 93/1991** – „Die Expedition ARKTIS VII mit FS ‚Polarstern‘, 1990. Bericht vom Fahrtabschnitt ARK VII/2“, herausgegeben von Gunther Krause
- Heft Nr. 94/1991** – „Die Entwicklung des Phytoplanktons im östlichen Weddellmeer (Antarktis) beim Übergang vom Spätwinter zum Frühjahr“, von Renate Scharek
- Heft Nr. 95/1991** – „Radioisotopenstratigraphie, Sedimentologie und Geochemie jungquartärer Sedimente des östlichen Arktischen Ozeans“, von Horst Bohrmann
- Heft Nr. 96/1991** – „Holozäne Sedimentationsentwicklung im Scoresby Sund, Ost-Grönland“, von Peter Marienfeld
- Heft Nr. 97/1991** – „Strukturelle Entwicklung und Abkühlungsgeschichte von Heimfrontfjella (Westliches Dronning Maud Land/Antarktika)“, von Joachim Jacobs
- Heft Nr. 98/1991** – „Zur Besiedlungsgeschichte des antarktischen Schelfes am Beispiel der Isopoda (Crustacea, Malacostraca)“, von Angelika Brandt
- **Heft Nr. 99/1992** – „The Antarctic ice sheet and environmental change: a three-dimensional modelling study“, by Philippe Huybrechts
 - **Heft Nr. 100/1992** – „Die Expeditionen ANTARKTIS IX/1-4 des Forschungsschiffes ‚Polarstern‘ 1990/91“ herausgegeben von Ulrich Bathmann, Meinhard Schulz-Baldes, Eberhard Fahrbach, Victor Smetacek und Hans-Wolfgang Hubberten
 - Heft Nr. 101/1992** – „Wechselbeziehungen zwischen Schwermetallkonzentrationen (Cd, Cu, Pb, Zn) im Meerwasser und in Zooplanktonorganismen (Copepoda) der Arktis und des Atlantiks“, von Christa Pohl
 - Heft Nr. 102/1992** – „Physiologie und Ultrastruktur der antarktischen Grünalge *Prasiola crispa* ssp. *antarctica* unter osmotischem Streß und Austrocknung“, von Andreas Jacob
 - **Heft Nr. 103/1992** – „Zur Ökologie der Fische im Weddellmeer“, von Gerd Hubold
 - Heft Nr. 104/1992** – „Mehrkanalige adaptive Filter für die Unterdrückung von multiplen Reflexionen in Verbindung mit der freien Oberfläche in marinen Seismogrammen“, von Andreas Rosenberger
 - Heft Nr. 105/1992** – „Radiation and Eddy Flux Experiment 1991 (REFLEX I)“, von Jörg Hartmann, Christoph Kottmeier und Christian Wamser
 - Heft Nr. 106/1992** – „Ostracoden im Epipelagial vor der Antarktischen Halbinsel - ein Beitrag zur Systematik sowie zur Verbreitung und Populationsstruktur unter Berücksichtigung der Saisonalität“, von Rüdiger Kock
 - **Heft Nr. 107/1992** – „ARCTIC '91: Die Expedition ARK-VIII/3 mit FS ‚Polarstern‘ 1991“, von Dieter K. Fütterer
 - Heft Nr. 108/1992** – „Dehnungsbeben an einer Störungszone im Ekström-Schelfeis nördlich der Georg-von-Neumayer-Station, Antarktis. – Eine Untersuchung mit seismologischen und geodätischen Methoden“, von Uwe Nixdorf.
 - **Heft Nr. 109/1992** – „Spätquartäre Sedimentation am Kontinentalrand des südöstlichen Weddellmeeres, Antarktis“, von Michael Weber.
 - **Heft Nr. 110/1992** – „Sedimentfazies und Bodenwasserstrom am Kontinentalhang des norwestlichen Weddellmeeres“, von Isa Brehme.
 - Heft Nr. 111/1992** – „Die Lebensbedingungen in den Solekanälchen des antarktischen Meereises“, von Jürgen Weissenberger.
 - Heft Nr. 112/1992** – „Zur Taxonomie von rezenten benthischen Foraminiferen aus dem Nansen Becken, Arktischer Ozean“, von Jutta Wollenburg.
 - Heft Nr. 113/1992** – „Die Expedition ARKTIS VIII/1 mit FS ‚Polarstern‘ 1991“, herausgegeben von Gerhard Kattner.
 - **Heft Nr. 114/1992** – „Die Gründungsphase deutscher Polarforschung, 1865 - 1875“, von Reinhard A. Krause.
 - Heft Nr. 115/1992** – „Scientific Cruise Report of the 1991 Arctic Expedition ARK VIII/2 of RV ‚Polarstern‘ (EPOS II)“, by Eike Racher.
 - Heft Nr. 116/1992** – „The Meteorological Data of the Georg-von-Neumayer-Station (Antarctica) for 1988, 1989, 1990 and 1991“, by Gert König-Langlo.
 - Heft Nr. 117/1992** – „Petrogenese des metamorphen Grundgebirges der zentralen Heimfrontfjella (westliches Dronning Maud Land / Antarktis)“, von Peter Schulze.
 - Heft Nr. 118/1993** – „Die mafischen Gänge der Shackleton Range / Antarktika: Petrographie, Geochemie, Isotopengeochemie und Paläomagnetik“, von Rüdiger Hotten.
 - **Heft Nr. 119/1993** – „Gefrierschutz bei Fischen der Polarmeere“, von Andreas P. A. Wöhrmann.
 - **Heft Nr. 120/1993** – „East Siberian Arctic Region Expedition '92: The Laptev Sea - its Significance for Arctic Sea-Ice Formation and Transpolar Sediment Flux“, by D. Dethleff, D. Nürnberg, E. Reimnitz, M. Saarso and Y. P. Sacchenko. – „Expedition to Novaja Zemlja and Franz Josef Land with RV ‚Dalnie Zelentsy‘“, by D. Nürnberg and E. Groth.

- * Heft Nr. 121/1993 – „Die Expedition ANTARKTIS X/3 mit FS ‚Polarstern‘ 1992“, herausgegeben von Michael Spindler, Gerhard Dieckmann und David Thomas
- Heft Nr. 122/1993 – „Die Beschreibung der Korngestalt mit Hilfe der Fourier-Analyse: Parametrisierung der morphologischen Eigenschaften von Sedimentpartikeln“, von Michael Diepenbroek.
- * Heft Nr. 123/1993 – „Zerstörungsfreie hochauflösende Dichteuntersuchungen mariner Sedimente“, von Sebastian Gerland.
- Heft Nr. 124/1993 – „Umsatz und Verteilung von Lipiden in arktischen marinen Organismen unter besonderer Berücksichtigung unterer trophischer Stufen“, von Martin Graeve.
- Heft Nr. 125/1993 – „Ökologie und Respiration ausgewählter arktischer Bodenfischarten“, von Christian F. von Dorrien.
- Heft Nr. 126/1993 – „Quantitative Bestimmung von Paläoumweltparametern des Antarktischen Oberflächenwassers im Spätquartier anhand von Transferfunktionen mit Diatomeen“, von Ulrich Zielinski
- * Heft Nr. 127/1993 – „Sedimenttransport durch das arktische Meereis: Die rezente lithogene und biogene Materialfracht“, von Ingo Wollenburg.
- Heft Nr. 128/1993 – „Cruise ANTARKTIS X/3 of RV ‚Polarstern‘: CTD-Report“, von Marek Zwierz.
- Heft Nr. 129/1993 – „Reproduktion und Lebenszyklen dominanter Copepodenarten aus dem Weddellmeer, Antarktis“, von Frank Kurbjeweit
- Heft Nr. 130/1993 – „Untersuchungen zu Temperaturregime und Massenhaushalt des Filchner-Ronne-Schelfeises, Antarktis, unter besonderer Berücksichtigung von Anfrrier- und Abschmelzprozessen“, von Klaus Grosfeld
- Heft Nr. 131/1993 – „Die Expedition ANTARKTIS X/5 mit FS ‚Polarstern‘ 1992“, herausgegeben von Rainer Gersonde
- Heft Nr. 132/1993 – „Bildung und Abgabe kurzkettiger halogener Kohlenwasserstoffe durch Makroalgen der Polarregionen“, von Frank Laturnus
- Heft Nr. 133/1994 – „Radiation and Eddy Flux Experiment 1993 (REFLEX II)“, by Christoph Kottmeier, Jörg Hartmann, Christian Wamser, Axel Bocher, Christof Lüpkes, Dietmar Freese and Wolfgang Cohrs
- * Heft Nr. 134/1994 – „The Expedition ARKTIS-IX/1“, edited by Hajo Eicken and Jens Meincke
- Heft Nr. 135/1994 – „Die Expeditionen ANTARKTIS X/6-8“, herausgegeben von Ulrich Bathmann, Victor Smetacek, Hein de Baar, Eberhard Fahrbach und Gunter Krause
- Heft Nr. 136/1994 – „Untersuchungen zur Ernährungsökologie von Kaiserpinguinen (*Aptenodytes forsteri*) und Königspinguinen (*Aptenodytes patagonicus*)“, von Klemens Pütz
- * Heft Nr. 137/1994 – „Die kälteozoische Vereisungsgeschichte der Antarktis“, von Werner U. Ehrmann
- Heft Nr. 138/1994 – „Untersuchungen stratosphärischer Aerosole vulkanischen Ursprungs und polarer stratosphärischer Wolken mit einem Mehrwellenlängen-Lidar auf Spitzbergen (79° N, 12° E)“, von Georg Beyerle
- Heft Nr. 139/1994 – „Charakterisierung der Isopodenfauna (Crustacea, Malacostraca) des Scotia-Bogens aus biogeographischer Sicht: Ein multivariater Ansatz“, von Holger Winkler.
- Heft Nr. 140/1994 – „Die Expedition ANTARKTIS X/4 mit FS ‚Polarstern‘ 1992“, herausgegeben von Peter Lemke
- Heft Nr. 141/1994 – „Satellitenaltimetrie über Eis – Anwendung des GEOSAT-Altimeters über dem Ekströmisen, Antarktis“, von Clemens Heiland
- Heft Nr. 142/1994 – „The 1993 Northeast Water Expedition. Scientific cruise report of RV ‚Polarstern‘ Arctic cruises ARK IX/2 and 3, USCG ‚Polar Bear‘ cruise NEWP and the NEWLand expedition“, edited by Hans-Jürgen Hirche and Gerhard Kattner
- Heft Nr. 143/1994 – „Detaillierte refraktionsseismische Untersuchungen im inneren Scoresby Sund Ost-Grönland“, von Notker Fechner
- Heft Nr. 144/1994 – „Russian-German Cooperation in the Siberian Shelf Seas: Geo-System Laptev Sea“, edited by Heidemarie Kassens, Hans-Wolfgang Hubberten, Sergey M. Pryamikov and Rüdiger Stein
- * Heft Nr. 145/1994 – „The 1993 Northeast Water Expedition. Data Report of RV ‚Polarstern‘ Arctic Cruises IX/2 and 3“, edited by Gerhard Kattner and Hans-Jürgen Hirche.
- Heft Nr. 146/1994 – „Radiation Measurements at the German Antarctic Station Neumayer 1982 - 1992“, by Torsten Schmidt and Gerd König-Langlo.
- Heft Nr. 147/1994 – „Krustenstrukturen und Verlauf des Kontinentalrandes im Weddell-See / Antarktis“, von Christian Hübscher.
- * Heft Nr. 148/1994 – „The expeditions NORILSK/TAYMYR 1993 and BUNGER OASIS 1993/94 of the AWI Research Unit Potsdam“, edited by Martin Melles.
- Heft Nr. 149/1994 – „Die Expedition ARCTIC '93. Der Fahrtabschnitt ARK-IX/4 mit FS ‚Polarstern‘ 1993“, herausgegeben von Dieter K. Fütterer.
- Heft Nr. 150/1994 – „Der Energiebedarf der Pygoscelis-Pinguine: eine Synopse“, von Boris M. Culik.
- Heft Nr. 151/1994 – „Russian-German Cooperation: The Transdrift I Expedition to the Laptev Sea“, edited by Heidemarie Kassens and Valeriy Y. Karpiv.
- Heft Nr. 152/1994 – „Die Expedition ANTARKTIS-X mit FS ‚Polarstern‘ 1992. Bericht von den Fahrtabschnitten / ANT-X / 1a und 2“, herausgegeben von Heinz Miller.
- Heft Nr. 153/1994 – „Aminosäuren und Huminstoffe im Stickstoffkreislauf polarer Meere“, von Ulrike Hubberten.
- Heft Nr. 154/1994 – „Regional and seasonal variability in the vertical distribution of mesozooplankton in the Greenland Sea“, by Claudio Richter.

- Heft Nr. 155/1995 – „Benthos in polaren Gewässern“, herausgegeben von Christian Wiencke und Wolf Arntz.
- Heft Nr. 156/1995 – „An adjoint model for the determination of the mean oceanic circulation, air-sea fluxes and mixing coefficients“, by Reiner Schlitzer.
- Heft Nr. 157/1995 – „Biochemische Untersuchungen zum Lipidstoffwechsel antarktischer Copepoden“, von Kirsten Fahl.
- ** Heft Nr. 158/1995 – „Die Deutsche Polarforschung seit der Jahrhundertwende und der Einfluß Erich von Drygalskis“, von Cornelia Lüdecke.
- * Heft Nr. 159/1995 – „The distribution of $\delta^{18}\text{O}$ in the Arctic Ocean: Implications for the freshwater balance of the halocline and the sources of deep and bottom waters“, by Dorothea Bauch.
- * Heft Nr. 160/1995 – „Rekonstruktion der spätquartären Tiefenwasserzirkulation und Produktivität im östlichen Südatlantik anhand von benthischen Foraminiferenvergesellschaftungen“, von Gerhard Schmiedl.
- Heft Nr. 161/1995 – „Der Einfluß von Salinität und Lichtintensität auf die Osmolytkonzentrationen, die Zellvolumina und die Wachstumsraten der antarktischen Eisdiatomeen *Chaetoceros sp.* und *Navicula sp.* unter besonderer Berücksichtigung der Aminosäure Prolin“, von Jürgen Nothnagel.
- Heft Nr. 162/1995 – „Meereistransportiertes lithogenes Feinmaterial in spätquartären Tiefseesedimenten des zentralen östlichen Arktischen Ozeans und der Framstraße“, von Thomas Letzig.
- Heft Nr. 163/1995 – „Die Expedition ANTARKTIS-XI/2 mit FS ‚Polarstern‘ 1993/94“, herausgegeben von Rainer Gersonde.
- Heft Nr. 164/1995 – „Regionale und altersabhängige Variation gesteinsmagnetischer Parameter in marinen Sedimenten der Arktis“, von Thomas Frederichs.
- Heft Nr. 165/1995 – „Vorkommen, Verteilung und Umsatz biogener organischer Spurenstoffe: Sterole in antarktischen Gewässern“, von Georg Hanke.
- Heft Nr. 166/1995 – „Vergleichende Untersuchungen eines optimierten dynamisch-thermodynamischen Meereismodells mit Beobachtungen im Weddellmeer“, von Holger Fischer.
- * Heft Nr. 167/1995 – „Rekonstruktionen von Paläo-Umweltparametern anhand von stabilen Isotopen und Faunen-Vergesellschaftungen planktischer Foraminiferen im Südatlantik“, von Hans-Stefan Niebler
- Heft Nr. 168/1995 – „Die Expedition ANTARKTIS XII mit FS ‚Polarstern‘ 1993/94. Bericht von den Fahrtabschnitten ANT XII/1 und 2“, herausgegeben von Gerhard Kattner und Dieter Karl Fütterer
- Heft Nr. 169/1995 – „Medizinische Untersuchung zur Circadianrhythmik und zum Verhalten bei Überwinterern auf einer antarktischen Forschungsstation“, von Hans Wortmann
- Heft-Nr. 170/1995 – DFG-Kolloquium: Terrestrische Geowissenschaften – Geologie und Geophysik der Antarktis.
- Heft Nr. 171/1995 – „Strukturentwicklung und Petrogenese des metamorphen Grundgebirges der nördlichen Heimfrontfjella (westliches Dronning Maud Land/Antarktika)“, von Wilfried Bauer.
- Heft Nr. 172/1995 – „Die Struktur der Erdkruste im Bereich des Scoresby Sund, Ostgrönland: Ergebnisse refraktionsseismischer und gravimetrischer Untersuchungen“, von Holger Mandler.
- Heft Nr. 173/1995 – „Paläozoische Akkretion am paläopazifischen Kontinentalrand der Antarktis in Nordvictorialand – P-T-D-Geschichte und Deformationsmechanismen im Bowers Terrane“, von Stefan Matzer.
- Heft Nr. 174/1995 – „The Expedition ARKTIS-X/2 of RV ‚Polarstern‘ in 1994“, edited by Hans-W. Hubberten
- Heft Nr. 175/1995 – „Russian-German Cooperation: The Expedition TAYMYR 1994“, edited by Christine Sievert and Gmitry Bolshiyayov.
- * Heft Nr. 176/1995 – „Russian-German Cooperation: Laptev Sea System“, edited by Heidemarie Kassens, Dieter Piepenburg, Jörn Thiede, Leonid Timokhov, Hans-Wolfgang Hubberten and Sergey M. Priamikov.
- Heft Nr. 177/1995 – „Organischer Kohlenstoff in spätquartären Sedimenten des Arktischen Ozeans: Terrigener Eintrag und marine Produktivität“, von Carsten J. Schubert
- Heft Nr. 178/1995 – „Cruise ANTARKTIS XII/4 of RV ‚Polarstern‘ in 1995: CTD-Report“, by Jüri Sildam.
- Heft Nr. 179/1995 – „Benthische Foraminiferenfaunen als Wassermassen-, Produktions- und Eisdriftanzeiger im Arktischen Ozean“, von Jutta Wollenburg.
- Heft Nr. 180/1995 – „Biogenopal und biogenes Barium als Indikatoren für spätquartäre Produktivitätsänderungen am antarktischen Kontinentalhang, atlantischer Sektor“, von Wolfgang J. Bonn.
- Heft Nr. 181/1995 – „Die Expedition ARKTIS X/1 des Forschungsschiffes ‚Polarstern‘ 1994“, herausgegeben von Eberhard Fahrbach.
- Heft Nr. 182/1995 – „Laptev Sea System: Expeditions in 1994“, edited by Heidemarie Kassens.
- Heft Nr. 183/1996 – „Interpretation digitaler Parasound Echolotaufzeichnungen im östlichen Arktischen Ozean auf der Grundlage physikalischer Sedimenteigenschaften“, von Uwe Bergmann.
- Heft Nr. 184/1996 – „Distribution and dynamics of inorganic nitrogen compounds in the troposphere of continental, coastal, marine and Arctic areas“, by María Dolores Andrés Hernández.
- Heft Nr. 185/1996 – „Verbreitung und Lebensweise der Aphroditen und Polynoiden (Polychaeta) im östlichen Weddellmeer und im Lazarevmeer (Antarktis)“, von Michael Stiller.
- Heft Nr. 186/1996 – „Reconstruction of Late Quaternary environmental conditions applying the natural radionuclides ^{230}Th , ^{10}Be , ^{231}Pa and ^{239}U : A study of deep-sea sediments from the eastern sector of the Antarctic Circumpolar Current System“, by Martin Frank.
- Heft Nr. 187/1996 – „The Meteorological Data of the Neumayer Station (Antarctica) for 1992, 1993 and 1994“, by Gert König-Langlo and Andreas Herber.
- Heft Nr. 188/1996 – „Die Expedition ANTARKTIS-XI/3 mit FS ‚Polarstern‘ 1994“, herausgegeben von Heinz Miller und Hannes Grobe.
- Heft Nr. 189/1996 – „Die Expedition ARKTIS-VII/3 mit FS ‚Polarstern‘ 1990“, herausgegeben von Heinz Miller und Hannes Grobe

- Heft Nr. 190/1996** – "Cruise report of the Joint Chilean-German-Italian Magellan 'Victor Hensen' Campaign in 1994", edited by Wolf Arntz and Matthias Gorny.
- Heft Nr. 191/1996** – „Leitfähigkeits- und Dichtemessung an Eisbohrkernen“, von Frank Wilhelms.
- Heft Nr. 192/1996** – „Photosynthese-Charakteristika und Lebensstrategie antarktischer Makroalgen“, von Gabriele Weykam.
- Heft Nr. 193/1996** – „Heterogene Reaktionen von N_2O_5 und Hbr und ihr Einfluß auf den Ozonabbau in der polaren Stratosphäre“, von Sabine Seisel.
- Heft Nr. 194/1996** – „Ökologie und Populationsdynamik antarktischer Ophiuroiden (Echinodermata)“, von Corinna Dahm.
- Heft Nr. 195/1996** – „Die planktische Foraminifere *Neogloboquadrina pachyderma* (Ehrenberg) im Weddellmeer, Antarktis“, von Doris Berberich.
- Heft Nr. 196/1996** – „Untersuchungen zum Beitrag chemischer und dynamischer Prozesse zur Variabilität des stratosphärischen Ozons über der Arktis“, von Birgit Heese.
- Heft Nr. 197/1996** – "The Expedition ARKTIS-XI/2 of 'Polarstern' in 1995", edited by Gunther Krause.
- Heft Nr. 198/1996** – „Geodynamik des Westantarktischen Riftsystems basierend auf Apatit-Spaltspuranalysen“, von Frank Lisker.
- Heft Nr. 199/1996** – "The 1993 Northeast Water Expedition. Data Report on CTD Measurements of RV 'Polarstern' Cruises ARKTIS IX/2 and 3", by Gerion Budéus and Wolfgang Schneider.
- Heft Nr. 200/1996** – "Stability of the Thermohaline Circulation in analytical and numerical models", by Gerrit Lohmann.
- Heft Nr. 201/1996** – „Trophische Beziehungen zwischen Makroalgen und Herbivoren in der Potter Cove (King George-Insel, Antarktis)“, von Katrin Iken.
- Heft Nr. 202/1996** – „Zur Verbreitung und Respiration ökologisch wichtiger Bodentiere in den Gewässern um Svalbard (Arktis)“, von Michael K. Schmid.
- Heft Nr. 203/1996** – „Dynamik, Rauigkeit und Alter des Meereises in der Arktis – Numerische Untersuchungen mit einem großskaligen Modell“, von Markus Harder.
- Heft Nr. 204/1996** – „Zur Parametrisierung der stabilen atmosphärischen Grenzschicht über einem antarktischen Schelfeis“, von Dörthe Handorf.
- Heft Nr. 205/1996** – "Textures and fabrics in the GRIP ice core, in relation to climate history and ice deformation", by Thorsteinn Thorsteinsson.
- Heft Nr. 206/1996** – „Der Ozean als Teil des gekoppelten Klimasystems: Versuch der Rekonstruktion der glazialen Zirkulation mit verschiedenen komplexen Atmosphärenkomponenten“, von Kerstin Fieg.
- Heft Nr. 207/1996** – „Lebensstrategien dominanter antarktischer Oithonidae (Cyclopoida, Copepoda) und Oncaeidae (Poecilostomatoida, Copepoda) im Bellingshausenmeer“, von Cornelia Metz.
- Heft Nr. 208/1996** – „Atmosphäreneinfluß bei der Fernerkundung von Meereis mit passiven Mikrowellenradiometern“, von Christoph Oelke.
- Heft Nr. 209/1996** – „Klassifikation von Radarsatellitendaten zur Meereiserkennung mit Hilfe von Line-Scanner-Messungen“, von Axel Bochert.
- Heft Nr. 210/1996** – „Die mit ausgewählten Schwämmen (Hexactinellida und Demospongiae) aus dem Weddellmeer, Antarktis, vergesellschaftete Fauna“, von Kathrin Kunzmann.
- Heft Nr. 211/1996** – "Russian-German Cooperation: The Expedition TAYMYR 1995 and the Expedition KOLYMA 1995", by Dima Yu. Bolshiyarov and Hans-W. Hubberten.
- Heft Nr. 212/1996** – "Surface-sediment composition and sedimentary processes in the central Arctic Ocean and along the Eurasian Continental Margin", by Ruediger Stein, Gennadij I. Ivanov, Michael A. Levitan, and Kirsten Fahl.
- Heft Nr. 213/1996** – „Gonadenentwicklung und Eiproduktion dreier *Calanus*-Arten (Copepoda): Freilandbeobachtungen, Histologie und Experimente“, von Barbara Niehof.
- Heft Nr. 214/1996** – „Numerische Modellierung der Übergangszone zwischen Eisschild und Eisschelf“, von Christoph Mayer.
- Heft Nr. 215/1996** – „Arbeiten der AWI-Forschungsstelle Potsdam in Antarktika, 1994/95“, herausgegeben von Ulrich Wand.
- Heft Nr. 216/1996** – „Rekonstruktion quartärer Klimaänderungen im atlantischen Sektor des Südpolarmeeres anhand von Radiolarien“, von Uta Brathauer.
- Heft Nr. 217/1996** – „Adaptive Semi-Lagrange-Finite-Elemente-Methode zur Lösung der Flachwassergleichungen: Implementierung und Parallelisierung“, von Jörn Behrens.
- Heft Nr. 218/1997** – "Radiation and Eddy Flux Experiment 1995 (REFLEX III)", by Jörg Hartmann, Axel Bochert, Dietmar Freese, Christoph Kottmeier, Dagmar Nagel and Andreas Reuter.
- Heft Nr. 219/1997** – „Die Expedition ANTARKTIS-XII mit FS „Polarstern“ 1995. Bericht vom Fahrtabschnitt ANT-XII/3, herausgegeben von Wilfried Jokat und Hans Oerter.
- Heft Nr. 220/1997** – „Ein Beitrag zum Schwerfeld im Bereich des Weddellmeeres, Antarktis. Nutzung von Altimetermessungen des GEOSAT und ERS-1“, von Tilo Schöne.
- Heft Nr. 221/1997** – „Die Expeditionen ANTARKTIS-XIII/1-2 des Forschungsschiffes „Polarstern“ 1995/96“, herausgegeben von Ulrich Bathmann, Mike Lukas und Victor Smetacek.
- Heft Nr. 222/1997** – "Tectonic Structures and Glaciomarine Sedimentation in the South-Eastern Weddell Sea from Seismic Reflection Data", by László Oszkó.

- Heft Nr. 223/1997** – „Bestimmung der Meereisdicke mit seismischen und elektromagnetisch-induktiven Verfahren“, von Christian Haas.
- Heft Nr. 224/1997** – „Troposphärische Ozonvariationen in Polarregionen“, von Silke Wessel.
- Heft Nr. 225/1997** – „Biologische und ökologische Untersuchungen zur kryopelagischen Amphipodenfauna des arktischen Meereises“, von Michael Poltermann.
- Heft Nr. 226/1997** – “Scientific Cruise Report of the Arctic Expedition ARK-XI/1 of RV 'Polarstern' in 1995”, edited by Eike Rachor.
- Heft Nr. 227/1997** – „Der Einfluß kompatibler Substanzen und Kryoprotektoren auf die Enzyme Malatdehydrogenase (MDH) und Glucose-6-phosphat-Dehydrogenase (G6P-DH) aus *Acrosiphonia arcta* (Chlorophyta) der Arktis“, von Katharina Kück.
- Heft Nr. 228/1997** – „Die Verbreitung epibenthischer Mollusken im chilenischen Beagle-Kanal“, von Katrin Linse.
- Heft Nr. 229/1997** – „Das Mesozooplankton im Laptevmeer und östlichen Nansen-Becken - Verteilung und Gemeinschaftsstrukturen im Spätsommer“, von Hinrich Hanssen.
- Heft Nr. 230/1997** – „Modell eines adaptierbaren, rechnergestützten, wissenschaftlichen Arbeitsplatzes am Alfred-Wegener-Institut für Polar- und Meeresforschung“, von Lutz-Peter Kurdelski
- Heft Nr. 231/1997** – „Zur Ökologie arktischer und antarktischer Fische: Aktivität, Sinnesleistungen und Verhalten“, von Christopher Zimmermann
- Heft Nr. 232/1997** – „Persistente chlororganische Verbindungen in hochantarktischen Fischen“, von Stephan Zimmermann
- Heft Nr. 233/1997** – „Zur Ökologie des Dimethylsulfoniumpropionat (DMSP)-Gehaltes temperierter und polarer Phytoplanktongemeinschaften im Vergleich mit Laborkulturen der Coccolithophorida *Emiliania huxleyi* und der antarktischen Diatomee *Nitzschia lecontei*“, von Doris Meyerdieter.
- Heft Nr. 234/1997** – „Die Expedition ARCTIC '96 des FS ‚Polarstern‘ (ARK XIII) mit der Arctic Climate System Study (ACSYS)“, von Ernst Augstein und den Fahrteilnehmern.
- Heft Nr. 235/1997** – „Polonium-210 und Blei-210 im Südpolarmeer: Natürliche Tracer für biologische und hydrographische Prozesse im Oberflächenwasser des Antarktischen Zirkumpolarstroms und des Weddellmeeres“, von Jana Friedrich
- Heft Nr. 236/1997** – “Determination of atmospheric trace gas amounts and corresponding natural isotopic ratios by means of ground-based FTIR spectroscopy in the high Arctic”, by Arndt Meier.
- Heft Nr. 237/1997** – “Russian-German Cooperation: The Expedition TAYMYR/SEVERNAYA ZEMLYA 1996”, edited by Martin Melles, Birgit Hagedorn and Dmitri Yu. Bolshiyarov
- Heft Nr. 238/1997** – “Life strategy and ecophysiology of Antarctic macroalgae”, by Iván M. Gómez.
- Heft Nr. 239/1997** – „Die Expedition ANTARKTIS XIII/4-5 des Forschungsschiffes ‚Polarstern‘ 1996“, herausgegeben von Eberhard Fahrbach und Dieter Gerdes.
- Heft Nr. 240/1997** – „Untersuchungen zur Chrom-Speziation in Meerwasser, Meereis und Schnee aus ausgewählten Gebieten der Arktis“, von Heide Giese.
- Heft Nr. 241/1997** – “Late Quaternary glacial history and paleoceanographic reconstructions along the East Greenland continental margin: Evidence from high-resolution records of stable isotopes and ice-rafted debris”, by Seung-Il Nam.
- Heft Nr. 242/1997** – “Thermal, hydrological and geochemical dynamics of the active layer at a continuous permafrost site, Taymyr Peninsula, Siberia”, by Julia Boike.
- Heft Nr. 243/1997** – „Zur Paläoozeanographie hoher Breiten: Stellvertreterdaten aus Foraminiferen“, von Andreas Mackensen.
- Heft Nr. 244/1997** – “The Geophysical Observatory at Neumayer Station, Antarctica, Geomagnetic and seismological observations in 1995 and 1996”, by Alfons Eckstaller, Thomas Schmidt, Viola Graw, Christian Müller and Johannes Rogenhagen.
- Heft Nr. 245/1997** – „Temperaturbedarf und Biogeographie mariner Makroalgen - Anpassung mariner Makroalgen an tiefe Temperaturen“, von Bettina Bischoff-Bäsmann.
- Heft Nr. 246/1997** – „Ökologische Untersuchungen zur Fauna des arktischen Meereises“, von Christine Friedrich.
- Heft Nr. 247/1997** – „Entstehung und Modifizierung von marinen gelösten organischen Substanzen“, von Berit Kirchoff.
- Heft Nr. 248/1997** – “Laptev Sea System: Expeditions in 1995”, edited by Heidemarie Kassens.
- Heft Nr. 249/1997** – “The Expedition ANTARKTIS XIII/3 (EASIZ I) of RV 'Polarstern' to the eastern Weddell Sea in 1996”, edited by Wolf Arntz and Julian Gutt.
- Heft Nr. 250/1997** – „Vergleichende Untersuchungen zur Ökologie und Biodiversität des Mega-Epibenthos der Arktis und Antarktis“, von Andreas Starmans.
- Heft Nr. 251/1997** – „Zeitliche und räumliche Verteilung von Mineralvergesellschaftungen in spätquartären Sedimenten des Arktischen Ozeans und ihre Nützlichkeit als Klimaindikatoren während der Glazial/Interglazial-Wechsel“, von Christoph Vogt.
- Heft Nr. 252/1997** – „Solitäre Ascidien in der Potter Cove (King George Island, Antarktis). Ihre ökologische Bedeutung und Populationsdynamik“, von Stephan Kühne.
- Heft Nr. 253/1997** – “Distribution and role of microprotozoa in the Southern Ocean”, by Christine Klaas.
- Heft Nr. 254/1997** – „Die spätquartäre Klima- und Umweltgeschichte der Bunger-Oase, Ostantarktis“, von Thomas Kulbe

- Heft Nr. 255/1997** – "Scientific Cruise Report of the Arctic Expedition ARK-XIII/2 of RV 'Polarstern' in 1997", edited by Ruediger Stein and Kirsten Fahl.
- Heft Nr. 256/1998** – „Das Radionuklid Tritium im Ozean: Meßverfahren und Verteilung von Tritium im Südatlantik und im Weddellmeer“, von Jürgen Süttenfuß.
- Heft Nr. 257/1998** – „Untersuchungen der Saisonalität von atmosphärischem Dimethylsulfid in der Arktis und Antarktis“, von Christoph Kleefeld.
- Heft Nr. 258/1998** – „Bellingshausen- und Amundsenmeer: Entwicklung eines Sedimentationsmodells“, von Frank-Oliver Nitsche.
- Heft Nr. 259/1998** – "The Expedition ANTARKTIS-XIV/4 of RV 'Polarstern' in 1997", by Dieter K. Fütterer.
- Heft Nr. 260/1998** – „Die Diatomeen der Laptevsee (Arktischer Ozean): Taxonomie und biogeographische Verbreitung“, von Holger Cremer
- Heft Nr. 261/1998** – „Die Krustenstruktur und Sedimentdecke des Eurasischen Beckens, Arktischer Ozean: Resultate aus seismischen und gravimetrischen Untersuchungen“, von Estella Weigelt.
- Heft Nr. 262/1998** – "The Expedition ARKTIS-XIII/3 of RV 'Polarstern' in 1997", by Gunther Krause.
- Heft Nr. 263/1998** – „Thermo-tektonische Entwicklung von Oates Land und der Shackleton Range (Antarktis) basierend auf Spaltspuranalysen“, von Thorsten Schäfer.
- Heft Nr. 264/1998** – „Messungen der stratosphärischen Spurengase ClO, HCl, O₃, N₂O, H₂O und OH mittels flugzeuggetragener Submillimeterwellen-Radiometrie“, von Joachim Urban.
- Heft Nr. 265/1998** – „Untersuchungen zu Massenhaushalt und Dynamik des Ronne Ice Shelves, Antarktis“, von Astrid Lambrecht.
- Heft Nr. 266/1998** – "Scientific Cruise Report of the Kara Sea Expedition of RV 'Akademic Boris Petrov' in 1997", edited by Jens Matthiessen and Oleg Stepanets.
- Heft Nr. 267/1998** – „Die Expedition ANTARKTIS-XIV mit FS ‚Polarstern‘ 1997. Bericht vom Fahrtabschnitt ANT-XIV/3“, herausgegeben von Wilfried Jokat und Hans Oerter.
- Heft Nr. 268/1998** – „Numerische Modellierung der Wechselwirkung zwischen Atmosphäre und Meereis in der arktischen Eisrandzone“, von Gerit Birnbaum.
- Heft Nr. 269/1998** – "Katabatic wind and Boundary Layer Front Experiment around Greenland (KABEG '97)", by Günther Heinemann.
- Heft Nr. 270/1998** – "Architecture and evolution of the continental crust of East Greenland from integrated geophysical studies", by Vera Schindwein.
- Heft Nr. 271/1998** – "Winter Expedition to the Southwestern Kara Sea - Investigations on Formation and Transport of Turbid Sea-Ice", by Dirk Dethleif, Per Loewe, Dominik Weiel, Hartmut Nies, Gesa Kuhlmann, Christian Bahe and Gennady Tarasov.
- Heft Nr. 272/1998** – „FTIR-Emissionsspektroskopische Untersuchungen der arktischen Atmosphäre“, von Edo Becker.
- Heft Nr. 273/1998** – „Sedimentation und Tektonik im Gebiet des Agulhas Rückens und des Agulhas Plateaus („SETA-RAP“)“, von Gabriele Uenzelmann-Neben.
- Heft Nr. 274/1998** – "The Expedition ANTARKTIS XIV/2", by Gerhard Kattner.
- Heft Nr. 275/1998** – „Die Auswirkung der 'NorthEastWater'-Polynya auf die Sedimentation von NO-Grönland und Untersuchungen zur Paläo-Ozeanographie seit dem Mittelwechsel“, von Hanne Notholt.
- Heft Nr. 276/1998** – „Interpretation und Analyse von Potentialfelddaten im Weddellmeer, Antarktis: der Zerfall des Superkontinents Gondwana“, von Michael Studinger.
- Heft Nr. 277/1998** – „Koordiniertes Programm Antarktisforschung“. Berichtskolloquium im Rahmen des Koordinierten Programms „Antarktisforschung mit vergleichenden Untersuchungen in arktischen Eisgebieten“, herausgegeben von Hubert Miller.
- Heft Nr. 278/1998** – „Messung stratosphärischer Spurengase über Ny-Ålesund, Spitzbergen, mit Hilfe eines bodengebundenen Mikrowellen-Radiometers“, von Uwe Raffalski.
- Heft Nr. 279/1998** – "Arctic Paleo-River Discharge (APARD). A New Research Programme of the Arctic Ocean Science Board (AOSB)", edited by Ruediger Stein.
- Heft Nr. 280/1998** – „Fernerkundungs- und GIS-Studien in Nordostgrönland“ von Friedrich Jung-Rothenhäusler.
- Heft Nr. 281/1998** – „Rekonstruktion der Oberflächenwassermassen der östlichen Laptevsee im Holozän anhand von aquatischen Palynomorphen“, von Martina Kunz-Pirrung.
- Heft Nr. 282/1998** – "Scavenging of ²³¹Pa and ²³⁰Th in the South Atlantic: Implications for the use of the ²³¹Pa/²³⁰Th ratio as a paleoproductivity proxy", by Hans-Jürgen Walter.
- Heft Nr. 283/1998** – „Sedimente im arktischen Meereis - Eintrag, Charakterisierung und Quantifizierung“, von Frank Lindemann.
- Heft Nr. 284/1998** – „Langzeitanalyse der antarktischen Meereisbedeckung aus passiven Mikrowellendaten“, von Christian H. Thomas.
- Heft Nr. 285/1998** – „Mechanismen und Grenzen der Temperaturanpassung beim Pierwurm *Arenicola marina* (L.)“, von Angela Sommer.
- Heft Nr. 286/1998** – „Energieumsätze benthischer Filtrierer der Potter Cove (King George Island, Antarktis)“, von Jens Kowalke.
- Heft Nr. 287/1998** – "Scientific Cooperation in the Russian Arctic: Research from the Barents Sea up to the Laptev Sea", edited by Eike Racher.

- Heft Nr. 288/1998** – „Alfred Wegener. Kommentiertes Verzeichnis der schriftlichen Dokumente seines Lebens und Wirkens“, von Ulrich Wutzke.
- Heft Nr. 289/1998** – „Retrieval of Atmospheric Water Vapor Content in Polar Regions Using Spaceborne Microwave Radiometry“, by Jungang Miao.
- Heft Nr. 290/1998** – „Strukturelle Entwicklung und Petrogenese des nördlichen Kristallingürtels der Shackleton Range, Antarktis: Proterozoische und Ross-orogene Krustendynamik am Rand des Ostantarktischen Kratons“, von Axel Brommer.
- Heft Nr. 291/1998** – „Dynamik des arktischen Meereises - Validierung verschiedener Rheologieansätze für die Anwendung in Klimamodellen“, von Martin Kreyscher.
- Heft Nr. 292/1998** – „Anthropogene organische Spurenstoffe im Arktischen Ozean, Untersuchungen chlorierter Biphenyle und Pestizide in der Laptevsee, technische und methodische Entwicklungen zur Probenahme in der Arktis und zur Spurenstoffanalyse“, von Sven Utschakowski.
- Heft Nr. 293/1998** – „Rekonstruktion der spätquartären Klima- und Umweltgeschichte der Schirmacher Oase und des Wohlthat Massivs (Ostantarktika)“, von Markus Julius Schwab.
- Heft Nr. 294/1998** – „Besiedlungsmuster der benthischen Makrofauna auf dem ostgrönländischen Kontinentalhang“, von Klaus Schnack.
- Heft Nr. 295/1998** – „Gehäuseuntersuchungen an planktischen Foraminiferen hoher Breiten: Hinweise auf Umweltveränderungen während der letzten 140.000 Jahre“, von Harald Hommers.
- Heft Nr. 296/1998** – „Scientific Cruise Report of the Arctic Expedition ARK-XIII/1 of RV 'Polarstern' in 1997“, edited by Michael Spindler, Wilhelm Hagen and Dorothea Stübing.
- Heft Nr. 297/1998** – „Radiometrische Messungen im arktischen Ozean - Vergleich von Theorie und Experiment“, von Klaus-Peter Johnsen.
- Heft Nr. 298/1998** – „Patterns and Controls of CO₂ Fluxes in Wet Tundra Types of the Taimyr Peninsula, Siberia - the Contribution of Soils and Mosses“, by Martin Sommerkorn.
- Heft Nr. 299/1998** – „The Potter Cove coastal ecosystem, Antarctica. Synopsis of research performed within the frame of the Argentinean-German Cooperation at the Dallmann Laboratory and Jubany Station (Kind George Island, Antarctica, 1991 - 1997)“, by Christian Wiencke, Gustavo Ferreyra, Wolf Arntz & Carlos Rinaldi.
- Heft Nr. 300/1999** – „The Kara Sea Expedition of RV 'Akademik Boris Petrov' 1997: First Results of a Joint Russian-German Pilot Study“, edited by Jens Matthiessen, Oleg V. Stepanets, Ruediger Stein, Dieter K. Fütterer, and Eric M. Galimov.
- Heft Nr. 301/1999** – „The Expedition ANTARKTIS XV/3 (EASIZ II)“, edited by Wolf E. Arntz and Julian Gutt.
- Heft Nr. 302/1999** – „Sterole im herbstlichen Weddellmeer (Antarktis): Großräumige Verteilung, Vorkommen und Umsatz“, von Anneke Mühlebach.
- Heft Nr. 303/1999** – „Polare stratosphärische Wolken: Lidar-Beobachtungen, Charakterisierung von Entstehung und Entwicklung“, von Jens Biele.
- Heft Nr. 304/1999** – „Spätquartäre Paläoumweltbedingungen am nördlichen Kontinentalrand der Barents- und Kara-See. Eine Multi-Parameter-Analyse“, von Jochen Knies.
- Heft Nr. 305/1999** – „Arctic Radiation and Turbulence Interaction Study (ARTIST)“, by Jörg Hartmann, Frank Albers, Stefania Argentini, Axel Bocher, Ubaldo Bonafé, Wolfgang Cohrs, Alessandro Conidi, Dietmar Freese, Teodoro Georgiadis, Alessandro Ippoliti, Lars Kaleschke, Christof Lüpkes, Uwe Maixner, Giangiuseppe Mastrantonio, Fabrizio Ravagnani, Andreas Reuter, Giuliano Trivellone and Angelo Viola.
- Heft Nr. 306/1999** – „German-Russian Cooperation: Biogeographic and biostratigraphic investigations on selected sediment cores from the Eurasian continental margin and marginal seas to analyze the Late Quaternary climatic variability“, edited by Robert R. Spielhagen, Max S. Barash, Gennady I. Ivanov, and Jörn Thiede.
- Heft Nr. 307/1999** – „Struktur und Kohlenstoffbedarf des Makrobenthos am Kontinentalhang Ostgrönlands“, von Dan Seiler.
- Heft Nr. 308/1999** – „ARCTIC '98: The Expedition ARK-XIV/1a of RV 'Polarstern' in 1998“, edited by Wilfried Jokat.
- Heft Nr. 309/1999** – „Variabilität der arktischen Ozonschicht: Analyse und Interpretation bodengebundener Millimeterwellenmessungen“, von Björn-Martin Sinnhuber.
- Heft Nr. 310/1999** – „Rekonstruktion von Meereisdrift und terrigenem Sedimenteintrag im Spätquartär: Schwermineralassoziationen in Sedimenten des Laptev-See-Kontinentalrandes und des zentralen Arktischen Ozeans“, von Marion Behrends.
- Heft Nr. 311/1999** – „Parameterisierung atmosphärischer Grenzschichtprozesse in einem regionalen Klimamodell der Arktis“, von Christoph Abegg.
- Heft Nr. 312/1999** – „Solare und terrestrische Strahlungswechselwirkung zwischen arktischen Eisflächen und Wolken“, von Dietmar Freese.
- Heft Nr. 313/1999** – „Snow accumulation on Ekströmsen, Antarctica“, by Elisabeth Schlosser, Hans Oerter and Wolfgang Graf.
- Heft Nr. 314/1999** – „Die Expedition ANTARKTIS XV/4 des Forschungsschiffes 'Polarstern' 1998“, herausgegeben von Eberhard Fahrbach.
- Heft Nr. 315/1999** – „Expeditions in Siberia in 1998“, edited by Volker Rachold.
- Heft Nr. 316/1999** – „Die postglaziale Sedimentationsgeschichte der Laptevsee: schwermineralogische und sedimentpetrographische Untersuchungen“, von Bernhard Peregovich.
- Heft-Nr. 317/1999** – „Adaption an niedrige Temperaturen: Lipide in Eisdiatomeen“, von Heidi Lehmal.
- Heft-Nr. 318/1999** – „Effiziente parallele Lösungsverfahren für elliptische partielle Differentialgleichungen in der numerischen Ozeanmodellierung“, von Natalja Rakowsky.

- Heft-Nr. 319/1999** – „The Ecology of Arctic Deep-Sea Copepods (Euchaetidae and Aetideidae). Aspects of their Distribution, Trophodynamics and Effect on the Carbon Flux“, by Holger Auel.
- Heft-Nr. 320/1999** – „Modellstudien zur arktischen stratosphärischen Chemie im Vergleich mit Meßdaten“, von Veronika Eyring.
- Heft-Nr. 321/1999** – „Analyse der optischen Eigenschaften des arktischen Aerosols“, von Dagmar Nagel.
- Heft-Nr. 322/1999** – „Messungen des arktischen stratosphärischen Ozons: Vergleich der Ozonmessungen in Ny-Ålesund, Spitzbergen, 1997 und 1998“, von Jens Langer
- Heft-Nr. 323/1999** – „Untersuchung struktureller Elemente des südöstlichen Weddellmeeres / Antarktis auf der Basis mariner Potentialfelddaten“, von Uwe F. Meyer.
- Heft-Nr. 324/1999** – „Geochemische Verwitterungstrends eines basaltischen Ausgangsgesteins nach dem spätpleistozänen Gletscherrückzug auf der Taimyrhalbinsel (Zentralibirien) - Rekonstruktion an einer sedimentären Abfolge des Lama Sees“, von Stefanie K. Harwart.
- Heft-Nr. 325/1999** – „Untersuchungen zur Hydrologie des arktischen Meereises - Konsequenzen für den kleinskaligen Stofftransport“, von Johannes Freitag.
- Heft-Nr. 326/1999** – „Die Expedition ANTARKTIS XIV/2 des Forschungsschiffes 'Polarstern' 1998“, herausgegeben von Eberhard Fahrbach.
- Heft-Nr. 327/1999** – „Gemeinschaftsanalytische Untersuchungen der Harpacticoidenfauna der Magellanregion, sowie erste similaritätsanalytische Vergleiche mit Assoziationen aus der Antarktis“, von Kai Horst George.
- Heft-Nr. 328/1999** – „Rekonstruktion der Paläo-Umweltbedingungen am Laptev-See-Kontinentalrand während der beiden letzten Glazial/Interglazial-Zyklen anhand sedimentologischer und mineralogischer Untersuchungen“, von Claudia Müller.
- Heft-Nr. 329/1999** – „Räumliche und zeitliche Variationen atmosphärischer Spurengase aus bodengebundenen Messungen mit Hilfe eines Michelson Interferometers“, von Justus Notholt.
- Heft-Nr. 330/1999** – „The 1998 Danish-German Excursion to Disko Island, West Greenland“, edited by Angelika Brandt, Helge A. Thomsen, Henning Heide-Jørgensen, Reinhardt M. Kristensen and Hilke Ruhberg.
- Heft-Nr. 331/1999** – „Poseidon“ Cruise No. 243 (Reykjavik - Greenland - Reykjavik, 24 August - 11 September 1998): Climate change and the Viking-age fjord environment of the Eastern Settlement, sw Greenland“, by Gerd Hoffmann, Antoon Kuijpers, and Jörn Thiede.
- Heft-Nr. 332/1999** – „Modeling of marine biogeochemical cycles with an emphasis on vertical particle fluxes“, by Regina Usbeck.
- Heft-Nr. 333/1999** – „Die Tanaidaceenfauna des Beagle-Kanals und ihre Beziehungen zur Fauna des antarktischen Festlandssockels“, von Anja Schmidt.
- Heft-Nr. 334/1999** – „D-Aminosäuren als Tracer für biogeochemische Prozesse im Fluß-Schelf-Ozean-System der Arktis“, von Hans Peter Fitznar.
- Heft-Nr. 335/1999** – „Ökophysiologische Ursachen der limitierten Verbreitung reptanter decapoder Krebse in der Antarktis“, von Markus Frederich.
- Heft-Nr. 336/1999** – „Ergebnisse der Untersuchung des grönländischen Inlandeises mit dem elektromagnetischen Reflexionsverfahren in der Umgebung von NGRIP“, von Fidan Göktas.
- Heft-Nr. 337/1999** – „Paleozoic and mesozoic tectono-thermal history of central Dronning Maud Land, East Antarctica, – evidence from fission-track thermochronology“, by Stefanie Meier.
- Heft-Nr. 338/1999** – „Probleme hoher Stoffwechselraten bei Cephalopoden aus verschiedenen geographischen Breiten“, von Susanne Zielinski.
- Heft-Nr. 339/1999** – „The Expedition ARKTIS XV/1“, edited by Gunther Krause.
- Heft-Nr. 340/1999** – „Microbial Properties and Habitats of Permafrost Soils on Taimyr Peninsula, Central Siberia“, by Nicolé Schmidt.
- Heft-Nr. 341/1999** – „Photoacclimation of phytoplankton in different biogeochemical provinces of the Southern Ocean and its significance for estimating primary production“, by Astrid Bracher.
- Heft-Nr. 342/1999** – „Modern and Late Quaternary Depositional Environment of the St. Anna Trough Area, Northern Kara Sea“, edited by Ruediger Stein, Kirsten Fahl, Gennadij I. Ivanov, Michael A. Levitan, and Gennady Tarasov.
- Heft-Nr. 343/1999** – „ESF-IMPACT Workshop/Oceanic impacts: mechanisms and environmental perturbations, 15 - 17 April 1999 in Bremerhaven“, edited by Rainer Gersonde and Alexander Deutsch.
- Heft-Nr. 344/1999** – „Die Klimageschichte der hohen nördlichen Breiten seit dem mittleren Miozän: Hinweise aus sedimentologischen- und mineralogischen Analysen (OPD Leg 151, zentrale Framstraße)“, von Amelie Winkler.
- Heft-Nr. 345/1999** – „Kurzfristige Klimaschwankungen im Scotiameer und Ergebnisse zur Kalbungsgeschichte der Antarktis während der letzten 200 000 Jahre“, von Annette Hofmann.
- Heft-Nr. 346/2000** – „Glazialmarine Sedimentationsentwicklung am westantarktischen Kontinentalrand im Amundsen- und Bellingshausenmeer - Hinweise auf Paläoumweltveränderungen während der quartären Klimazyklen“, von Claus-Dieter Hillenbrand
- Heft-Nr. 347/2000** – „Zur Ökologie des Phytoplanktons im arktischen Laptevmeer - ein jahreszeitlicher Vergleich“, von Kirsten Tuschling.
- Heft-Nr. 348/2000** – „Untersuchungen zum Fettstoffwechsel des Südlichen See-Elefanten (*Mirounga leonina* L.) in der Antarktis“, von Sven Ramdohr.
- Heft-Nr. 349/2000** – „Licht- und Temperatureinfluß auf den enzymatischen Oxidationsschutz der antarktischen Eisdiatomee *Entomoneis kufferathii* Manguin“, von Raimund Schriek.

Heft-Nr. 350/2000 – „Die Expedition ARKTIS XV/3 des Forschungsschiffes 'Polarstern' 1999“
herausgegeben von Ursula Schauer.

Heft-Nr. 351/2000 – „Dissolution kinetics of biogenic silica in marine environments“, by Dirk Rickert.

* verfüllend of print.
** nur noch beim Autor/only from the author.

